PROCEEDINGS OF THE KECK GEOLOGY CONSORTIUM

Volume 31
2018
2017-2018 Projects

Dr. Cameron Davidson and Dr. Karl Wirth, Editors
Co-Directors, Keck Geology Consortium

Marga Miller
Keck Geology Consortium Administrative Assistant
Macalester College

Keck Geology Consortium
Macalester College
1600 Grand Ave, St. Paul, MN 55105
(651) 696-6108, Info@KeckGeology.org

ISSN# 1528-7491

Funding Provided by:
Keck Geology Consortium Member Institutions
The National Science Foundation Grant NSF-REU 1659322

PROCEEDINGS OF THE KECK GEOLOGY CONSORTIUM

ISSN# 1528-7491

2017-2018 Projects

Cameron Davidson Editor and Co-Director Carleton College	Keck Geology Consortium Macalester College 1600 Grand Ave. St Paul, MN 55105	Karl Wirth Editor and Co-Director Macalester College

Keck Geology Consortium Member Institutions:

Amherst College, Beloit College, Carleton College, Colgate University, The College of Wooster, The Colorado College, Franklin & Marshall College, Macalester College, Mt Holyoke College, Oberlin College, Pomona College, Smith College, Trinity University, Union College, Washington & Lee University, Wesleyan University, Whitman College

2017-2018 GATEWAY PROJECT

EXPLORING GEOCHRONOLOGY: DATING YOUNG LAVA FLOWS AND OLD TREES IN DECLINE
Faculty: MEAGEN POLLOCK, The College of Wooster and GREG WILES, The College of Wooster
Students: JOHSUA CHARLTON, The College of Wooster, ALORA CRUZ, Macalester College, MYRON MALISSE LUMMUS, Trinity University, KERENSA LOADHOLT, Oberlin College, CHRISTOPHER MESSERICH, Washington and Lee University, PA NHIA MOUA, Carleton College, SAMUEL PATZKOWSKY, Franklin and Marshall College, EMILY RANDALL, The College of Wooster, MADISON LILITH ROSEN, Mt Holyoke College, ADDISON THOMPSON, Pitzer College

2017-2018 ADVANCED PROJECTS

HAZARDS OF THE CARIBBEAN: THE HISTORY OF MAGMA CHAMBERS, ERUPTIONS, LANDSLIDES, STREAMS, AND FUMEROLES IN DOMINICA
Faculty: HOLLI FREY, Union College, AMANDA SCHMIDT, Oberlin College, EROUSCILLA JOSEPH, University of West Indies Seismic Research Center, LAURA WATERS, Sonoma State University
Students: JESSICA BERSSON, Whitman College, JACQUELINE BUSKOP, Wesleyan University, JUSTIN CASAUS, Sonoma State University, NOLAN EBNER, Macalester College, SARAH HICKERNELL, Union College, MARCUS HILL, Oberlin College, ANDREW HOLLYDAY, Middlebury College, TARYN ISENBURG, Mount Holyoke College, COLE JIMERSON, The College of Wooster, DEXTER KOPAS, Beloit College, ABADIE LUDLAM, Union College, CHLOE MOORE, Amherst College, MAZI-MAZTHIS C. ONYEALI, University of Colorado, Boulder, CLARISSA SMITH, Carleton College, HALEY TALBOT-WENDLANDT, KIRA TOMENCHOK, Washington & Lee University, KATHRYN VONSYDOW

UNRAVELING ANTARCTIC ICE SHEET DYNAMICS VIEWED THROUGH A MARINE DEPTH TRANSECT NEAR THE SOUTH ORKNEY MICROCONTINENT, WEDDELL SEA (IODP)
Faculty: SUZANNE O'CONNELL, Wesleyan University and JOSEPH ORTIZ, Kent State University
Students: EDUARDO CENTENO, Wesleyan University, MARK LAPAN, Colgate University, FORREST W. LLOYD, Beloit College

Short Contributions – Geochronology Gateway Project

Short Contributions – Dominica Advanced Project

UNDERSTANDING THE EFFECTS OF LARGE STORMS ON DOMINICA: AN ANALYSIS USING GIS AND REPEAT PHOTOGRAPHY
MARCUS HILL, Oberlin College
Research Advisor: Amanda Schmidt

STRATIGRAPHY AND GEOCHEMISTRY OF A FOND ST. JEAN CINDER CONE, DOMINICA
TARYN ISENBURG, Mount Holyoke College
Research Advisors: Steve Dunn and Holli Frey

RIVER DEVELOPMENT AND INCISION ON DOMINICA, WEST INDIES
COLE JIMERSON, The College of Wooster
Research Advisor: Amanda Schmidt

AN INVESTIGATION OF THE INFLUENCES ON THE GEOCHEMISTRY OF STREAMS IN DOMINICA, LESSER ANTILLES: 2014-2017
DEXTER KOPAS, Beloit College
Research Advisors: Susan Swanson, Erouscilla Joseph, and Holli Frey

DECOMPRESSION AND HEATING INDUCED AMPHIBOLE BREAKDOWN IN EFFUSIVE VOLCANISM ON DOMINICA, LESSER ANTILLES
ABADIE LUDLAM, Union College
Research Advisor: Holli Frey

INVESTIGATING VOLCANIC-HYDROTHERMAL SYSTEMS IN DOMINICA, LESSER ANTILLES: TEMPORAL CHANGES IN THE CHEMICAL COMPOSITION OF HYDROTHERMAL FLUIDS FOR VOLCANIC MONITORING USING GEOTHERMOMETERS
MAZI-MAZTHIS C. ONYEALI, University of Colorado, Boulder
Research Advisors: Holli Frey, Erouscilla Joseph, and Lon Abbott

INVESTIGATION OF MINERAL ALTERATION IN ANDESITE AND DACITE FROM THREE DIFFERENT VOLCANO HYDROTHERMAL SYSTEMS ON DOMINICA, LESSER ANTILLES
CLARISSA ITZEL VILLEGAS SMITH, Carleton College
Research Advisors: Cameron Davidson, Holli Frey, and Erouscilla Joseph

COMPOSITION AND SHORT-TIMESCALE EROSION PATTERNS OF RIVER SEDIMENTS ON DOMINICA
HALEY TALBOT-WENDLANDT, Ohio Wesleyan University
Research Advisor: Bart Martin

APPROXIMATING METEORIC ^{10}BE USING THE CONCENTRATION OF ACID-EXTRACTABLE GRAIN COATINGS: A CASE STUDY TRACING EROSION DEPTH ON DOMINICA, LESSER ANTILLES
KIRA TOMENCHOK, Washington and Lee University
Research Advisors: David Harbor and Amanda Schmidt

EVIDENCE FOR COLD, HYDROUS PARENTAL MAGMAS ON DOMINICA: PETROLOGY OF THE FOUNDLAND BASALTS
KATHRYN VONSYDOW, California State University San Bernardino
Research Advisors: Laura Waters (Sedona College), Holli Frey (Union College), and Joan E. Fryxell (California State University San Bernardino)

Short Contributions – IODP Advanced Project

Learning Science Through Research
Published by Keck Geology Consortium

Short Contributions
Keck Geology Consortium
Volume 31
May 2018

EXPLORING GEOCHRONOLOGY: DATING YOUNG LAVA FLOWS AND OLD TREES IN DECLINE

Faculty:
MEAGEN POLLOCK, The College of Wooster
GREG WILES, The College of Wooster

Students:
JOHSUA CHARLTON, The College of Wooster; **ALORA CRUZ,** Macalester College;
MYRON MALISSE LUMMUS, Trinity University; **KERENSA LOADHOLT,** Oberlin College;
CHRISTOPHER MESSERICH, Washington and Lee; **PA NHIA MOUA,** Carleton College;
SAMUEL PATZKOWSKY, Franklin and Marshall; **EMILY RANDALL,** The College of Wooster;
MADISON LILITH ROSEN, Mount Holyoke; **ADDISON THOMPSON,** Pitzer College

INTRODUCTION

In the summer of 2017, 10 students participated in a 5-week Gateway project hosted at The College of Wooster (Figure 1). Students conducted research in two teams led by co-directors Meagen Pollock and Greg Wiles. Team Utah (led by Pollock) investigated the age of young basaltic lava flows in Utah's Ice Springs Volcanic Field (ISVF). The goals of the Utah project were to constrain the timing of ISVF volcanism relative to the development of the Black Rock Desert (BRD), revise the lava flow emplacement history, and test the classification of the ISVF as a polymagmatic compound monogenetic field. Team Alaska (led by Wiles) reconstructed the growth history and recent climate response of yellow-cedar in Juneau, Alaska. The goals of the Alaska project were to sample tree-ring sites along elevational transects in the Juneau region and develop chronologies (ring-width and Blue Intensity (BI) records) to compare these records with meteorological records from stations along the Gulf of Alaska and with gridded data from the North Pacific. These comparisons allow us to better understand the forest decline in the region.

Figure 1. (a) Team Alaska. From left to right: Kerensa Loadholt, Alora Cruz, Chris Messerich, Malisse Lummus, and Josh Charlton. (b) Team Utah. From left to right: Pa Nhia Moua, Addison Thompson, Emily Randall, Madison Rosen, and Sam Patzkowsky.

Both projects began at Wooster, where the groups learned how to core trees and describe samples in preparation for field work. The teams then went to their respective field sites, where they collected data and interacted with professional geoscientists. The students shared their experiences on the Wooster Geologists blog and highlights included visits to the Alaska State Museum and the Utah Core Repository. When the teams returned to Wooster, they embarked on the analytical component of the research project. For the Utah project, students prepared samples for geochemical analysis by X-ray Fluorescence (XRF) in Wooster's X-ray lab and sent samples to external labs for trace element analysis. Students also prepared samples for bulk 36Cl analysis at the Purdue PRIME lab and used previous cosmogenic data with the CRONUS Earth Web Calculator to estimate an age for ISVF. For the Alaska project, students collected ring-width and BI time series records in the Wooster Tree Ring Lab. The tree-ring chronologies were compared with station climate data from the Juneau area and with a variety of gridded climate records available on Climate Explorer.

The teams achieved their research objectives and presented their work at the 2017 GSA annual meeting in Seattle, Washington. Team Utah's poster was titled New Cosmogenic and VML Dates and Revised Emplacement History of the Ice Springs Volcanic Field in the Black Rock Desert, Utah (Patzkowsky et al., 2017). Team Alaska's poster was titled Yellow Cedar Growth Response to Decadal Climatic Shifts at Cedar Lake, Juneau, Alaska (Charlton et al., 2017). Their GSA posters can be found on the Keck Geology Consortium website. This short contribution summarizes their work and highlights their key findings.

ICE SPRINGS VOLCANIC FIELD, BLACK ROCK DESERT, UTAH

Utah's Black Rock Desert (BRD), located in the Basin & Range Province, contains 7+ unique volcanic fields, all 1 Ma or younger (Condie and Barsky, 1972). Ice Springs Volcanic Field (ISVF) is one of youngest BRD units, dated at 660 ± 170 years ago (Figure 2, Valestro et al., 1972). ISVF is hypothesized to be a compound polygenetic volcano due to multiple cinder cones (Miter, Terrace, Pocket, & Crescent), eruptions, and magma batches (Nemeth and Kereszturi, 2015;

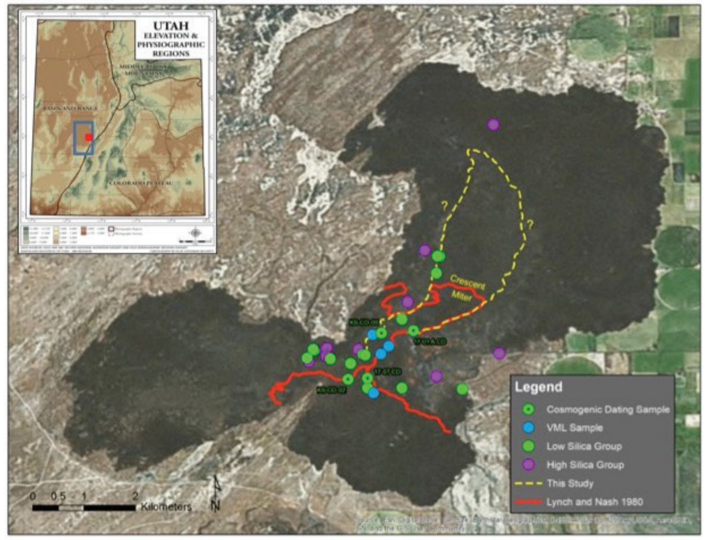

Figure 2. Map of Ice Springs Volcanic Field. Circles show locations of low silica (green) and high silica (purple) samples. VML (blue) and cosmogenic dating (dot) samples are located in the area west of the cones. Boundaries of Lynch and Nash (1980) are in red. Proposed boundaries from this study are in yellow. Inset map shows location of Ice Springs Volcanic Field (red square) in Utah's Black Rock Desert (blue rectangle).

Williams, 2016). Individual flows boundaries have been previously defined (Gilbert, 1890; Hoover, 1974; Lynch and Nash, 1980), but have been called into question based on recent mapping and geochemical analysis (Figure 2, Thompson, 2009; Sims, 2013). The development of robust dating methods (Cosmogenic Dating & Varnish Microlamination (VML)) makes it possible to more accurately determine the date of young lava flows in the ISVF. This study aims to determine the flows' emplacement sequence and ages in order to place the ISVF in geologic context and improve understanding of its eruption history.

Our approach combines mapping and geochemical investigations with multiple dating techniques. Eight samples from the Miter and Crescent flows were collected for major element geochemical analysis by XRF at The College of Wooster. Two additional pahoehoe samples were collected from the Miter/Terrace boundary and within the Miter flow for cosmogenic 36Cl dating at the Purdue PRIME lab. The CRONUS calculator (Marrero et al., 2015) was used to find minimum and maximum ages for the lava flows based on variations in erosion rates, density, and scaling framework. VML ultra-thin thin sections (Goldsmith, 2011; Liu and Broecker, 2013) were made from samples of the Miter/Terrace flows to independently estimate the age.

Age estimates from VML and cosmogenic 36Cl methods are approximately the same and significantly older than previous estimates (Figure 3). Two VML samples yielded the oldest dates of ~12,500 years, based on distinct layering that could be correlated to established VML stratigraphy in the western U.S. (Figure 3a, Liu and Broecker, 2013). The 36Cl age range of the sample from the Miter/Terrace boundary (CD-02) is 9.4 (± 1.3) to 10.9 (± 1.6) kyr. The 36Cl age range for the Miter flow (CD-05) is 10.9 (± 1.6) to 11.3 (± 1.5) kyr (Figure 3b). Our cosmogenic age ranges for ISVF are significantly older than those previously found by Valastro et al. (1972; 660 ±170 years) and Hoover (1974; 1 - 4 kyr), but are still viable as they would have been post Lake Bonneville at an elevation of ~1,400m (Figure 3b, Lifton et al., 2015).

Our mapping and geochemical analyses also disagree with previous observations (Figures 2 and 3c). Two previously identified ISVF compositional groups are distinct in major and trace elements, and are referred to as “high silica” and “low silica” lava flows (Lynch & Nash, 1980; Nelson & Tingey, 1997; Thompson, 2009; Sims, 2013; Matesich, 2014). High silica lavas are correlated with the oldest lava flows, originating from Crescent. Low silica lavas correlate with the Miter and Terrace eruptions. Samples from this study that are currently mapped at Miter overlap with Crescent flows; those that are currently mapped as Crescent overlap with Miter and Terrace flows (Figure 3c). The new geochemical data suggest that the previous boundary between the Miter and Crescent flows is either not in the correct location or that the chemistry of the Crescent flow is much more complex than previously thought. We propose a new Miter/Crescent boundary based on geochemistry (Figure 2).

In summary, new cosmogenic dates for the ISVF range from 9.4 (±1.3) - 11.3 (±1.5) kyr, similar to VML ages of ~12.5 kyr. These ages are much older than previous estimates, but still consistent with the geologic history of the BRD and Lake Bonneville. Additional geochemical data fill gaps in previous sampling and suggest newly mapped boundaries between the Crescent and Miter lava flows. The ages of ISVF flows and its multiple eruptions support its

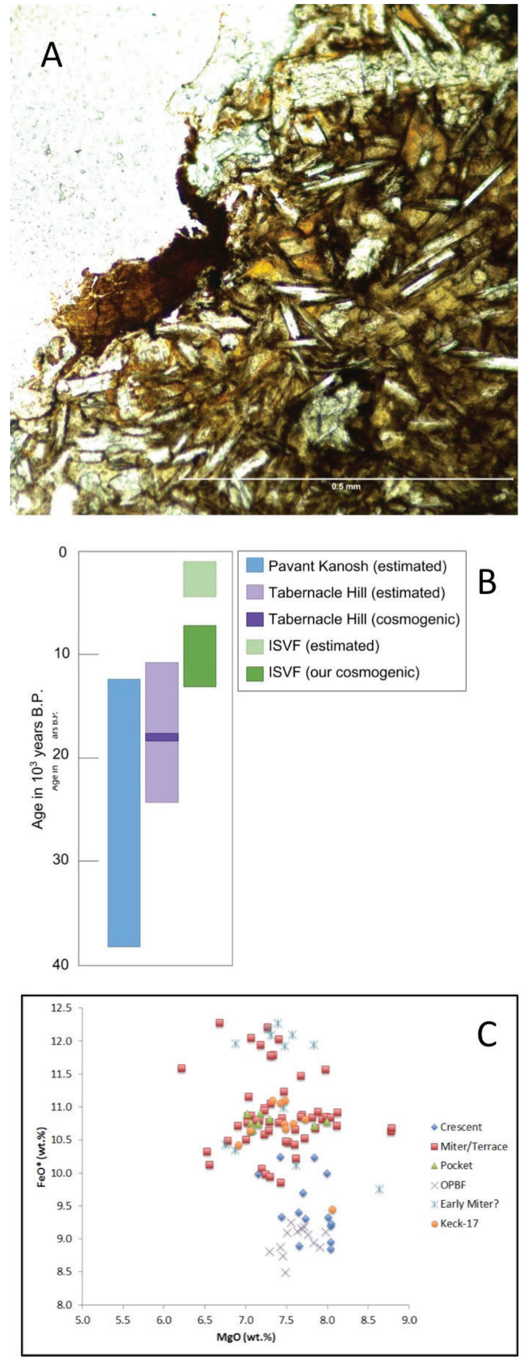

Figure 3. (a) VML sample yields a date of ~12,500 as indicated by the distinct layering and representation of layer WP0 (from Liu and Broecker, 2013) at the base. (b) Our cosmogenic age range for ISVF (dark green) in relation to the Pavant Kanosh estimated age (blue; Condie and Barsky, 1972), Tabernacle Hill estimated age (light purple; Condie and Barsky, 1972; Hoover, 1974), Tabernacle Hill cosmogenic age (dark purple; Lifton et al., 2015), and ISVF estimated age (light green, Hoover, 1974). (c) FeO vs. MgO (in wt.%) for ISVF. Crescent flows show low FeO* compared to Miter and Terrace. Samples from this study that are currently mapped as Miter (OPBF and one Keck-17) overlap with Crescent flows; those that are currently mapped as Crescent (Keck-17) overlap with Miter and Terrace flows. Previous geochemistry from Lynch and Nash, 1980; Nelson and Tingey, 1997; Thompson, 2009; and Matesich, 2014.*

classification as a compound polygenetic volcano according to the Nemeth and Kereszturi (2015). Additional ages and geochemical sampling can clarify details of the eruption history of an area of local importance for its economic mining operations and potential for geothermal energy development.

YELLOW CEDAR, JUNEAU, ALASKA

The decline of yellow-cedar (Callitropsis nootkatensis D. Don; Oerst. Ex D.P. Little) is an ongoing forest response to climate change that has been linked to warming temperatures, earlier snow melt, and a transition of snow to rain, which all lead to a loss of snowpack. Snow protects vulnerable small roots of this shallow-rooting species and thus the trees are more susceptible to frost damage (Shaberg et al., 2011; Hennon et al. 2012, 2016). Extensive work, testing this hypothesis is underway, in part, driven by consideration of listing the species as endangered (Bidlack et al., 2017; Buma et al., 2017).

We examined the climate response of a well-replicated composite tree-ring chronology from three sites in the Juneau, Alaska region (Figure 4). Ring-widths (RW) and latewood blue intensity measurements (LBi) were measured, developed into tree ring series, and the climate response was analyzed in this region where snowfall is decreasing as temperature and rainfall increase. LBi is a proxy for maximum latewood density and is a less expensive alternative (Björklund et al., 2014; Wilson et al., 2017). We present the RW and LBi records and examine their potential for climate reconstruction and interpret results in the context of the yellow-cedar decline.

Trees were cored at the three sites (Figure 4). Increment cores were mounted on sticks and sanded to a high polish, scanned as high-resolution image files, and analyzed using CDendro 8.1 and CooRecorder 8.1. The final combined RW and LBi chronologies incorporate 179 series from 113 trees and we examined the record back to CE 1400 where the series are sufficiently replicated (Figure 5c).

The two chronologies were correlated with monthly maximum average temperatures within the coordinates 57 o-62o N, 130 o -140o W (Harris et al., 2014; Figure 5b) for the CE 1900-2014 interval. For precipitation,

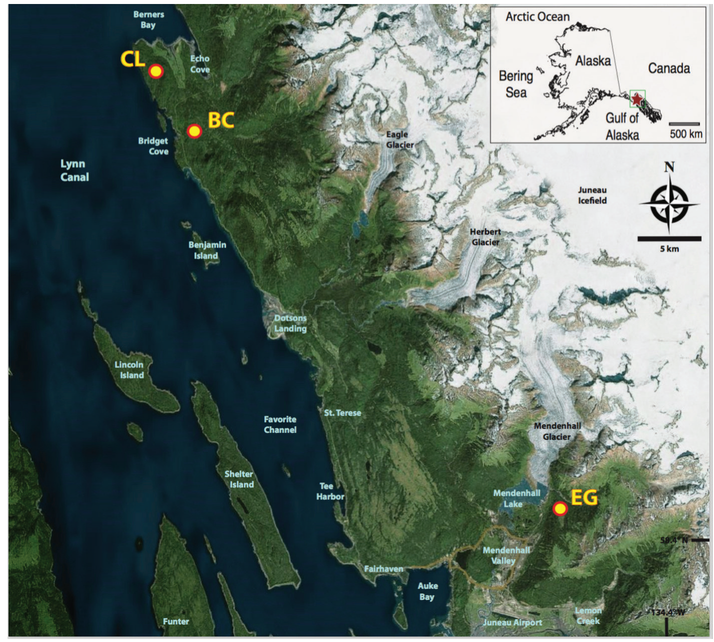

Figure 4. Map of the three yellow cedar tree-ring sites near Juneau, Alaska. CL- Cedar Lake, BC – Bridget Cove, and EG – East Glacier. The ring-width and latewood blue intensity chronology for this study were generated from a composite from the three sites. The box in the inset location map outlines the region from which temperature records were averaged.

we assembled the monthly Juneau total precipitation records for 1949-2014 extracted from Climate Explorer (Trouet and Oldenborgh, 2013).

The RW and LBi series shows strong synchronous decadal variability throughout the record (CE 1400-1975) until they diverge notably after about 1975 (Figure 5a), when the LBi record decreases and the RW series drops, and then generally increases through recent decades. Climate comparisons were made for the standard dendroclimatic year that consisted of March through December of the previous year of growth and January through October of the year of growth (not shown). The RW series did not show a strong climate response and is not considered further. For the LBi, the strongest correlation was with January-August maximum mean temperature (Figure 5b), which correlates at 0.62 for the interval 1902-1975 ($p<0.00001$). We identified a marked decrease in correlation after 1976 (Figure 5b) and then a recovery in correlation in the recent decades.

For precipitation, we correlated monthly totals with the LBi series (Figure 5c) for the early period from 1949-1975; there were no significant correlations at the 95% confidence levels for this interval. However, for the interval after 1975, there is a strong negative relationship with the LBi and with total July-September precipitation (Figure 5c). This observation suggests that high rainfall during these late summer months into the early fall is detrimental to tree growth.

In contrast with the temperature response, which shows a recovery from negative to positive correlation after about 2001 (Figure 5b), the precipitation response remains negative (Figure 5c).

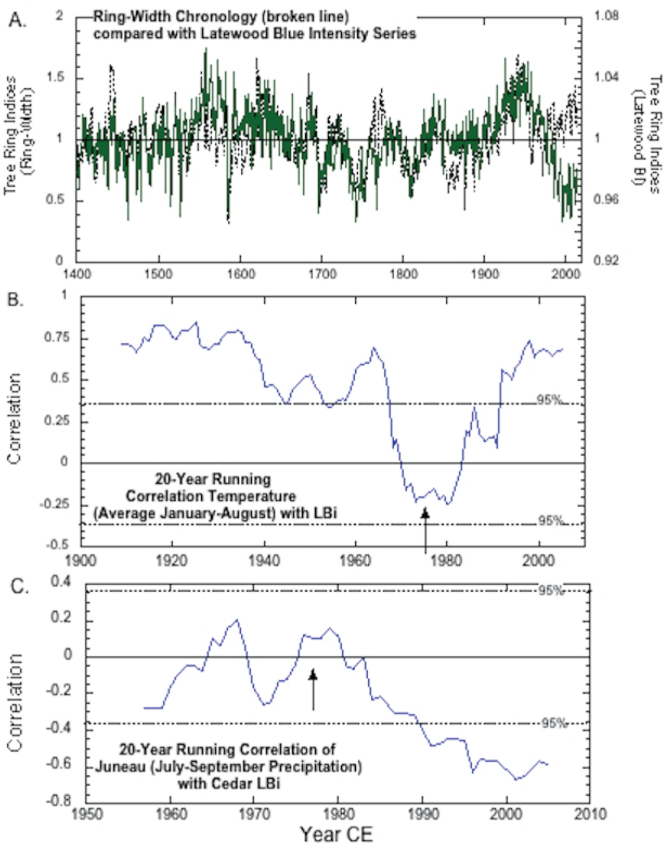

Figure 5. (a) Ring-width series compared with the latewood blue intensity chronology, note how the two series diverge after the mid 1970s. (b) 20-year running correlations between average maximum temperatures for January through August with the latewood blue intensity (LBi) record. Up until the mid-1970s regime shift (arrow) in the North Pacific the LBi and temperature records are strongly correlated. After the shift in temperature associated with the regime shift the LBi loses its temperature sensitivity and appears to recover in recent decades. (c) Total July through September precipitation records compared with the LBi record. Here the 20-year running correlation shows a negative relationship beginning on the 1980s and persisting through recent decades.

This study is the first to generate and analyze the climate signal in Blue Intensity chronologies from Alaska yellow-cedar. The well-replicated LBi chronology shows a much stronger sensitivity to temperature than ring-width and furthermore, the BI records from this species are sufficiently sensitive to be an important species in dendroclimatology.
The LBi record however, indicates a nonstationarity in climate response after the well-documented 1976-77 climate shift. This shift in southeast Alaska forced warmer temperatures, less snow and more rain to the region. Comparisons of monthly climate records with the well-replicated LBiI chronology show a strong positive January-August average temperature signal becoming negative after 1976 with some recovery to a positive response in recent decades. This observation is consistent with previous work on climate response of yellow cedar and the associated cedar decline forced by warming temperatures causing this shallow-rooting species to be vulnerable to rootlets freezing as a leading hypothesis for the loss of trees at some sites. In addition to the changes in temperature response, warm-season precipitation (total July-September) increases are linked to negative excursions in the latewood BI suggesting that this parameter may also be sensitive to moisture variability.

CONCLUSIONS

Ten Gateway students conducted cutting-edge geochronological research, making original intellectual contributions to the fields of volcanology and dendrochronology. Team Utah applied cosmogenic and varnish microlamination dating methods to investigate the emplacement history of Ice Springs Volcanic Field in the Black Rock Desert, Utah. They determined that Ice Springs Volcanic field is significantly older (~10 ka) than previous estimates. Their work resulted in revised lava flow boundaries and emplacement history for the Ice Springs Volcanic Field, enhancing the understanding of a local area of economic interest for its quarrying and potential to provide geothermal energy. Team Alaska applied dendrochronological methods to investigate the decline of yellow cedar in Cedar Lake north of Juneau, Alaska. Their study is the first to generate and analyze the climate signal in Blue Intensity (BI) chronologies from Alaska yellow-cedar. Their findings support the leading hypothesis for cedar decline and provide well replicated ring-width and BI records for further research. Environmental changes in the region are proceeding rapidly and their contribution provides a case study to understand how yellow-cedar and other species may respond to rapid climate change.

ACKNOWLEDGEMENTS

This material is based upon work supported by the Keck Geology Consortium and the National Science Foundation under Grant No. 1659322. Additional funding was provided by The College of Wooster Wengerd Fund and NSF-AGS-1502186. Thanks to Red Dome Quarry, who owns ISVF and gave us permission to access their land during this research. We appreciate the assistance of Brian Buma, John Krapek, and the Department of Natural Resources at the University of Alaska Southeast. Thanks to Shelley Judge for critical feedback on our project and to Patrice Reeder and Nick Wiesenberg for technical support.

REFERENCES

Bidlack, A., Bisbing, S., Buma, B., D'Amore, D., Hennon, P., Heutte, T., Krapek, J., Mulvey, R., and Oakes, L., 2017, Alternative interpretation and scale-based context for "No evidence of recent (1995–2013) decrease of yellow-cedar in Alaska" (Barrett and Pattison 2017): Canadian Journal of Forest Research, 2017, v. 47, p. 1145-1151.

Björklund, J. A., Gunnarson, B. E., Seftigen, K., Esper, J., and Linderholm, H. W., 2014, Blue intensity and density from northern Fennoscandian tree rings, exploring the potential to improve summer temperature reconstructions with earlywood information: Climate of the Past, v. 10, p. 877-885, https://doi.org/10.5194/cp-10-877-2014.

Buma B, Hennon PE, Harrington CA, Popkin JR, Krapek J, Lamb MS, Oakes LE, Saunders S, Zeglen S. 2017, Emerging climate-driven disturbance processes: widespread mortality associated with snow-to-rain transitions across 10° of latitude and half the range of a climate-threatened conifer. Global Change Biol. v. 23, p. 2903-2914.

Charlton, J., Cruz, A.J., Lummus, M.M., Loadholt, K., Messerich, C., Wiles, G., Buma, B., and Krapek, J., 2017, Yellow cedar growth response to decadal climatic shifts at Cedar Lake, Juneau, Alaska: GSA Abstracts with Programs, V. 49(6), doi: 10.1130/abs/2017AM-298740.

Condie, K.C., and Barsky, C.K., 1972, Origin of Quaternary basalts from the Black Rock desert region, Utah: Geological Society of America Bulletin, v. 83, p. 333–352.

Gilbert, G.K., 1890, Lake Bonneville: United States Geological Survey, monograph 1, 438 p.

Goldsmith Y., 2011, Characterizing rock varnish developed on earliest Holocene Negev flint artifacts as a potential paleoenvironmental or paleoclimatic indicator: The Hebrew University, Jerusalem, report GSI/33/2011.

Harris, I. P. D. J., Jones, P. D., Osborn, T. J., and Lister, D. H., 2014, Updated high-resolution grids of monthly climatic observations – the CRU TS3. 10 Dataset: Int. J. Climatol., v. 34, p. 623–642.

Hennon, P. E., D'Amore, D. V., Schaberg, P. G., Wittwer, D. T., & Shanley, C. S., 2012, Shifting climate, altered niche, and a dynamic conservation strategy for yellow-cedar in the North Pacific coastal rainforest: BioScience, v. 62, p. 147–158.

Hennon, P. E., McKenzie, C. M., D'Amore, D., Wittwer, D. T., Mulvey, R. L., Lamb, M. S., Cronn, R. C., 2016, A climate adaptation strategy for conservation and management of yellow-cedar in Alaska: PNW-GTR-917. Portland, Oregon, USA: US Department of Agriculture, Forest Service, Pacific Northwest Research Station.

Hoover, J.D., 1974, Periodic Quaternary volcanism in the Black Rock Desert, Utah: Brigham Young University, 70 p.

Lifton, N., Caffee, M., Finkel, R., Marrero, Shasta., Nishiizumi, K., Phillips, F.M.,Goehring, B., Gosse, J., Stone, J., Schaefer, J., Theriault, B., Timothy Jull, A.J., Fifield, K. 2014, In situ cosmogenic nuclide production rate calibration for the CRONUS-Earth project from Lake Bonneville, Utah, -shoreline features: Quaternary Geochronology, 26, 56-69, doi: 10.1016/j.quageo.2014.11.002

Liu, T and Broecker, W.S., 2013, Millennial-scale varnish microlamination dating of late Pleistocene geomorphic features in the drylands of western USA: Geomorphology, 187, 38-60.

Lynch, W.C., and Nash, W.P., 1980, Chemical trends in the Ice Springs Basalt, Black Rock Desert, Utah: U.S. Government Documents (Utah Regional Depository), 86 p.

Marrero, S.M., Phillips, F.M., Borchers B., Lifton N., Aumer R., Blaco G., 2015, Cosmogenic Nuclide Systematics and the CRONUScalc Program: Quaternary Geochronology.

Matesich, C., 2014, Geochemical Analysis of Basalt Flows from Miter Crater in Ice Springs Volcanic Field, Utah: [Undergraduate Thesis] The College of Wooster.

Nelson, S. T., and Tingey, D. G., 1997, Time-transgressive and extension-related basaltic volcanism in southwest Utah and vicinity: Geological Society of America Bulletin, 109(10), 1249-1265.

Németh, K., and Kereszturi, G., 2015, Monogenetic volcanism: personal views and discussion: International Journal of Earth Science, 2131-2146.

Patzkowsky, S., Randall, E., Rosen, M.L., Thompson, A., Moua, P.N., Schantz, K., Pollock, M., Judge, S.A., Williams, M., and Matesich, C., 2017, New cosmogenic and VML dates and revised emplacement history of the Ice Springs Volcanic Field in the Black Rock Desert, Utah: GSA Abstracts with Programs, v. 49(6), doi: 10.1130/abs/2017AM-306786.

Schaberg, P. G., D'Amore, D. V., Hennon, P. E., Halman, J. M., & Hawley, G. J., 2011, Do limited cold tolerance and shallow depth of roots contribute to yellow-cedar decline?: Forest Ecology and Management, v. 262,p. 2142–2150.

Sims, W., 2013, Geochemical and geospatial analysis: Mapping of Miter's lava flows in Ice Springs Volcanic Field, Black Rock Desert, Utah: [Undergraduate Thesis] The College of Wooster.

Thompson, J., 2009, Crustal assimilation mechanisms in continental basalts: the Ice Springs flow, Utah: University of Iowa, 203 p.

Trouet, V., Van Oldenborgh, J., 2013, KNMI Climate Explorer: A Web-Based Research Tool for High-Resolution Paleoclimatology: Tree-Ring Research v. 69, p. 3-13. DOI:10.3959/1536-1098-69.1.3

Valastro, S., Davis, E.M., and Varela, A.G., 1972, University of Texas at Austin radiocarbon dates, IX: Radiocarbon, v. 14, p. 461–485.

Williams, M., 2016, Emplacement processes and monogenetic classification of Ice Springs Volcanic Field, central Utah: [Undergraduate Thesis] The College of Wooster.

Wilson, R., D'Arrigo, R., Andreu-Hayles, L., Oelkers, R., Wiles, G., Anchukaitis, K., and Davi, N., 2017, Experiments based on blue intensity for reconstructing North Pacific temperatures along the Gulf of Alaska: Climate of the Past, v. 13, p. 1007-1022, https://doi.org/10.5194/cp-13-1007-2017.

KECK Geology Consortium
Learning Science Through Research
Published by Keck Geology Consortium

Short Contributions
Keck Geology Consortium
Volume 31
May 2018

HAZARDS IN THE CARIBBEAN: THE HISTORY OF MAGMA CHAMBERS, ERUPTIONS, LANDSLIDES, STREAMS, AND FUMEROLES IN DOMINICA

HOLLI FREY, Union College
AMANDA SCHMIDT, Oberlin College
EROUSCILLA JOSEPH, University of West Indies Seismic Research Center
LAURA WATERS, Sonoma State University

INTRODUCTION

The Caribbean has been the site of significant historic volcanism, from the ongoing eruptions in Monserrat to the devesating eruptions of Mt. Pelee, Martinique and Soufriere, St. Vincent in 1902, in which ~32,000 people perished. However, the island with the most volcanic hazard risk is Dominica, which experienced the largest explosive eruption in the Caribbean in the last 200 kyr (~58 km^3) and features nine potentially active volcanic centers that are Pleistocene or younger in age (Carey and Sigurdsson, 1980; Lindsay et al., 2005), and had phreatic eruptions in the Valley of Desolation in 1880 and 1997. The landscape of Dominica has been shaped by its volcanic history and tropical climate, as evidenced by its heavily weathered terrains and preponderance of landslides. It is characterized by lava domes and extensive block and ash flows and explosive deposits, as well as numerous geothermal areas with fumeroles and steam vents. Multiple shallow seismic swarms since the late 1990s (Lindsay et al., 2003, Smith et al., 2013) suggest the region may be undergoing a periodic of volcanic unrest.

Today, Dominica is known as the Nature Island of the Caribbean and significant efforts have been made to increase tourism. There are numerous eco-tourism sites and the Waitukubuli National Trail, an island-wide 185 km hiking trail, was recently completed. The tourism sites feature active geothermal areas, with fumeroles and steam vents, as well as older lava flows and explosive deposits of pumice and ash. Dominica's volcanic unrest has also drawn the attention of the scientific community. Increased levels of volcano-seismic activity in the northern and southern portions of the island since the late 1990s prompted a reassement of the geologic hazards of Dominica (Lindsay et al., 2003) and targeted GPS monitoring campaigns. One volcano in northern Dominca, Morne aux Diables (MAD) was recently studied by VUELCO (Volcanic unrest in Europe and Latin America: Phenomenology, eruption precursors, hazard forecast, and risk mitigation), a consortium of scientists seeking an understanding of the processes behind volcanic unrest and the ability to forecast its outcome. In Dominica, VUELCO aimed to use existing seismic, GPS, and geochemical data from geothermal areas around MAD to better model and understand geothermal systems as a potential precursor to eruptive activity. A VUELCO workshop was held in Dominica in May 2015 (attended by Frey and Joseph), in which researchers presented their preliminary findings and participated in an eruption crisis simulation exercise with local government officials and disaster management organizations. The consensus was that more primary research and baseline monitoring would be valuable and help with future risk assessments.

GEOLOGIC SETTING

The Lesser Antilles arc in the eastern Caribbean is approximately 850 km in length and extends from St. Kitts in the north to Grenada in the south with a total of 11 volcanic islands (Fig. 1). The volcanism is caused by the westward subduction of the 90 Ma

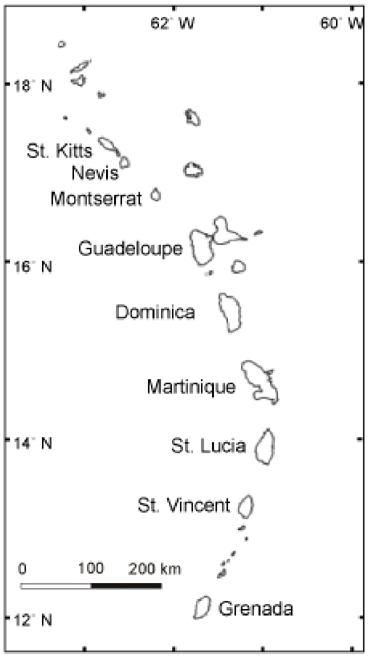

Figure 1. Geographic map of the Lesser Antilles volcanic arc.

North American Plate under the Caribbean Plate. The Lesser Antilles island arc is segmented, with the north trending at 330° and the south trending at 020° (Arculus and Wills, 1980; Wadge and Shepherd, 1984). The slab dip angle is approximately 50-60° in the north and 60-90° in the south. The northern volcanic islands (north of Martinique) have high levels of seismicity and a subduction rate of 2.0 cm/yr (DeMets et al., 2000) whereas the southern volcanic islands do not have a history of large earthquakes and the rate of subduction is slower, only 1.8 cm/yr (DeMets et al., 2000). Dominica is located in the central portion of the arc, where these segments converge, with a 45-50° dipping Wadati-Benioff zone approximately 160-180 km beneath the volcanic front (Lindsay et al., 2005b). The physical segmentation and differences in subduction rates may drive the voluminous volcanism observed on Dominica. Dominica is considered to be the most volcanically productive and hazardous island in the arc, with nine potentially active volcanic centers, the majority of which are located within 10 km of the capital of Roseau, located in the southern portion of the island (Lindsay et al., 2005b).

Dominica is a 750 km^2 island (Fig. 2) of rugged topography and pristine rainforest which features nine volcanic centers that are <2.6 Ma in age (Lindsay et al., 2005a). Dominica's coastlines and interior valleys abound with thick (>20 m) ignimbrite deposits, composed of pumice clasts, rock fragments, and ash from solidified pyroclastic flows. Some ignimbrites are welded and up to 200 m thick in valleys in central Dominica, with thickness generally decreasing towards the coast. Ash from these eruptions has blanketed nearby Caribbean islands and the eastern Caribbean Sea. Although only ~3 km^3 of debris from the explosive eruptions remains in the central valleys of Dominica today, the distribution and thickness of ash found in the drill cores of oceanic material in the Caribbean Sea allowed for an estimation of the material that erupted in the past. More than 58 km^3 of material was erupted from Dominica, making it the largest explosive eruption in the Caribbean in the last 200 kyr (Sigurdsson, 1972; Carey and Sigurdsson, 1980).

There have been no documented explosive eruptions of large magnitude in Dominica in the last 20 kyr. The most recent activity involving magma was a lava

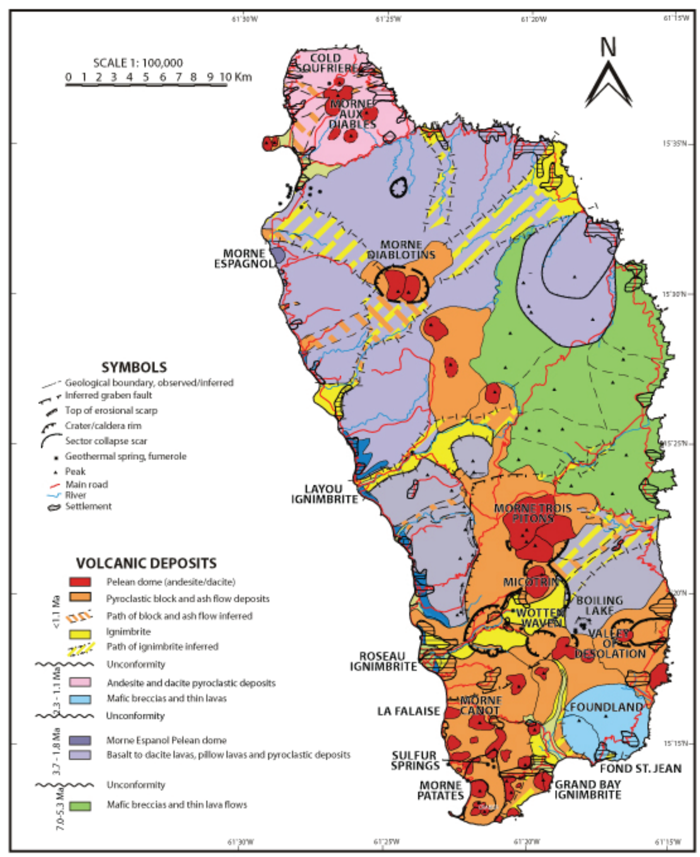

Figure 2. Geologic map of Dominica adapted from Smith et al. (2013).

dome collapse. Lava domes form when degassed and now very viscous magma reaches the surface. They often post-date explosive eruptions, in which most of the volatiles (H_2O, CO_2, H_2S) are released. Lava dome growth can occur over decades with the slow extrusion of magma building a steep-sided dome. Periodically, these domes become over-steepened and collapse, jettisoning large angular blocks of lava downslope to form block and ash deposits. There are numerous block and ash deposits found throughout the island. The youngest block and ash deposit is thought to be in southern Dominica, which has an abundance of lava domes. Arcaheological investigations in the late 1970s unearthed clay pots beneath an ash horizon near the village of Soufrierre. Charcoal within the ash was dated at 450 ± 90 years B.P. (Roobol et al., 1983).

Dominica's most recent volcanic activity was several explosions of steam and ash violently ejected from hydrothermal vents. Phreatic eruptions ocurred in the Valley of Desolation in 1880 and 1997, covering an area <1 km^2 with a thin (~2 cm) layer of ash (Lindsay et al., 2005b). The Valley of Desolation is an active hydrothermal area and popular hiking destination of tourists. The name is likely derived from the stark landscape, devoid of vegetation from past steam explosions. The smell of rotten eggs from the release of sulphur dioxide permeates the valley and sulphur crystals ring many of the fumeroles or steam vents that hiss as they release gas. Hot, acidic mudpots up to 2 m in diameter bubble, gurgle and pop, releasing carbon dioxide. At the far end of the valley lies Boiling Lake, a 75 m volcanic lake that is is typically very hot (80-90 ˚C) and acidic (pH of 3-5). The Valley of Desolation and Boiling Lake exist bcause magma is present beneath the surface, heating the groundwater and releasing volcanic gasses like CO_2 and SO_2.

In addition to the older volcanic deposits and active hydrothermal areas, Dominica's volcanic present is recorded by earthquake swarms. The earthquakes are typically shallow (<5 km) and of fairly low magnitude (<4.0), often ocurring in rapid succession or swarms. Often an increase in the frequency of seismicity or the magnitude of earthquakes is one of the first indicators that a volcano may become active again. Since monitoring in Dominica began in 1952 by the University of the West Indies Seismic Research Center (UWI-SRC), there have been several periods of more intense seismicity, particularly in the last two decades in northern and southern Dominica. In 2003, >1000 earthquakes were recorded in northern Dominica, all of which were under magnitude 3.5. The same region experienced another period of increased seismicity from 2009-2012. On October 21, 2009, twenty-one earthquakes were reported overnight, and two were felt in the town Portsmouth, damaging local buildings. The earthquake swarms in southern Dominica occurred in the mid-late 1990s. None of these periods of heightened seismicity were a precursor to a volcanic eruption and the earthquake tremors returned to background levels. In the last few years, there have been two clusters of low magnitude shallow earthquakes, one in Sulphur Springs, an active geothermal region, and one in Salisbury, a coastal village built on ~80 ka ignimbrite deposits.

STUDENT PROJECTS

The Dominica Keck project is the inaugural Frontier project of the Keck Consortium. The goal of a Frontier project is to bring together a larger group of students and faculty to approach a problem or geologic setting from a multi-disciplinary perspective. The rugged volcanic landscape of Dominica afforded us the opportunity to investigate a relatively active volcanic system that has not been well studied. A better characterization of the geologic history and current conditions on Dominica will add critical knowledge that may help us better understand volcanic unrest and the threat of eruptions and other natural disasters, such as landslides induced by hurricanes. The work presented herein pre-dates by two months the devastating Cat. V Hurricane Maria, which destroyed much of the island in September, 2017. However, Schmidt returned to Dominica in January, 2018 to collect post-Maria sediment from the rivers.

Through our two-week field season in Dominica and subsequent analytical work in various labs, we explore various petrologic and volcanic questions, the interaction of hydrothermal gasses with fluids, and how a volcanic landscape erodes in a tropical climate. The project builds on previous work by Frey and students, funded by National Geographic, and by Joseph and the on-going monitoring efforts of the UWI-SRC. This previous work has been presented at

AGU, GSA, NE GSA, and IAVCEI and the focus of more than a dozen senior theses. Schmidt received a RAPID NSF grant following Hurricane Maria to study the effects of the storms on the landscape, so she will be continuing work initiated on this project. Fifteen students from fourteen institutions completed projects and initial results were presented at AGU in December, 2017. Summaries of their findings are presented below.

Petrology (Frey and Waters)

Despite its hazard potential and number of volcanoes, Dominica's volcanic history and geology have been somewhat poorly studied, likely owing to the country's rugged terrain, humid climate, and lack of easily accessible outcrop. Detailed petrologic studies of the lava domes have been restricted to the southern Plat Pays volcanic complex (Wills, 1974; Roobol et al., 1983; Lindsay et al., 2003; Lindsay et al., 2005; Gurenko et al., 2005; Halama et al., 2006). Smith et al. (2013) presented an island-wide reconnaissance of the bulk and mineral chemistry of many lava domes and flows, as well as the explosive deposits found throughout the island. More detailed characterizations have been published for the Grand Savanne ignimbrite (>22 ka; Sparks et al., 1980), Roseau ignimbrite (~28-46 ka; Sigurdsson, 1972; Carey and Sigurdsson, 1980; Howe et al., 2014; Boudon et al., 2017) and Grand Bay ignimbrite (~39 ka; Lindsay et al., 2005).

The petrology student projects span an array of topics, but all took advantage of scanning electron microscopy to image minerals and textures, as well as to do quantitative analysis, which allowed for the quantification of intensive variables like temperature (Ghiorso and Evans, 2008) and water content (Waters and Lange, 2015).

Jessie Bersson (Whitman College) evaluated whether changing intensive variables (e.g., pressure, temperature) and/or compositional variables (e.g., water contents) were responsible for the oscillation between explosive and effusive volcanism at Wotten Waven caldera by conducting a detailed petrologic study on the ignimbrites and lava domes. Plagioclase, ilmenite and magnetite were analyzed in several pumice clasts from the Roseau Ignimbrite and samples of lava from a fresh rock fall from the Micotrin lava dome using electron dispersion spectroscopy (Union College) and the electron microprobe (University of California, Davis). Compositions of mineral phases are incorporated into a geo-thermometer and hygrometer to determine the temperatures and water contents in equilibrium with the melts at the time of crystallization. The results reveal that the Roseau ignimbrite had pre-eruptive conditions that were colder and more hydrous than the Micotrin lava dome. These results broadly inform how the caldera cycle of volcanism proceeds in Dominica; the first phase is defined by a colder, hydrous explosive eruption, which is followed by a second, hotter, extrusive phase that results in a lava dome.

Justin Casaus (Sonoma State University) compared the pre-eruptive intensive variables and plagioclase compositions between the Layou ignimbrite and the Morne Trois Piton lava dome forming eruption to understand what caused a changing in eruptive style. Fe-Ti oxides and plagioclase compositions were measured using the electron dispersion spectroscopy (Union College) and the electron microprobe (University of California, Davis). Fe-Ti oxide compositions were incorporated into a model thermometer to determine pre-eruptive temperatures. These temperatures and plagioclase compositions were incorporated into a model hygrometer to determine pre-eruptive water contents. Hygrometry results reveal that plagioclase crystals in both the ignimbrite and the lava dome record a continuous range of water contents, and that crystallization in the ignimbrite began at higher water contents (i.e., pressures) than the dome. If the dome is derived from the same magmatic source as the ignimbrite, then some mechanism to induce heating is required. The dome lavas notably contain mafic enclaves, and comparison with other studies in the literature suggests these enclaves were the source of additional heat, which could have caused the extrusion of the lava dome.

Nolan Ebner (Macalaster College) mapped a 15 m-thick ignimbrite sequence near Fond St. Jean in southern Dominica and compared the stratigraphy, geochemistry, mineralogy, and intensive variables to the nearby Grand Bay Ignimbrite, a hypothesized more proximal unit in an ignimbrite sequence (Lindsay et al., 2005). Unlike the unconsolidated ignimbrite units of Grand Bay, Fond St. Jean exhibited several sub-meter to meter scale graded layers with varying proportions and sizes of pumice and lithic clasts, as well as abundance of ash. The bulk chemistry of the units was distinctive, with pumice clasts from Grand Bay typically exhibiting a homogeneous chemistry, whereas pumice clasts from Fond St. Jean displayed significant variability, and lacked linear trends which would reflect a genetic relationship due to fractional crystallization. REE trends between the units are not parallel, also suggesting different sources. The mineral assemblages of the units are comparable, but Fond St. Jean is less crystal-rich and contains ~4% amphibole, which is absent in Grand Bay. Mineral compositions and zoning of plagioclase, pyroxenes, and oxides, were comparable, leading to broadly similar calculated intensive variables. However, the stratigraphy and bulk chemistry clearly demonstrate the lack of a genetic relationship between the deposits, so the Fond St. Jean Ignimbrite must now be considered a distinct unit.

Sarah Hickernall (Union College) investigated enclaves in the andesitic Morne Micotrin lava dome, which post-dates the explosive Roseau Ignimbrite. Enclaves were basaltic andesite and classified as coarse- or fine-grained. Bulk rock geochemistry showed linear trends for some elements and chondrite-normalized patterns were parallel for the host and coarse-grained enclaves. However, several elements did not show linear trends and REE in the fine-grained enclaves were depleted, suggesting fractional crystallization cannot explain the variation. Open system behavior is further supported by variable abundances and compositional analyses of mineral phases (plag + cpx + opx + qtz + ox). Plagioclase ranged in composition from $An_{45\text{-}94}$, with normal and reverse zoning. Plagioclase rims within the enclaves contained significant potassium, suggesting a unique crystallization history. Pyroxene in the enclaves typically displayed reverse zoning and cpx was found primarily only as rims on opx in the coarse-grained enclaves. Oxides within the enclaves exhibited significant exsolution and two-oxide thermometry yielded two sets of temperatures, ~50˚C hotter and cooler than the host andesite. The enclaves confirm open system behavior and suggest that mafic recharge may trigger eruptions on Dominica, similar to nearby Montserrat.

Taryn Isenburg (Mt. Holyoke College) mapped a 35 m sequence of massive basaltic flows, scoria, lapilli, and ash lenses, associated with a previously undescribed cinder cone within the Foundland Center in southern Dominica near Fond St. Jean. All units contain plagioclase + olivine + clinopyroxene + orthopyroxene + titanomagnetite + spinel and have similar mineral compositions. Plagioclase are typically normally zoned with An-rich cores and more sodic rims. Olivine in most units ranges in composition from Fo55-70. With respect to whole-rock chemistry, the Fond St. Jean basalts are the most primitive on the island (48-52 wt% SiO_2), with relatively high Al_2O_3 (20-23 wt%) and low MgO (4-5 wt%). Within the section, there is no systematic compositional variation. Trace and REE abundances are typical of oceanic island arcs, with a slight affinity for MORBs. However, some trace element ratios such as Th/La indicate the Fond St. Jean basalts were contaminated by sediments and are not derived directly from uncontaminated mantle. Therefore, it is difficult to model these basalts as a parental magma that underwent crystal fractionation to produce the voluminous intermediate material on Dominica.

Abadie Ludlam (Union College) studied the breakdown of amphibole in four andesitic-dacitic lava domes from across the island. Due to its limited stability, amphibole undergoes reactions, attributed to a decrease in pressure and/or an increase in temperature (>950 ˚C). Thickness of reaction rims of amphiboles has been used a proxy for ascent rate in some volcanic systems like Mount St. Helens. In Dominica, two lava domes (La Falaise and Canot) had amphibole phenocrysts that were complete replaced by a mixture of plagioclase, orthopyroxene, clinopyroxene, and Fe-Ti oxides. Four different textures were identified in these samples, with variable crystal sizes, zoning, and degree of disaggregation. Amphibole in Morne Patates had thin (10-50 μm) reaction rims, composed of similar mineralogy, but devoid of clinopyroxene. Amphibole in Morne Espagnole featured amphibole with slightly thicker reaction rims, with inner portions containing clinopyroxene, but lacking in the outermost rim. There were no compositional, chronological, or geographical constraints on the observed textures. The different textures were attributed to decompression (completely reacted crystals) and heating (thin, cpx-absent rims), based on comparison of textures with the literature and temperatures obtained by two-oxide thermometry.

Clarissa Itzel Villegas Smith (Carleton College) analyzed the hydrothermal alteration of andesitic clasts from three different geothermal areas on the island: Cold Soufriere, Valley of Desolation, and Sulfur Springs. The hydrothermal waters of Dominica are acid-sulphate in composition and the degree of hydrothermal alteration appears to be a function of the temperature and amount of surface water of the particular geothermal area. XRD analysis of clast rinds and Rietveld analysis of the XRD spectra identified fifteen different minerals, including silica polymorphs, hematite, alunite minerals, sulfates, sulfides, and feldspars. Silica polymorphs are dominant with about 70% of the samples containing cristobalite, likely replacing plagioclase, as observed in elemental maps of the clast-rind boundary. The minerals present are typical of rock alteration by low temperature (<300 ˚C) acid-sulfate fluids, suggesting that the alteration is a result of mixing of shallow sulfate water and gasses. One sample from the Cold Soufriere included a fine-grained mix of iron, sulfur, and titanium, which is a rare combination of elements, previously described in Martian soils.

Katie Von Sydow (Cal State San Bernadino) conducted a geochemical and petrographic study on mafic lavas from Foundland in southern Dominica. The most voluminous eruptions on Dominica are the intermediate (~60 wt% SiO_2) lava domes and ignimbrites, and eruptions of basalt occur in relatively low frequency in most locations across the island. Foundland, a relatively remote region in southeastern Dominica, and proto-Morne aux Diables (northern Dominica), however, feature basaltic volcanism in relatively great abundance. This study aims to compare new samples from Foundland to those from proto-Morne aux Diables (Smith et al., 2013) on the basis of whole rock geochemistry, modal abundances, and compositions of phenocrysts to determine if the mafic lavas are likely from the same source. Major element concentrations were determined using XRF analyses at Pomona College and reveal that the mafic lavas in Foundland span a range in composition from low magnesium, high aluminum basalts to andesite. All lavas contained a similar phenocryst assemblage consisting of plagioclase + olivine + clinopyroxene + orthopyroxene + Fe-Ti oxides (mostly magnetite). In a single sample, hornblende was observed. Foundland lavas have many commonalities with the proto-Morne aux Diables basalts, suggesting that they could be derived from a similar source; however, the phase assemblage in the Foundland lavas requires them to evolve to colder, more hydrous, and more crystalline conditions.

Fluids and Gasses (Joseph)

Volcanic gases and hydrothermal waters were sampled from five (5) hydrothermal areas across the island (Valley of Desolation, Sulphur Spring, Watten Waven, Galion and Penville Cold Soufriere; Fig. 2) to determine temporal and spatial deviations from baseline geochemical conditions. This information would contribute to the volcanic monitoring efforts, of the UWI Seismic Research Center, on Dominica of a potential monitor for volcanic unrest. Additionally, water samples were also collected from meteoric streams to continue a three-year long monitoring project determining what controls chemical/isotopic variation, and analyzing the potential lasting effects of severe tropical storms (i.e. Tropical Storm Erika, August 2015), which frequently trigger mass wasting events. With updated gas and water chemistry and isotopic data for the period 2014 to 2017, it was possible to re-evaluate the characteristics of these systems, which were last reported in 2011.

Jackie Buskop (Wesleyan University) studied volcanic gasses from multiple geothermal areas. Baseline monitoring of hydrothermal gases of Dominica for the period 2000 – 2006 show compositions typical of those found in arc-type settings, with N_2 excess and low amounts of He and Ar (Joseph et al., 2011). The 2017 study presents new data on sulphur and nitrogen isotopes to evaluate contributions from various source components. Fumaroles appear to reflect a deeper source contribution as compared to thermal waters with differences in acidity, temperature, TDS, $\delta^{18}O$, and δD observed. Preliminary results show high CH_4/CO_2 ratios for gases from Dominica, which are indicative of a significant hydrothermal contribution to these fluids. However, high helium isotope compositions of 6.6 – 8.3 R/Ra indicate a clear magmatic origin. This is consistent with the previously established baseline gas chemistry of the hydrothermal systems on Dominica. Notably $\delta^{34}S$ values of Dominica fits well with other arc volcanic gases, which are heavier than MORB or plume volcanic gases. This is consistent with the subduction of $\delta^{34}S$-enriched seawater sulphate and recycling of sulphur through arc volcanoes. The $\delta^{15}N$ values for the hydrothermal gases indicate a lack of N_2 contributed from the organic sediment component of the subduction plate. This may be explained by its diversion to the overriding crust rather than subduction into the mantle (Elkins et al., 2006; Fischer et al., 2002; Zimmer et al., 2004).

Dexter Kopas (Beloit College) studied water samples collected from meteoric streams to continue a three-year long monitoring project determining what controls chemical/isotopic variation, and analyzing the potential lasting effects of severe tropical storms (i.e. Tropical Storm Erika, August 2015), which frequently trigger mass wasting events. Over four years from 2014-2017, water chemistry was tested from 56 Dominican streams. This presented an opportunity to obtain a general overview of the major stream geochemistry and stable isotope composition on the island. It also facilitated the investigation of the major environmental controls on stream geochemistry in the tropics, considering multiple and potentially complex interactions among these factors. Major stream geochemistry show that waters sourced by hydrothermal springs are geochemically similar to their hydrothermal source, and generally contain more SO_4 and Cl. Isotopically, purely meteoric streams and meteoric streams with a known hydrothermal influence differ significantly (α=0.05). The mean differences are 0.19‰ for $\delta^{18}O$, and 0.46‰ for δD. Dominica's west coast is slightly more enriched in $\delta^{18}O$ compared to the east coast, by ~0.15‰ (α=0.05). However, there is no significant difference in δD. The results obtained suggest that there is no single dominant environmental influence on Dominican rivers and that environmental influences are multiple and complex. The lack of correlations suggest that neither dominant wind direction nor precipitation amount influence east-west differences in $\delta^{18}O$. Hydrothermal sites are a significant influence on stream ion chemistry, which may be dependent on the relative amounts and type of discharge compared to that of the stream water.

Mazi Mathias-Onyeali (University of Colorado) analyzed the waters from geothermal areas, comparing data from published work (Joseph et al., 2011) and ongoing studies since 2014 (Metzger et al., 2015; Metzger et al., 2016; DeFranco et al., 2016). Recent changes in chemistry of the waters have indicated that while the origin of the hydrothermal systems are still dominantly meteoric ($\delta^{18}O$ = -3 to 8‰ and δD = -5 to 18‰), surface evaporation effects and variable amounts of mixing with shallow ground waters play an important role. The general composition of the waters for most of the hydrothermal systems studied indicate no significant changes, with the exception of the Boiling Lake, which experienced a draining event in November 2016 which lasted for 6 weeks. Decreases in temperature, pH, Na, K, and Cl were seen post draining, while SO_4 remained relatively low (66 ppm), but showed a small increase. The chemistry of the Boiling Lake appears to show significant changes in response to changes in the groundwater system.

Geomorphology (Schmidt)

Stochastic processes, such as landslides and large tropical storms, are known to be a major driving factor in setting erosion rates over geologic timescales (Kirchner et al., 2001). However, the effects of individual events are difficult to quantify, in part because there are rarely data available from before the event. In addition, tropical environments are typically underrepresented in geomorphic studies compared to temperate and polar locations (Portenga and Bierman, 2011). The geomorphology part of this Frontier project is focused on documenting geomorphic effects of landslides and generally quantifying controls on erosion for Dominica, thus expanding studies of Caribbean erosion from one watershed in Puerto Rico (Brown et al., 1995; Riebe et al., 2003) to also include 20 watersheds on Dominica. Prior work on geomorphology in Dominica has been limited to studies of landslides and debris flows (Degraff et al., 2010; Rouse, 1990), soils (Reading, 1991; Rouse et al., 1986), and chemical weathering (Goldsmith et al., 2010; Rad et al., 2013), but we are unaware of any prior work using detrital sediments to characterize basin-average erosional processes.

Measuring sediment movement across the landscape – where it comes from, where it is stored, and where it ends up – is fundamental to the study of Earth surface processes. However, until recently, quantifying rates of sediment production, storage, and delivery to channels from hillslopes were difficult, if not impossible, tasks. Doing so required unique situations where one could assume that single measurements of sediment movement were representative of longer time frames. What was needed was a system to trace sediment movement over longer periods of time.

Over the past 20 years, isotopic analysis has opened new ways of quantifying the amount and source of sediment moving over the landscape and through river systems over time scales ranging from tens to millions of years (Stokes and Walling, 2003). In this project we are analyzing four fallout radionuclides: ^{137}Cs, ^{210}Pb, ^{7}Be, and ^{10}Be in detrital sediments (Figure 2). We are also using x-ray fluorescence, x-ray diffraction, and concentration of acid-extractable grain coatings as additional proxies of erosional depth and degree of sediment weathering. Students used these chemical measurements of sediment in conjunction with basin analyses in GIS (including slope, rainfall, number and size of landslides, and land use) to characterize spatial patterns of erosion on Dominica over short and long timescales. The four geomorphology student projects each focus on a different piece of the puzzle of understanding erosion on Dominica (Fig. 3).

Marcus Hill (Oberlin College) studied the effects of large storms on landslides and channel geomorphology. He (and other Keck students) mapped landslides on Dominica before and after Tropical Storm Erika and Hurricane Maria. He also used photos he took in the field and those previously taken by PI Frey and her students to complete a repeat photography project. These photos include photos taken before and after both Tropical Storm Erika and Hurricane Maria. Changes observed due to Hurricane Maria included widening and narrowing channels, aggradation and incision, and both deposition and erosion of sediment. Some channels had no noticeable differences in photos whereas others were unrecognizable in the field even when we knew for certain that we were at the exact same spot we sampled just a few months before. In short, there were no systematic changes he detected across the island. However, he found that changes were typically greater on the west side of the island than the east side. In addition, he observed significant transport of very large boulders into and out of sampling sites, suggesting that the debris flows triggered by Hurricane Maria had extremely high power to move sediment.

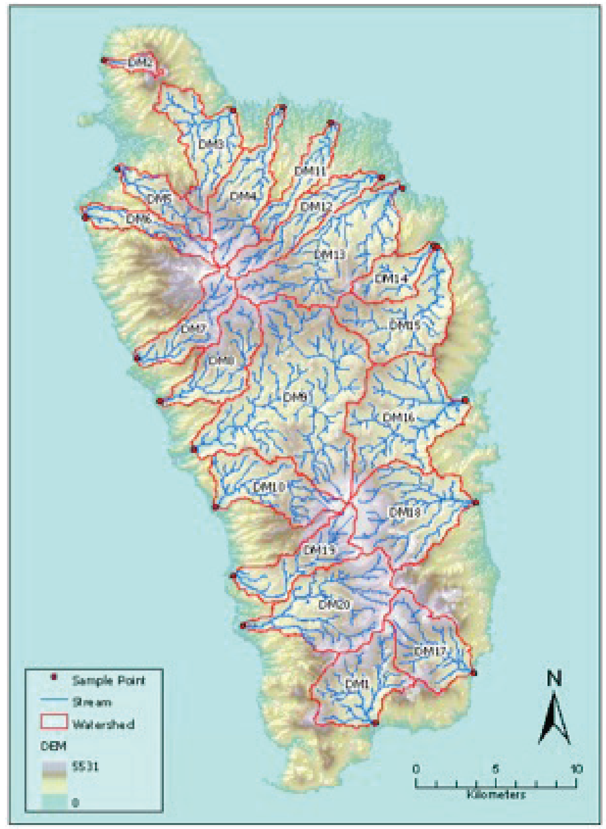

Figure 3. DEM created in GIS depicting the watersheds and major river systems in Dominica.

Cole Jimerson (College of Wooster) used previously reported ignimbrite ages (Frey et al., 2015) to calculate incision rates by rivers into the ignimbrite deposits and combined this with an analysis of basin-average parameters such as slope, rainfall, and landslide frequency to understand what best controls fluvial incision into ignimbrites. Cole found that incision rates are highest for younger ignimbrites (up to ~6 mm/yr for ignimbrites <25 ka) and that rates sharply drop to <1 mm/yr for ignimbrites more than 80 ka. Rivers incising into younger ignimbrites also tended to have steeper channels (especially through the ignimbrites) and multiple knickpoints along the longitudinal profile. Channels incised into older ignimbrites are inferred to have incised completely through the ignimbrite and to be eroding into lava or block and ash flows. These channels have less steep channels without knickpoints. Incision rates correlate best with normalized channel steepness, a measure of channel steepness that is scaled for upstream area. Combined with millennial timescale erosion rates (which are in process but not completed in time for this volume), this could provide a unique comparison of incision to basin-average erosion rates.

Haley Talbot-Wendlandt (Ohio Wesleyan University) analyzed the composition of detrital sediments (measured with XRF and XRD), the concentration of ^{7}Be in the sediment, and the activity of ^{137}Cs and ^{210}Pb in the sediment. Haley found that the XRD spectra of sediment is similar for all sites sampled, suggesting that all rivers are sourcing similarly weathered sediments. The XRF data vary more across the island and suggest that the composition of fine-grained sediments (<63 µm) has more information about the source of sediments than the composition of coarse grained sediments (250-850 µm). Haley also analyzed the location of landslides on the island due to Tropical Storm Erika and Hurricane Maria in relation to landslide hazard maps for the island. She found that the landslide hazard maps were largely accurate with most landslides happening in high hazard locations.

Kira Tomenchok (Washington & Lee University) measured the concentration of acid-extractable grain coatings using an ICP-OES and is comparing the concentration of grain coatings to the concentration of fallout ^{10}Be in detrital samples. Her analysis of the concentration of grain coatings and ^{10}Be in detrital sediments indicate the depth at which material was sourced from in the upstream watershed over long timescales (Greene, 2016) and may correlate with landslide frequency in the upstream watershed.

ACKNOWLEDGEMENTS

This material is based upon work supported by the Keck Geology Consortium and the National Science Foundation Grant No. 1659322 and permitted by the Dominican Ministry of Forestry. Special thanks to Matthew Manon (Union College) for guiding the SEM, ICP-MS, IC, XRD, and p-XRF analyses at Union College. We also owe a huge debt to Bill Neubeck (Union College), who tuned around ~50 thin-sections and ~20 grain mounts in less than a week, and Deb Klein (Union College) who assisted with logistics on campus. We are grateful to Nancy Osler and the staff at the Arcbold Tropical Research Center at the Springfield Estate in Dominica who provided us with great food and a place to stay in the field. We'd also like to acknowledge the analytical facilities and personnel at Union College (IRMS lab), UC Davis (electron microprobe facility), UVM (^{10}Be extraction), LLNL (^{10}Be analyses), and INGV (gas analyses). Thank you to Karl Wirth (Macalaster) who spent some time with us in the field and Cam Davidson (Carleton) who supported us at AGU. Also a special thanks to all of the home advisors who helped guide the project during the academic year: Sue Swanson (Beloit), Kristen Nicolaysen (Whitman), Steve Dunn (Mt. Holyoke), Cam Davidson (Carleton), Karl Wirth (Macalster), Joan Fryxell (Cal State San Bernadino), Joop Varekamp and Tim Ku (Wesleyan), Ron Abbot (U of Colorado), Dave Harbor (Washington & Lee), Meagan Pollack (College of Wooster), and Bart Martin (Ohio Wesleyan). We would also like to acknowledge the hospitality and strength of the people of Dominica; their tropical paradise was devastated by Hurricane Maria two months after our project. In the face of such adversity, the Dominicans will be resilient and adapt to their ever-changing landscape.

REFERENCES

Annen, C., Blundy, J.D. and Sparks, R.S.J. (2006) The genesis of intermediate and silicic magmas in deep crustal hot zones. Journal of Petrology 47: 505-539.

Arculus, R.J., Wills, K.J.A. (1980) The petrology of plutonic blocks and inclusions from the Lesser Antilles Arc. Journal of Petrology 21: 743-799.

Bellon H (1989) Reconnaissance chronologique des deux premieres phases d'activite volcanique en Dominique (Petites Antilles). CR Acad Sci Paris 306:1487-1492.

Belousova, E.A., Griffin, W.L., O'Reilly, S.Y., Fisher, N.I. (2002) Apatite as an indicator mineral for mineral exploration: trace element compositions and their relationship to host Rock. Journal of Geochemical Exploration 76:45-69.

Brown, E.T., Stallard, R.F., Larsen, M.C., Raisbeck, G.M. and Yiou, F. (1995) Denudation rates determined from the accumulation of *in-situ* produced ^{10}Be in the Luquillo Experimental Forest, Puerto Rico. Earth and Planetary Science Letters 129, 193-202.

Carey, S.N., Sigurdsson, H. (1980) The Roseau ash: deep-sea tephra deposits from a major eruption on Dominica, Lesser Antilles arc. Journal of Volcanology and Geothermal Research 7: 67-86.

DeFranco, K.*, Frey, H.M. and Manon, M.R.F. (2016) Establishing island-wide water characterization in a volcano-hydrothermal system in Dominica, Lesser Antilles. Northeastern section Geological Society of America Abstracts with Programs. Vol. 48, No. 2.

Degraff, J.V., James, A. and Breheny, P. (2010) The formation and persistence of the Matthieu landslide-dam lake, Dominica, WI. Environmental & Engineering Geoscience 16, 73-89.

Demange J, Leborne H, Traineau H, Westercamp D (1985) Histoire volcano-structurale de la Region sud de la Dominique. Bureau de Recherches Geologiques et Minieres, Institut Mixte de Recherches Geothermiques, Rapport 85 SGN 068 IRG-GTH: 1-114.

DeMets, C., Jansma, P.E., Mattioli, G.S., Dixon, T.H., Farina, F., Bilham, R., Calais, E., Mann, P. (2000) GPS geodetic constraints on Caribbean-North American plate motion. Geophysical Research Letters 27: 437-440.

Elkins, L. J., T. P. Fischer, D. R. Hilton, Z. D. Sharp, S. McKnight, and J. Walker (2006) Tracing nitrogen in volcanic and geothermal volatiles from the Nicaraguan volcanic front. Geochimica et Cosmochimica Acta 70: 5215-5235.

Fischer, T.P., Hildon, D.R., Zimmer, M.M., Shaw, A.M., Sharp, Z.D., Walker, J.A. (2002) Subduction and recycling of nitrogen along the Central American Margin. Science 297: 1154-1157.

Frey, H., Manon, M. and Brehm, S. (2015) Fingerprinting young ignimbrites in Dominica (Lesser Antilles): Constraints from bulk REEs, apatite chemistry, and U-Th zircon chronology, AGU Fall Meeting Abstracts.

Frey, H.M. and Lange, R.A. (2011) Petrologic complexity in andesites and dacites from the Tequila volcanic field, Mexico: Resolving the effects of degassing vs. magma mixing: Contributions to Mineralogy and Petrology 162: 415-445.

Ghiorso, M.S., and Evans, B.W. (2008). Thermodynamics of rhombahedral oxide solid solutions and a revision of the Fe-Ti two-oxide geothermometer and oxygen-barometer. American Journal of Science, 308: 957-1039.

Goldsmith, S.T., Carey, A.E., Johnson, B.M., Welch, S.E., Lyons, W.B., McDowell, W.H. and Pigott, J.S. (2010) Stream Geochemistry, Chemical Weathering and CO_2 Consumption Potential of Andesitic Terrains, Dominica, Lesser Antilles. Geochimica Et Cosmochimica Acta 74.1: 85-103.

Greene, E.S. (2016) Comparing meteoric ^{10}Be, *in situ* ^{10}Be, and native ^{9}Be across a diverse set of watersheds, Geology. University of Vermont, Burlington, VT, p. 118.

Gurenko, A.A., Trumbull, R.B., Thomas, R., Lindsay, J.M. (2005) A melt inclusion record of volatiles, trace elements and Li-B isotope variations in a single magma system from the Plat Pays volcanic complex, Dominica, Lesser Antilles. Journal of Petrology 46: 2495-2526.

Halama, R., Boudin, G., Villemant, B., Joron, J.L., Le Fraint, A., Komorowski, J.C. (2006) Pre-eruptive crystallization conditions of mafic and silicic magmas at the Plat Pays volcanic complex, Dominica (Lesser Antilles). Journal of Volcanology and Geothermal Research 153: 200-220.

Howe, T.M., Lindsay, J.M., and Shane, P. (2105a) Eruption of young andesitic-dacitic magmatic systems beneath Dominica, Lesser Antilles: Journal of Volcanology and Geothermal Research 297:9-88.

Howe, T.M., Schmitt, A.K., Lindsay, J.M., Shane, P., and Stockli, D.F (2015b) Time scales of intra-oceanic arc magmatism from combined U-Th and (U-Th)/He zircon geochronology of Dominica, Lesser Antilles: Geochemistry, Geophysics, Geosystems 16:347-365.

Howe, T.M., Lindsay, J.M., Shane, P., Schmitt, A.K., and Stockli, D.F. (2014) Re-evaluation of the Roseau Tuff eruptive sequence and other Ignimbrites in Dominica, Lesser Antilles. Journal of Quaternary Science 29(6): 531-546.

Joseph, E.P., Fournier, N., Lindsay, J.M., Fischer, T.B. (2011) Gas and water geochemistry of geothermal systems in Dominica, Lesser Antilles island Arc, Journal of Volcanology and Geothermal Research. 206:1-14.

Joseph, E.P., Fournier, N., Lindsay, J.M., Robertson, R., and Beckles, D. (2013) Chemical and isotopic characteristics of geothermal fluids from Sulphur Springs, Saint Lucia. Journal of Volcanology and Geothermal Research 254: 23-36.

Kirchner, J.W., Finkel, R.C., Riebe, C.S., Granger, D.E., Clayton, J.L., King, J.G. and Megahan, W.F. (2001) Mountain erosion over 10 yr, 10 k.y., and 10 m.y. time scales. Geology 29, 591-594.

Lindsay, J.M., Stasiuk, M.V., Shepherd, J.B. (2003) Geological history and potential hazards of the late- Pleistocene to Recent Plat Pays volcanic complex, Dominica, Lesser Antilles, Bulletin of Volcanology 65: 201–220.

Lindsay, J. M., Trumball, R.B., Siebel, W. (2005a) Geochemistry and petrogenesis of Late Pleistocene to recent volcanism in southern Dominica, Lesser Antilles. Journal of Volcanology and Geothermal Research 148: 253-294.

Lindsay, J.M., Smith, A.L., Roobol, M.J., and Stasiuk, M.V. (2005b) Dominica: Volcanic Hazards of the Lesser Antilles. Seismic Research Unit, The University of the West Indies, Trinidad and Tobago.

Metzger, T.*, Frey, H.M., Manon, M.R.F., and DeFranco, K.* (2016) Island-wide isotopic analysis of meteoric and hydrothermal waters in Dominica, Lesser Antilles. Geological Society of America Abstracts with Programs. Vol. 48, No. 7.

Metzger, T.*, Frey, H.M., and Manon, M.R.F. (2015) Water geochemistry analysis of streams and hydrothermal waters in Dominica, Lesser Antilles. Northeastern section Geological Society of America Abstracts with Programs, Vol. 47.

Monjaret, M.C. (1985) Contribution a l'etude de l'arc des Petites Antilles. Le Volcanisme de la Dominique. Donnees chronologiques, mineralogiques et geochimiques. Unpublished Thesis, Universite de Bretagne Occidentale, 1-77.

Portenga, E.W. and Bierman, P. (2011) Understanding Earth's eroding surface with 10Be. GSA Today 21, 4-10.

Rad, S., Rivé, K., Vittecoq, B., Cerdan, O. and Allègre, C.J. (2013) Chemical weathering and erosion rates in the Lesser Antilles: An overview in Guadeloupe, Martinique and Dominica. Journal of South American Earth Sciences 45, 331-344.

Reading, A.J. (1991) Stability of tropical residual soils from Dominica, West Indies. Eng Geol 31, 27-44.

Riebe, C.S., Kirchner, J.W. and Finkel, R.C. (2003) Long-term rates of chemical weathering and physical erosion from cosmogenic nuclides and geochemical mass balance. Geochim Cosmochim Ac 67, 4411-4427.

Rivé, K., Gaillardet, J., Agrinier, P. and Rad, S. (2013) Carbon Isotopes in the Rivers from the Lesser Antilles: Origin of the Carbonic Acid Consumed by Weathering Reactions in the Lesser Antilles. Earth Surface Processes and Landforms 38: 1020-035.

Roobol MJ, Wright JV, Smith AL (1983) Calderas or gravity-slide structures in the Lesser Antilles island arc? Journal of Volcanology and Geothermal Research 19: 121-134.

Rouse, C. (1990) The mechanics of small tropical flowslides in Dominica, West Indies. Eng Geol 29, 227-239.

Rouse, W., Reading, A. and Walsh, R. (1986) Volcanic soil properties in Dominica, West Indies. Eng Geol 23, 1-28.

Ruzie, L., Aubaud, C., Morira, M., Agrinier, P., Dessert, C., Greau, C., and Crispi, O. (2013) Carbon and helium isotopes in thermal springs of La Soufriere volcano (Guadeloupe, Lesser Antilles): Implications for volcano monitoring. Chemical Geology 359: 70-80.

Sigurdsson, H. (1972) Partly-welded pyroclastic flow deposits in Dominica, Lesser Antilles, Bulletin of Volcanology 36: 148-163.

Smith, A.L., Roobol, M.J., Mattioli, G.S., Fryxell, J.E., Daly, G.E., Fernandez, L.A. (2013) The Volcanic Geology of the Mid-Arc Island of Dominica, Lesser Antilles—The Surface Expression of an Island-Arc Batholith. The Geological Society of America, Special Paper, 496.

Sparks, R.S.J., Sigurdsson, H., and Carey, S.N. (1980) The entrance of pyroclastic flows into the sea I. Oceanographic and geologic evidence from Dominica, Lesser Antilles. Journal of Volcanology and Geothermal Research 7(1): 87-96.

Stokes, S. and Walling, D.E. (2003) Radiogenic and isotopic methods for direct dating of fluvial sediments, in: Kondolf, G.M., Piegay, H. (Eds.), Tools in Fluvial Geomorphology. John Wiley and Sons, West Sussex, pp. 233-267.

Wadge, G., and Shephard, J.B. (1984) Segmentation of the Lesser Antilles subduction zone. Earth and Planetary Science Letters 71; 297-304.

Waters, L.E., and Lange, R.A. (2015). An updated calibration of the plagioclase-liquid hygrometer-thermometer applicable to basalts through rhyolites. American Mineralogist, 100: 2172-2184.

Wills K (1974) The Geological History of Southern Dominica and Plutonic Nodules from the Lesser Antilles. PhD Thesis, University of Durham.

Zimmer, Mindy M., Tobias P. Fischer, David R. Hilton, Guillermo E. Alvarado, Zachary D. Sharp, and James A. Walker (2004) Nitrogen systematics and gas fluxes of subduction zones: insights from Costa Rica arc volatiles. Geochemistry, Geophysics, Geosystems 5: Q05J11, doi:10.1029/2003GC000651.

KECK Geology Consortium
Learning Science Through Research
Published by Keck Geology Consortium

Short Contributions
Keck Geology Consortium
Volume 31
May 2018

EXPLOSIVE TO EFFUSIVE TRANSITION IN INTERMEDIATE VOLCANISM: AN ANALYSIS OF CHANGING MAGMA SYSTEM CONDITIONS IN DOMINICA

JESSICA BERSSON, Whitman College
Research Advisor: Kirsten Nicolaysen, Whitman College

INTRODUCTION

The oscillation between explosive and effusive intermediate (58-65 wt% SiO_2) volcanism at Wotten Waven Caldera on Dominica, an island in the Lesser Antilles Arc, provides an opportunity to investigate temporal changes in the magmatic system. In order to determine possible explanations for the shifting eruptive style a detailed petrologic analysis of phenocrysts is conducted to determine commonalities or changes in pre-eruptive conditions (i.e., intensive variables) for the Roseau Ignimbrite Group (~1-65 ka) (i.e., the explosive end-member) and the Micotrin Lava Dome (~1.1-26 ka) (i.e., the effusive end-member), from the Wotten Waven magma system (Frey, 2016; Howe et al., 2014; Lindsay et al., 2005). Samples from the Micotrin Lava Dome and from multiple units of the Roseau Ignimbrite were collected and analyzed for major element chemistry, trace element chemistry, and mineral geochemistry. Oxide geothermometry (Ghiorso and Evans, 2008) demonstrates pre-eruptive magma temperatures and oxygen fugacity (fO_2). Plagioclase hygrometry (Waters and Lange, 2015) reveals melt water content at the time of peak crystallization of plagioclase. These variables define pressure conditions of the magma storage at the time of the eruptions of the Roseau Ignimbrite and the effusion of the Micotrin Lava Dome. This study aims to better define the magmatic evolution of the source and the shift in volcanism from explosive to effusive by integrating a petrological analysis with past and ongoing geochronological research. Here we see a disparity in SiO_2 content, pre-eruptive temperatures, melt water content, and pressure between the ignimbrite and dome deposits suggesting a complex evolution of the magma system beneath Micotrin. Understanding the progression of this complex magma system informs the volcanic hazards Dominica is exposed to, as the capital Roseau (pop. 15,000) sits atop the thick Roseau Ignimbrite Sequence down valley of the Micotrin Lava Dome.

AREA OF STUDY

Tectonics of Dominica & the Lesser Antilles Arc

The Island of Dominica is located centrally on the Lesser Antilles island arc, at the eastern boundary of the Caribbean Sea. The Lesser Antilles island arc, active since the Eocene, is the surface expression of the westward subduction of the North American Plate beneath the Caribbean plate (Lindsay et al., 2005). Dominica is dominated by intermediate pyroclastic deposits and lava domes sourced from nine volcanic centers trending north-south, forming the island's distinct spine. High precipitation rates promote a densely vegetated, rugged landscape with high relief, largely limiting outcrop access to ocean cliffs, valley walls, and quarries. Volcaniclastic fans at the mouth of major valley drainages represent the scarce flat topography on Dominica, and the location of the island's main population centers. Dominica exhibits signs of volcanic unrest, hydrothermal activity, and seismic swarms, which warrant further research into the islands' magma systems to inform potential volcanic hazards, especially given its history of irregular explosive eruptions.

Wotten Waven Caldera

The extensive Roseau Ignimbrite Sequence (~1 – 65 ka) and subsequent Micotrin Lava Dome (~1.1 – 26 ka) have been attributed to the Wotten Waven Caldera, located in central southern Dominica, based on proximity (Lindsay et al., 2005; Smith et al., 2013; Boudon et al., 2017). The caldera is elongate south to southwest extending 7 km by 4.5 km with partially fault controlled margins and a subsidence volume between 5 and 7.7 km^3 (Smith et al., 2013). The Roseau Ignimbrite Sequence is composed of multiple units representing pulses of explosive activity and subsequent caldera collapse. The Micotrin Lava Dome Complex extruded within the Wotten Waven Caldera following caldera collapse, analogous to, but at a larger scale than, the resurgent lava dome extruded at Mt. St. Helens between 2004 and 2008. Wotten Waven deposits are andesitic to dacitic in composition (58-65 wt% SiO_2). The shift from explosive, ignimbrite-forming eruptions to effusive dome-forming activity resembles the classic caldera cycle of Smith and Bailey (1968), defined by oscillations of plinian and peléan style volcanism. Smith et al. (2013) suggest the characteristic alternations may represent volcanic responses to specific conditions (i.e. temperature, water content) within the magma reservoir.

Roseau Ignimbrite and Micotrin Lava Dome Complex

Plinian eruptive activity produced the Wotten Waven caldera and associated Roseau pyroclastic deposits. The Roseau Ignimbrite Sequence is composed of three distinct stratigraphic units representing multiple eruptive periods, exposed within the caldera and throughout the Roseau Valley (Demange et al., 1985; Smith et al., 2013). Unit 1 is a thick, relatively uniform welded ignimbrite interpreted as deposited from a singular collapse of a plinian eruption column (Smith et al., 2013). Unit 2 is unwelded and contains a paleosol present at Kings Hill, representing a period of inactivity and suggesting at least two distinct eruptive events are represented. Unit 3 is unique in that it contains both unwelded pyroclastic deposits and intermittent block-and-ash flow deposits (Smith et al., 2013). The block-and-ash flows tend to overlie pyroclastic deposits suggesting dome extrusion marks the end of the main eruptive series and represents the transition from plinian to peléan activity (Smith et al., 2013). These block-and-ash flow deposits represent the extrusion, over steepening, and collapse of a lava dome and have been attributed to the Micotrin Lava Dome Complex, two coalesced domes located on the northeastern margin of the Wotten Waven Caldera (Demange et al., 1985).

METHODS

Roseau Ignimbrite and Micotrin Dome samples were collected over multiple field seasons (2015, 2016, and 2017) led by Holli Frey. Samples were powdered and analyzed for major and trace elements using ICP-OES at Acme Labs and ICP-MS at Union College. Samples were prepared as thin sections for microbeam analyses. Compositions of magnetite, ilmenite and plagioclase were collected using energy dispersive spectrometry (EDS) with the Zeiss EVO-MA15 Scanning Electron Microscope (SEM) at Union College. The EDS analyses were conducted following a calibration method, where the initial beam intensity is obtained by collecting the energy emitted by a copper plate, then EDS spectra are collected for natural mineral standards in the Union College collection (e.g., grossular, ilmenite, magnetite, anorthite). Compositions of magnetite, ilmenite and plagioclase were also collected using the Cameca SX-100 electron microprobe (EPMA) at University of California Davis. For EPMA analyses, a beam intensity of 15 KeV was used along with an intensity of 20 μm and 10 μm for oxides and plagioclase, respectively. Oxide analyses were repeated on samples that were analyzed at Union College to test the robustness of the EDS calibration method.

RESULTS

Petrography

Both deposits are saturated in five phenocrysts (plagioclase + orthopyroxene + clinopyroxene + ilmenite + magnetite +/- amphibole +/- quartz) but with notable differences: lava dome deposits contain more quartz and relict amphiboles. Ignimbrite deposits are glass-rich, whereas the Micotrin Dome deposits contain little glass with microcrystalline matrices (Fig. 1).

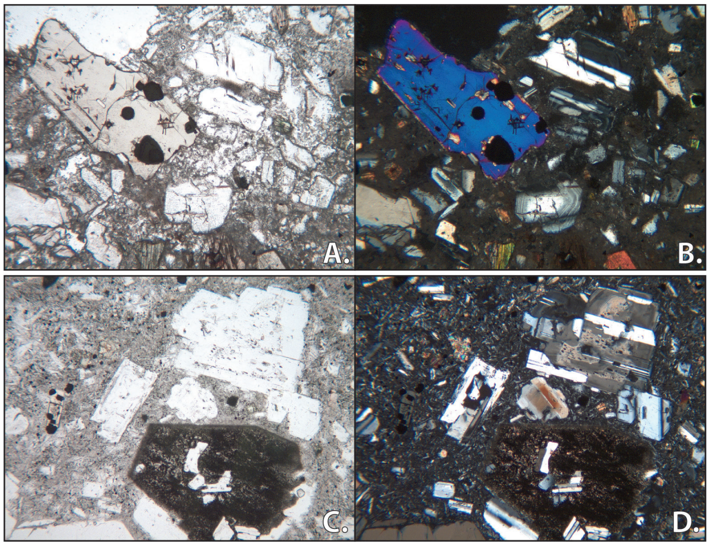

Figure 1. Roseau Ignimbrite sample RI-13 (A., PPL, 40x; B., XPL, 40x) contains plagioclase + clinopyroxene + orthopyroxene + ilmenite + magnetite grains with broken boundaries and a glass matrix, characteristic of pyroclastic deposits. Micotrin Dome sample MI-7 (C., PPL, 40x; D., XPL, 40x) contains a similar mineral assemblage as well as quartz and relict amphibole. MI-7 contains euhedral grains with a microcrystalline matrix.

Whole Rock Geochemistry

Major element chemistry reveals Micotrin Lava Dome deposits have lower SiO_2 contents than Roseau Ignimbrite Group deposits (Fig. 2). Younger Roseau Ignimbrites (Casso Ignimbrite) have largely lower SiO_2 contents than older Roseau Ignimbrites (Kings Hill Ignimbrite). In contrast trace elements, normalized to chondrite, illustrate the homogeneity of Wotten Waven deposits. Notably, younger deposits (Micotrin Lava Dome and Casso Ignimbrites being roughly the same age) have progressively lower LREE values, suggesting greater extent of partial melting of the mantle.

Oxide and Plagioclase Compositions

Most samples were analyzed using EDS at Union College (MI-1B, MI-7, RI-9, RI-10, RI-13, RI-15, KH-4). At UC Davis, EPMA analysis tested additional samples (MI-8, MI-9, RI-1A, RI-9) and validated Union College EDS analyses by reanalyzing samples (RI-9 and RI-13). Samples analyzed using both EDS and EPMA exhibit largely consistent oxide compositions with slightly elevated TiO_2 levels in EDS data. This inflation of TiO_2 under-predicts fO_2 values using geothermometry analysis. Consequently, fO_2 analysis was not the focus of this study. Samples containing chemically weathered oxides show dissolution of magnetite and ilmenite grains in EDS and EPMA as well as highly variable compositions. Samples exhibiting a weathering trend are distinct (Fig. 3) and are not used to calculate pre-eruptive temperatures and fO_2. Ignimbrite deposits have more calcic plagioclase, with rims and cores ranging from An_{24} to An_{93}, than subsequent Micotrin Dome deposits, with rims and cores ranging from An_{45} to An_{85} (Fig. 4).

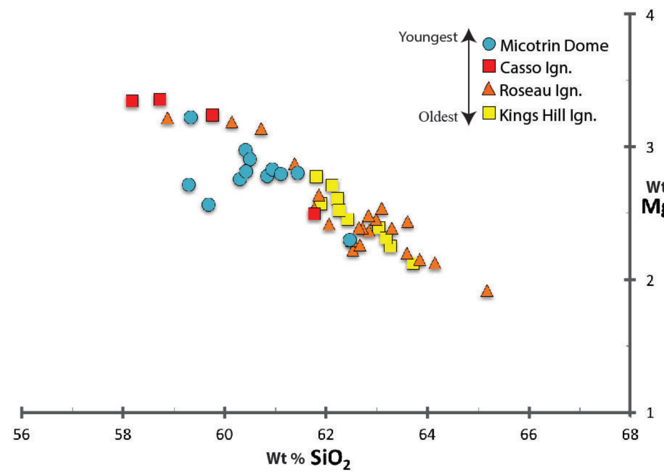

Figure 2. Major element geochemistry reveals younger deposits (Micotrin) have generally lower silica contents than older ignimbrite deposits (Kings Hill).

Determination of Intensive Variables

Fe-Ti oxide geothermometry using magnetite-ilmenite pairs reveals pre-eruptive conditions of the magma storage, including temperature and oxygen fugacity (fO_2) of the melt immediately before eruption. Oxide data was processed using the Hora et al. (2013) model, which applies the Ghiorso and Evans (2008) formulation of the Fe-Ti oxide thermometer and the Bacon and Hirschmann (1988) test for equilibrium. Roseau Ignimbrites demonstrate lower pre-eruptive temperatures (mean = 831˚C) and higher fO_2 (mean = 0.40 ΔNNO) values than subsequent Micotrin Lava Dome deposits (mean = 851˚C, 0.30 ΔNNO)(Fig. 3).

Plagioclase hygrometry reveals melt water content at the time of peak plagioclase crystallization using the measured albite and anorthite components. Plagioclase

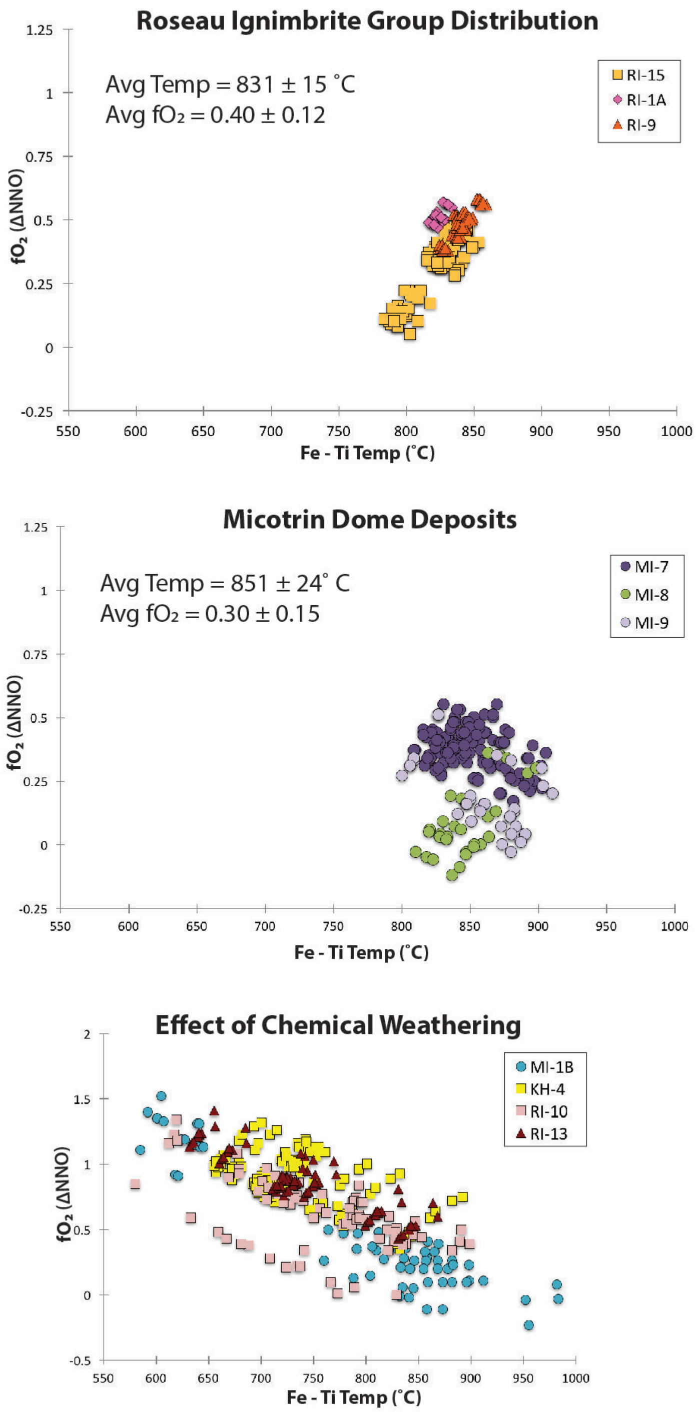

Figure 3. Oxide geothermometry reveals the pre-eruptive conditions of the magma system. Here we see pre-eruptive temperatures plotted against fO_2. Each symbol represents an oxide pair within the sample. Samples showing a trend characteristic of chemical weathering have been separated, illustrating the limitations of fieldwork on a tropical island with a high precipitation rate.

data was processed using the Waters and Lange (2015) plagioclase-liquid exchange hygrometer. This model incorporates independent Fe-Ti temperatures, plagioclase chemistry, and a proxy for melt composition, ideally interstitial glass. The microcrystalline matrix of Micotrin Dome deposits hosts little glass, so whole rock was used to supplement and better describe the water content in the changing conditions of the melt. Within each sample the most calcic plagioclase compositions were analyzed using whole rock composition to determine maximum water contents. The most sodic plagioclase compositions were analyzed using interstitial glass composition to determine the minimum water content. Accordingly, Roseau Ignimbrite deposits exhibit higher magmatic water contents (10.1-4.6 wt % H_2O) than subsequent Micotrin Dome lavas (7.1-2.8 wt% H_2O).

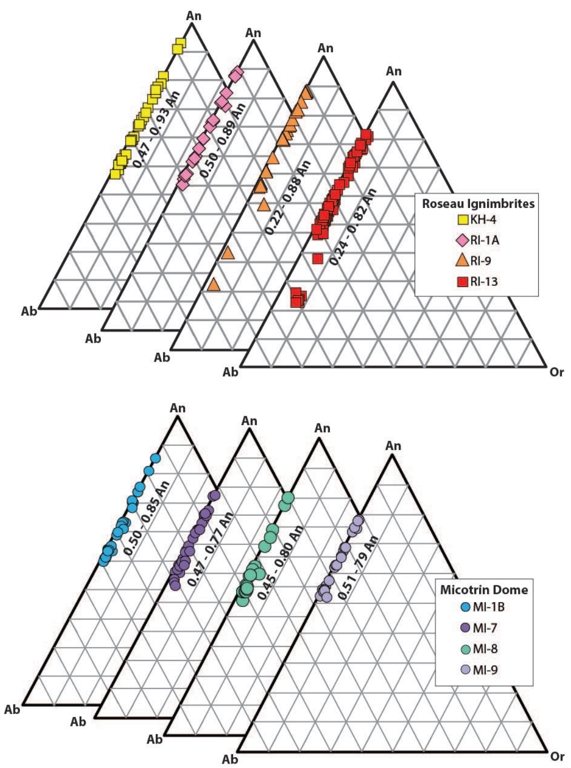

Figure 4. Plagioclase ternary diagrams show the spread of anorthite (An) and albite (Ab) components. Data include rims and cores.

DISCUSSION

This study establishes that the overall pattern of magmatism observed at Wotten Waven Caldera includes an initial, explosive interval of cold hydrous andesitic ignimbrites, followed by a second interval consisting of an effusive eruption of andesite with hotter pre-eruptive temperatures. Petrographic analysis reveals microcrystalline matrices of Micotrin Dome deposits, suggesting slow magmatic ascent. Whole rock geochemistry (Fig. 2) reveals Wotten Waven became less evolved over time, regardless of eruptive style. Oxide geothermometry reveals Micotrin Dome deposits to have higher pre-eruptive temperatures than previous Roseau Ignimbrite deposits. The decreasing silica content and increasing temperature found at Wotten Waven raises questions, as a homogenous, discrete magma body would be expected to become more siliceous, due to fractional crystallization, and cooler over time.

Phase Diagram

This phase diagram (Fig. 5) allows us to visualize the intensive variables (eruption temperature, pressure, water content) at Wotten Waven by plotting our natural samples against experimentally determined phase stability curves for a liquid with a composition similar to our samples (Holz et al., 2005). The water contents, calculated from the application of plagioclase-liquid hygrometry, are plotted as a function of the pre-eruptive temperature determined for each of our samples. Our samples have delineated a pattern consistent with crystallization coincident with magma ascent. Moreover, we find consistency between our samples and the phase equilibrium experiments and we conclude: (1) The Ignimbrites are colder, and the water contents recorded by plagioclase crystallization are consistent with the position of the plagioclase-stability curve at higher pressures for lower temperatures. (2) Plagioclase crystallization ceases above the quartz-in curve in the ignimbrites, which may suggest that crystallization in the ignimbrite ceases at these conditions. This is consistent with the absence of quartz as a phenocryst phase in our ignimbrite samples.

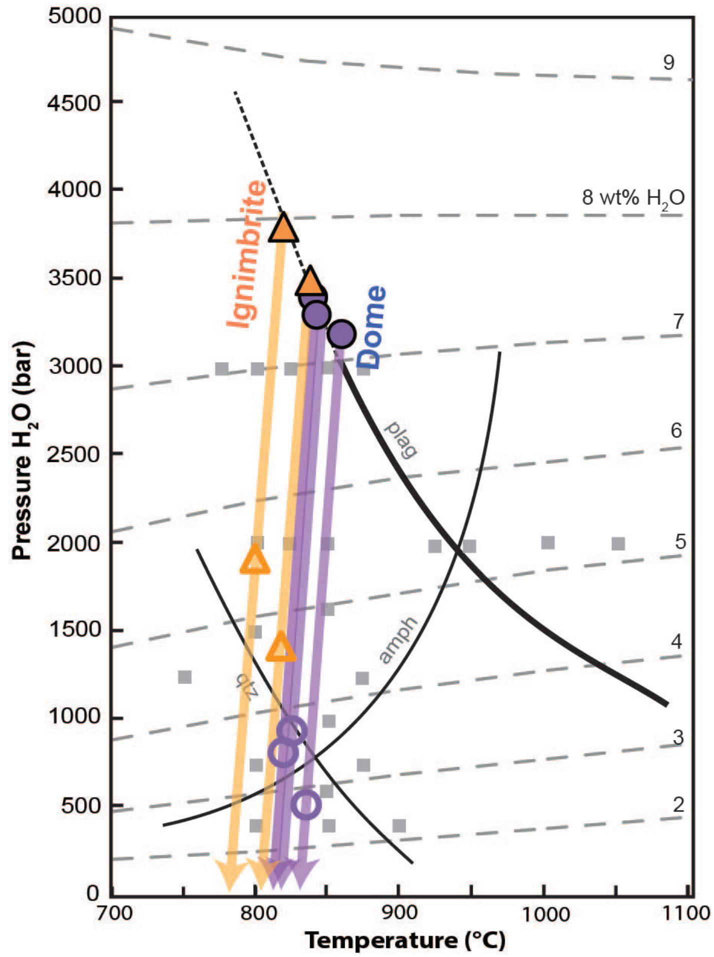

Figure 5. Phase diagram shows Wotten Waven deposits plotted against experimental data of a deposit with similar composition. Lines represent the evolution of the liquid as the system is evolving and decompressing in the time before eruption. Solid symbols represent maximum water content, indicating the onset of crystallization based on plagioclase hygrometry. Hollow symbols represent minimum water content, indicating the end of crystallization based on plagioclase hygrometry. Modified from Holz et al. (2005).

CONCLUSION

Systematic variations in magmatic conditions between Roseau Ignimbrite and Micotrin Lava Dome deposits raise questions about the mechanism of magmatic evolution. Why does Wotten Waven Caldera experience a decrease in SiO_2 content, an increase in pre-eruptive temperatures, and a decrease in melt water content during its evolution from explosive to effusive volcanism? Here, we consider three interpretations of the data. First, Micotrin Lava Dome may be sourced from a separate magmatic body than that of the Roseau Ignimbrites, and has taken advantage of the existing conduit system. The homogeneity of trace elements from both deposits, however, suggest they are sourced from the same magma system. Another interpretation is that Micotrin Lava Dome reflects the introduction of a hotter, more mafic melt to the system, adding heat and volatiles to the system while lowering the silica content. This idea of magmatic mafic recharge at Wotten Waven is supported by the presence of enclaves in the Micotrin Dome deposits, suggesting magma-mixing (Hickernell, 2018). A final alternative interpretation of the data is that Micotrin Lava Dome represents the last breath of a singular magma body that is stratified in both temperature and volatile content. Understanding the complexities of the magmatic evolution at Wotten Waven informs the hazards Dominica is exposed to and provides insight into the mechanism of volcanic expression at this magma system.

ACKNOWLEDGEMENTS

This material is based upon work supported by the Keck Geology Consortium and the National Science Foundation under Grant no. 1659322. I'd like to express my immense gratitude to Laura Waters, Holli Frey, and Kirsten Nicolaysen for their invaluable guidance and encouragement. Thank you to Matt Manon for his support and instruction. This research would not have been possible without the generous support of the Keck Geology Consortium, Whitman College, and Union College.

REFERENCES

Bacon, C.R. and Hirschmann, M.M. (1988) Mg/Mn partitioning as a test for equilibrium between coexisting Fe–Ti oxides. American Mineralogist 73: 57–61.

Boudon, G., Balcone-Boissard, H., Solaro, C., and Martel, C. (2017) Revised chronostratigraphy of recurrent ignimbrite eruptions in Dominica (Lesser Antilles Arc): Implications on the behavior of the magma plumbing system. Journal of Volcanology and Geothermal Research 343: 135-154.

Demange, J., Leborne, H., Traineau, H., and Westercamp, D. (1985) Histoire Volcano-Structurale De La Region Sud de la Dominique. Institute Mixte Recherches Geothermiques, 114p.

Frey, H.M. (2016) Dominica: The Sleeping Giant in the Caribbean. F&M Scientist.

Ghiorso, M.S. and Evans, B.W. (2008) Thermodynamics of rhombohedral oxide solid solutions and a revision of the Fe–Ti two-oxide geothermometer and oxygen-barometer. American Journal of Science 308: 957–1039.

Hickernell, S. (2018) Magma Mixing: Magmatic Enclaves in Morne Micotrin, Domincia. 31st Keck Symposium Volume.

Holtz, F., Sato, H., Lewis, J., Behrens, H. and Nakada, S. (2005) Experimental petrology of the 1991-1995 Unzen Dacite, Japan. Part 1: Phase relations, phase composition, and pre-eruptive conditions. Journal of Petrology 46 (2): 319-337.

Howe, T.M., Lindsay, J.M., Shane, P., Schmitt, A.K., and Stockli, D.F. (2014) Re-evaluation of the Roseau Tuff eruptive sequence and other Ignimbrites in Dominica, Lesser Antilles. Journal of Quaternary Science 29(6): 531–546.

Hora, J.M., Kronz, A., Moller-McNett, S. and Worner, G. (2013) An Excel-based tool for evaluating and visualizing geothermobarometry data. Computers and Geoscience 56: 178-185.

Lindsay, J.M., Smith, A.L., Roobol, M.J., and Stasiuk, M.V. (2005) Dominica: Volcanic Hazards of the Lesser Antilles. Seismic Research Unit, The University of the West Indies, Trinidad and Tobago. 279 p.

Sigurdsson, H. (1972) Partly-welded pyroclastic flow deposits in Dominica, Lesser Antilles, Bulletin of Volcanology 36: 148–163.

Smith, A.L., Roobol, M.J., Mattioli, G.S., Fryxell, J.E., Daly, G.E., Fernandez, L.A. (2013) The Volcanic Geology of the Mid-Arc Island of Dominica, Lesser Antilles—The Surface Expression of an Island-Arc Batholith. The Geological Society of America, Special Paper, V496, 249p.

Smith, R. and Bailey, R. (1968) Resurgent Cauldrons. Geological Society of America Memoir 116: 613-662.

Sun, S. and McDonough, W.F. (1989) Chemical and isotopic systematics of oceanic basalts: implications for mantle composition and processes. Geological Society, London, Special Publications 42: 313–345.

Wang, Y., Pan, H., Li, H. and Wang, C. (2007) Force field of the TMGL ionic liquid and the solubility and SO2 and CO2 in the TMGL from molecular dynamics simulation. Journal of Physical Chemistry 111(35): 10461-10467.

Waters, L. and Lange, R. (2015) An updated calibration of the plagioclase-liquid hygrometer-thermometer applicable to basalts through rhyolites. American Mineralogist 100(10): 2172-2184.

KECK Geology Consortium
Learning Science Through Research
Published by Keck Geology Consortium
Short Contributions
Keck Geology Consortium
Volume 31
May 2018

SOURCES OF VOLCANIC GASES FROM DOMINICA, LESSER ANTILLES

JACQUELINE BUSKOP, Wesleyan University
Research Advisors: Erouscilla (Pat) Joseph (University of the West Indies, Trinidad), **Johan C. Varekamp** (Wesleyan University), **Timothy C. Ku** (Wesleyan University), and **Salvatore Inguaggiato** (Instituto Nazionale di Geofisica e Vulcanologia, Palermo, Italy)

INTRODUCTION

Dominica boasts nine young volcanic complexes, five of which have associated geothermal fields. Volcano hydrothermal monitoring provides information on temperature, origin, and secular changes in chemical composition of volcanic fluids and informs on potential volcanic hazards to which the public may be exposed. We sampled low temperature fumaroles and measured bulk gas composition and isotope ratios of N, He, S, and C for hydrothermal areas across the island. Isotope ratios enable us to track the gas sources for each hydrothermal system. Gas source components of a subduction zone volcano include the subducting slab with subducted sediment, the earth's mantle, crustal rocks just below the volcano, and the ubiquitous ambient air contamination.

SOURCE COMPONENTS FROM STABLE ISOTOPE SYSTEMATICS

The general isotopic compositions of volcanic gases from different tectonic settings is well established and can help define their source components (Poorter et al., 1991; Giggenbach 1991, 1992). The $\delta^{15}N$ of mid-ocean ridge basalts (MORB) is approximately -5‰, whereas atmospheric N_2 is 0‰, and terrigenous sediments typically have values of +6 to +7‰ (Fischer et al., 2002). The contrasts in $\delta^{15}N$ values of the gases allow this isotope system to be used as a potential tracer of volatile recycling from subducted sediments along the Lesser Antilles arc.

The $^3He/^4He$ ratios can be used to discriminate between mantle and crustal gases. An air-normalized $(^3He/^4He)_R$ of mantle gases ~30 has been used as evidence for the existence of a 'primordial' un-degassed deep mantle reservoir, whereas MORB has $(^3He/^4He)_R$ = ~ +8 ± 1 (Class and Goldstein, 2005). Terrigenous sediment rich in U and Th results in high ^4He concentrations and low $(^3He/^4He)_R$. Thus, $(^3He/^4He)_R$ can aid in identifying different mantle volatiles from recycled subducted sediment sources: Low $(^3He/^4He)_R$ reflects recycled terrigeneous material enriched in radiogenic ^4He, whereas high $(^3He/^4He)_R$ values indicate a magmatic mantle component.

Cosmochemical constraints suggest that sulfur may make up ~ 9-12% of the Earth's core whereas the remaining S cycles through the rest of the solid Earth (Dreibus and Palme, 1996). Mantle $\delta^{34}S$ values are close to 0‰, with a value of -1.28± 0.33‰ proposed by Labidi and Moreira (2013). Subducted marine sediment may carry sulfate (gypsum, anhydrite) with near seawater $\delta^{34}S$ values (+18 to +25 ‰), whereas altered sea floor and organic rich shales may be rich in sulfides with $\delta^{34}S$ values down to -15‰ or lower. Thus, either very high or very low $\delta^{34}S$ values may point to recycled sedimentary sulfur, whereas values close to 0‰ represent mantle sulfur contributions. High temperature, volcanic sulfur-bearing gases consist mainly of SO_2 with minor amounts of H_2S, whereas low temperature fumaroles and geothermal gases are rich in H_2S and carry little to no SO_2. The $\delta^{34}S$ of H_2S in fumaroles at arc volcanoes ranges from +1.6 to -5.2‰ in the eastern Indonesian arc (Poorter et al., 1991) and was found to be relatively uniform

(2.5 ± 0.28‰) at Milos in Greece (Gilhooly et al., 2014). Many low temperature fumaroles precipitated native S as a result of the oxidation of H_2S, which may range in $\delta^{34}S$ from -4.7 to +3.2‰ in Eastern Indonesia (Poorter et al., 1991).

Carbon occurs in the upper mantle as CO_2, CO, CH_4 and COS (Deines, 1992). The $\delta^{13}C$ of mantle carbon is -5 ± 2 ‰ (Schidlowski, 1995). Subducted sedimentary carbon may consist of carbonates ($\delta^{13}C$ = ~0‰) or shales rich in organic matter ($\delta^{13}C$ = -20 to -30‰), whereas the altered ocean slab may carry substantial carbonate of marine derivation ($\delta^{13}C$ = 0‰). Most arc volcanoes carry up to 75% of their CO_2 from recycled sedimentary carbon (Varekamp et al., 1992). Ambient atmospheric CO_2, currently at ~411ppmv has $\delta^{13}C$ = -8.5‰.

The combination of S and C isotope systematics of volcanic gases enables us to distinguish between volatile recycling of subducted black shales (low $\delta^{13}C$ and low $\delta^{34}S$) versus carbonates – terrigenous sediment with high $\delta^{34}S$ and close to 0‰ for $\delta^{13}C$.

STUDY AREA

Gas samples were taken from five geothermal sites on Dominica. Four of the five sites are located in the southern portion of the island and the Cold Soufriere is located on the northern tip of the island. The best-known site, the Valley of Desolation (VoD), has numerous fumaroles and bubbling pools over an area of ~0.5km^2 (Joseph et al., 2011). Reported fumarole temperatures from the VoD over the last century have been between 91°C and 99°C while bubbling water pools have temperatures in the range 40°C - 96°C (Joseph et al., 2011). The 2017 temperature observations are consistent with these historical records, with the VoD having some of the hottest features with temperatures of 99°C for both the Bubbling Pool South and the Black Bubbler.

Sulfur Springs is the second hottest site at 91°C, characterized by sulfurous fumaroles and hot pools with a plethora of bright yellow sulfur deposits surrounding gaseous vents. Galion is the third hottest fumarolic site at 87.5°C. Many bright yellow sulfur deposits were present around gaseous vents. Sulfur Springs and Galion activity is part of the Plat Pays volcanic complex (Joseph et al., 2011). Watten Waven is characterized by numerous bubbling pools and fumaroles with a temperature of 59°C, and its activity is part of the Watten Waven/Micotrin volcanic complex. The coldest hydrothermal site, at 24°C, is aptly named Cold Soufriere. It lacks fumaroles, H_2S odors, and kaipohan geothermal features (Joseph et al., 2011).

METHODOLOGY

Cleaned, empty Giggenbach flasks were weighed before being prepared for sampling. Approximately 50ml of a 5M NaOH solution was then funneled into each Giggenbach flask. The Giggenbach flasks next were evacuated with a hand pump, and then re-weighed. A separate set of Giggenbach flasks were prepared as well and bulk gas composition was analyzed at the INVG laboratory in Palermo, Sicily.

Gas from bubbling pools were sampled at the VoD, Cold Soufriere and Watten Waven sites. Dry fumarolic vents were sampled at Sulfur Springs and Galion. Thus, the standard methods described by Giggenbach and Goguel (1989) had to be adapted for the variation in the type of geothermal feature sampled. For bubbling pool sites, a funnel was attached to the end of a tube covering the most vigorously bubbling spots in the pool which was connected to the inlet of the Giggenbach flask. The Giggenbach flask was opened and gases seeped up the tube and into the flask. The flask was held open as long as gases bubbled through the NaOH solution. Once bubbling in the flask slowed down, the flask was closed to allow absorption of soluble gases, and after a few seconds, the flask was opened again to allow more gas to bubble through the flask. This process is repeated four to five times to ensure that as much gas was collected as the flask could hold. Careful attention was paid that no liquid from the pool entered the flasks.

For the fumarolic vents at Galion and Sulfur Springs, a ~1m titanium tube was gently hammered into the surface layer as close as possible to the hottest portion of the fumarole. A glass connector was fitted to the top of the Ti-tube, and the Giggenbach flask fitted with a ground glass joint onto the connector. The same protocol of opening and closing the flask when bubbling intensity decreased was followed. We paid

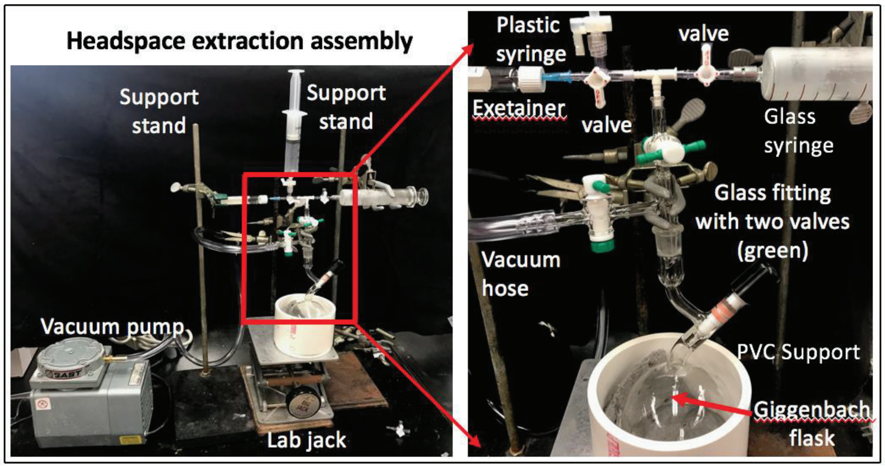

Figure 1: Manifold that was used to draw headspace gases from the Giggenbach flasks. The glass manifold was first evacuated, then the headspace gas in the Giggenbach flask was allowed to expand into the glass syringe before isolating the volume above the upper green valve. The gas was then injected into the Exetainer. This process was repeated as many times as possible for each sample.

attention to the high temperatures of the fumaroles as well as avoided H_2S inhalation during sampling.

Ambient air samples were collected with a 100ml syringe at varying distances from the vents and then injected in pre-evacuated 'Exetainers' for $\delta^{13}C(CO_2)$ analysis. The syringe was pumped full and emptied several times to avoid sample carry-over and contamination. At bubbling pool sites, the syringe was filled as close to the most vigorously bubbling portion of the pool; at fumarolic vents, filled as close to the opening as possible. For atmospheric, samples, the syringe was pumped at least 0.5km away from any fumarole or bubbling pool site. Analyses for $\delta^{13}C(CO_2)$ and CO_2 concentrations were done at the UC Davis Stable Isotope Lab.

Bright yellow sulfur precipitates close to the vents were taken from VoD, Sulfur Springs, Galion, and Cold Soufriere. Samples were homogenized and analyzed for mineralogy by XRD at Wesleyan University, and for $\delta^{34}S$ at the OASIC Lab at Louisiana State University. The sulfur was precipitated as $BaSO_4$ and gravimetric analysis of the Giggenbach flask solutions followed the method of Fahlquist and Janik (1992). The $BaSO_4$ precipitate was analyzed for $\delta^{34}S$ at the OASIC Lab at LSU. Headspace gases were transferred into pre-evacuated exetainers using an extraction line and a gas-tight syringe as a pump (Fig. 1). Samples were balanced to near atmospheric pressures with UHP He prior to analyses. Aliquots of the Giggenbach flask headspace gases were sent to the UC Davis Stable Isotope Lab for $\delta^{15}N$-N_2 analyses.

RESULTS

Bulk gas composition

Volcanic, magmatic, and hydrothermal gases are dominant in H_2O and CO_2. Volcanic and magmatic gases are characterized by high SO_2, HCl, HF, and CO while hydrothermal gases lack these constituents due to mixing with aquifers (Fischer and Chiodini, 2015). Gas compositions analyzed at INVG indicate N_2/Ar ratios typical of arc-type gases (Figure 2), as defined by Giggenbach (1996), suggesting N_2 addition from subducted sediments (Joseph et al., 2011). However, some of the hydrothermal fluids contain deeper source components as indicated by a significant excess of N_2 possibly due to the addition of nitrogen from the subducting slab (Fischer and Chiodini, 2015). This is especially true for discharges from Galion, Sulfur Springs, and VoD.

Nitrogen isotope composition

The $\delta^{15}N$ results are used to trace the possible sources of the excess N_2 in these gases.

The measured $\delta^{15}N$ values (Fig. 3) range from -0.84‰ (Galion) to +0.24‰ (VoD Black Bubbler). Galion,

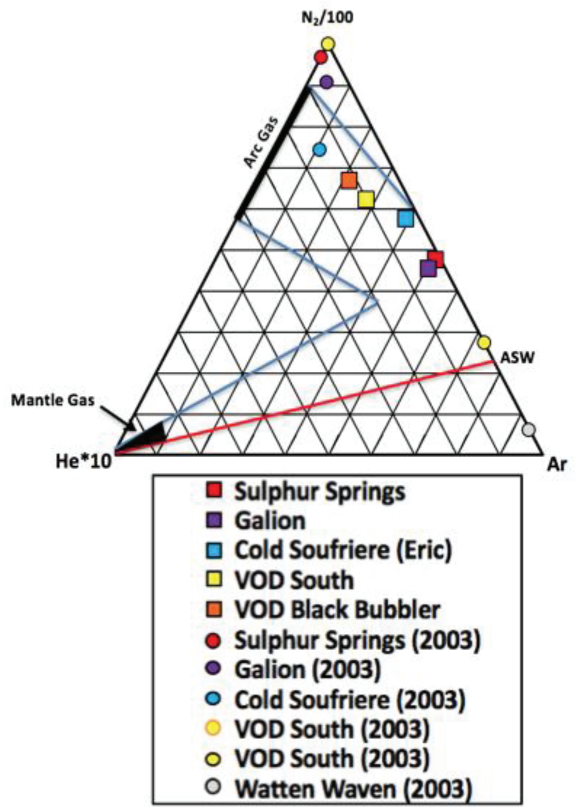

Figure 2: Bulk gas compositions in a He-Ar-N_2 ternary plot, indicating bulk gas compositions with some excess N_2 (arc type gases) and some with stronger air influences.

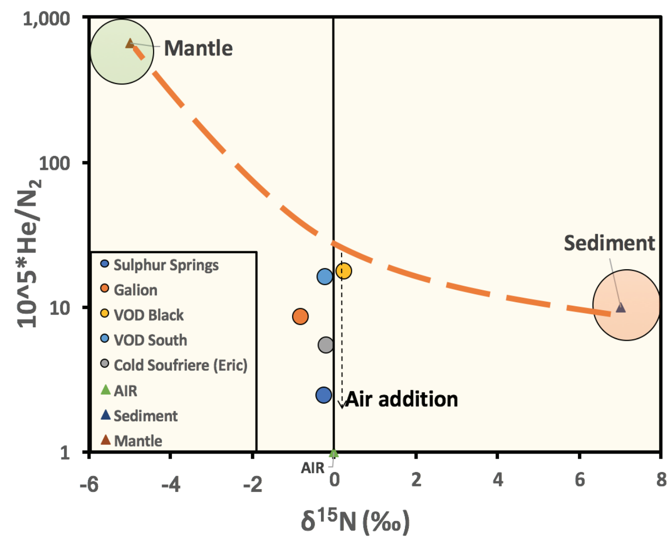

Figure 3: The $(^3He/^4He)_R$ and $\delta^{15}N$ isotopic diagram shows potential mixtures between mantle, and subducted components and mixing with ambient air. One sample suite plots on a mixing curve of ambient air with a component that is strongly leaning to mantle compositions, whereas some of the other samples show a larger contribution from the subducted complex.

Sulfur Springs (-0.25‰), Cold Soufriere (-0.19‰), and VoD South (-0.23‰). All these $\delta^{15}N$ values are considerably lower than the 0‰ of air and the typical values for terrigenous sediment (+6 to +7‰). These negative $\delta^{15}N$ values may have been sourced from the mantle (-5‰). Galion, Sulfur Springs, Cold Soufriere, VoD South have intermediate $\delta^{15}N$ values possibly the result of mixing between mantle, subducted-sediment, and the common air end member.

Helium isotope composition

After correction for air contamination, He isotope data range from 6.65 to 8.39 R/Ra. These analyses are just below to close to MORB values (R/R_A) = ~8, indicating a mantle origin for the He with small contributions of subducted sediment. Lower R/Ra values at Sulfur Springs (6.77) and Cold Soufriere (6.65) especially could indicate addition of subducted sediments. Nonetheless, the helium isotope signature indicates largely a mantle derived gas with a small input from recycled sediment.

Sulfur isotope composition

Sulfur isotope data of all the analyzed gases range from +2‰ to +12‰ (Fig. 4). Sulfur isotope values of the five bubbling pools have a great range: Cold Soufriere (+4.6‰), VoD Black Bubbler (+1.5‰), VoD South (+2.3‰) and Watten Waven (+12.1‰). The two dry fumarolic sites are Galion (+2.6‰) and Sulfur Springs (+4.3‰). The highest temperature features at VoD (99˚C) and Galion (87.5˚C), have $\delta^{34}S$ values closest to mantle values, with some indication of the presence of subducted marine sulfates in the source region.

The surficial native sulfur has more negative $\delta^{34}S$, while the gas phase sulfur has more positive $\delta^{34}S$. During equilibrium isotope partition, the higher oxidation state species will have the highest $\delta^{34}S$. An exception to this rule is the precipitation of native S through oxidation of H_2S: under equilibrium conditions at 200-400°C, where S_8 binds with itself and S_2^- oxidizes to S_0 and the precipitate on the ground is “isotopically lighter”. During this process, the remaining gas will become heavier (Rayleigh fractionation), which may

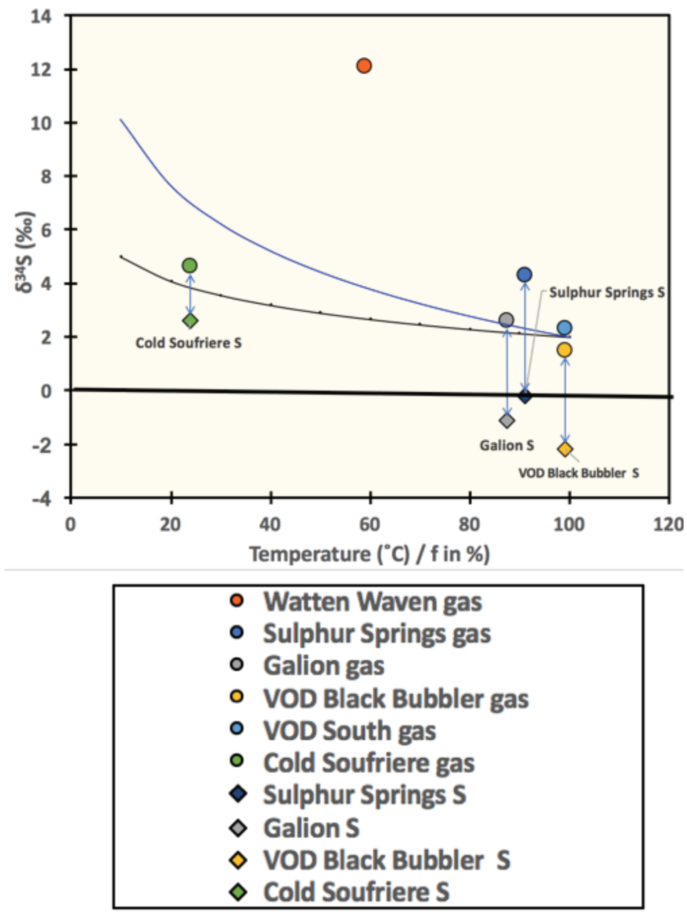

Figure 4: Temperatures of the various sampling locations with $\delta^{34}S$ values, both for gases and associated solid sulfur. The latter are always isotopically lighter than the gases. Also shown are two different temperature Rayleigh fractionation curves for the crystallization of solid sulfur from H_2S; the temperature scale is then used as the % of remaining gas. These curves show the heavier $\delta^{34}S$ values in the remaining gas with progressive extraction of solid sulfur during precipitation in the air.

drive up gas sulfur values to high extremes with extensive sulfur fractionation. The $\delta^{34}S$ values for solid sulfur from Cold Soufriere (+2.6‰), Galion (-1.1‰), Sulfur Springs (-0.2‰), and the VoD Black Bubbler (-2.2‰) evidence this type of fractionation, as all of the solid sulfur values are more negative than their respective gas counterparts (Figure 4).

The $\delta^{34}S$ value of +12‰ of the Watten Waven sample is of interest due to its "isotopically very heavy" nature compared to all other samples that are < +4.6‰ in $\delta^{34}S$. This outlier data point may be the result of extreme sulfur extraction from its gas (unlikely) or the result of SO_2 disproportionation deep in the crust at high temperatures (200-400˚C). The two samples with the highest $\delta^{34}S$ are from cool bubbling pools (Watten Waven, +12.1‰) and Cold Soufriere, +4.62‰) and fractionation at modest temperature between aqueous and gas sulfur species may be another explanation. Watten Waven solid sulfur deposits were lacking in 2017 but should be looked for during the next field campaign.

Carbon isotope composition

The air samples have contributions from ambient CO_2 and from geothermal/volcanic CO_2 and a $1/CO_2$ versus $\delta^{13}C(CO_2)$ (Keeling plot) is a suitable tool to derive potential mixing endmembers (Figure 5). Plotting $\delta^{13}C(CO_2)$ vs $1000/CO_2$ (in ppmv) results in a more or less linear mixing array between the volcanic and ambient endmembers. The ambient pole plots at 400 ppm and -8.5‰ and the array of data intersects the y axis ('100% CO_2') near the -2.5‰ value, close to standard mantle $\delta^{13}C$ values of -5 +/- 2 ‰. Samples (Fig. 5) taken close to Nancy's Pool at Cold Soufriere (-4.6‰) and the fumarole at Sulfur Springs (-1.7‰)

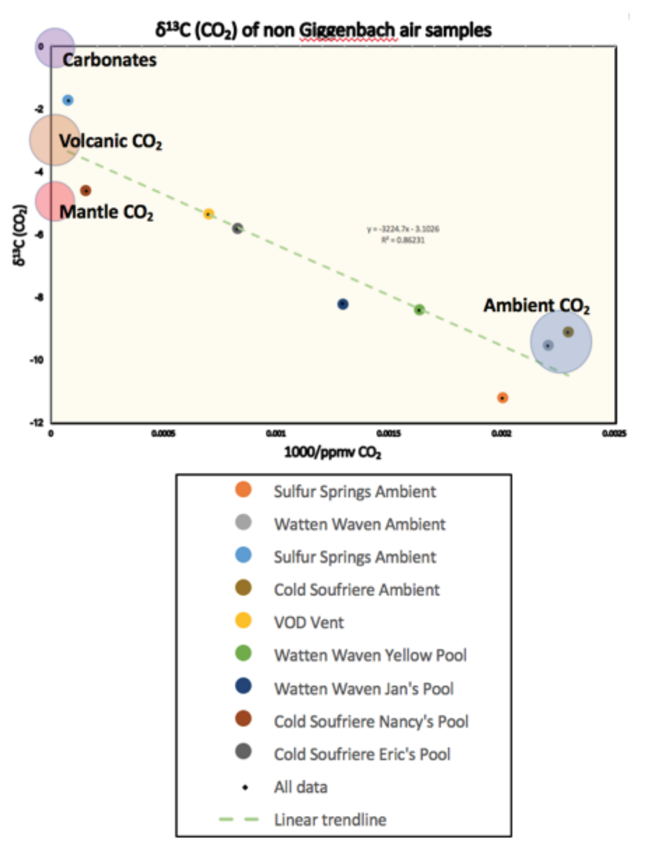

Figure 5: Keeling diagram with $\delta^{13}C$ (CO_2) vs 1000/ppmv CO_2. A mixing line is drawn between ambient air and the samples, providing a best estimate for the volcanic component of $\delta^{13}C$ (CO_2) = -2.5‰, well within the mantle range.

have CO_2 concentrations well above ambient and $\delta^{13}C(CO_2)$ closer to mantle values. Samples taken ~0.5km away from any geothermal site plot well within the ambient CO_2 endmember. All other points plot between the two endmembers, indicating mixing between ambient and volcanic CO_2.

CONCLUSIONS

The suite of gas and stable isotope analyses shows a variation between gases with strong mantle affinities, as indicated by high $(^3He/^4He)_R$, low $\delta^{13}C(CO_2)$ and $\delta^{34}S$ and $\delta^{15}N$, and a suite of gases that point more towards small contributions derived from subducted sediment. These hydrothermal gases of Dominica are rich in N_2, H_2, H_2S, and CH_4, pointing more to a geothermal origin than pure volcanic gases directly derived from the underlying magma. It appears that these gases have partially equilibrated in an intermediate geothermal reservoir prior to their emission at the surface. Continued monitoring of these fumarolic sites will allow for greater insight into the geothermal processes in the subsoil of Dominica and possibly may aid in the monitoring of future volcanic activity.

ACKNOWLEDGEMENTS

This material is based upon work supported by the Keck Geology Consortium and the National Science Foundation under Grant No. 1659322.

REFERENCES

Class, C., and Goldstein, S.L., 2005, Evolution of helium isotopes in the Earth's mantle: Nature, v. 436, p. 1107-1112.

Deines, P., 1992, Mantle Carbon: Concentration, Mode of Occurrence, and Isotopic Composition in Schidlowski, M., Golubic, S., Kimberley, M.M., McKirdy, D.M., Trudinger, P.A., eds., Early Organic Evolution: Springer, Berlin, Heidelberg, p. 133-146.

Dreibus, G., and Palme, H., 1996, Cosmochemical constraints on the sulfur content in the Earth's core: Journal of the Geochemical Society and The Meteoritical Society v. 60, p. 1125-1130.

Fahlquist, L.S., and Janik, C.J., 1992, Procedures for collecting and analyzing gas samples from geothermal systems: U.S. Geological Survey Open-File Report 92-211, 21 p.

Fischer, T.P., and Chiodini, G., 2015, Volcanic, Magmatic, and Hydrothermal Gases in Sigurdsson, H., Houghton, B., McNutt, S., Rymer, H., and Stix, J., eds., Encyclopedia of Volcanoes: Academic Press, Elsevier, London, San Diego, Waltham, Oxford, p.779-797.

Fischer, T.P., Hilton, D.R., Zimmer, M.M., Shaw, A.M., Sharp, Z.D., Walker, J.A., 2002, Subduction and recycling of nitrogen along the Central American Margin: Science, v. 297, p. 1154-1157.

Giggenbach, W.F., 1991, Chemical Techniques in Geothermal Exploration: Application of Geochemistry in Geothermal Reservoir Development: UNITAR/UNDP Centre on Small Energy Resources, New York, p. 253-273.

Giggenbach W.F., 1992, Isotopic shifts in waters from geothermal and volcanic systems along convergent plate boundaries and their origin: Earth and Planetary Science Letters 113 (4), p. 495-510.

Giggenbach, W.F., 1996, Chemical composition of volcanic gases in Scarpa, r., Tilling, RI.I, eds., IAVCEI-UNESCO: Monitoring and Mitigation of Volcano Hazards, Springer, Berlin, p. 221-256.

Giggenbach, W.F., and Goguel, R.L., 1989, Collection and analysis of geothermal and volcanicwater and gas discharges, Department of Scientific and Industrial Research, Chemistry Divison. Report No.: CD 240, Petone.

Gilhooly, W.P., Fike, D.A., Drushcel, G.K., Kafantaris, F.A., Price, R.E., and Amend, J.P., 2014, Sulfur and oxygen isotope insight into sulfur cycling in shallow-sea hydrothermal vents, Milos, Greece: Geochemical Transactions, v. 14, p. 1-19.

Joseph, E.P., Fournier, N., Lindsay, J. and Fischer, T., 2001, Gas and water geochemistry of geothermal systems in Dominica, Lesser Antilles island arc: Journal of Volcanology and Geothermal Research, v. 206(1-2), p. 1-14.

Labidi, J., and Moreira, M., 2013, Non-chondritic sulphur isotope composition of the terrestrial mantle: Nature, v. 501, p. 208-211.

Poorter, R.P.E., Varekamp, J.C., Poreda, R.J., vanBergen, M.J. and Kreulen, R., 1991: Geochemistry and isotopic composition of volcanic gases from the Banda and Eastern Sunda arcs, Indonesia, Geochim. Cosmochim. Acta 55, 3795-3807.

Schidlowski, M., 1995, Isotope fractionations in the terrestrial carbon cycle: A brief overview: Advances in Space Research, v. 15, p. 441-449.

Varekamp J.C., Kreulen R., Poorter R.P.E. and VanBergen M.J. 1992: Carbon sources of arc volcanism with applications for the carbon cycle. Terra Nova v. 4, p. 363-373.

KECK Geology Consortium

Learning Science Through Research

Published by Keck Geology Consortium

Short Contributions
Keck Geology Consortium
Volume 31
May 2018

A PETROLOGIC EVALUATION OF THE LAYOU IGNIMBRITE AND MORNE TROIS PITON LAVA DOME: HOW DO CHANGES IN PRE-ERUPTIVE CONDITIONS AFFECT ERUPTIVE BEHAVIOR?

JUSTIN CASAUS, Sonoma State University
Research Advisor: Laura Waters

INTRODUCTION

One of the most active volcanic centers in the Central Lesser Antilles is the island of Dominica, which features nine active volcanic centers, periodic earthquake swarms and seismic activity, as well as phreatic eruptions (non-magmatic explosive steam eruption) (Lindsay et al., 2005). The frequency with which Dominica features voluminous eruptions of pyroclastic andesite flows presents an immediate hazard for communities on Dominica and underscores the importance of investigating the pre-eruptive storage conditions experienced by previous eruptions to determine whether or not mechanisms that can induce eruption can be identified. Here, we evaluate the Layou Ignimbrite and the Morne Trois Piton dome to discern any variations in their pre-eruptive intensive variables, which may explain the shift in eruptive behavior.

GEOLOGIC SETTING

Dominica is located in the Central Lesser Antilles island arc, located in the Eastern Caribbean Ocean, where the North and South American plates are subducting beneath the Caribbean plate at an average angle of 70° and a rate of 1.9 cm/yr (DeMets et al., 2000). Dominican volcanics range in composition from mafic (basalt) to intermediate (andesite) (48-63 wt.% SiO_2); dacites (63-70 wt.% SiO_2) are occasionally observed (Smith et al., 2013). Notably, the more silicic lavas typically explosively erupt as ignimbrites or effusively erupt as domes. The Layou Ignimbrite is the most evolved composition on the island. Mapping by Smith et al. (2013) reveals that its likely source is approximately the location of the present day edifice Morne Trois Piton, a crystal rich lava dome. The Layou ignimbrite is dramatically exposed along the Layou River, where incision has exposed a ~4 m section of interbedded pumice clasts and ash. Though Dominica is highly vegetated, the Morne Trois Piton dome is actively quarried, which provides excellent exposures of fresh rock in the interior of the dome.

METHODS

Rock samples of the Morne Trois Piton lava dome were collected from a quarry located on the northern side of the dome. Samples were selected to accurately reflect the observed heterogeneity in the outcrop. We observed light- and dark-grey banding of various crystal-rich andesite, as well as numerous inclusions. Layou ignimbrite samples and most data were obtained by Frey and research students over three field seasons. Morne Trois Piton rock samples were cut and processed into thin sections for microbeam analyses at Union College, Schenectady New York. Samples of the Light Grey and Dark Grey portions of the Morne Trois Piton rock samples were first crushed to approximately 1 cm or smaller using a RockLabs laboratory hydraulic crusher/breaker. The crushed samples were then reduced to powder using the RockLabs aluminum oxide grinding vessel. For whole rock composition analysis by ICP-OES, the powdered samples were sent to Acme Labs. The remaining portion of the powdered samples were first dissolved using hydrofluoric acid,

Table 1: Whole Rock Geochemistry and Modal Abundances

	Ignimbrite					Dome				
Descriptor	Pumice Clast 1	Pumice Clast 2	Pumice Clast 3	Pumice Clast 4	**Average Pumice**	Dark Grey	Dark Grey	Dark Grey	**Average Dark Grey**	**Light Grey**
Sample	LV-1	LV-2	LV-3A	LV-4		MTP-2D-A	MTP-Q-DG	MTP-2A-A		MTP-Q-LG
SiO_2	64.49	65.74	64.18	65.67	65.02	62.33	62.04	62.49	62.29	63.17
TiO_2	0.44	0.39	0.45	0.38	0.41	0.5	0.52	0.48	0.5	0.47
Al_2O_3	16.59	16.45	16.43	16.42	16.47	16.9	17.2	17.11	17.07	17.03
FeO^T	5.2	4.67	5.35	4.68	4.97	5.9	5.92	5.69	5.84	5.34
MnO	0.14	0.13	0.15	0.14	0.14	0.15	0.15	0.14	0.15	0.14
MgO	2.09	1.71	2.18	1.72	1.92	2.48	2.53	2.33	2.45	2.23
CaO	5.58	5.3	5.7	5.39	5.49	6.23	6.34	6.22	6.27	6.14
Na_2O	3.22	3.34	3.26	3.37	3.3	3.27	3.35	3.31	3.31	3.35
K_2O	1.56	1.63	1.58	1.6	1.59	1.46	1.4	1.48	1.45	1.51
P_2O_5	0.1	0.12	0.12	0.11	0.11	0.12	0.1	0.11	0.11	0.1
Total	99.42	99.5	99.4	99.48	99.45	99.34	99.94	99.37	99.55	99.93
Modal Abundances										
Plag	10.8	11.2	13.8	20.4	14.1	34.6	27.4	35.3	32.4	34.6
Cpx	2.9	0.6	1.8	1.4	1.7	3.3	2.5	3.9	3.2	2.1
Opx	2.1	1	1.8	1.3	1.5	2.9	6.6	2.3	3.9	5.7
Ox	1.7	0.9	1.6	1.4	1.4	3.3	2.9	1.6	2.6	3.6
Hbl	2.1	2	2.2	2.2	2.2	2.3	0.7	0.6	1.2	0.8
Qtz	0	0.4	0.1	0.2	0.2	1.4	0	0.4	0.6	0
gdms	69.6	62.5	59.6	60.1	63	48.4	52.6	45.2	48.7	44.6
ves	10.8	21.4	17.1	12.9	15.5	3.9	7.3	10.7	7.3	8.6
Total	100	100	97.9	99.9	99.5	100	100	100	100	100

Plag, plagioclase; cpx, clinopyroxene; opx, orthopyroxene; ox, fe-ti oxides; hbl, hornblende; qtz, quartz; gdms, groundmass; ves, vesicles

then nitric acid. The dissolved samples were then analyzed for trace elements using a PerkinElmer/Sciex Elan 6100 DRC inductively coupled plasma mass spectrometer on site at Union College of Schenectady, New York. Point count analyses consisting of 1000 points were performed using PETROG's stepping stage and PetrogLite on site at Union College. Point counts of the Layou Ignimbrite samples were additionally compared to previous students counts to ensure accuracy.

Plagioclase, ilmenite, and magnetite were analyzed in each sample using a standard carbon coating of thin sections in the Zeiss EVO MA15 scanning electron microscope (SEM) located at Union College of Schenectady, New York. The Zeiss SEM was utilized for the back scatter electron (BSE) imaging and quantitative analyses with the Bruker electron dispersive spectrometer (EDS). Spectra analyses were collected over a period of 30 seconds. The EDS analyses were conducted following a calibration method, where the initial beam intensity is obtained by collecting the energy emitted by a copper plate, and then EDS spectra are collected for natural mineral standards in the Union College collection. Plagioclase, ilmenite, and magnetite were reanalyzed in select samples using the Cameca SX-100 Electron Microprobe using wavelength dispersive spectrometry (WDS) at the University of California Davis. For analyses conducted with the electron microprobe, a beam intensity of 15 KeV was used along with an intensity of 20 µm and 10 µm for oxides and plagioclase, respectively.

RESULTS

Sample Petrography and Whole Rock Geochemistry

Point counts from three different thin sections reveal that the Layou Ignimbrite contains 22% crystals on average (including vesicles) and is multiply saturated in seven phenocrystic phases (plagioclase + hornblende + clinopyroxene +orthopyroxene + ilmenite + magnetite + quartz) as shown in Table 1. The pumice samples have an average vesicularity of ~15% .The Morne Trois Piton dome is intermediate in composition and contains approximately 45% crystals and a phase assemblage identical to the Layou Ignimbrite with a few notable distinctions. The Morne Trois Piton samples have more plagioclase, hornblende crystals in the dome are significantly reacted, quartz in the dome samples occurs in a greater abundance and size, and there are notably fewer vesicles– consistent with an effusive eruption. Analyses of pumices from the Layou Ignimbrite reveal that there is little heterogeneity between clasts, and that the Layou Ignimbrite is dacitic and one of the most evolved rocks erupted on

Table 2: Ilmenite and Magnetite Compositions

	Dome				Ignimbrite	
	Dark Grey			Light Grey		
Sample	MTP-2D-A	MTP-2A	MTP-Q	MTP-Q	LV1	LV2
Phase	IL	IL	IL	IL	IL	IL
No. of Analyses	10	10	9	10	15	10
SiO2	0.03	0.02	0.11	0.01	0.08	0.03
TiO2	46.43	46.09	45.29	45.53	48.42	46.54
Al2O3	0.15	0.13	0.14	0.12	0.26	0.14
Fe2O3	13.38	14.32	15.37	15.15	11.18	12.69
V2O3	0.15	0.13	0.15	0.11	0.00	0.12
Cr2O3	0.01	0.01	0.00	0.01	0.06	0.01
FeO	36.80	36.43	35.72	35.98	39.75	37.32
MnO	0.92	0.90	0.94	1.04	0.42	0.85
MgO	1.66	1.79	1.75	1.71	1.31	1.54
CaO	0.05	0.03	0.04	0.03	0.03	0.03
Total	99.57	99.86	99.51	99.70	101.52	99.27
$X_{Ilmenite}$	79.12	77.86	76.84	77.00	83.89	80.32
$\pm 1\sigma$ $X_{Ilmenite}$	3.42	1.04	1.45	1.94	1.21	0.46
Phase	MT	MT	MT	MT	MT	MT
No. of Analyses	11	12	10	10	12	11.00
SiO2	0.09	0.08	0.07	0.08	0.13	0.08
TiO2	9.89	10.64	9.66	9.40	9.64	9.61
Al2O3	1.44	1.49	1.41	1.37	1.98	1.86
Fe2O3	47.58	46.47	48.13	48.74	48.00	47.53
V2O3	0.66	0.66	0.62	0.54	0.35	0.58
Cr2O3	0.03	0.03	0.02	0.03	0.06	0.03
FeO	38.66	39.21	38.19	37.87	39.67	38.52
MnO	0.56	0.62	0.57	0.65	0.00	0.52
MgO	0.79	0.94	0.93	0.86	0.57	0.74
CaO	0.02	0.02	0.01	0.04	0.03	0.02
Total	99.73	100.17	99.61	99.58	100.43	99.50
$X_{Ulvospinel}$	28.03	29.98	27.39	26.69	27.12	27.26
$\pm 1\sigma$ $X_{Ulvospinel}$	2.60	1.74	1.75	1.43	0.61	0.37
T (°C)	798±39	834±15	821 ±27	812±21	769 ±12	793 ± 7
ΔNNO	0.10±0.2	0.23±0.1	0.38±0.17	0.4±0.1	-0.1±0.1	0.1±0.1

Temperature and ΔNNO are average ($\pm 1\sigma$) from all possible pairings of ilmenite and titanomagnetite analyses and the model of Ghiorso and Evans (2008).

the island. Analyses of the Morne Trois Piton dome samples show that the dome is andesitic. Additionally, analyses of specific samples on a color basis reveal trivial compositional differences. The light grey samples are slightly more evolved than the dark grey samples, as they have lower concentrations of CaO and FeO (though the difference is not remarkable).

Oxide Compositions

Ilmenite and magnetite crystals span a relatively narrow range in composition (Table 2). All possible pairs of ilmenite and magnetite within the Layou Ignimbrite and Morne Trois Piton samples were tested using the Bacon & Hirschmann (1988) assessment of equilibrium. The oxide pairs plotted from the Layou Ignimbrite fall well within the defined upper and lower limits, whereas oxide pairs from Morne Trois Piton samples spanned a range but broadly overlapped with the equilibrium criteria.

Plagioclase Compositions

Plagioclase compositions (corresponding to 127 analyses of two samples) in the Layou Ignimbrite (Fig. 1a) span a continuous range from An_{88} to An_{42}. Both samples have calcic plagioclase compositions that gradually increase in abundance to form a distinct peak at ~An_{54} then rapidly decrease in abundance to more sodic compositions An_{44}. Plagioclase in the Morne Trois Piton samples form a slightly more complex pattern in compositions; compositions (shown as a histogram in Fig 1b) occur in three models, one occurring at ~An_{90}, another at ~An_{72}, and a third occurring at ~ An_{54}. Upon close inspection the majority of the plagioclase compositions that form the peak at An_{90} come from a single large calcic plagioclase in a dark grey sample from the Morne Trois Piton dome. The remaining two peaks come from core-to-rim plagioclase analyses of relatively euhedral crystals, which produce this bimodal pattern. The Morne Trois Piton samples share a similarity with the Layou Ignimbrite as the position of the most sodic peak is also ~An_{54}.

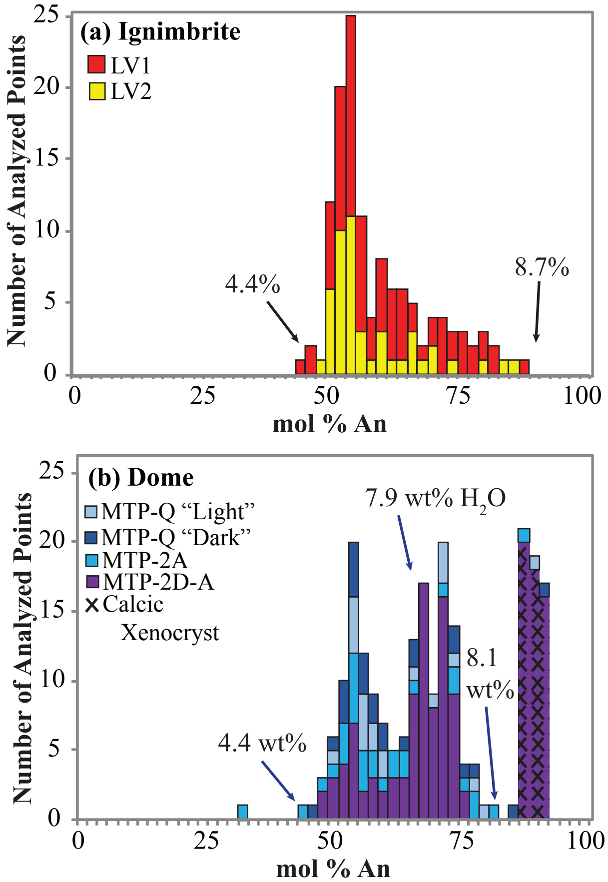

Figure 1: Plagioclase compositions for the (a) Layou Ignimbrite and the and the (b) Morne Trois Piton Lava dome are shown as histograms as a function of mol% An (see text for detailed discussion)

Calculation of Intensive Variables

Pre-eruptive temperatures were calculated by incorporating the compositions of ilmenite and magnetite (Table 2) into the model of Ghiorso & Evans (2008). Oxide pairs from two pumice samples from the Layou Ignimbrite revealed tightly constrained pre-eruptive temperatures of 769 ± 12°C and 794 ± 7°C (Table 2). Oxide pairs from the Morne Trois Piton samples returned a minimum pre-eruption temperature of 798 ± 40°C and maximum temperature of 834 ±15°C (Fig. 2). Oxygen fugacities (relative to the ΔNNO buffer) for the samples range between ~0 and +1, which is consistent with an arc setting. Water contents in equilibrium with the melt at the time plagioclase crystallized in the ignimbrite and the dome are estimated using the plagioclase-liquid hygrometer of Waters & Lange (2015). The pre-eruptive temperatures, calcic plagioclase compositions and whole rock compositions are incorporated in the hygrometer to calculate the maximum water contents. Temperatures, the most sodic plagioclase compositions and the interstitial melt compositions are used to estimate the minimum water contents at the time of plagioclase crystallization. Water contents in equilibrium with the melt at the time of plagioclase crystallization for the Layou Ignimbrite range from ~8.4 wt% to 4.4 wt% H_2O. Water contents in equilibrium with the melt at the time of plagioclase crystallization for the Morne Trois Piton Dome are calculating using only those compositions that are probable phenocrysts (compositions of ~ An_{90} are excluded) and return in a range of H_2O contents from 8.1 to 4.4 wt%.

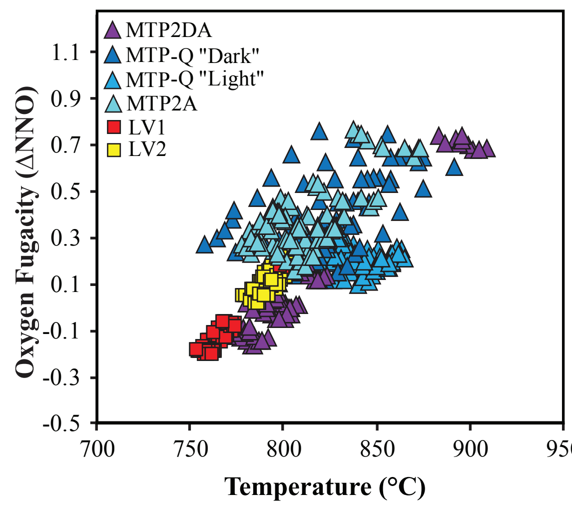

Figure 2: Pre-eruptive temperatures and oxygen fugacities are shown for lava dome samples (triangles, cool colors) and ignimbrites (squares, warm colors). Samples from the lava dome are shifted to hotter temperatures, whereas those from the pumice clasts from the ignimbrites are shifted to cooler temperatures.

DISCUSSION

An outstanding question surrounding arc volcanism is what is the mechanism that that causes a change in eruptive style. The Layou ignimbrite and the Morne Trois Piton Dome provide an opportunity to examine this question as they both erupted from the same edifice in two entirely different styles. The phenocryst assemblages and intensive variables allow us to assess possible pre-eruptive conditions that may have influenced eruptive style. Notably, one of the biggest differences between the Layou ignimbrite and the Morne Trois Piton Dome are the degree of crystallinity and the pre-eruptive temperatures. The Morne Trois Piton Dome is twice as crystalline as the Layou ignimbrite, which is consistent with an effusive eruptive style (e.g., if the eruption is slower there could be more time to crystallize). A surprising observation is that the Morne Trois Piton dome erupted after the Layou Ignimbrite, and has a hotter temperature.

The temperatures and the phase assemblage are evaluated using a phase diagram from the literature based on experiments from Holtz et al. (2005) conducted on a melt with a composition similar to the Layou Ignimbrite and the Morne Trois Piton Dome (Fig. 3). Each sample is shown on the diagram as an arrow plotted at its pre-eruptive temperature (a slight angle is shown to reflect the adiabatic cooling that occurs during ascent). The water contents derived from the hygrometer that correspond to the most calcic and most sodic plagioclase composition are also shown (as boxes) for each sample at its pre-eruptive temperature. The water contents recorded by plagioclase compositions show changing melt H_2O contents (and or temperature; Waters & Lange, 2015), and the ignimbrites are colder and more hydrous than the domes. The diagram suggests that the ignimbrites were sourced from deeper in the crust than the domes. This model however is problematic, as the ignimbrite erupted before the dome and is also colder than the dome; some mechanism to induce heating is required if they are from the same source.

The domes notably contain mafic enclaves, which are largely absent in the ignimbrites and could be the mechanism delivering heat into the magmatic source, mobilizing the magma. The enclaves in the Morne Trois Piton dome, studied by Howe et al. (2015), have compositions that broadly correspond to basaltic andesite and are saturated in plagioclase + clinopyroxene + orthopyroxene + magnetite + hornblende. Application of the two pyroxene thermometer of Putirka (2008) to clinopyroxene and orthopyroxene crystals in Morne Trois Piton enclaves by Howe et al (2015) reveals that the enclaves record temperatures of 920-1080°C, demonstrating that they could be the source of the heat that shifted the dome temperatures upward. The volcanism at Morne Trois Piton broadly follows and informs the caldera cycle defined by Smith & Bailey (1968), which initially begins with small dome

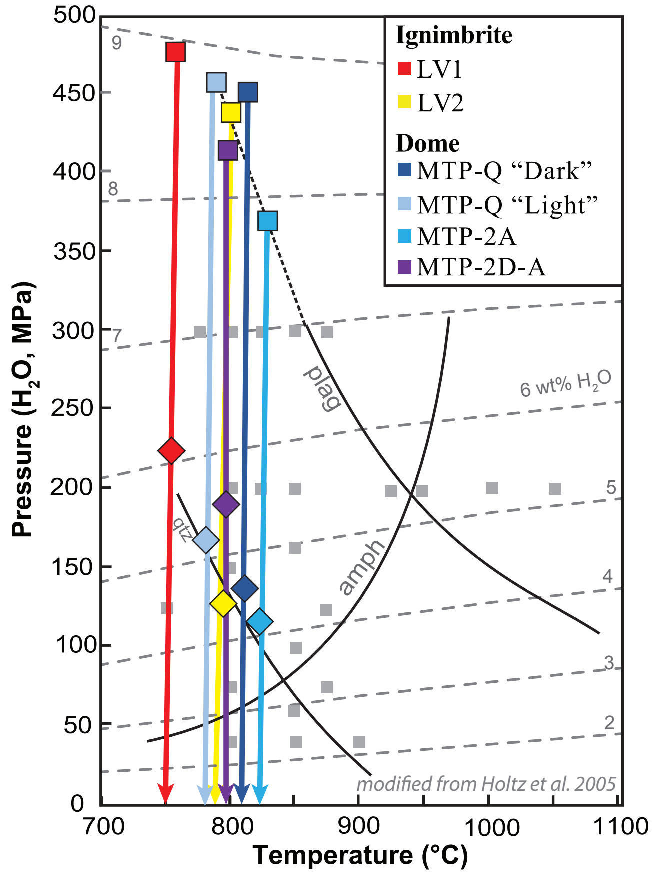

Figure 3: The samples from the Layou Ignimbrite and the Morne Trois Piton Lava dome are plotted at their pre-eruptive temperatures (Table 2) on a phase diagram from Holtz et al. (2005). Experiments that are used to define the phase boundaries are shown as grey squares, also shown are isopleths of dissolved H_2O that correspond to temperatures and and pressure on the diagram for an andesite liquid calculated using Zhang et al. (2007). The maximum water contents (corresponding to the most calcic plagioclase composition) are shown as squares. The minimum water contents (corresponding to the most sodic plagioclase compositions) are shown as diamonds (see text for discussion).

forming eruptions, followed by fumarolic activity, and then they systems enters caldera collapse and an explosive phase; the pattern in volcanism then repeats. The caldera cycle broadly applies to the eruption of the Layou ignimbrite, followed by the formation of the Micotrin dome. The samples suggest that, for Dominica, the explosive phase is shifted to colder temperatures, where explosion is driven by fluid saturation (as indicated by the presence of highly vesiculated pumices), and the hotter, lava dome forming phase, where extrusion is driven by an influx of heat to the source (as indicated temperatures of enclaves; Howe et al. 2015).

CONCLUSION

The Layou ignimbrite and the Morne Trois Piton lava dome represent different phases of the caldera cycle for Dominica. With respect to these two deposits, the Layou ignimbrite erupted at cold temperatures and high water contents, which is consistent with its general, vesiculated morphology. The Morne Trois Piton lava dome erupted later at hotter pre-eruptive temperatures and lower total water contents. This suggests both a shallowing and a heating of the source. The likely source of the influx heat that mobilized the magma to for Morne Trois Piton are the abundant mafic enclaves, which contain a phenocryst assemblage that records elevated (>1000°C) temperatures. These results, combined with those from Wotten Waven caldera, suggests that the caldera cycle, as it applies to Domincia, consists of cold-explosive volcanism, followed by hot, effusive volcanism mobilized by a mafic injection (i.e., enclaves).

ACKNOWLEDGEMENTS

This material is based upon work supported by the Keck Geology Consortium and the National Science Foundation under Grant no. 1659322. I'd like to express my immense gratitude to Laura Waters and Holli Frey. This research would not have been possible without the generous support of the Keck Geology Consortium and Union College.

REFERENCES

Ghiorso, M.S. and Evans, B.W., 2008, Thermodynamics of Rhombohedral Oxide Solid Solutions and a Revision of the Fe-Ti Two-oxide Geothermometer and Oxygen-barometer: American Journal of Science, v. 208, p. 957 – 1039.

Grove, T.L., Elkins-Tanton, L.T., Parman, S.W., Chatterjee, N., Müntener, O., and Gaetani, G.A., 2003, Fractional crystallization and mantle-melting controls on calc-alkaline differentiation trends: Contributions to Mineralogy and Petrology, v. 145, doi: 10.1007/s00410-003-0448-z.

Howe, T.M., Lindsay, J.M., and Shane, P., 2015, Evolution of young andesitic-dacitic magmatic systems beneath Dominica, Lesser Antilles: Journal of Volcanology and Geothermal Research, v. 298. 69-88.

Lindsay, J.M., Smith, A.L., Roobol, M.J., and Stasiuk, M.V., 2005, Volcanic Hazard Atlas of the Lesser Antilles: Dominica: West Indies, Seismic Research Centre, 279 p.

Putirka, K.D., 2008, Thermometers and barometers for volcanic systems, in: Putirka, K. D., and Tepley, F. eds., Reviews in Mineralogy and Geochemistry vol. 69, p 61-120

Smith, R.L. & Bailey, R.A., 1968, Resurgent cauldrons, in Coats, R.R., Hay, R.L., and Anderson, C.A., eds., Studies in Volcanology: Geological Society of America Memoir, v. 116, p. 613-662.

Smith, A.L., Roobol, M.J., Mattioli, G.S. Fryxell, J.E., Daly, G.E., and Fernandez, L.A., 2013, The Volcanic Geology of the Mid-Arc Island of Dominica, Lesser Antilles: The Surface Expression of an Island-Arc Batholith: Boulder, Colorado, Geological Society of America Special Paper 496, 249 p.

Waters, L.E., and Lange, R.A., 2015, An updated calibration of the plagioclase-liquid hygrometer-thermometer applicable to basalts through rhyolites. American Mineralogist, 100: 2172-2184.

Zhang, Y., Xu, Z., Zhu, M., and Wang, H., 2007, Silicate melt properties and volcanic eruptions. Reviews of Geophysics 45, RG4004

KECK Geology Consortium
Learning Science Through Research
Published by Keck Geology Consortium

Short Contributions
Keck Geology Consortium
Volume 31
May 2018

A RE-EXAMINATION OF THE IGNIMBRITE AT FOND ST. JEAN, DOMINICA

NOLAN EBNER, Macalester College
Research Advisors: Holli Frey, Union College and Karl Wirth, Macalester College

INTRODUCTION AND PREVIOUS WORK

With nine potentially active volcanic centers and a history that includes some of the largest explosive eruptions in the Caribbean, the island of Dominica is widely regarded as being vulnerable to considerable volcanic hazards. Detailed knowledge of the frequency, magnitude, and distribution of volcanic eruptions is central to hazard assessment and risk mitigation on the island. Stratigraphic and geochemical fingerprinting of volcanic deposits is essential for unravelling the complex eruptive history of Dominica and understanding local volcanic hazards.

Past studies have identified five main ignimbrite depositing events on Dominica: Grand Savanne (22.2 ka; Sparks et al., 1980), Layou (79.7 ka ± 4.8 ka; Howe et al., 2014), Grand Bay (43 ka ± 13 ka; Frey et al., 2016), Roseau (29.343 ka ± 362 ka; Lindsay et al., 2005), and Grand Fond (27.6 ka ± 0.6 ka; Carey and Sigurdsson, 1980). An ignimbrite at Fond St. Jean (38.9 ka ± 0.4 ka; Lindsay et al., 2005) has previously been associated with the Grand Bay ignimbrite (Lindsay et al., 2003), however significant mineralogical differences and an intervening ridge call this supposition into question (Smith et al., 2013; Boudon et al., 2017) but a detailed study of Fond St. Jean has yet to be completed. Exposures of the Grand Bay ignimbrite, along the southern coast and approximately 1.5 km inland, reveal it as a massive 9-14 meter thick unconsolidated coarse grained deposit. In this study I address two main goals related to the ignimbrite at Fond St. Jean:

1. Provide a detailed characterization of the ignimbrite at Fond St. Jean.

2. Determine the nature of the relationship between the ignimbrites at Fond St. Jean and Grand Bay.

Below we describe new stratigraphic measurements, petrographic analyses, and mineral and whole rock geochemical data that indicate that the ignimbrites at Fond St. Jean and Grand Bay are significantly dissimilar as to suggest that they originated from separate eruptive events.

METHODS

Field

The study area focuses on the ignimbrite and immediately underlying stratigraphic units exposed at Fond St. Jean. We measured a section at Fond St. Jean using an improvised four meter long Jacob's staff. Descriptions of the ignimbrite build on the previous work of Lindsay et al. (2003), Lindsay et al. (2005), Smith et al. (2013), Howe et al. (2014), and Boudon et al. (2017).

For this study we collected samples of pumice, ash, and lithic fragments from the lowermost two meters of the section leaving the uppermost six meters of the vertical face unsampled. Sampled pumice clasts and lithic fragments ranged from 6 to 15 cm. Ash was scraped from the ignimbrite and sieved to < 2 mm.

Laboratory

Thin sections were prepared from the collected pumice samples. To establish mineral abundances 1500 grain point counts were done on thin sections from Fond St. Jean and Grand Bay. The remaining pumice, lithic, and ash samples were powdered for analysis of major and trace elements. In total, fifteen pumice clasts from Fond St. Jean and twenty-two pumice samples from Grand Bay were analyzed for major and minor elements. Trace element analysis was completed at Union College by ICP-MS following guidelines of the ICP-MS analytical facility (Hollocher, 2016). Major element analysis was completed at Acme Labs via ICP-OES.

SEM

We analyzed carbon coated thin sections of pumice taken from the lowermost two meters at Fond St. Jean and representative Grand Bay samples using a Zeiss EVO-MA15 Scanning Electron Microscope (SEM) at Union College and a JEOL JSM-6610LV SEM at Macalester College. Analyses focused on titanomagnetite, ilmenite, orthopyroxene, clinopyroxene, and plagioclase with slightly differing beam conditions for each group. For the oxide minerals, we used an accelerating voltage of 20 kV and beam current of 1.75 nA. Pyroxene, plagioclase, and glass were analyzed using 10 kV and 1.00 nA. Each grain analysis reflects the average of fifteen short (5-10 sec duration; from which we used V, Mn, Ni, Zn) and three long (45-50 sec; from which we used Si, Ti, Al, Fe, Mg, Ca) raster analyses. Sample analyses were corrected for beam drift using correction factors determined by comparison of measured and published values for Smithsonian mineral standards (Jarosweich et al. 1980) (Ilmenite, Roberts Victor Mine Garnet, Rockport Fayalite, Kakanui Augite, Natural Bridge Diopside, Plagioclase, Johnstown Hypersthene, Great Sitkin Island Anorthite) and Taylor mineral standards (V, Cr, Ni, Mn, Zn).

RESULTS

Field

The lowermost four meters of this section, beginning immediately on the southwestern side of town, are composed of six layers of largely matrix dominated block and ash flows with lithic clasts and volcanic bombs (1-50 cm in diameter). Overlying these are three, one-meter thick basalt flows that range in vesicularity from 5% (middle flow) to 50% (lower and upper flows). Above the basalt flows are thin ash laminations (< 0.2 m thick), which drape over blocks (40-50 cm) of the vesicular basalt from the underlying layer. A massive scoria deposit (<4 cm diameter clasts) spans the next two meters and is overlain by approximately 3 meters intensely weathered material. Above the weathered profile is four meters of reworked and largely unconsolidated volcanic materials.

The ignimbrite overlies the reworked materials on a sharp unconformable contact and spans 8 meters before being overwhelmed by vegetation. The ignimbrite can be divided into 8 horizons (A through H in ascending order; Figure 1). Beginning at the base of the ignimbrite (13 meters above the base of the section), Horizon A is a one meter thick clast-supported ignimbrite consisting of 75% pumice clasts (5-7 cm diameter) and 3-5% lithic clasts (< 1 cm diameter) in an ash matrix (20%). The final 0.2 m of the bed transitions to laminations of ash. Horizon B (1.2 meters thick) is similar to Horizon A, but the ash laminations constitute a greater thickness (0.4 m). Horizons C, B, and D all consist of pumice dominated ignimbrite followed by ash dominated ignimbrite but with varying thicknesses of each layer (Figure 1). Horizon E, is comprised of 0.6 m of pumice rich ignimbrite, however, it contains up to 10% lithic fragments and 65-70% pumice. Horizon F and horizon G are two additional expressions of pumice dominated ignimbrite followed by an ash dominated layer. Horizon F is 0.8 m of ignimbrite with 75% pumice clasts and 3-5% lithic clasts (less than the previous horizons).

Petrographic Analysis

An analysis of four thin sections of representative samples from the lowermost two meters of ignimbrite at Fond St. Jean (Figure 2A) consist mostly of glass (63%), with minor vesicles (20%) and mineral grains (17%). Mineral abundances at Fond St. Jean, renormalized to exclude glass and vesicles, include 80% plagioclase, 8% orthopyroxene, 2%

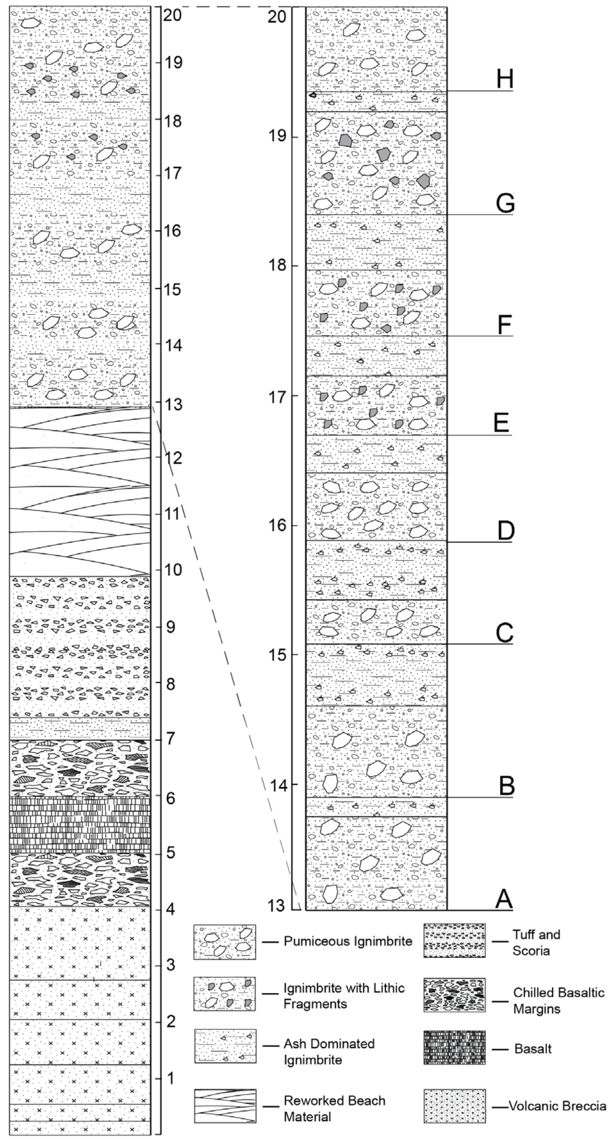

Figure 1. Stratigraphic column of exposed volcanic materials at Fond St. Jean (left). Exposed in the uppermost 7 meters of the section (13-20 m above base), the ignimbrite at Fond St. Jean (enlarged on the right), consists mostly of reversely graded beds composed of pumice clasts, lithic clasts, and ash.

clinopyroxene, 6% Fe-Ti oxides, and 4% hornblende. Four thin sections from Grand Bay (Figure 2B) were examined and consist on average of 63% glass, 10% vesicles, and 27% crystal grains. At Grand Bay, mineral re-normalized mineral abundances are 81% plagioclase, 11% orthopyroxene, 4% clinopyroxene, 4% and Fe-Ti oxides.

Mineral Compositions

Plagioclase phenocrysts (n=10) from Fond St. Jean have compositions that vary in anorthite content

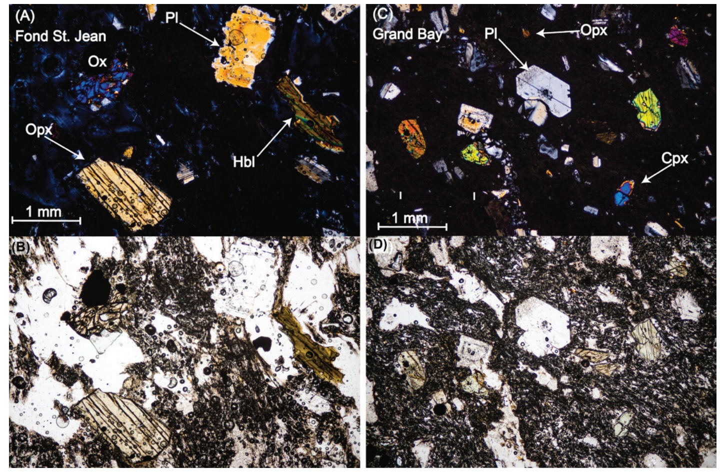

Figure 2. Photomicrographs of cross polarized (A and C) and plain (B and D) of ignimbrite from Fond St. Jean (A and B) and Grand Bay (C and D) showing plagioclase (Pl), orthopyroxene (Opx), clinopyroxene (Cpx), and oxides (Ox) in samples from both localities, in addition to hornblende (Hbl) at Fond St. Jean. Samples from Fond St. Jean are more vesicular and less crystal rich than those from Grand Bay.

(An_{57-78}). The cores of phenocrysts average An_{58-72} and are generally more calcic than the rims (An_{58-78}), indicating normal, although oscillatory, zoning. In contrast, Fond St. Jean pyroxene phenocrysts from four samples do not show evidence of compositional zonation; orthopyroxene compositions average Wo_2 En_{55} Fs_{42} and clinopyroxene averages Wo_{44} En_{38} Fs_{18}. Magnetite phenocrysts from Fond St. Jean pumice clasts (n=5) average 77.65 wt% FeO^t and 10.98% wt% TiO_2, and ilmenite compositions average 47.56 wt% FeOt and 46.20 wt% TiO_2. Plagioclase phenocrysts (n=10) from Grand Bay ignimbrite have core compositions that average An_{51-88} and are generally more calcic than the rims (An_{52-68}), indicating generally normal zoning. Grand Bay orthopyroxene compositions averaged from four samples are Wo_2 En_{55} Fs_{42}; clinopyroxene averages Wo_{43} En_{38} Fs_{19}. Magnetite phenocrysts from Grand Bay pumice clasts have average compositions (n=6) of 79.49% FeO^t and 10.04% TiO_2; ilmenite compositions average 48.97% FeO^t and 46.49% TiO_2.

Whole Rock Geochemistry

Whole rock analyses of Fond St. Jean pumice clasts (n=15) form high (63.0 to 64.5 wt% SiO_2) and low (60.5 to 62% wt% SiO_2) clusters based on silica content (Figure 3). Fond St. Jean samples also show higher wt% K_2O (1.7%) and Al_2O_3 (18.0%), and lower wt% $Fe_2O_3^t$ (5.5%), MgO (1.7%), Na_2O (3.1%), and

TiO_2 (0.5%) than samples from Grand Bay. Lithic clasts have greater amounts of MgO (4.5%) relative to ash (2.5%), pumice clasts (1.5%), and pumice glass (0.2%). Lithic clasts and ash are basaltic (49-51% wt % SiO_2), while glass from pumice clasts is rhyolitic (75-76% wt % SiO_2) (Figure 5A). Trace element compositions (e.g., Rb, Zr, REE) do not exhibit the same bimodal clustering demonstrated by silica and some major elements and in general are less enriched in incompatible trace elements compared to Grand Bay (Figure 5B and 5C). The REE patterns of Fond St. Jean pumice are LREE-enriched, have a distinct negative Eu anomalies (Eu/Eu* = 0.70-0.90), and have spoon-shaped HREEs.

Whole rock analyses of Grand Bay pumice clasts (n=22) exhibit more limited silica contents (61.2 to 63.4 wt % SiO_2), higher wt% $Fe_2O_3^t$ (6.3%), MgO (2.3%), Na_2O (3.4%), and TiO_2 (0.5%), and lower wt% K_2O (1.5%) and Al_2O_3 (16.8%) when compared with Fond St. Jean samples (Figure 3A-F). In general, incompatible trace elements are more enriched in ignimbrite samples from Fond St. Jean compared with Grand Bay (Figure 5B, 5C). Ash has greater amounts of MgO (3.2%) relative to pumice clasts (2.2%) and pumice glass (0.05%), however, ash is basaltic andesitic in composition (56% wt % SiO_2), whereas pumice glass is rhyolitic (79-80% wt % SiO_2)(Figure 5A). Grand Bay pumice samples have LREE-enriched patterns similar to Fond St. Jean, but with less negative Eu anomalies (Eu/Eu* = 0.82-0.95).

DISCUSSION AND CONCLUSIONS

Ignimbrite deposits across Dominica can be difficult to compare because of the relative homogeneity of their stratigraphic and geochemical signatures. However, Lindsay et al. (2003) described differences between the ignimbrites at Fond St. Jean and Grand Bay when he suggested the Fond St. Jean ignimbrite to be the result of a more evolved magmatic system than Grand Bay. Recent work (Smith et al., 2003; Boudon et al., 2003) has called this association into question, though no detailed studies have been conducted aside from this one. Our results advance the calls for disassociation based on in depth stratigraphic and geochemical disparities.

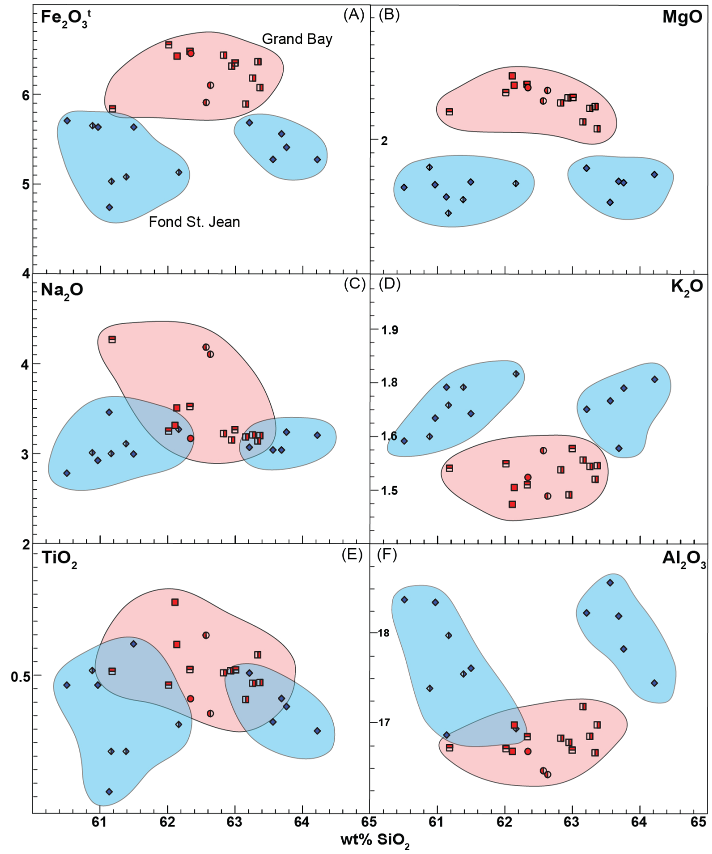

Figure 3. Major element Harker plots of Fond St. Jean (blue diamonds and shading) and Grand Bay (red squares and shading) pumice clasts. Note, at Fond St. Jean silica clusters tend not to correlate with changes in other major element concentrations.

If the ignimbrite at Fond St. Jean is a lateral equivalent of the Grand Bay ignimbrite, then the two should share common stratigraphic features, with some dissimilarities owed to distance from source. However, stratigraphic evidence from this study suggests there is little to no resemblance between the ignimbrites at Fond St. Jean and Grand Bay. At Fond St. Jean, normally graded ignimbrite beds of pumice clasts, lithic clasts, and ash are evidence of pulsating magmatism (Figure 1). In contrast, the massive and unsorted nature of both outcrops of the Grand Bay ignimbrite suggest a single large eruptive event.

If the ignimbrites at Fond St. Jean and Grand Bay were erupted from the same magma chamber and during the same event, then minerals in both should share similar growth conditions and histories. Although samples from both ignimbrites contain similar amounts of glass (62-63%), Fond St. Jean samples were more vesicular (19.7% versus 9.6%, respectively) and less

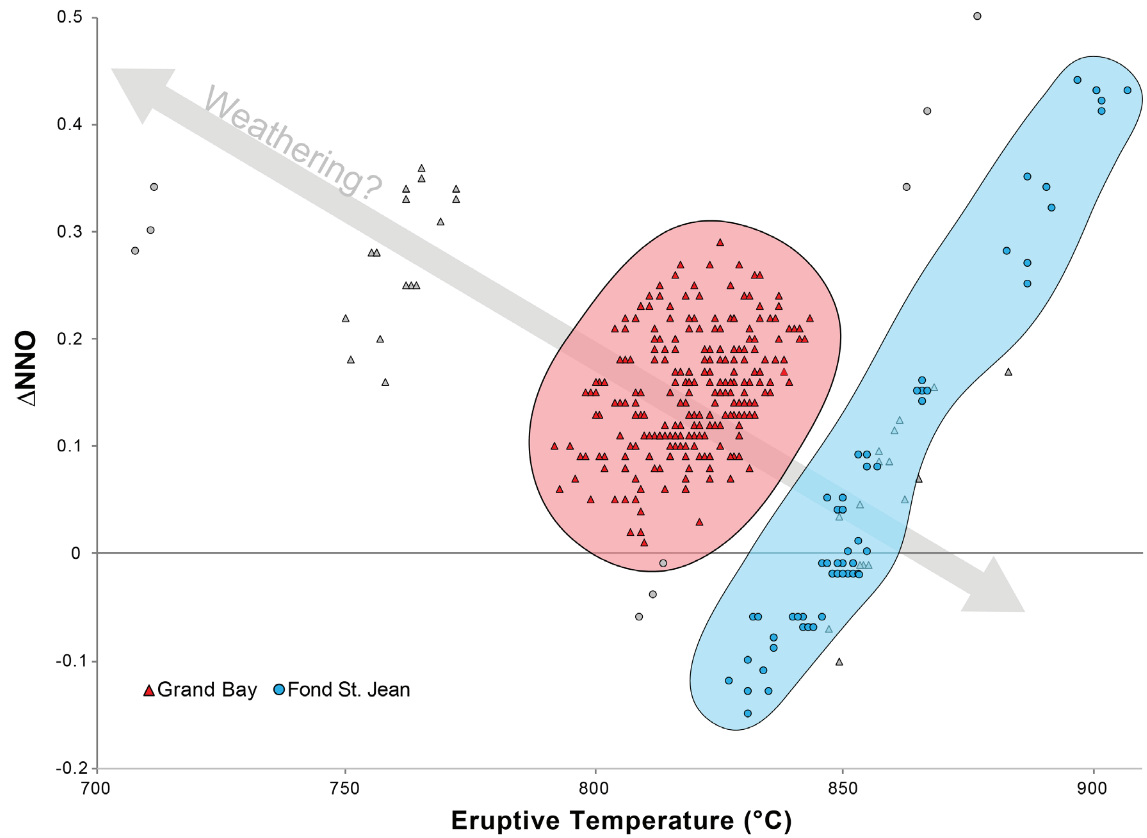

Figure 4. Clusters of magnetite-ilmenite derived eruptive temperatures from pumice samples of Fond St. Jean (blue) and Grand Bay (red). Mineral pairs from Fond St. Jean display an average temperature of 860 ± 21 °C (ΔNNO = 0.07), while those from Grand Bay average 822 + 13 °C (ΔNNO = 0.15). Oxide pairs that did not pass the Bacon and Hirschmann test of equilibrium (1988) (gray) were not included in average values.

crystal rich (17% versus 27%, respectively) than those from Grand Bay. While mineral phases and abundances are roughly similar, the ubiquitous presence of amphibole at Fond St. Jean is distinct given its total absence in Grand Bay pumice clasts. Plagioclase crystals at both localities exhibit oscillatory zoning and anorthite compositions (An_{57-78} versus An_{51-88}, respectively) with significant overlap between Fond St. Jean and Grand Bay samples, and so do not illuminate the relationship between these two ignimbrites. Pyroxene and oxide compositions are also not helpful in this regard. The similar mineral compositions of the two ignimbrites suggest that even if deposits resulted from different eruptions, then they were likely derived from similar magmatic sources and processes.

Another valuable tool in distinguishing igneous deposits is two-oxide geothermobarometry, which we can use to infer temperature and oxygen fugacity relative to the nickel-nickel oxide buffer (ΔNNO) during mineral growth. Geothermobarometry performed on 74 magnetite-ilmenite pairs from Fond St. Jean display an average temperature of 860 ± 21 °C (ΔNNO = 0.07) ranging from 830 °C to 915 °C (ΔNNO = -0.14 to 0.44) (Figure 4). Fe-Ti pairs that did not pass the Bacon and Hirschmann test of equilibrium (1988) were not included in average values of temperature or fugacity (Figure 4). Temperatures derived from 291 magnetite-ilmenite pairs from Grand Bay average 822 + 13°C (ΔNNO = 0.15) trending from 792 °C to 844 °C (ΔNNO = 0.01 to 0.29). While both Fond St. Jean oxide pairs exhibit a positive trend in temperature and oxygen fugacity, temperatures at Fond St. Jean were notably higher than those from Grand Bay.

Plagioclase hygrometry, using the method of Waters and Lange (2015), allows insight into water contents of the source magma. Hygrometry reveals slightly drier magmatic conditions at Fond St. Jean (7.3 to 7.1

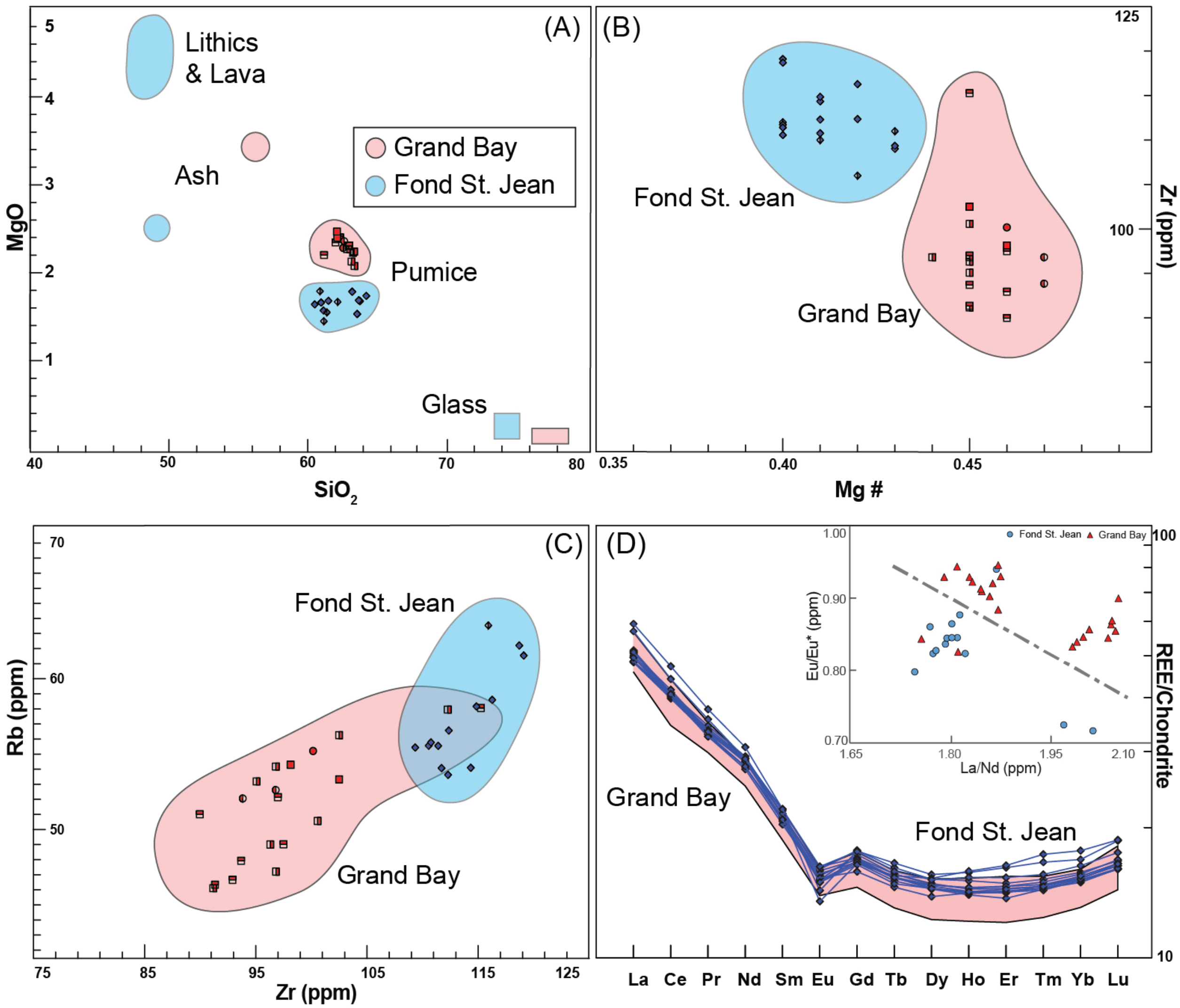

Figure 5. Whole rock geochemistry on ash, pumice and lithic clasts, and glass reveal separate groupings between Grand Bay and Fond St. Jean (A). Fond St. Jean has lower Mg #s ([Mg]/[Mg + Fe+2]) and higher amounts of Zr relative to Grand Bay (B), as well as generally greater concentrations of Rb and Zr (C). REE elements show similar patterns between the two ignimbrites (D) though Fond St. Jean samples exhibit generally lower La/Nd and lower Eu anomalies than those from Grand Bay (Eu/Eu = 0.7 to 0.9 and 0.82 to 0.95, respectively) at a given concentration of La/Nd (D inset).*

wt % H_2O) compared to those at Grand Bay (7.8 to 7.3 wt % H_2O). However, these differences are slight and may not be significant given the relatively large errors in these measurements. Interestingly, the drier conditions implied by hygrometry for Fond St. Jean, relative to Grand Bay, seem counterintuitive given the presence of amphibole at Fond St. Jean.

Whole rock geochemistry reveals that the ignimbrites at Fond St. John and Grand Bay have distinct chemical fingerprints. Where Fond St. Jean samples exhibit high and low silica components, those from Grand Bay plot as a single intermediate group. Furthermore, Fond St. Jean pumice glass compositions are less siliceous than those from Grand Bay (75-76% and 79-80% wt % SiO_2, respectively), and so must come from different magmatic sources. Overall, Fond St. Jean samples are less enriched in compatible major elements (e.g., $Fe_2O_3^t$ and MgO; Figure 3) suggesting that it was derived from a more evolved magmatic system. Analyses of incompatible trace elements (e.g., Zr, Rb) reveal a similar story; Fond St. Jean pumice samples consistently exhibit higher incompatible trace element abundances at a given Mg # (Figure 5B, 5C). REE patterns are very similar between the Fond St. Jean and Grand Bay ignimbrites, however, Fond

St. Jean samples generally exhibit lower La/Nd and more negative Eu anomalies (Eu/Eu* = 0.7 to 0.9 and 0.82 to 0.95, respectively) at a given level of LREE enrichment (Figure 5D). The lower Eu abundances at Fond St. Jean could be the result of greater plagioclase fractionation, either during melting in the source or during crystallization in a magma chamber, or to varying degrees of crustal contamination.

In summary, significant differences in stratigraphy, mineralogy, mineral chemistry, and whole-rock compositions suggest that the similarly aged ignimbrites at Fond St. Jean and Grand Bay likely stem from different eruptive events. However, similarities in mineral abundances and compositions do not preclude derivation of these two ignimbrites from different batches of magma at a shared volcanic source. Disassociation of these two ignimbrites also calls into question whether other ignimbrites along the southeastern coast (e.g., Petit Savane; Boudon et al., 2017) might also represent additional eruptive events. If an inland, more proximal, expression of the Fond St. Jean ignimbrite can be located, it might help to further illuminate the origin of this eruption.

ACKNOWLEDGEMENTS

This material is based upon work supported by the Keck Geology Consortium and the National Science Foundation under Grant No. 1659322. Thank you to Holli Frey and Karl Wirth for your guidance and enthusiasm every step of the way. Many thanks to Laura Waters, Amanda Schmidt, and Pat Joseph for your help on Dominica and beyond. This project could not have been completed without the assistance and support of Jeff Thole, Matthew Manon, Bill Neubeck, all of my Keck peers, and of course the staff of the Archbold Tropical Research and Education Center in Dominica.

REFERENCES

Bacon, C.R., and Hirschmann, M.M., 1988, Mg/Mn Partitioning As a Test for Equilibrium between Coexisting Fe-Ti Oxides. American Mineralogist, 73(1-2), 1-200.

Boudon, G., Balcone-Boissard, H., Solaro, C., and Martel, C., 2017, Revised chronostratigraphy of recurrent ignimbritic eruptions in Dominica (Lesser antilles arc): Implications on the behavior of the magma plumbing system. Journal of Volcanology and Geothermal Research, 343, 135-154. doi:10.1016/j.jvolgeores.2017.06.022

Carey, S.N., and Sigurdsson, H., 1980, The Roseau ash: deep-sea tephra deposits from a major eruption on Dominica, Lesser Antilles arc. Journal of Volcanology and Geothermal Research 7: 67–86.

Frey, H.M., Manon, M.R.F., Brehm, S., Babiak, R., 2016, The U-Th zircon chornology revelas protracted cold storage and subsequent rejuvenation in magma reservoirs beneath Dominica, Lesser Antilles, Abstract [V53D-315] presented at the 2016 Fall Meeting, AGU, San Francisco, Calif., 12-16 Dec.

Ghiorso, M.S., and Evans, B.W., 2008, Thermodynamics of rhombohedral oxide solid solutions and a revision of the Fe-Ti two-oxide geothermometer and oxygen-barometer. American Journal of Science, 308(9), 957-1039. doi:10.2475/09.2008.01

Hollocher, K., 2016, ICP-MS Analytical Facility, Retrieved on 3/19/2018 from http://minerva.union.edu/hollochk/icp-ms/index.html

Howe, T.M., Lindsay, J.M., Shane, P., Schmitt, A.K., and Stockli, D.F., 2014, Re-evaluation of the Roseau Tuff eruptive sequence and other Ignimbrites in Dominica, Lesser Antilles. Journal of Quaternary Science 29(6): 531–546.

Jarosewich, E., Nelen, J.A., and Norbers, J.A., 1980, Reference Samples for Electron Microprobe Analysis. Geostandards Newsletter, 4(1), 43-47. doi:10.1007/s00445-002-0253-y

Lindsay, J., Stasiuk, M., & Shepherd, J., 2003, Geological history and potential hazards of the late-Pleistocene to recent plat pays volcanic complex, Dominica, Lesser Antilles. Bulletin of Volcanology, 65(2-3), 201-220. doi:10.1007/s00445-002-0253-y

Lindsay, J.M., Smith, A.L., Roobol, M.J., and Stasiuk, M.V., 2005, Dominica: Volcanic Hazards of the Lesser Antilles. Seismic Research Unit, The University of the West Indies, Trinidad and Tobago.

Smith, A., Roobol, M.J., Mattioli, G., Fryxell, J., Daly, G., Fernandez, L.A., 2013, The Volcanic Geology of the Mid-Arc Island of Dominica, Lesser Antilles—The Surface Expression of an Island-Arc Batholith. Special Paper of the Geological Society of America. 496. 249. 10.1130/2013.2496.

Union College ICP-MS Analytical Facility. Retrevied on 3/19/18 from http://minerva.union.edu/hollochk/icp-ms/index.html

Waters, L. E., & Lange, R. A., 2015, An updated calibration of the plagioclase-liquid hygrometer-thermometer applicable to basalts through rhyolites. American Mineralogist, 100(10), 2172-2184. DOI: 10.2138/am-2015-5232.

KECK Geology Consortium

Learning Science Through Research

Published by Keck Geology Consortium

Short Contributions
Keck Geology Consortium
Volume 31
May 2018

MAGMATIC ENCLAVES AND MAGMA MIXING IN MORNE MICOTRIN, DOMINICA

SARAH HICKERNELL, Union College
Research Advisor: Holli Frey

INTRODUCTION

Morne Micotrin in Dominica, Lesser Antilles is an andesitic lava dome located on the northeastern margin of the Wotten Waven caldera, an active geothermal area (Smith et al., 2013). Micotrin is comprised of two coalesced domes, formed within 3.5 km diameter craters. Located at the head of the 8 km Roseau Valley, Wotten Waven and Micotrin are the most likely source for the ~3 km^3 of pyroclastic deposits filling the valley (Sigurdsson, 1972). Dominica's capital city Roseau, with a population of 17,000, sits at the bottom of this valley. A series of explosive eruptions formed the Roseau Sequence between 20 and 70 ka, with a ~6 ka deposit at Casso being the youngest dated (Howe et al., 2014; Frey et al., 2016). Block-and-ash flows from Micotrin near the top of the Roseau Sequence suggests that major period of dome growth occurred following explosive eruption (Smith et al., 2013). Micotrin last erupted explosively approximately 1 ka, and therefore poses a risk to the adjacent valley and island of Dominica as a whole (Lindsay et al., 2005). Shallow seismicity in Wotten Waven and volcanic earthquakes beneath Micotrin suggest that the magmatic system that initially formed Micotrin is still active at depth. Further, warm streams flowing down the dome's eastern flank stain their banks orange, suggesting geothermal springs may be feeding streams at higher elevations (Lindsay et al., 2005).

The presence of mafic enclaves has been documented in Dominica at several lava domes, and suggests that magma mixing and mingling processes at depth are shaping the evolution of the lava domes (Howe et al., 2015; Halama et al., 2006). Mafic enclaves, volumes of compositionally unique magma emplaced into a host, are evidence of mafic injection into a silicic system. Mafic injections introduce volatiles, heat, and pressure, and push the magmatic system out of equilibrium. Injections can therefore be eruption triggers, and by studying enclaves one can determine the extent of disequilibrium caused by mafic injection. Enclaves give insight into the nature of the mafic magma, and comparison to the host can allow one to reconstruct how the mafic magma impacted the silicic host. During the Soufriere Hills eruption in nearby Montserrat from 1995 until 2012, several types of mafic enclaves were documented in the host andesite, and their characteristics were studied to help reconstruct the nature of the magma chamber, and the ultimate source feeding the eruption (Plail et al., 2014; Barclay et al., 2010; Mann et al., 2010). Additionally, the increase in abundance of mafic enclaves has been correlated to an increase in intensity of the eruption event, supporting the idea that injections at depth are keeping the system active (Barclay et al., 2010). Considering its geographic proximity to Dominica and the ability to continuously monitor this modern eruption, Soufriere Hills serves as a functional analog for the magmatic systems beneath Dominica.

Through this study, we aim to better understand the magmatic system beneath Dominica and understand eruption triggers by characterizing the mafic enclaves found in the host rock of Morne Micotrin. Two main types of enclaves, coarse-grained and fine-grained, can be found in Micotrin, and these enclave types differ significantly from the host rock as well as from one another. Relatively large-scale characteristics, including mineral assemblage, vesicles, boundaries, and reactions, as well as finer-scale characteristics, including individual mineral zoning and whole rock, phenocryst, and glass compositions, have been thoroughly examined to help determine the nature of the differing magmas.

METHODS

We sampled a quarry on the western flank of Micotrin, based on the availability of relatively fresh, unweathered rock and abundance of enclaves observed at this site during past visits. Several samples of each enclave type were collected to determine the extent of variability amongst enclaves.

Following fieldwork, sample preparation was conducted at Union College in Schenectady, NY. After cutting down the samples, rock powders were made by placing the samples into a hydraulic press and then powdered by agitation in a Spex 15 cm aluminum oxide puck mill. The powders were sent to Acme Labs in Vancouver, Canada for ICP-OES analysis of major elements. Trace elements were analyzed at Union College on an ICP-MS using 200 mg powdered samples. The powders were dissolved and analyzed by the procedure outlined in Hollocher et al. (2007). The major element compositions of plagioclase, pyroxenes, oxides, and glass were analyzed with a Zeiss EVO MA15 using energy-dispersive spectroscopy (EDS). Back-scattered electron (BSE) imagery was utilized to image and observe zonation patterns in individual phenocrysts, whereas EDS was utilized for quantitative analyses. Pyroxenes and oxides were analyzed using a 5 um beam spot. Oxides were standardized on spinel for Mg and Al, rutile for Ti, hematite for Fe, and spessartine for Si, Ca, and Mn. For plagioclase, we used a 100 µm rastered beam and standardized on PX69 for Mg and Si, GKFS for K, amilia albite for Na, and grossular for Al and Ca. Pyroxenes were standardized on grossular for Al and Ca, PX69 for Si and Mg, hede for Fe and Mn, acmite for Na, and GKFS for K.

To calculate melt temperatures, we used all possible pairs of Fe-Ti oxides and the geothermometer of Ghiorso and Evans (2008). To determine water content we utilized a plagioclase hygrometer, which requires the input of the average melt temperature, whole melt/rock composition, and highest anorthite content plagioclase (Waters and Lange, 2015).

RESULTS

Petrography

Mineral abundances were determined by point counting five different enclaves (500-1000 points, depending on enclave size). Fine-grained enclaves contain 50.6% plagioclase, 10.9% opx, 6.6% cpx, 6.8% oxides, 5.3% quartz, 17.2% vesicles, and 2.5% microlites. Coarse-grained enclaves contain 52.5% plagioclase, 10.7% opx, 0.5% cpx, 8.4% oxides, 2.2% quartz, 13.7% vesicles, and 11.8% microlites. Fine-grained enclave pyroxenes tend to grow outward from inner nucleation points, and average 0.01-0.02 cm. Fine-grained enclave plagioclase average 0.05, with larger phenocrysts up to 0.1 cm. Coarse-grained enclave pyroxenes tend average 0.05 cm in size, whereas plagioclase average 0.1 cm.

Fine-grained enclave boundaries are quite distinct. The host contains a relatively dark, fine-grained matrix that is absent in the enclaves. Coarse-grained enclave boundaries can be sharp to diffuse, which may be due in part to the large size of the phenocrysts obscuring the transition. Both enclave types are more vesicular than the host, however the coarse-grained enclaves tend to be notably more vesicular than the fine-grained enclaves (Figure 1). It does not appear that there is extensive transfer of material between the enclaves and the host based on observation of phenocryst textures.

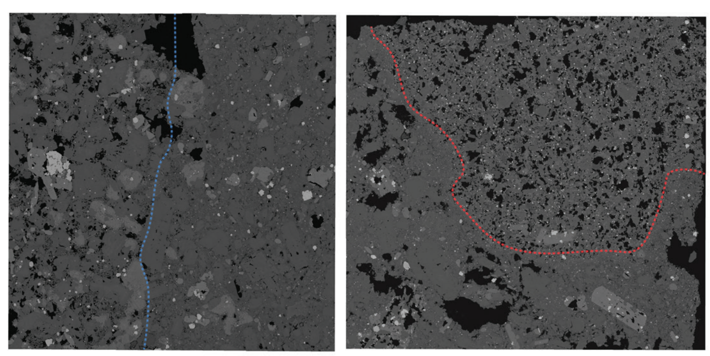

Figure 1. Back-scattered electron maps of a coarse-grained enclave (left) and fine-grained enclave (right). The dotted lines indicate the boundaries between enclave and host. Note the high vesicularity and lack of matrix in the enclaves. Coarse-grained enclave field of view ~1 cm, fine-grained enclave field of view ~1.3 cm.

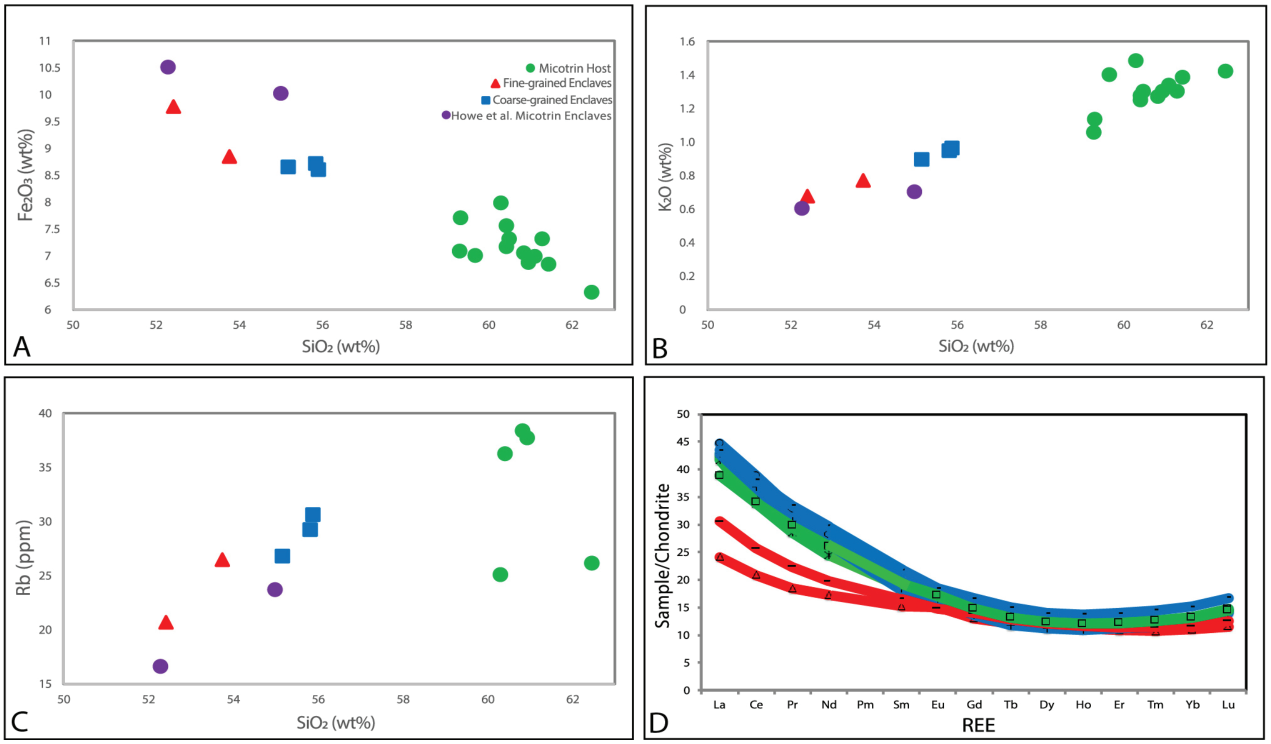

Figure 2. Morne Micotrin whole rock geochemistry. Major elements (A and B), trace elements (C) and rare earth elements (D) were analyzed to determine compositional differences between the two enclave types and the host.

Bulk Chemistry

Major element analysis reveals that both the fine-grained enclaves (52-54 wt% SiO_2) and the coarse-grained enclaves (55-56 wt% SiO_2) are more mafic than the host andesite (59-62 wt% SiO_2). Enclaves are relatively enriched in Fe, Mg, and Ca. The enclaves are relatively depleted in K. Al and Na abundances are comparable across both enclaves and the host. The fine-grained enclaves differ most compositionally from the host, with the coarse-grained enclaves tending to plot as an intermediate (Figure 2).

The enclaves are depleted in some trace elements compared to the host, including Rb, Ba, and Sr. Other elements, including Zr, show little to no difference in concentration across the enclave types and host (Figure 2).

Rare earth element concentrations relative to chondrite were plotted to determine possible genetic relationships between the enclaves and the host. The coarse-grained enclaves' and host's trends are nearly parallel, whereas the fine-grained enclaves' trend dips in the light REE (Figure 2).

Plagioclase

Plagioclase phenocrysts in the host, as well as the enclaves, exhibit dark rims of grainy-looking, very small inclusions. In some samples, this texture occurs in rims around the core of the phenocryst, whereas in others this texture is extensive throughout the crystal. Under BSE, this texture appears to be inclusions or reaction phases that are too small for individual analysis.

Plagioclase phenocrysts in coarse-grained enclaves are normally- and reversely-zoned, and range from approximately An_{45-88} with some outliers (Figure 3). Several plagioclase rims in coarse-grained enclaves have a potassic component, up to 10 weight% orthoclase (Figure 4). Fine-grained enclave plagioclase phenocrysts also appear both normally- and reversely-zoned, and range from An_{48-94} (Figure 3). Some plagioclase rims were quite potassic in the fine-grained enclaves, up to 42 weight% orthoclase (Figure 4). The host plagioclase is normally- and reversely-zoned and has comparable average anorthite compositions, however the host lacks orthoclase rims. Additionally, the host plagioclase has lower maximum anorthite content (An77) than both enclave types (Figure 4).

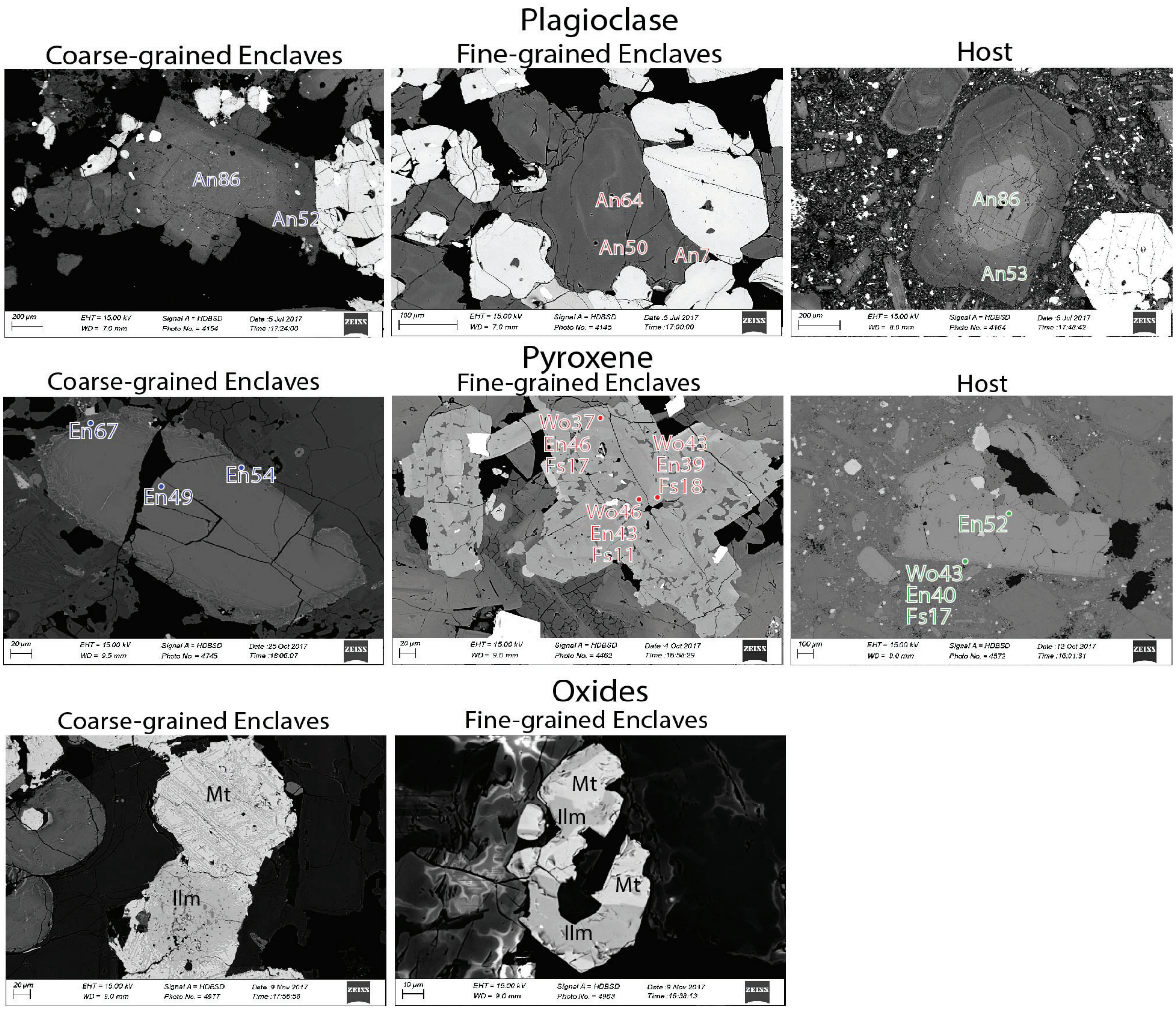

Figure 3. Characteristic back-scattered electron images of typical phases in each enclave type and the host showing zoning and example compositions.

Pyroxene

Pyroxene in the host is reversely- and normally-zoned, with compositionally distinct cores and rims. Both enclave types are more complex, with frequent patchy and oscillatory zoning throughout the pyroxene phenocrysts (Figure 3). Clinopyroxene is quite scarce in coarse-grained enclaves, occurring primarily as rims on orthopyroxenes. Mg-rich rims are abundant in both enclave types, as phenocrysts are commonly reversely zoned. Fine-grained enclave pyroxene cores tend to be Ca-enriched relative to coarse-grained enclave pyroxenes, and clinopyroxene is much more abundant in fine-grained enclaves than in coarse-grained. Mg-rich rims are common in fine-grained enclaves as well, however Fe-rich rims also occur (Figure 5). The host pyroxene compositions are relatively tightly clustered relative to the enclaves, and have similar compositional ranges to the enclaves (En_{50-70})(Figure 5).

Oxides

Oxides in both enclave types occur as magnetite and ilmenite, and are relatively titanium-enriched. The enclave oxides are highly exsolved, particularly in the coarse-grained enclaves (Figure 3). Oxides occur as independent phases as well as inclusions, particularly in pyroxenes. The high degree of exsolution in the enclave oxides led to a relatively high degree of analytical uncertainty. In comparison, the host oxides are far less exsolved and yield more reliable analyses.

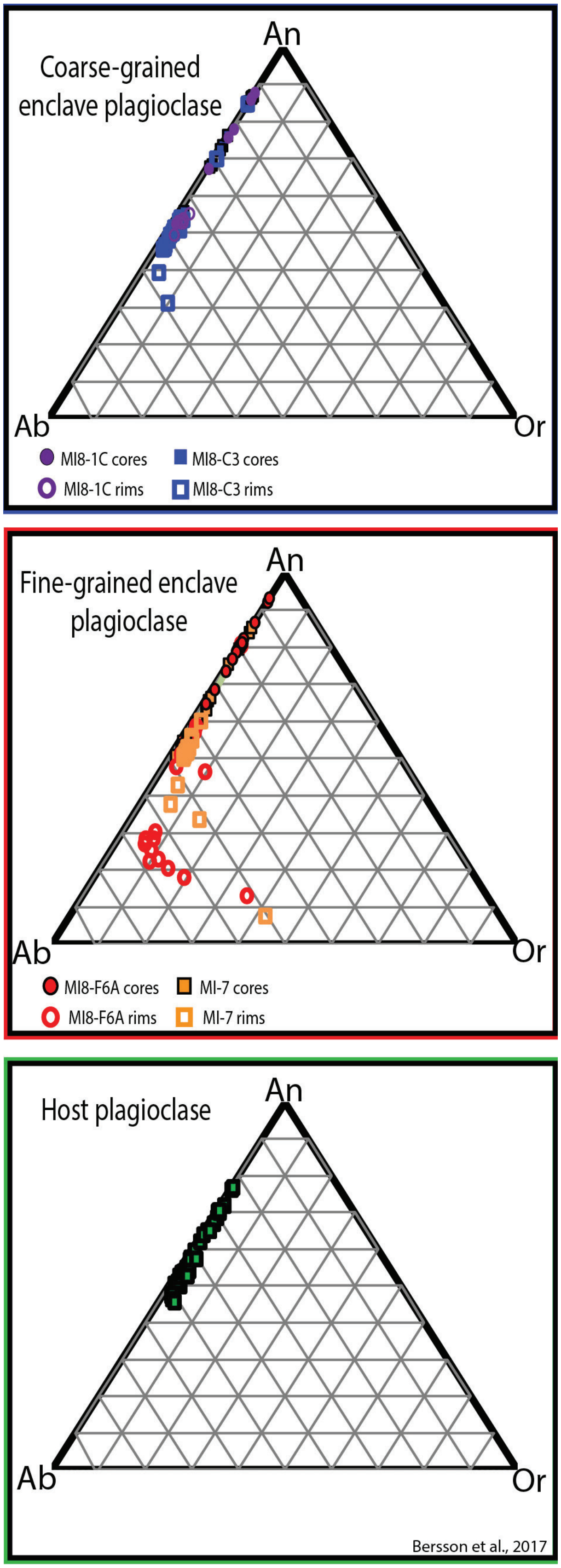

Figure 4. Plagioclase ternaries for feldspar phenocrysts analyzed in both enclave types and the host. Note the lack of potassium-rich analyses in the host relative to the enclaves.

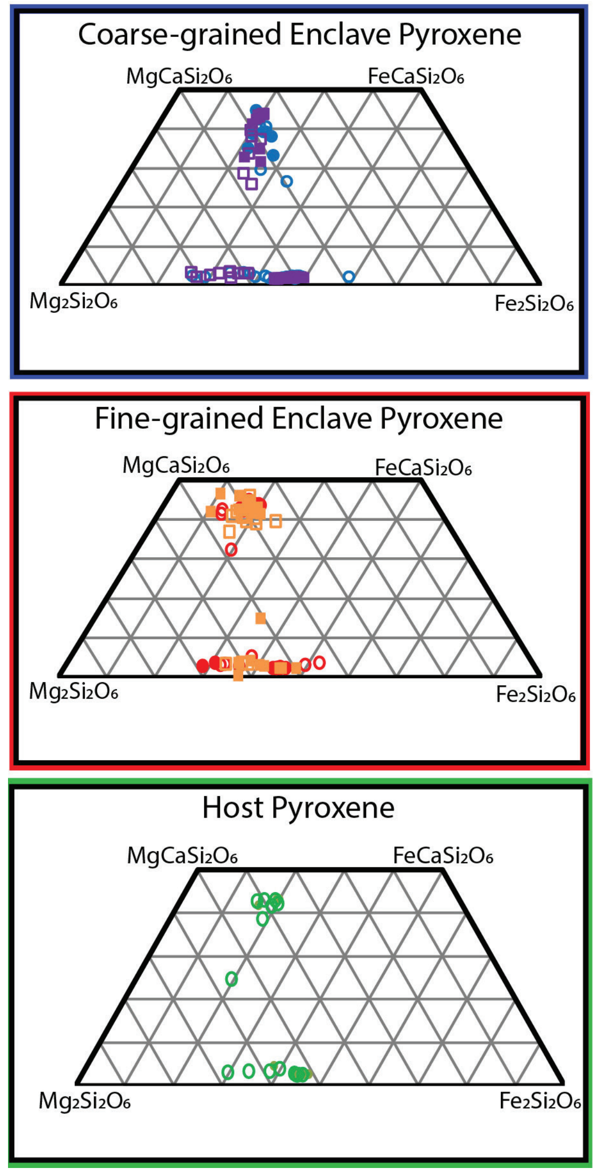

Figure 5. Pyroxene quadrilaterals for pyroxene phenocrysts analyzed in both enclave types and the host. Note the Mg-rich rims and the wide spread in the enclave data relative to the host.

Calculation of Intensive variables: Geothermometry and Hygrometer

Magnetite and ilmenite were targeted in both enclave types and the host to employ a two-oxide geothermometer (Ghiorso and Evans, 2008) for reconstruction of melt temperatures and oxygen fugacity. The coarse-grained enclaves yield temperatures of 890 ± 91°C and 774 ± 168°C. Coarse-grained enclaves yield fO_2 values of 1.00 ± 0.23 and 1.49 ± 1.22 relative to ΔNNO. Fine-grained enclaves yield temperatures of 891 ± 74°C and 794 ± 60°C, and fO_2 values of 0.42 ± 0.23 and 0.60 ± 0.21 relative to ΔNNO. In comparison, the host oxides yield a temperature of 851 ± 24°C and average fO_2 of 0.30 ± 0.15 relative to ΔNNO (Bersson et al., 2018).

Based on the highest anorthite plagioclase in each sample type, a plagioclase hygrometer was utilized to determine the water content of the melt. Coarse-grained enclaves contain up to 10 weight% H_2O and fine-grained enclaves contain up to 9.7 weight% H_2O, whereas the host contains up to 6.4 weight% H_2O (Waters and Lange, 2015).

DISCUSSION

Major element analysis of both enclave types and the host reveals that the enclaves differ compositionally from the host andesite in several major and trace elements. Major element compositions tend to have linear trends, with the fine-grained enclaves being most dissimilar from the host (Figure 2). Enclave compositions are also comparable to enclaves analyzed from other volcanic centers on Dominica (Howe et al., 2015; Halama et al., 2006). When comparing REE to chondrite, we find that coarse-grained enclaves and the host plot similarly, suggesting a process such as fractional crystallization could account for the differences observed (Figure 2). However, the fine-grained enclaves' plot is not parallel to the host and coarse-grained enclave. This suggests that another mechanism must be considered to account for the fine-grained enclaves, such as a higher degree of partial melt. Fractional crystallization alone cannot account for the trend differences observed.

The plagioclase compositions from both enclave types to the host is comparable ($An_{45} – An_{80}$), however the compositions in the enclaves reach higher anorthite contents than the host (up to An_{94}). Additionally, the potassic rims observed in the enclaves is absent in the host (Figure 4). The trend of the feldspar compositions in each enclave type generally follows the plagioclase solvus. This suggests that the enclaves may have a unique thermal history relative to the host. The enclave plagioclase was in a melt for a longer period of time than the host, allowing K into the crystal structure. Therefore, the source of the enclaves and their melt may be unique relative to the host as well. Further, both enclave types have higher water content than the host based on plagioclase hygrometery (Waters and Lange, 2015). The higher water content in the enclaves suggests that when a mafic injection occurred, forming these enclaves, it also introduced a greater concentration of water. Water is an important volatile in volcanic systems, and its introduction may have caused unrest in Micotrin and potentially triggered eruption.

Pyroxene rims in both enclave types are Mg-rich, and the reverse zoning commonly observed may be insight into how mafic injections changed the melt in Micotrin over time. Injections would have introduced more magnesium into the system, which could then be preferentially incorporated into pyroxene rims. This trend is observed in the host as well, but to a lesser degree. Further, the cpx compositions in the enclave vary widely, with 20% wollastonite variation (Figure 5). The host is more tightly-clustered in comparison. This suggests that the enclaves may have been experiencing changing melt conditions over time, whereas the host melt was relatively consistent.

The temperatures obtained from two oxide geothermometry have a high level of error associated with them, and therefore a more robust estimate on the temperatures of both enclave types' melts is desirable. However, based on fO_2 data, it appears that weathering and oxidation plays a greater role in the enclave oxides and their exsolution than in the host.

Based on the data compiled in this study, it is apparent that the enclaves have a unique history relative to the host. The fine-grained enclaves cannot be related to the coarse-grained enclaves or the host by fractional crystallization alone, and supports an open-system model of the magma chamber underlying Morne Micotrin. Additionally, potassic plagioclase rims in both enclave types suggests that both enclave types have undergone heating and dynamic magma chamber conditions to a greater degree than the host. The heating that the enclaves experienced may have reinvigorated the magma chamber beneath Micotrin as well, and resulted in a period of volcanic unrest from Micotrin or Wotten Waven. By better understanding how enclaves have formed and how they differ from the host, we can better model the larger magmatic system at depth and explain possible sources of eruptive episodes.

ACKNOWLEDGEMENTS

This material is based upon work supported by the Keck Geology Consortium and the National Science Foundation under Grant No. 1659322. Thanks to Holli Frey, Matt Manon, and Laura Waters for their guidance and advice throughout my research experience, and thanks to the other Keck researchers on this project for help in the field.

REFERENCES

Barclay, J., Herd, R.A., Edwards, B.R., Christopher, T., Kiddle, E.J., Plail, M, and Donovon, A. (2010). Caught in the act: Implications for the increasing abundance of mafic enclaves during the recent eruptive episodes of the Soufriere Hills Volcano, Montserrat. Geophysical Research Letters, 37.

Bersson, J.J., Waters, L.E., Frey, H.M., Nicolaysen, K.P., and Manon, M.R.F. (2017). Explosive to Effuse Transition in Intermediate Volcanism: An Analysis of Changing Magma System Conditions in Dominica. 2017 American Geophysical Union Fall Meeting, V43A-0516.

Frey, H. M., Manon, M.R.F., Brehm, S., and Babiak, R.N. (2016). U-Th zircon chronology reveals protracted cold storage and subsequent rejuvenation in magma reservoirs beneath Dominica, Lesser Antilles. 2016 American Geophysical Union Fall Meeting, V53D-3157.

Ghiorso, M.S., and Evans, B.W. (2008). Thermodynamics of rhombahedral oxide solid solutions and a revision of the Fe-Ti two-oxide geothermometer and oxygen-barometer. American Journal of Science, 308: 957-1039.

Halama, R., Boudon, G., Villemant, B., Joron, J.-L., Le Friant, A., and Komorowski, J.-C. (2006). Pre-eruptive crystallization conditions of mafic and silicic magmas at the Plat Pays volcanic complex, Dominica (Lesser Antilles). Journal of Volcanology and Geothermal Research, 153: 200-220.

Hollocher, K., Robinson, P., Terry, M.P., and Walsh, E. (2007). Application of major- and trace-element geochemistry to refine U-Pb zircon, and Sm/Nd or Lu/Hf sampling targets for geochronology of HP and UHP eclogites, Western Gneiss Region, Norway. American Mineralogist, 92: 1919-1924.

Howe, T.M., Lindsay, J.M., and Shane, P. (2015). Evolution of young andesitic-dacitic magmatic systems beneath Dominica, Lesser Antilles. Journal of Volcanology and Geothermal Research, 297: 69-88.

Lindsay, J.M., Smith, A.L., Roobol, M.J., and Stasiuk, M.V. (2005). Volcanic Hazard Atlas of the Lesser Antilles: Dominica. Seismic Research Unit, University of the West Indies.

Mann, C.P. (2010). Magma chamber dynamics at Soufriere Hills volcano, Montserrat. PhD thesis.

Plail, M., Barclay, J., Humphreys, M.C.S., Edmonds, M., Herd, R.A., and Christopher, T.E. (2014). Characterization of mafic enclaves in the erupted products of Soufriere Hills Volcano, Montserrat, 2009 to 2010. Geological Society of London Memoirs, 39: 343-360.

Sigurdsson, H. (1972). Partly-welded pyroclast flow deposits in Dominica, Lesser Antilles. Bulletin of Volcanology, 36: 148-163.

Smith, A.L., Roobol, M.J., Matioli, G.S., Fryxell, J.E., Daly, G.E., and Fernandez, L.A. (2013). The Volcanic Geology of the Mid-Arc Island of Dominica. Geological Society of America Special Paper, 496.

Waters, L.E., and Lange, R.A. (2015). An updated calibration of the plagioclase-liquid hygrometer-thermometer applicable to basalts through rhyolites. American Mineralogist, 100: 2172-2184.

KECK Geology Consortium
Learning Science Through Research
Published by Keck Geology Consortium

Short Contributions
Keck Geology Consortium
Volume 31
May 2018

UNDERSTANDING THE EFFECTS OF LARGE STORMS ON DOMINICA: AN ANALYSIS USING GIS AND REPEAT PHOTOGRAPHY

MARCUS HILL, Oberlin College
Research Advisor: Amanda Schmidt

INTRODUCTION

Understanding the full extent to which landscapes change over extended periods of time due to natural and anthropogenic causes is a challenging task. An image can start to come together using existing data, but it is difficult to contextualize an environment from numeric values alone. Keeping track of the progression of a site over time is important and provides potential information for the future. One methodology employed in the past which produces measurable and meaningful results is the use of repeat photography (Bierman, 2007; Frankl et al., 2011; Hoffman, 2010; Khan et al., 2013; Webb et al., 2010). Depending on how the method is implemented, both temporal and spatial data can be obtained from a series of photographs. To see the best results over a specific area, the location and time interval between photos have to robust and considerate of the features encompassed (Grove et al., 2013). For this study we documented the changes experienced across Dominica before and after Hurricane Maria in 2018 and Tropical Storm Erika in 2015.

The geomorphic history—and current status—of Dominica is absent from most published research (Rad et al., 2006). The small (750 km^2) island is located in the Lesser Antilles, in the southern Caribbean. It is situated on the convergent plate boundary between the subducting North American Plate and the overriding Caribbean plate, with nine potentially active volcanic sites (Long, 2017). Government provided data indicates an average annual rainfall ranging from 1,700 - 2,650 mm across the island. Located in a tropic climate, Dominica experiences a wet season ranging from mid-June to mid-November, and dry season beginning in late January to the middle of April, although it rains regularly year around (Dominica Meteorological Service, 2018). The island is over 85% vegetated and has an average slope of 19 degrees (Jimerson, this volume).

There have been 14 hurricanes which have crossed the island from 1880 - 2000 according to NOAA records (2017). In the recent past there have been two large events, Tropical Storm Erika in 2015 and Hurricane Maria in 2017. These events caused wide-spread changes to the island including inducing landslides, felling trees, and likely impacting all of the water systems on Dominica. These changes can be most evidently seen within the rivers and channels across the island over time. Using images taken over several years, both temporal and spatial comparisons were made. Conditions like average grain size, channel width, and vegetation density are compared within each channel individually over each field season. This specificity allows for broader, channel to channel comparisons to be made. To compliment the island-wide approach of understanding the effects these storm systems had on Dominica, a GIS analysis of the landslides visible from satellite imagery was also conducted.

METHOD

Google Earth Pro was used to identify the presence and relative magnitudes of landslides on the island prior to Hurricane Maria; any disturbance in vegetated features that did not appear to be anthropogenic in origin was noted. The imagery provided by Google

Earth Pro ranges in age from 2015-2017, within this paper I refer to it all as Summer 2017 data. A qualitative assessment of age of these features was recorded to attempt to discern more recent features from older events which still visually affected the landscape. This same process was repeated using satellite imagery provided after both Tropical Storm Erika and Hurricane Maria had passed over the island. We then transferred these points into ArcGIS to begin qualitatively assessing the affect these events had on the landscape.

We identified the 20 largest watersheds on Dominica prior to arrival to obtain representative information from the entire island. At each location we photographed distinguishing and characteristic features, such as: channel width, sediment size, human activity/construction, water clarity, etc. Every location within these previously identified 20 watersheds was sampled both during June 2017 and January 2018. Samples and pictures taken during the summer field season begin with DM-0XX while the winter seasons samples begin with DM-1XX. We also conducted an in-depth analysis of the Roseau watershed, DM-X20, with eleven more samples collected along the mainstem and tributaries of the Roseau river. Within this analysis, thirteen locations were sampled during earlier field expeditions in either 2014 or 2015. These photosets are particularly useful as they capture both before and after Tropical Storm Erika and Hurricane Maria.

While searching for evidence of landslides, there were noticeable patches across the island with missing foliage and uprooted or bare trees visible from satellite. These instances were noted alongside the post Maria landslides, although no such indication was visible for the analysis conducted over the summer. Post Maria satellite imagery for the island was also blocked by clouds in certain regions. This prevented fully accurate datasets from being created and can be seen sparse coverage for much of DM-X09, DM-X015, DM-X016, DM-X018 (Fig. 1). This makes it difficult to accurately determine if there is actually a preference for debris flows on the western coast.

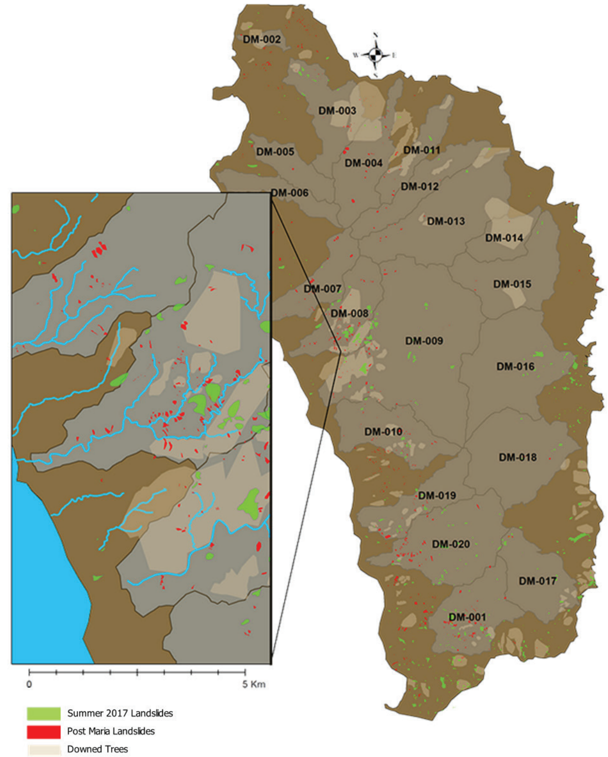

Figure 1. Map view of Dominica indicating regions of visible earth present from satellite imagery from each field season, shown in red and green. Brown regions indicate felled or barren trees.

GIS RESULTS

The landslide analysis results indicate a strong westward trend for the development of landslides on the island (Fig. 1). Within both image sets that were analyzed, more than half of the mass wasting events occurring on the island took place on the western coast, accounting for 58% of the summer 2017 events and 77% after Maria. Figure 1 also shows that 672 landslides occurred after Hurricane Maria compared to the 486 seen in the summer of 2017. The trends for each set of events noticeably differed when looking at average size and elevation. While there were more landslide events after the hurricane, they tended to be smaller in comparison to what was seen in the summer. The number of events resulting from the hurricane increased with elevation until reaching its peak at 300-400 m, whereas the peak for the earlier landslides was at 100-200 m. (Fig. 2).

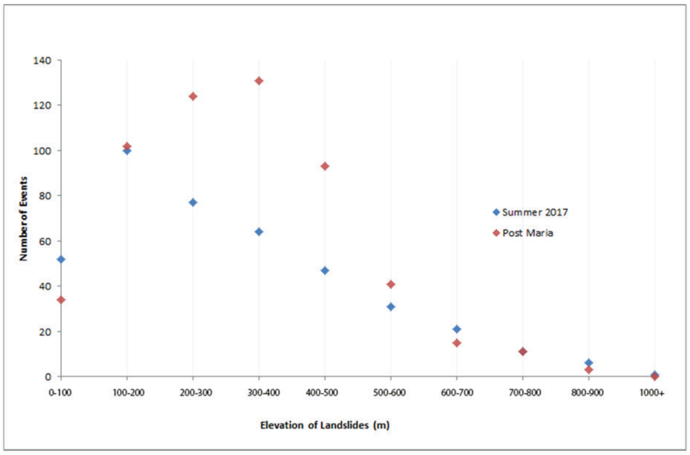

Figure 2. Frequency of events against the average elevation of landslides. Google Earth satellite imagery (Summer 2017) and satellite images available following Hurricane Maria (Post Maria)

PHOTOGRAPHY RESULTS

As the majority of the images were taken at the same location during the trip in January as the ones taken in June, many environmental conditions can be seen changing across the island. Within the 20 watersheds, 16 of them displayed a significant increase in the presence of gravel to cobble sized material, while three—DM-X07, DM-X09, and DM-X13—showed little to no variation, and one, DM-X12, showed reduced presence of cobbles (Fig. 3). There was a significant increase in the presence of boulder-size rocks compared to what was seen over the summer within DM-X01, DM-X05, DM-X06, DM-X10, and DM-X12. Aside from DM-X12, these previously mentioned sites are all on the west coast of Dominica. DM-X17 was the only site to have fewer boulders in or near the channel during the post-Maria visit than it had during the summer (Fig. 4).

There was widespread loss of vegetation due to Hurricane Maria. DM-X01, DM-X06, DM-X10, DM-X12, DM-X15, DM-X16, DM-X18 and DM-X09 all experienced severe vegetative loss, with very apparent changes to bank structure, size and location (Fig. 3, Fig 4). Of these eight locations, four were on each coast of Dominica. Most of these sites converted previously dirt banks into elongated cobble bars or flood plain structures. Seven of the remaining twelve locations appeared to be mostly the same in both seasons, and the last five sites show mild-to-moderate loss of plant material.

Channel size varied noticeably across the field seasons for twelve sites as well (Fig. 3). Eight of these twelve sites became much wider while four became narrower. DM-X07 was unique in that it changed channels, reoccupying a previously deserted one. Five of the seven streams that became wider were found

Sample	Cobbles Present	Boulders Present	Vegetation	Channel size	Channel path	Coast
DM-X01	yes, more	yes	severe loss	much wider	curved	West
DM-X02	yes, more	fewer than before	moderate loss	Slightly wider to no change	straight/step pool	West
DM-X03	yes, more	no	Minor to no loss	Slightly wider to no change	straight/step pool	East
DM-X04	yes, more	no	moderate loss	much wider	curved	East
DM-X05	yes, more	yes	moderate loss	Slightly wider to no change	slightly curved	West
DM-X06	yes, more	yes	severe loss	much wider, deeper	curved	West
DM-X07	Little to no change	no	Minor to no loss	wider, jumped	straight	West
DM-X08	yes, more	no	Minor to no loss	much wider, deeper	curved	West
DM-X09	Little to no change	no	Minor to no loss	Slightly wider to no change	curved	West
DM-X10	yes, more	yes	severe loss	much wider	straight/steps	West
DM-X11	yes, more	no	moderate loss	narrower	curved	East
DM-X12	fewer, but larger	yes	severe loss	much wider	curved	East
DM-X13	Little to no change	no	Minor to no loss	Slightly wider to no change	curved	East
DM-X14	yes, more	no	moderate loss	Slightly wider to no change	curved	East
DM-X15	yes, more	no	severe loss	narrower	curved	East
DM-X16	yes, more	no	severe loss	narrower	straight	East
DM-X17	yes, more	fewer than before	Minor to no loss	much wider	straight	East
DM-X18	yes, more	no	severe loss	Slightly wider to no change	straight	East
DM-X19	yes, more	no	severe loss	narrower	curved	West
DM-X20	yes, more	no	Minor to no loss	Slightly wider to no change	curved	West
DM-X21	Little to no change	yes	severe loss	Slightly wider to no change	straight	West
DM-X22	yes, more	fewer than before	moderate loss	much wider	straight	West
DM-X23	fewer, but larger	yes	moderate loss	narrower	slightly curved	West
DM-X24L	yes, more	yes	severe loss	narrower	slightly curved	West
DM-X25R	yes, more	yes	severe loss	wider	slightly curved	west
DM-X26	yes, more	no	moderate loss	wider	curved	west
DM-X27	Little to no change	no	severe loss	Slightly wider to no change	curved	west
DM-X28	Little to no change	no	Minor to no loss	Slightly wider to no change	straight/step pool	west

Figure 3. Comparisons of the features seen in the repeat photography between 2017 and 2018.

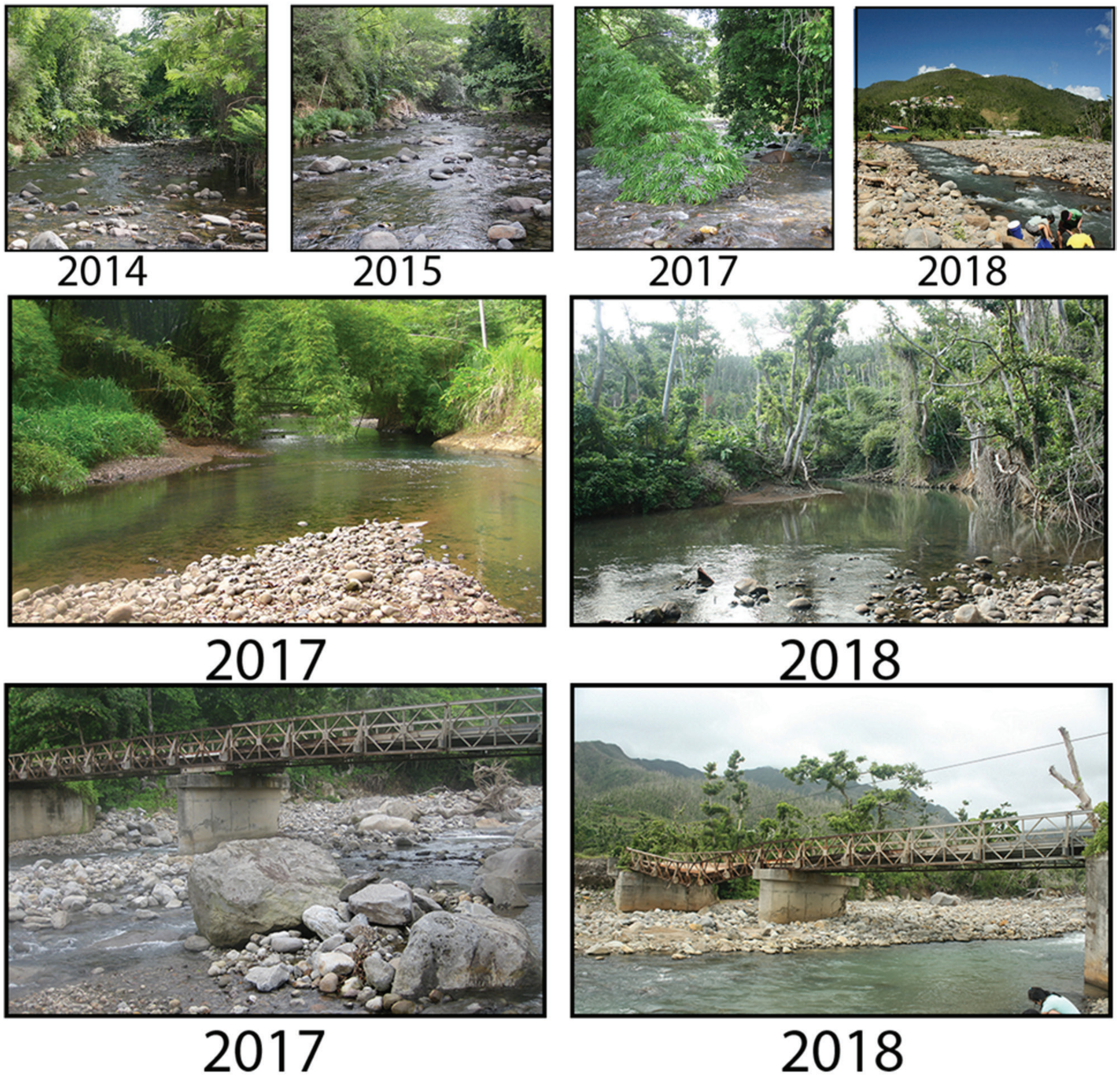

Figure 4. Images in order from top to bottom: DM-X10, DM-X03, DM-X17. DM-X10 showcases the development of cobble banks, DM-X03 is relatively unchanged environment and DM-X17 shows the expulsion of boulders from the channel.

in watersheds on the west coast of the island. Three of the four streams which became narrower were on the east coast. While resampling, it was noted that many of the channels became much more sinuous than what was seen over the summer. Thirteen of the twenty channels have noticeably changed shape or direction. Of the seven that remained straight, three began developing a step-pool structure. There was no noticeable trend to determine on which side of the island these transformations took place.

As the first set of information was gathered during the wet season and the second set was during the dry, accurate comparisons and assessments of water depth and speed cannot be made. I will note, however, that generally the rivers were all deeper despite it being the dry season. Specifically, at the four locations where the channels became narrower the stream was much more deeply incised.

The trends within the Roseau watershed mirrored the patterns exhibited across the rest of the island. Significant vegetation loss, widening of the channels, evidence of larger sediment in the channel ranging from cobbles to boulders and creation of cobble banks. There was also a fairly large gradient in the amount of variability experienced across the sites; DM-X24L was unrecognizable between the two seasons while DM-X20 was extremely similar to the conditions over the summer.

DISCUSSION

The satellite imagery analysis demonstrates frequent, small to medium scale alterations to the surface of island resulting from the storm. The frequent and shallow nature of the landslides depicted in Figure 1 agrees with the findings of Bucknam et al. and their case study of the landslides produced on Guatemala as a result of Hurricane Mitch (2001). Shallow debris flows were the most common resulting feature from the storm, present in large quantities across the environment. The magnitude and longevity of the storm seem to play important roles in understanding the types of mass-wasting events that will occur. Just as Hurricane Mitch did with Guatemala, Tropical Storm Erika lingered over Dominica for a prolonged period of time, compared to the faster nature of Hurricane Maria. Although Hurricane Maria was more powerful, because the rainfall was not as sustained as what was experienced with Erika, fewer large mass-wasting events could happen.

There was significant channel change across the island. DM-X07 was one of the most interesting locations to resample as it was the only place which completely changed original channels. Figure 5 describes the channel as seen in the summer with the darker blue line and what was seen in January with the lighter blue line. There is evidence that extreme flooding conditions which also induce landslides can reroute waterflow into previously abandoned channels (Wang et al., 2015; Tiron et al., 2009). This may likely be the case of a cut-off resulting from a debris-flow, as Figure 1 shows there are a number of landslides within this particular watershed.

The GIS findings indicate that the geomorphic processes on the island respond differently depending on the severity of the storms. Figures 1 and 2 highlight the variation in landslide frequency, presence and elevation between each field season. Hurricane Maria induced a greater number of landslides at a much higher average elevation than what was seen with the summer landslide data. Despite these differences, both Figure 1 and 3 generally report a westerly storm preference across the island, although these data are disputed by local accounts from islanders. Several anecdotal accounts argue that the eastern portion of Dominica experienced Hurricane Maria more

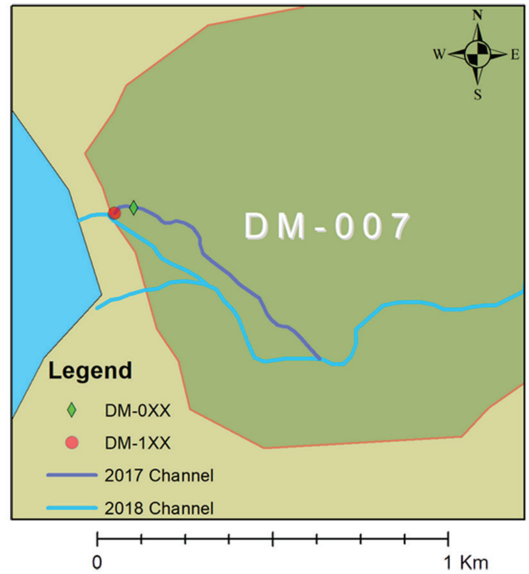

Figure 5. The only location among our sample sites to have completely changed original channels between field seasons.

dramatically, which could be supported with some of the changes seen in Figure 3.

It is difficult to determine if one side of Dominica was more greatly affected than the other. The presence of large (1 m+ sized) boulders in river channels was primarily restricted to the islands western streams. Only two of the seven instances where channel development indicated the movement of these materials occurred on the east coast. One of the two instances on the east coast was the removal of these boulders from the channel (Fig. 3). While the water did not appear to be able to move such massive rocks at the time of sampling, they were able to at some point during the storm. This would allow for the assumption of other water channels based along the east coast to move similar material.

Four locations did see the body of the stream become narrower, DM-X11, DM-X15, DM-X16, DM-X19. Three of these sites were located on the east coast while DM-X19 was found on the west side of Dominica. These streams were all narrower due to an increased presence or new occurrence of cobble banks and bars. The widespread integration of highly coarse-grained material supports the previously mentioned finding suggesting that the East coast of the island experienced similarly strengthened forces.

CONCLUSION

Despite having a high average slope across the island, the highly vegetated nature of Dominica allows for a large amount of stability under normal conditions. The presence of large magnitude mass-wasting events is rare, even in the wake of the two most recent large-scale weather events. The stability of river channels varies across the island, with GIS analysis indicating that the western coast was more dramatically affected. Though hard to confirm with obscured satellite imagery, the use of ground-truthing and repeat photography appear to be verify these findings. More than half the sites experienced obvious and profound disturbance to vegetation near and along the stream channel due to Hurricane Maria. At most sites there was an increased presence in coarse, rocky material, often replacing previously vegetated banks for cobble bars and banks instead. There were five locations along the west coast which also had newly introduced boulders into the stream profile compared to only two on the east coast. The data and image sets used within this study lead us to believe not all the rivers were affected equally and that there was a westerly bias with the storms.

ACKNOWLEDGEMENTS

This material is based upon work supported by the Keck Geology Consortium and the National Science Foundation under Grant No. 1659322, in collaboration with the Government of Dominica and Union College. Many thanks to Holli Frey, Laura Waters, Pat Joseph, and the rest of the KECK 2017 students who also participated on this project. I'd like to specifically thank Amanda Schmidt, Kira Tomenchok, Haley Talbot-Wendlandt, and Cole Jimerson for their assistance and support throughout this project. Three other students have also been very influential in keeping this project going: Nathan Daniel, Ely Bordt, and Melinda Quock have all been great partners and co-investigators to work on this data with.

REFERENCES

Bucknam, R.,C., J. Coe, M. Mota ChavarrÃa, J. Godt, A. Tarr C., L. Bradley, S. Rafferty, D. Hancock, R. Dart L., and M. Johnson L. (2001), Landslides Triggered by Hurricane Mitch in Guatemalaâ€" Inventory and Discussion.

Dominica Meteorological Service (2018), Climate Data, Weather.gov.dm. Available from: http://www.weather.gov.dm/climate-data (Accessed 15 March 2018)

Frankl, A., J. Nyssen, M. De Dapper, and M. Haile (2011), Linking long-term gully and river channel dynamics to environmental change using repeat photography (Northern Ethiopia), Geomorphology (Amsterdam, Netherlands), 129(3), 238-251.

Hoffman, M. T. and R. F. Rohde (2011), Rivers Through Time: Historical Changes in the Riparian Vegetation of the Semi-Arid, Winter Rainfall Region of South Africa in Response to Climate and Land Use, Journal of the History of Biology, 44(1), 59-80, doi:10.1007/s10739-010-9246-4.

Jugaru Tiron, L., J. Le Coz, M. Provansal, and N. Panin (2009), Flow and sediment processes in a cutoff meander of the Danube Delta during episodic flooding, Geomorphology (Amsterdam, Netherlands), 106(3), 186-197.

Khan, S. F., S. F. Khan, U. Kamp, and L. A. Owen (2013), Documenting five years of landsliding after the 2005 Kashmir earthquake, using repeat photography, Geomorphology (Amsterdam, Netherlands), 197, 45-55.

National Oceanic and Atmospheric Administration (2017), Hurricanes, Coast.noaa.gov. Available from: https://coast.noaa.gov/hurricanes/ (Accessed 15 March 2018)

Long, D. (2017), Geology | | a virtual Dominica, Avirtualdominica.com. Available from: http://www.avirtualdominica.com/project/geology/

R. Grove, J., J. R. Grove, J. Croke, and C. Thompson (2013), Quantifying different riverbank erosion processes during an extreme flood event, Earth Surf. Process. Landforms, 38(12), 1393-1406.

Rad, S., P. Louvat, C. Gorge, J. Gaillardet, and C. Allègre (2006), River dissolved and solid loads in the Lesser Antilles: New insight into basalt weathering processes, Journal of Geochemical Exploration, 88(1-3), 308-312, doi:10.1016/j.gexplo.2005.08.063.

Webb, R. H., D. E. Boyer, and R. M. Turner (2010), Repeat photography: methods and applications in the natural sciences, Island Press, Washington.

Learning Science Through Research
Published by Keck Geology Consortium

Short Contributions
Keck Geology Consortium
Volume 31
May 2018

STRATIGRAPHY AND GEOCHEMISTRY OF A FOND ST. JEAN CINDER CONE, DOMINICA

TARYN ISENBURG, Mount Holyoke College
Research Advisors: Steve Dunn and Holli Frey

INTRODUCTION

Dominica is an island nation located near the center of the Lesser Antilles Island Arc, and it is primarily composed of subaerial lava flows and pyroclastic deposits, which give rise to a rugged terrain (Smith et al., 2013). Due to the warm and wet climate, weathering rates are high, and a thick layer of soil covers much of the geology, making it difficult to map. As a result, large portions of the island, especially volcanic centers, are grouped together on geologic maps as large cohesive units. One such unit is Foundland Center, surrounding the historically active Foundland stratovolcano, which is mapped as a 25 km2 block of mafic flow rocks (Smith et al., 2013).

Foundland Center is unusual in that it is the only mafic volcanic center on the island, which is otherwise composed of intermediate rocks ranging from andesites to dacites (Smith et al., 2013). Previous analyses of rocks from Foundland Center indicate that lapilli collected from Fond St. Jean, a town within Foundland, is some of the most mafic and primitive material from the island (Wills, 1976).

This study analyzes the stratigraphy and geochemistry of geologic material composing a cinder cone at Fond St. Jean. The purpose of this study is to characterize the mineralogy, textures, and composition of the most primitive material on Dominica and determine if it is a parental source to more evolved lavas on the island. A study of the evolution of material emplaced within Foundland may provide insight into the evolution of mafic magma. Furthermore, studying variations in the texture of materials deposited by the cinder cone gives insight into how styles of volcanism changed at Fond St. Jean.

METHODOLOGY

Fond St. Jean is located on the southeastern shore of Dominica, situated within the Foundland Stratovolcano. A dome shaped structure within Fond St. Jean was identified as a weathered and partially eroded cinder cone. The dome is composed of repetitive layers of massive basaltic flow rocks, scoria, ash, and lapilli units. A continuous outcrop of the material composing the cinder cone is exposed by a road cut, along which all samples and additional data were collected (Fig. 1 a-d). Field work consisted of collecting samples, measuring the thickness of units composing the outcrop, and collecting coordinates and elevation measurements using ArcGIS software.

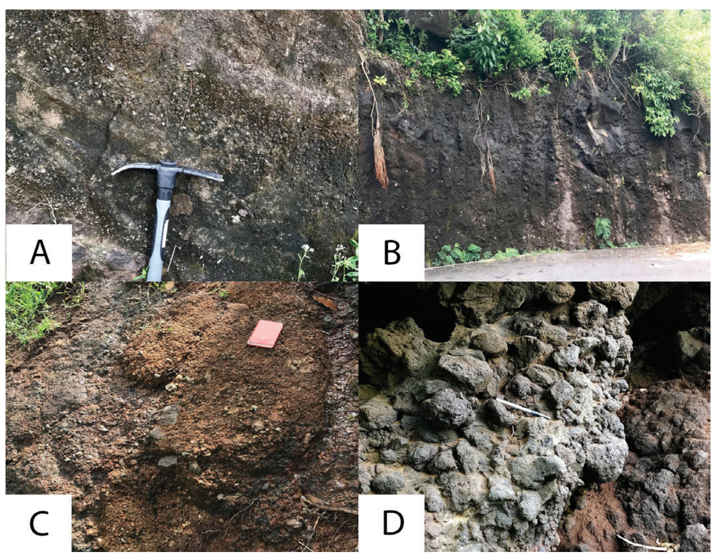

Figure 1. Unit photos taken along the road cut exposing the Fond St. Jean cinder cone. Physical characteristics, textures, and mineralogy separate units such as lapilli in soft flow rocks (a), massive flows (b), brecciated basalt (c), and scoria (d).

In the lab thin sections of all samples except the lapilli were cut. Lapilli were made into micromounts by selecting the glassiest pieces and placing them into plastic rings, which were then filled with epoxy, cut through the center, and polished. Thin section and micromount mineralogy was analyzed on a petrographic microscope and mineral compositions were analyzed on a scanning electron microscope (SEM) both at Union College and Mount Holyoke College. Plagioclase, olivine, and oxides were the main phases analyzed on the SEM by energy dispersive spectrometry (EDS). Additionally, rock samples were crushed into powders, which were analyzed by inductively coupled plasma optical emission spectrometry (ICP-OES) and inductively coupled plasma mass spectrometry (ICP-MS) to determine major element and trace element compositions, respectively. ICP-OES was conducted at Acme Labs in Vancouver, Canada, and ICP-MS was conducted at Union College, following procedures of Hollocher and Joaquin, 1995.

RESULTS

Stratiography

The stratigraphic sequence of the cinder cone includes 35 m of basaltic material including brecciated lava flows, massive flow rocks, scoria, ash, and lapilli (Fig. 2). The sequence begins with a 2-3 m thick basal unit of basaltic breccia overlain by repetitive layers of massive and rubbly flow rocks, which range from 1 to 10 m in thickness. These flows transition into an additional 2 m thick scoria deposit capped by a meter of massive basalt, which sits beneath another 3-4 m scoria deposit. Another layer of massive flow then transitions to three units of alternating lapilli and ash lenses. Lapilli units are 0.25 m in thickness, but pinch and swell regularly, and ash lenses are roughly 0.25 m thick.

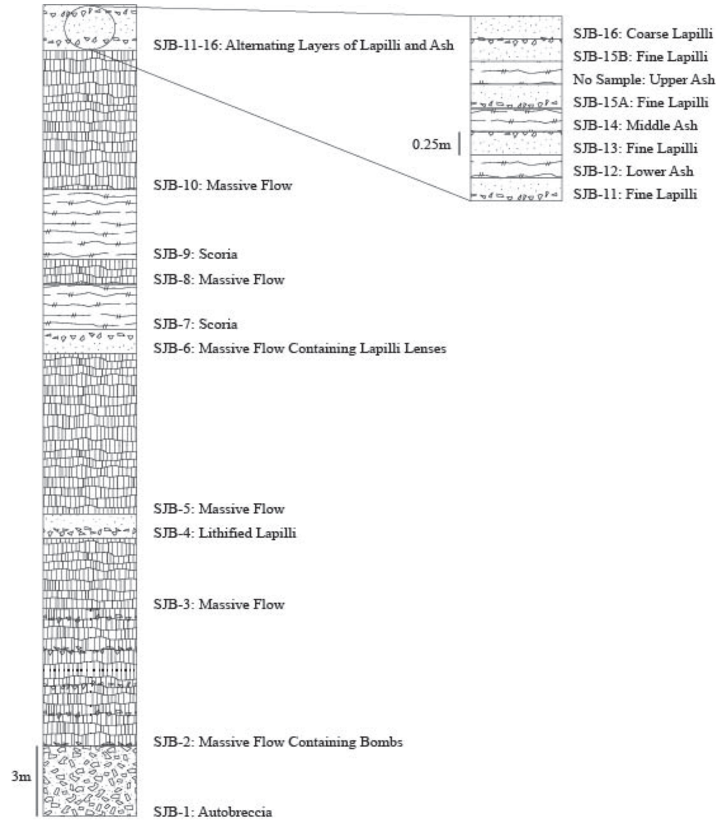

Figure 2. Idealized stratigraphic column of the cinder cone at Fond St. Jean. Overall thickness of the sampled section is 35 m. Unit boundaries were established where changes in the appearance or mineralogy of the outcrop were obvious. The boundary between many units was gradational, so the beginning of a new unit was marked where the rocks completely transitioned into a new appearance, behavior, or mineralogy.

Petrography

All units contain plagioclase + olivine + clinopyroxene + orthopyroxene + titanomagnetite. Plagioclase is the most dominant phase in each unit, and commonly appears as 1-3 mm scale phenocrysts (Fig. 3a). Plagioclase habit ranges from tabular euhedral to broken and anhedral depending on the unit (Fig. 3a-c). Phenocrysts of olivine and both pyroxenes are equally common in thin section, and both appear as single mm scale rounded, subhedral grains (Fig. 3a). Olivine grains are at least partially altered to iddingsite in every unit. Phenocrysts of all minerals are fractured or broken in every unit, but phenocrysts in massive flow units have lighter fractures than phenocrysts in other units. Phenocrysts from ash, lapilli, and scoria units are more likely to contain broken, anhedral grains (Fig. 3c). Titanomagnetites are present throughout the section and occur as poorly mixed sub-mm scale minerals. A matrix of fine grained, intergranular plagioclase, olivine, and pyroxene surrounds phenocrysts in every unit.

Matrix olivine crystals occasionally have reaction rims showing alteration to micron scale pyroxene (Fig. 3d). Other minerals do not consistently show alteration, though plagioclase textures do change based on the unit they are in. Plagioclase in the lapilli and ash units

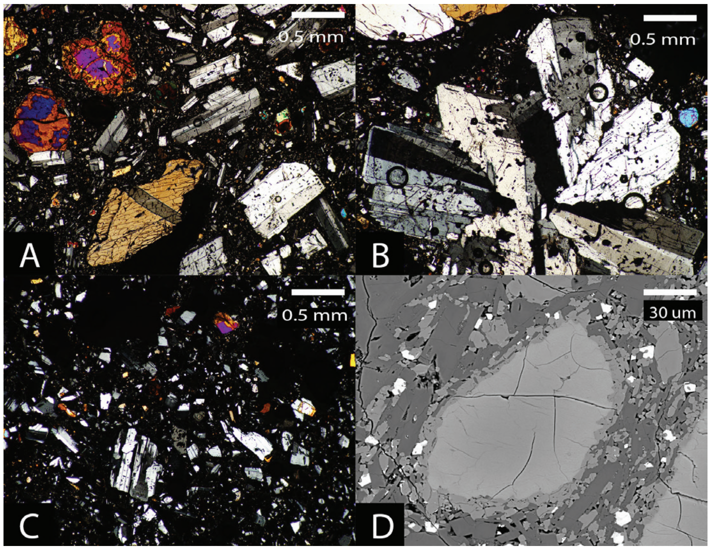

Figure 3. Photomicrographs (3a-c) and a backscattered electron image (3d) of minerals in thin section. SJB-10 (3a, x4 mag.) is a massive flow containing phenocrysts of tabular plagioclase, rounded and subhedral olivine with alteration to iddingsite, and subhedral clinopyroxene, which is partly obscured by a bubble in the thin section. SJB-9 (3b, x4 mag.) is a scoria unit containing large glomerocrysts of plagioclase. SJB-14 (3c, x4 mag.) is an ash unit containing broken phenocrysts of plagioclase, olivine, and both pyroxenes. The brecciated basalt unit SJB-1 (3d) shows matrix olivine with reaction rims altered to pyroxene.

are usually broken and surrounded by intergranular matrix (Fig. 3c). Plagioclase in the massive flows and scoria units are more likely to form glomerocrysts with each other and pyroxene grains (Fig 3b).

Mineral Compositions

Mineral compositions are similar throughout the stratigraphic column. Massive flows contain similar, weakly zoned plagioclase cores (An_{84-94}) with 10-30 µm sodic rims (An_{58-78}, most rims are <An_{68}). Plagioclase microlites (long axis <100 µm) span a wide range of compositions (An_{50-90}). Lapilli units contain crystal rims ranging in composition from An_{58-86} and cores ranging from An_{84-92}, with the exception of a single core with the composition of An_{61}. Scoria units follow a similar trend, with plagioclase cores ranging from An_{84-90} and rims ranging from An_{53-66}. The autobreccia unit again follows the same trend, with plagioclase cores ranging in composition from An_{80-87} and rims ranging from An_{60-64}. Olivine in most units ranges in composition from Fo_{55-70}, with the exception of a single lapilli unit where only Fo_{55} was identified. Spinels are ubiquitous throughout each of the units and are consistently poorly mixed titanomagnetites.

Whole Rock Chemistry

Compared to other available whole rock analyses (accessed on http://georoc.mpch-mainz.gwdg.de/georoc/ September 28, 2017; Brown et al., 1977; Halama et al., 2006; Howe et al., 2014, 2015; Lindsay et al., 2005; Smith et al., 2013), the samples from Fond St. Jean are basalts and contain the highest amount of iron and magnesium by oxide weight percent and the lowest amount of silica (~48-50 wt% SiO_2), potassium, and sodium by oxide weight percent of all of the rocks analyzed on Dominica (Fig. 4). Plots of oxide weight percent for each sample vs. the relative height at which they were collected in the stratigraphic column show that major element compositions vary up section, but not systemtically. In general, SiO_2 wt % gradually decreases up section from ~50 wt% to 48 wt%. Al_2O_3 content gradually increases up section from ~20 wt % to 23 wt %. MgO remains relatively consistent at 4-5 wt % throughout the section.

Rare earth elements from these samples are consistent with typical island arcs, though some samples are slightly less enriched in light rare earth elements and more enriched in heavy rare earth elements (Fig. 4). Discrimination plots show that the majority of samples have major and trace element compositions that are consistent with island arc basalts (Fig. 5). Some samples are slightly depleted in strontium or enriched in zirconium, similar to mid-ocean ridge basalts, but these make up a minority of the samples (Fig. 5). Trace element ratios that may monitor sediment contribution to arc magmas are fairly consistent throughout the column, with Th/La ratios ranging from 0.12 to 0.36 (most ratios are >0.20).

DISCUSSION AND CONCLUSION

Stratigraphy of the cinder cone, in addition to unit textures that were used to establish boundaries and transitions within the stratigraphic section indicate that both explosive and effusive styles of volcanism were critical during cinder cone deposition. Flow rocks indicate more effusive styles of volcanism whereas brecciated flows, scoria, lapilli, and ash indicate more explosive styles of volcanism. Alternating emplacement of these units alone cannot be used

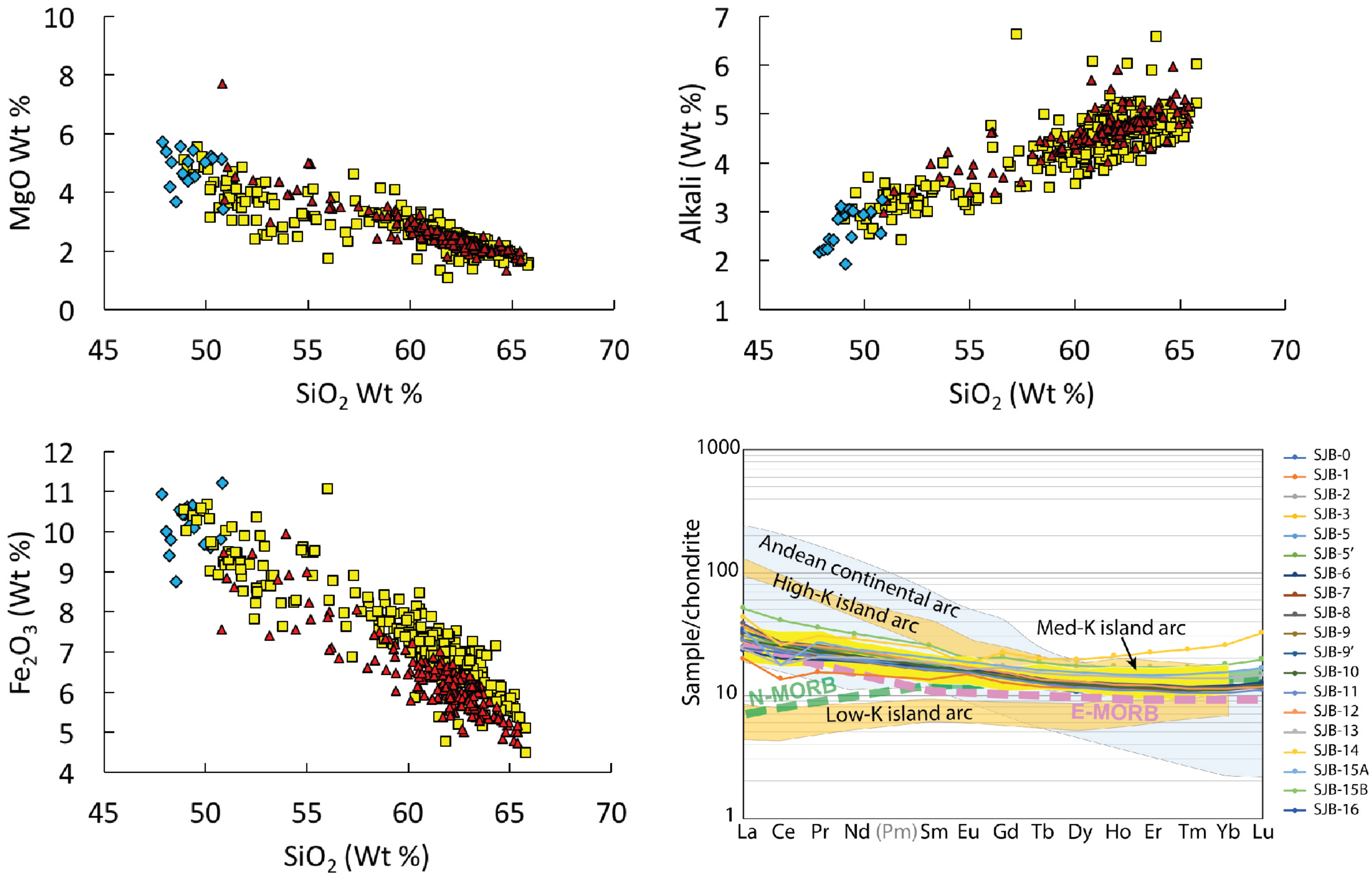

Figure 4. Harker diagrams comparing major element compositions and a rare earth element plot. On the harker diagrams, blue diamonds represent rocks collected in this study. Red triangles represent data collected and shared on the GeoRock database (accessed on http://georoc.mpch-mainz.gwdg.de/georoc/ September 28, 2017). Yellow boxes represent data collected by Smith et al. (2013). The rare earth element plot shows that these samples are consistent with medium K island arc rocks. All trace elements are normalized after McDonough and Sun, 1995.

to determine the temporal relationship of eruptive styles, as lava flows can disrupt pyroclastic deposits after emplacement through a number of complex mechanisms (Brown et al. 2015).

Consistency in mineralogy and mineral compositions throughout the stratigraphic section indicates that the material being emplaced did not undergo dramatic evolution as emplacement proceeded in this particular location. Major element compositions are also fairly consistent throughout the column. While some general trends in major element compositions exist for certain oxides, the column does not show consistent and continual increase or decrease in major element oxide compositions. This indicates that magma emplacement was complex and did not simply progress from the most primitive and mafic material to continually more mature material.

The material collected for this study is some of Dominica's most mafic and primitive material on record (Fig. 4). Major and trace element plots provide evidence that these rocks are well behaved island arc basalts (Fig. 5). Trace element ratios, such as Th/La, can be used to track sediment contribution at subduction zones (Plank, 2005). These samples yield Th/La ratios close to 0.2-0.3, which is consistent with Th/La ratios of subducting sediments in the Lesser Antilles (Plank, 2005). These values indicate that the samples collected in this study have been contaminated by sediment contribution instead of being derived directly from uncontaminated mantle, which has Th/La ratios closer to 0.1 (Plank, 2005).

A comprehensive study of cumulate blocks from samples throughout the Lesser Antilles provides insight on fractional crystallization processes on each island (Arculus et al. 1980). On Dominica, intermediate

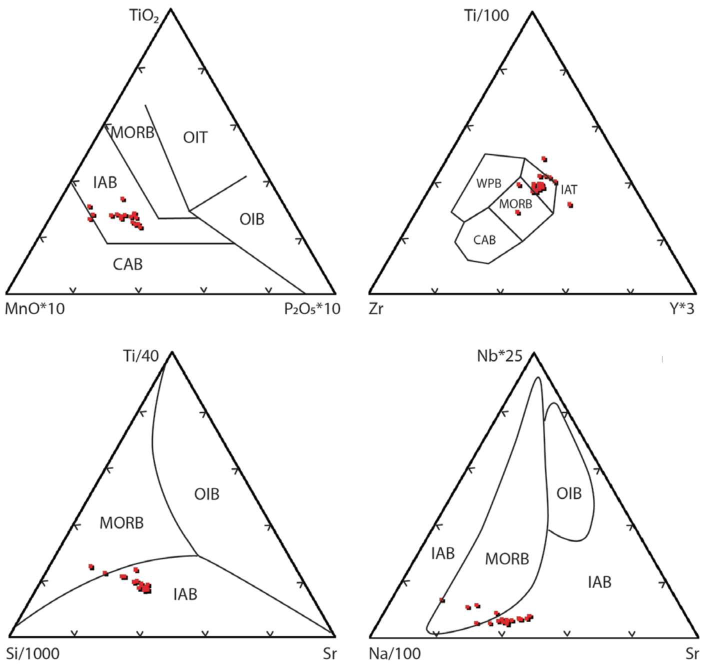

Figure 5. Discrimination diagrams after Vermeesh, 2006. Major and trace elements show that the samples collected at Fond St. Jean are consistent with ocean island basalts.

rocks contain mafic blocks that provide evidence for fractional crystallization at mid crustal depths (Arculus et al.,1980). This process may explain why Dominica is dominated by intermediate rocks, as cumulates likely removed mafic phases from the parent magma, leaving a more evolved melt to erupt. This study, however, finds no evidence for this fractional crystallization process at Fond St. Jean, and concludes that direct emplacement of the parent magma has occurred instead.

This study may be broadened in the future by utilizing mixing models to generally determine what type of mantle the parent magma was derived from, and what percent of the magma composition is due to sediment contamination. Unfortunately, the ability to model solid-melt processes and calculate a more specific mantle composition from which the parent magma was derived is limited by sediment contamination in these samples.

ACKNOWLEDGEMENTS

This material is based upon work supported by the Keck Geology Consortium and the National Science Foundation under Grant No. 1659322. I would like to thank Holli Frey and Laura Waters for their assistance and guidance throughout my project. I would also like to thank Steve Dunn for additional guidance and support.

REFERENCES

Arculus, R.J., and Wills, K.J.A., 1980. The petrology of plutonic blocks and inclusions from the Lesser Antilles island arc. Journal of Petrology 21, 743-799.

Brown, G.M., Holland, J.G., Sigurdsson, H., Tomblin, J.F., 1977. Geochemistry of Lesser Antilles volcanic arc. Geochimica et Cosmochimica Acta 41, 785-801.

Brown, R.J., Thordardson, T., Self, S., Blake, S., 2015. Disruption of tephra fall deposits caused by lava flows during basaltic eruptions. Bulletin of Volcanology 77, 1-15.

Halama, R., Bourdon, G., Villemant, B., Joron, J.-L., Le Friant, A., Komorowski, J.-C., 2006. Pre-eruptive crystallization conditions of mafic and silicic magmas at the Plat Pays volcanic complex, Dominica (Lesser Antilles). Journal of Volcanology and Geothermal Research 153, 200-220.

Hollocher, Kurt and Ruiz, Joaquin, 1995. Major and trace element determinations on NIST glass standard refererence materials 611, 612, 614 and 1834 by inductively coupled plasma mass spectrometry. Geostandards Newsletter 19, 27-34.

Howe, T.M., Lindsay, J.M., Shane, P.A., Schmitt, A.K., and Stockli, D.F., 2014. Re-evaluation of the Roseau Tuff eruptive sequence and other ignimbrites in Dominica, Lesser Antilles. Journal of Quaternary Science 29, 531-546.

Howe, T.M., Lindsay, J.M., and Shane, P.A., 2015. Evolution of young andesitic-dacitic magmatic systems beneath Dominica, Lesser Antilles. Journal of Volcanology and Geothermal Research 297, 69-88.

Lindsay, J.M., Trumbull, R.B., and Siebel, W., 2005. Geochemistry and petrogenesis of late Pleistocene to recent volcanism in southern Dominica, Lesser Antilles. Journal of Volcanology and Geothermal Research 148, 253-294.

McDonough, W.F. and Sun, S.-s., 1995. The composition of the earth. Chemical Geology 120, 223-253.

Pearce, J.A. and Cann, J.R., 1973. Tectonic setting of basic volcanic rocks determined using trace element analyses. Earth and Planetary Science Letters 19, 290–300.

Plank, T., 2005. Constraints from thorium/lanthanum on sediment recycling at subduction zones and the evolution of the continents. Journal of Petrology 46, 921-944.

Smith, A.L., Roobol, M.J., Mattioli, G.S., Fryxell, J.E., Daly, G.E., and Fernandez, L.A., 2013. The volcanic geology of the mid-arc island of Dominica, Lesser Antilles—The surface expression of an island-arc batholith. Geological Society of America Special Paper 496, pp. 249. doi:10.1130/2013.2496.

Wills, K.J.A., 1976. The geological history of southern Dominica and plutonic nodules from the Lesser Antilles. Ph.D Thesis, Durham University, 222pp.

Vermeesch, P., 2006. Tectonic discrimination diagrams revisited. Geochemistry Geophysics Geosystems 7, 1-55. doi:10.1029/2005GC001092.

Learning Science Through Research
Published by Keck Geology Consortium

Short Contributions
Keck Geology Consortium
Volume 31
May 2018

RIVER DEVELOPMENT AND INCISION ON DOMINICA, WEST INDIES

COLE JIMERSON, The College of Wooster
Research Advisor: Amanda Schmidt

INTRODUCTION

Understanding the tectonic and climatic forces influencing the shape and history of Earth's surface has become a key undertaking in geomorphology (Gonzalez et al., 2016). Throughout the world, controls on river development include tectonics, bedrock lithology, storm pulses, landslides, and glaciers (Pike, 2010). Climatic and topographic variables such as mean basin slope, basin relief, seismicity, and precipitation have previously shown strong influence on erosion and incision rates (Portenga and Bierman, 2011; Covault et al., 2013; Willenbring et al., 2013; Harel et al., 2016). Although controls on erosion rates have been determined in many diverse landscapes, there has been little work on understanding river development and controls in the Lesser Antilles (Allen, 2017).

The tropical volcanic rivers on Dominica make up one of the largest river densities in the world and are accompanied by steep slopes, high mean annual rainfall, many landslides, and tropical storms creating a highly erosive landscape (Table 1; Neumann et al., 1978; Reading, 1991; Goldsmith et al., 2010; Ogden, 2016). Determining spatial patterns of geomorphic characteristics such as local relief, slope, rainfall, and channel steepness across Dominica brings insights of the effects of volcanic activity, tropical humid climate, great relief, and tropical storm pulses on geomorphic processes occurring on Caribbean islands. Minimum incision rates provide insights into the pace of river incision following pyroclastic flows filling the valleys. Long profiles show trends in channel gradients and are used to understand lithological influences on river down cutting (Duvall et al., 2004; Cyr et al., 2014). Comparisons between incision rates to local climatic, lithological, topographic variables and long profiles allow for relative controls on geomorphic process to be established.

Table 1. Climatic and topographic geomorphic characteristics of the 20 largest rivers on Dominica.

Name	Local Relief (m)	M.A.P (mm/year)	Mean Basin Slope (%)	Area (km²)	% Area Landslide Covered (landslides mapped)	Mean chi coordinate
Geneva River	1471.9	4592.7	26.2	1723.8	24.69% (140)	3.04
Lamothe River	597.7	3312.2	23.2	306.9	0.00% (0)	2.73
Blenheim River	590.7	3684.6	18.8	1850.1	2.67%(23)	3.25
Hampstead River	1132.4	5156.2	18.9	1994.5	0.27%(7)	4.81
Picard River	781.9	3774.9	18.9	685.9	0.00%(0)	3.56
Espagnole River	1132.2	3577.5	16.8	1371.8	3.33%(5)	4.71
Batali River	1099.3	4653.6	20.8	1245.5	5.40%(18)	3.71
Macoucherie River	786.3	5235.8	19.7	1787.0	40.51%(103)	4.41
Layou River	1429.4	5555.2	16.6	6389.7	17.23%(139)	5.89
Belfast River	1485.6	4197.3	19.0	1832.1	5.48%(41)	3.35
Mamelabou River	568.1	4435	15.1	1254.5	11.93%(12)	4.66
Toulaman River	1057.4	5062.3	16.6	1543.3	1.92%(17)	5.36
Melville Hall River	949.1	5512.8	16.0	3086.6	5.09%(7)	4.66
Pagua River (North)	621.3	4866.6	19.0	694.9	2.89% (4)	3.21
Pagua River (South)	629.6	5069	17.2	1732.8	2.69%(16)	4.25
Castle Bruce River	1340.2	5624.9	17.2	2545.1	8.79%(84)	3.12
White River	1500.1	5157.2	27.1	1588.4	20.14%(82)	2.92
Rosalie River	1452.1	5922	23.7	3113.6	19.74%(75)	3.68
Boeri River	1474.4	4694.9	20.3	1407.9	11.74%(35)	4.05
Roseau River	1461.1	5091.5	21.0	2815.8	31.59%(126)	4.29

METHODS

A variety of topographic, climatic, and geologic variables (elevation, slope, rainfall, lithology) are compared to minimum rates of incision. To analyze spatial patterns of steepness, local relief and basin-average slope were calculated using the Advanced

Spaceborne Thermal Emission and Reflections Radiometer (ASTER) Global Digital Elevation Model (GDEM) Version 2 (NASA et al., 2009). Basin-averaged mean annual rainfall was calculated using precipitation data from Lang (1967). Landslide data was collected by Marcus Hall (Oberlin College) and Haley Talbot-Wendlandt (Ohio Wesleyan University), determining the total amount of landslides in each watershed and the area covered by landslides using Google Earth (Tomenchok et al., 2017). Channel profile analysis was completed using LSDTopoTools (Mudd et al., 2014). LSDTopoTools extracts the (chi) χ coordinate value, which represent the steepness of the river normalized for the upstream area and show the channel gradient throughout the entire river (Mudd et al., 2014). Long profiles of the rivers were created using LSDTopoTools then resampled using the geologic map of Dominica to determine the type of rock that is underlying the channel (Roobol and Smith, 2004). The steepness of the channel typically increases as the streams experience transitions in rock strengths, while consistently weak rock strengths yield lower channel slopes (Duvall et al., 2004).

Incision rates were determined for nine of the rivers on Dominica using ArcGIS (Fig. 1). Ignimbrite age dates for the sampled rivers were previously established from zircon dating (Howe et al., 2014; Frey et al., 2015). Transects across the channels were created within the extent of the dated ignimbrites. Once transects were created, the changes in elevation from the top to the bottom of the channels were recorded and divided by the age of the ignimbrites to determine minimum incision rate.

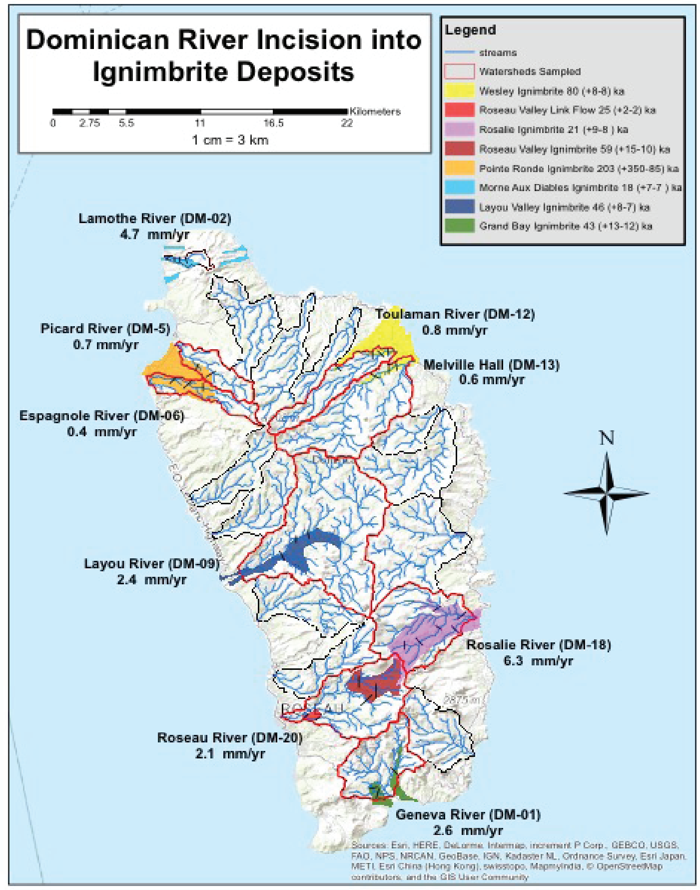

Figure 1. Average rates of minimum incision into the underlying ignimbrite deposits are the greatest in the southern rivers. Lowest rates of incision are in the northern rivers, with the exception of the northern-most Lamothe river.

RESULTS

Geomorphic Characteristics

To quantify the characteristics of the rivers of Dominica, basin average statistics were determined for topographic and climatic variables that influence erosional processes. Digitalizing and extracting mean annual rainfall data from Lang (1967), average annual rainfall of the 20 watersheds on Dominica is 4759 mm/yr. Watersheds on the eastern side of the island have mean annual precipitation rates approximately 600 mm/yr greater than the watersheds on the western side. The local relief, difference of the minimum and maximum elevations, and mean basin slope are the highest in the southern watersheds while local relief and slope are much lower in northern watersheds (Table 1). Linear regressions comparing the geomorphic characteristics of Dominica show that mean annual rainfall correlates strongly with mean normalized channel steepness (chi). Of the 934 landslides mapped, the southern watersheds tended to have the greatest number of landslides and percentage of area covered in landslides.

Incision Rates

Minimum incision rates were established for nine rivers on Dominica (Fig. 1) using transects across the river channels that flow through dated ignimbrite deposits (Howe et al., 2014; Frey et al., 2015). Incision rates of the rivers are relatively higher in the south of the island, except for the northernmost Lamothe River, which had the second highest average

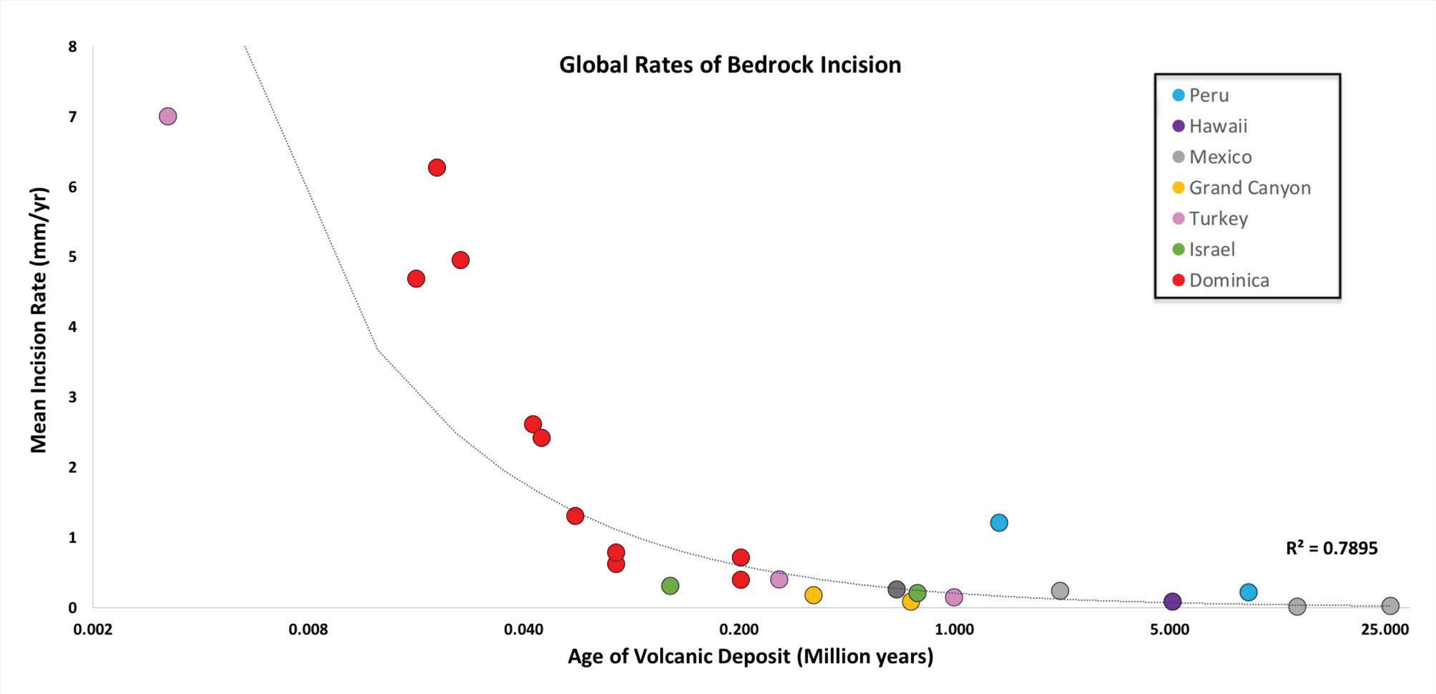

Figure 2. Incision rates show an exponential decrease with increasing ignimbrite age until ~80 ka where incision rates decrease much slower (Howe et al., 2014; Frey et al., 2015). The rivers that are incising into younger ignimbrite deposits that are less than ~50ka, showed higher incision rates and had a broader range in rates. Rivers incising older ignimbrites (~80 – 200ka) have more consistent lower incision rates. Previous studies show that this trend continues as bedrock ages increase, showing minor decreases in incision after ~200 ka.

incision rate (4.7 mm/yr) (Fig. 1). The Rosalie River in the southeast had the highest minimum incision rate (6.3 mm/yr) into the Rosalie ignimbrite (Fig. 1). The Rosalie, Roseau, Geneva, and Layou Rivers in the south, with the higher incision rates, tended to have the greatest local relief and mean basin slope (Table 1). Linear regressions show incision rates of the nine rivers are significantly correlated with mean normalized channel steepness (chi) ($p < 0.05$) and the percent of the basin area covered in mapped landslides ($p < 0.05$).

Incision rates tended to also be higher in younger ignimbrite deposits (Fig. 1, 2). Rivers with ignimbrite deposits less than ~50 ka have the highest rates of incision ranging from 2.1 – 6.3 mm/yr (Fig. 2). Although the Wesley Ignimbrite is slightly younger than the Pointe Ronde Ignimbrite, the rivers flowing through both are experiencing similarly low rates of incision (0.4 – 0.7 mm/yr) (Fig. 2).

Channel Analysis

Long profiles show that rivers with high incision rates into ignimbrite deposits have steeper slopes in the ignimbrite sections of the main channel, while rivers with low incision rates show lower slopes in ignimbrite sections (Fig. 3). The Roseau, Layou, and Rosalie Rivers, with high incision rates display the greatest slope in the channel segments of ignimbrite which occur frequently throughout the profiles (Fig. 1, 3). In the Toulaman, Melville Hall, and Espagnole Rivers, with low incision rates, long profiles show decreased slopes in ignimbrite sections and primarily consist of block and ash flow deposits rather than ignimbrite deposits (Fig. 3). The slope gradient in these channel profiles is greater in the block and ash flow deposits and display a much more linear shape, lacking any distinct knickpoints.

DISCUSSION

The rivers on Dominica, like many volcanic landscapes that are responding to eruptions, show increased initial incision followed by exponential

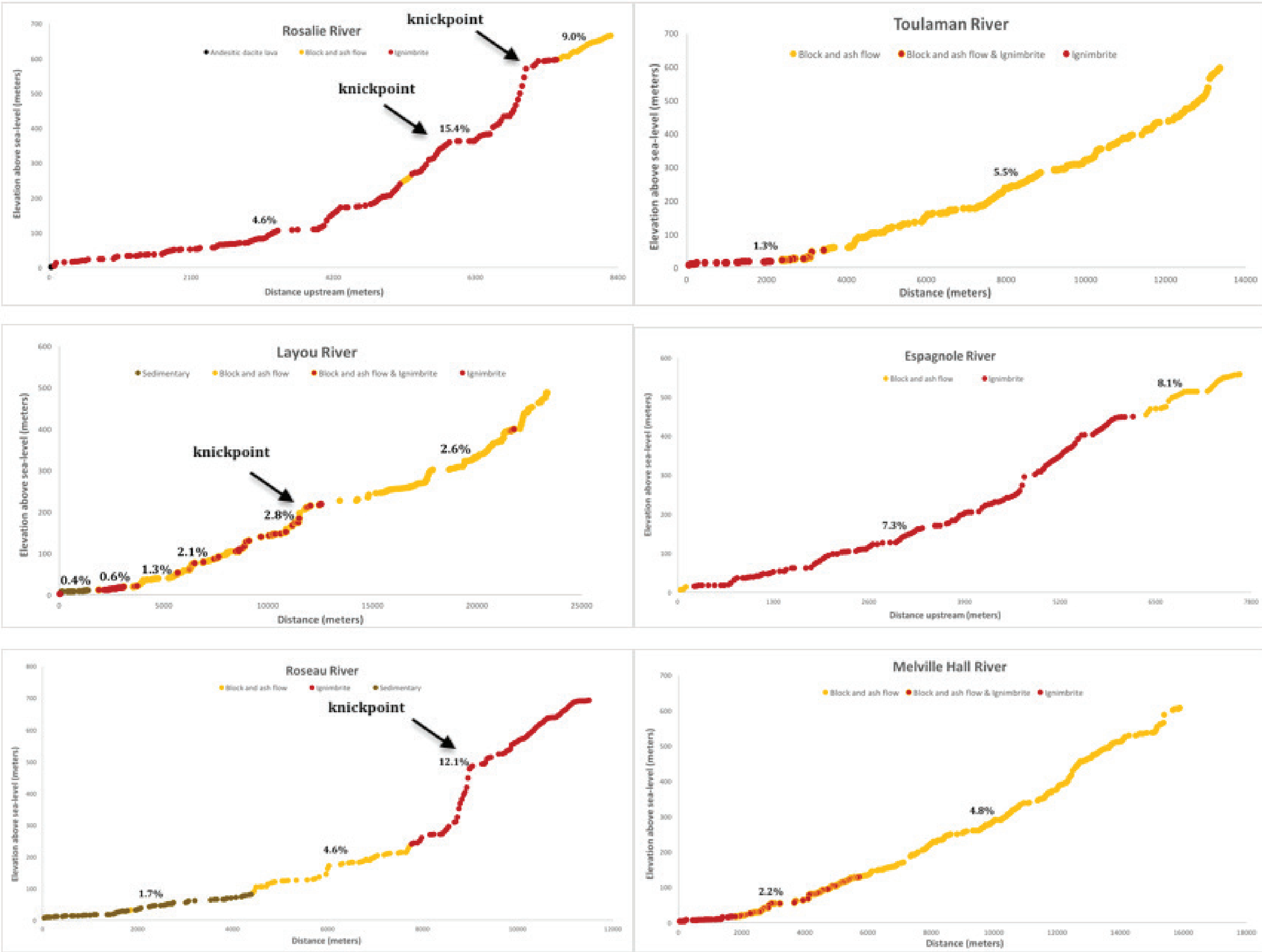

Figure 3. (Right) The Espagnole, Melville Hall, and Toulaman Rivers show steeper slopes in channel segments of block and ash flow deposits than segments of ignimbrite. These northern rivers also had the lowest minimum incision rates (0.4 -0.8 mm/yr), than the southern rivers with higher incision and steeper channels in ignimbrite segments. (Left) Ignimbrite deposit segments are the steepest in The Roseau, Layou, and Rosalie Rivers showing distinct knickpoints in these areas. The increasing steepness in ignimbrite sections in these channels align well with the higher rates of minimum incision (6.3 – 2.4 mm/yr) that the rivers are experiencing.

decrease over time (Thouret, 1999). Incision rates into young ignimbrite deposits less than ~25 ka are very high and are reduced to approximately half in ignimbrite deposits that are between ~43 – 46 ka (Fig. 2). This pattern continues with increasing ignimbrite age as deposits ~59 ka drop approximately 50% again. (Howe et al., 2014; Frey et al., 2015). Incision rates into ignimbrite deposits show a distinct tendency of decreasing around 50% every ~20 ka (Fig. 2). After ~80 ka, incision rates begin to decrease at a progressively slower pace. Incision rates into much older ignimbrite deposits in Peru (Thouret et al., 2007) and Mexico (Montgomery et al., 2003) demonstrate a similar result with incision in deposits < 1.4 Ma being five times greater than incision into deposits 9 – 13 Ma and continuing to decrease as ages increase (Fig. 2). Studies on river incision into basalt lava flows followed a similar trend, where local incision rates were lower in the oldest deposits, with all deposits >100 ka having incision rates below 0.4 mm/yr (Fig. 2; Seidl et al., 1994; Righter et al., 1997; Karlstrom et al., 2007; Seyrek et al., 2008; Maddy et al., 2012; van Gorp et al., 2013; Shtober-Zisu et al., 2017). Long profiles further express this pace of incision as rivers with higher incision rates and younger ignimbrite deposits show multiple knickpoints that represent changes in lithology and erodibility (Cyr et al., 2014) and steeper channel slopes throughout ignimbrite segments (Fig. 3).

On the other hand, rivers with lower incision rates lacked knickpoints and had less lithological changes throughout the channels, suggesting that the rivers have fully incised through these ignimbrite deposits reaching the less erodible underlying bedrock.

The incision rates of Dominica's rivers into the ignimbrite deposits are greater in southern watersheds that tended to have both higher mean basin slopes, local relief, and more area covered by landslides (Fig. 4). Although relief and slope have been shown to correlate with erosion, the percent of watershed area covered in landslides and mean (chi) normalized channel gradient show the strongest influence on incision rates ($p < 0.05$). Increased landsliding is how hillslopes adjust in response to rapid fluvial incision (Burbank et al., 1996) and is a primary mechanism in which landscapes respond to high rates of tectonic uplift (Montgomery and Brandon, 2002; Larson and Montgomery, 2012). Mean incision rates significantly influence mean channel steepness as increased down-cutting leads to channels becoming steeper and have been directly linked to increased erosion especially after hillslopes reach their slope threshold (Kirby and Whipple, 2001; Lague and Davy, 2003; Safran et al., 2005; Wobus et al., 2006). Ultimately, the high annual rainfall, basin slope, and local relief, causes increased landslides and channel steepness, allowing incision to be higher in the southern watersheds.

CONCLUSION

Dominica gives us insights into younger Pleistocene ignimbrite incision rates over the past ~ 200 ka. Our data suggest that mean incision rates of 4.67 – 6.26 mm/yr since ~ 18 – 25 ka, decrease approximately 50% every ~20 ka until ~80 ka, when incision rates reach 0.61 – 0.78 mm/yr and remain similar in

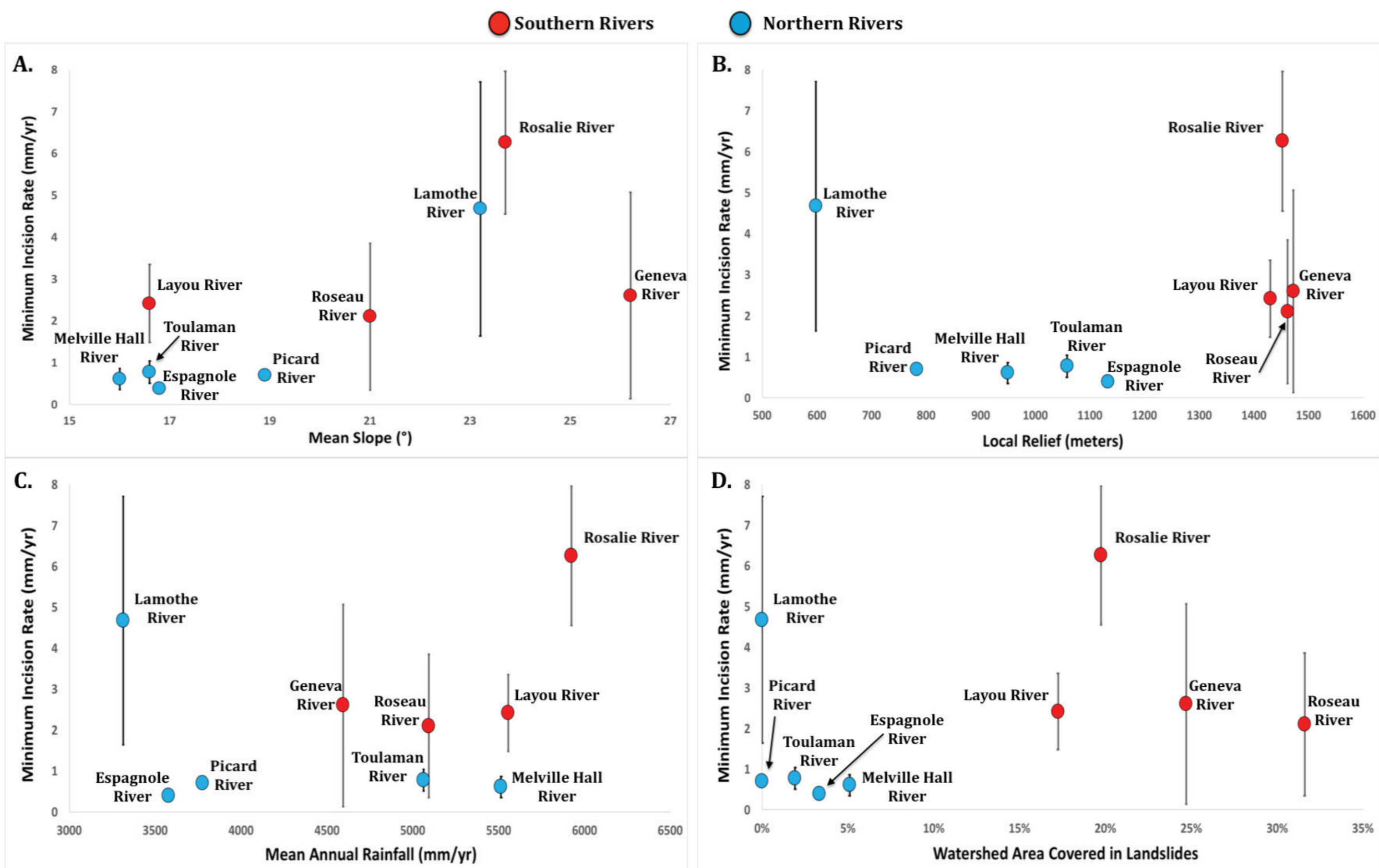

Figure 4. Incision rates across Dominica compared to influential geomorphic characteristics exhibiting both higher rates of incision and topographic/climatic variables in the southern watersheds (red). Northern watersheds (blue) with lower incision rates typically had lower (A.) mean basin slopes, (B.) local relief, (C.) mean annual rainfall, and (D.) area covered in landslides.

~203 ka ignimbrite deposits at 0.39 – 0.7 mm/yr (Fig. 2). Incision rates were most significantly correlated with the percent of watershed area landslide covered, identifying that hillslopes respond to fast fluvial incision through increased frequency of landsliding (Burbank et al., 1996, Montgomery and Brandon, 2002). Normalized chi coordinate values correlated significantly with mean incision rates, strengthening the relationship between river incision and channel steepness that lead to increased erosion (Safran et al., 2005). Long profiles of the rivers on Dominica present lithologic controls on incision, where steep slopes and knickpoints are prominent in segments of the channel consisting of ignimbrite (Fig. 3). Correlations between mean (chi) normalized channel steepness and landslide coverage with incision rates, show that increased climatic and topographic variables drive incision process through landsliding and channel steepening.

ACKNOWLEDGEMENTS

This material is based upon work supported by the Keck Geology Consortium and the National Science Foundation under Grant No. 1659322. I would like to thank the Keck Geology Consortium for the research opportunity and experience to conduct research on Dominica, West Indies and the Dominica Ministry of Forestry for providing permits for this research. Thanks to Holi Frey at Union College for coordinating the Keck project and my Keck Advisor Amanda Schmidt at Oberlin College for the information and data required to carry out this study. Special thanks go to the Geomorph research team: Marcus Hall, Kira Tomenchok, and Haley Talbot-Wendlandt for assistance in the field, lab and supplying data for this study.

REFERENCES

Allen, C.D., 2017, Landscapes and Landforms of the Lesser Antilles: Springer, p. 326.

Burbank, D.W., Leland, J., Fielding, E., and Anderson, R.S., 1996, Bedrock incision, rock uplift and threshold hillslopes in the northwestern Himalayas: Nature, v. 379, p. 505.

Covault, J.A., Craddock, W.H., Romans, B.W., Fildani, A., and Gosai, M., 2013, Spatial and Temporal Variations in Landscape Evolution: Historic and Longer-Term Sediment Flux through Global Catchments: The Journal of Geology, v. 121, p. 35–56.

Cyr, A.J., Granger, D.E., Olivetti, V., and Molin, P., 2014, Distinguishing between tectonic and lithologic controls on bedrock channel longitudinal profiles using cosmogenic ^{10}Be erosion rates and channel steepness index: Geomorphology, v. 209, p. 27–38.

Duvall, A., Kirby, E., and Burbank, D., 2004, Tectonic and lithologic controls on bedrock channel profiles and processes in coastal California: Journal of Geophysical Research: Earth Surface, v. 109, p. F03002.

Frey, H.M., Manon, M.R., and Brehm, S., 2015, Fingerprinting young ignimbrites in Dominica (Lesser Antilles): Constraints from bulk REEs, apatite chemistry, and U-Th zircon chronology: AGU Fall Meeting Abstracts, http://adsabs.harvard.edu/abs/2015AGUFM.V51F3104F (accessed October 2017).

Goldsmith, S.T., Carey, A.E., Johnson, B.M., Welch, S.A., Lyons, W.B., McDowell, W.H., and Pigott, J.S., 2010, Stream geochemistry, chemical weathering and CO_2 consumption potential of andesitic terrains, Dominica, Lesser Antilles: Geochimica et Cosmochimica Acta, v. 74, p. 85–103.

Harel, M.-A., Mudd, S.M., and Attal, M., 2016, Global analysis of the stream power law parameters based on worldwide ^{10}Be denudation rates: Geomorphology, v. 268, p. 184–196.

Howe, T.M., Schmitt, A.K., Lindsay, J.M., Shane, P., and Stockli, D.F., 2015, Time scales of intra-oceanic arc magmatism from combined U-Th and (U-Th)/He zircon geochronology of Dominica, Lesser Antilles: Geochemistry, Geophysics, Geosystems, v. 16, p. 347–365.

Karlstrom, K.E., Crow, R.S., Peters, L., McIntosh, W., Raucci, J., Crossey, L.J., Umhoefer, P., and Dunbar, N., 2007, $^{40}Ar/^{39}Ar$ and field studies of Quaternary basalts in Grand Canyon and model for carving Grand Canyon: Quantifying the interaction of river incision and normal faulting across the western edge of the Colorado Plateau: GSA Bulletin, v. 119, p. 1283–1312.

Kirby, E., and Whipple, K., 2001, Quantifying differential rock-uplift rates via stream profile analysis: Geology, v. 29, p. 415.

Lague, D., Crave, A., and Davy, P., 2003, Laboratory experiments simulating the geomorphic response to tectonic uplift: GEOMORPHIC RESPONSE TO TECTONIC UPLIFT: Journal of Geophysical Research: Solid Earth, v. 108, p. ETG 3-1-ETG 3-20.

Lang, D.M., 1967, Soil and land-use surveys No. 21. Dominica.: Soil and land-use surveys No. 21. Dominica., https://www.cabdirect.org/cabdirect/abstract/19721905097 (accessed January 2018).

Larsen, I.J., and Montgomery, D.R., 2012, Landslide erosion coupled to tectonics and river incision: Nature Geoscience, v. 5, p. 468–473.

Maddy, D., Demir, T., Veldkamp, A., Bridgland, D.R., Stemerdink, C., Schriek, T.V.D., and Schreve, D., 2012, The obliquity-controlled early Pleistocene terrace sequence of the Gediz River, western Turkey: a revised correlation and chronology: Journal of the Geological Society, v. 169, p. 67–82.

Montgomery, D.R., and Brandon, M.T., 2002, Topographic controls on erosion rates in tectonically active mountain ranges: Earth and Planetary Science Letters, v. 201, p. 481–489.

Montgomery, D.R., and López-Blanco, J., 2003, Post-Oligocene river incision, southern Sierra Madre Occidental, Mexico: Geomorphology, v. 55, p. 235–247.

Mudd, S.M., Attal, M., Milodowski, D.T., Grieve, S.W.D., and Valters, D.A., 2014, A statistical framework to quantify spatial variation in channel gradients using the integral method of channel profile analysis: CHANNEL SEGMENT FITTING: Journal of Geophysical Research: Earth Surface, v. 119, p. 138–152.

NASA/METI/AIST/Japan Spacesystems, and U.S./Japan ASTER Science Team, 2009, ASTER Global Digital Elevation Model: Terra ASTER v. 2. NASA EOSDIS Land Processes DAAC, “ASTER GDEM is a product of METI and NASA.” doi: 10.5067/ASTER/ASTGTM.002.

Neuman, C.J., Cry, G.W., Caso, E.L., and Jarvinen, B.R., 1978, Tropical cyclones of the north Atlantic Ocean, 1871–1977: National Climatic Center. US Department of Commerce. National Oceanic and Atmospheric Administration. Asheville, NC.

Ogden, F.L., 2016, Evidence of equilibrium peak runoff rates in steep tropical terrain on the island of Dominica during Tropical Storm Erika, August 27, 201: Journal of Hydrology, v. 542, p. 35–46.

Pike, A.S., Scatena, F.N., and Wohl, E.E., 2010, Lithological and fluvial controls on the geomorphology of tropical montane stream channels in Puerto Rico: Earth Surface Processes and Landforms, v. 35, p. 1402–1417.

Portenga, E.W., and Bierman, P.R., 2011, Understanding Earth’s eroding surface with 10Be: GSA Today, v. 21, p. 4–10.

Reading, A.J., 1991, Stability of tropical residual soils from Dominica, West Indies: Engineering Geology, v. 31, p. 27–44.

Righter, K., 1997, High bedrock incision rates in the Atenguillo River valley, Jalisco, Western Mexico: Earth Surface Processes and Landforms, v. 22, p. 337–343.

Roobol, M.J. and Smith, A.L., 2004, Geologic Map of Dominica, West Indies: CHARIM (Caribbean Handbook on Risk Information Management), 2016, http://charim-geonode.net/layers/geonode:geology_dominica#more.

Safran, E.B., Bierman, P.R., Aalto, R., Dunne, T., Whipple, K.X., and Caffee, M., 2005, Erosion rates driven by channel network incision in the Bolivian Andes: Earth Surface Processes and Landforms, v. 30, p. 1007–1024.

Seidl, M.A., Dietrich, W.E., and Kirchner, J.W., 1994, Longitudinal Profile Development into Bedrock: An Analysis of Hawaiian Channels: The Journal of Geology, v. 102, p. 457–474.

Seyrek, A., Demir, T., Pringle, M., Yurtmen, S., Westaway, R., Bridgland, D., Beck, A., and Rowbotham, G., 2008, Late Cenozoic uplift of the Amanos Mountains and incision of the Middle Ceyhan river gorge, southern Turkey; Ar–Ar dating of the Düziçi basalt: Geomorphology, v. 97, p. 321–355.

Shtober-Zisu, N., Inbar, M., Mor, D., Jicha, B.R., and Singer, B.S., 2018, Drainage development and incision rates in an Upper Pleistocene Basalt-Limestone Boundary Channel: The Sa'ar Stream, Golan Heights, Israel: Geomorphology, v. 303, p. 417–433.

Sosa Gonzalez, V., Bierman, P.R., Fernandes, N.F., and Rood, D.H., 2016, Long-term background denudation rates of southern and southeastern Brazilian watersheds estimated with cosmogenic ^{10}Be: Geomorphology, v. 268, p. 54–63.

Thouret, J. C., 1999, Volcanic geomorphology—an overview: Earth-Science Reviews, v. 47, p. 95–131.

Thouret, J.-C., Wörner, G., Gunnell, Y., Singer, B., Zhang, X., and Souriot, T., 2007, Geochronologic and stratigraphic constraints on canyon incision and Miocene uplift of the Central Andes in Peru: Earth and Planetary Science Letters, v. 263, p. 151–166.

Tomenchok, K., Jimerson, C., Talbot-Wendlandt, H., and Hill, M., 2017, Landslides and Volcanoes: Fingerprinting Erosional Processes on a tropical island, Lesser Antilles: AGU Fall Meeting Abstracts.

Van Gorp, W., Veldkamp, A., Temme, A.J.A.M., Maddy, D., Demir, T., van der Schriek, T., Reimann, T., Wallinga, J., Wijbrans, J., and Schoorl, J.M., 2013, Fluvial response to Holocene volcanic damming and breaching in the Gediz and Geren rivers, western Turkey: Geomorphology, v. 201, p. 430–448.

Willenbring, J.K., Codilean, A.T., and McElroy, B., 2013, Earth is (mostly) flat: Apportionment of the flux of continental sediment over millennial time scales: Geology, v. 41, p. 343–346.

Wobus, C., Whipple, K.X., Kirby, E., Snyder, N., Johnson, J., Spyropolou, K., Crosby, B., and Sheehan, D., 2006, Tectonics from topography: Procedures, promise, and pitfalls, in Special Paper 398: Tectonics, Climate, and Landscape Evolution, Geological Society of America, v. 398, p. 55–74.

KECK Geology Consortium
Learning Science Through Research
Published by Keck Geology Consortium

Short Contributions
Keck Geology Consortium
Volume 31
May 2018

AN INVESTIGATION OF THE INFLUENCES ON THE GEOCHEMISTRY OF STREAMS IN DOMINICA, LESSER ANTILLES: 2014-2017

DEXTER KOPAS, Beloit College
Research Advisors: Susan Swanson, Erouscilla Joseph, and Holli Frey

INTRODUCTION

The chemical makeup of stream waters is a reflection of the environment upstream. Two important tools in determining water provenance are stable isotopes ($\delta^{18}O$ and $\delta^{2}H$) and major ion concentrations, both useful for determining environmental influences in tropical climates (Lachniet and Patterson, 2009, Goldsmith et al., 2010). Much is known about the relationships between environmental factors and stream chemistry in the temperate catchments of North America and Europe; however, little is known about tropical volcanic regions (McDowell et al., 1995, Johnson et al., 1997,). This project will serve to give a general overview of the major environmental controls on stream stable isotope and major ion geochemistry in Dominica and, by extension, the surrounding Lesser Antilles considering multiple and potentially complex interactions of these factors. With a baseline knowledge of the current controls on chemistry, future changes to this baseline can be explored.

Located at the center of the Lesser Antilles archipelago, the island nation of Dominica presents an interesting study area to investigate the environmental influences on stream geochemistry in the tropics. The island features a population of 74,000, active volcanism, one of the world's greatest stream den-sities, with 350 streams over an area of 751 km^2, and high precipitation rates up to 10,000 mm/yr in the mountainous interior. Synthesizing data collected in projects led by Holli Frey over the last four years, this study aims to characterize the impact of environmental factors to stream water chemistry, examining precipitation patterns and hydrothermal activity (Metzger et al., 2015; DeFranco et al., 2016; Metzger et al., 2016).

Several impacts are possible from climatic factors. The dominant wind direction in Dominica is east to west, with the interior mountains presenting a mild rain shadow. As rainout occurs in this direction, east coast precipitation may be more isotopically enriched than on the west coast (Lachniet and Patterson, 2009). At higher altitudes in the central mountains, lower temperatures may drive precipitation to be more isotopically depleted. If local rainout is an important control, then catchment precipitation may be inversely correlated with $\delta^{18}O$. Tropical storms often have a source different from normal weather, such that a sudden rainfall event may temporarily alter the isotopic signature of surface streams (Good et al., 2014). Tropical Storm Erika, which hit Dominica in August of 2015, presents an interesting opportunity to test this relationship, having dropped over 500 mm of rainfall in a single day (Ogden, 2016). If any of these effects are significant, they should impact the isotopic signature of meteorically-fed surface waters.

At hydrothermal springs near volcanic centers, meteorically sourced water is altered through subsurface geothermal processes, wherein high temperatures encourage faster equilibration between water and bedrock. Downstream, rivers with hydrothermal sites in their catchments may be enriched in both $\delta^{18}O$ and $\delta^{2}H$, and the stream water may exhibit an ionic signature that is similar to the hydrothermal source. These effects should be proportional to the relative input of hydrothermally altered waters to a given stream and diminish going downstream from the hydrothermal source.

METHODS

This study is primarily concerned with a four-year collection of stream and spring samples. From 2014 to 2017, annual samples were collected in June from a total of 104 water bodies. Samples were collected from streams, both near coastal outlets as well as upstream. Coastal samples were collected closest to the shore while remaining out of the influence of seawater. The major hydrothermal springs on the island were also sampled directly from orifices (Fig. 1).

The suite of 104 sample sites was classified depending on three criteria. In terms of hydrothermal influence, four categories are used. Samples from streams with at least one hydrothermal site in their catchment are classified as mostly meteoric with some hydrothermal input, or Hyd-met, while those without any hydrothermal sites upstream are classified as purely meteoric, or Met. This was determined using the placement of hydrothermal areas from Smith and Roobol's 2013 geologic map of Dominica in relation to stream basins in a geographic information system (GIS). Samples collected directly from hydrothermal pools are classified as hydrothermal, or Hyd. Samples are further differentiated into coastal (<2 km from the coast) and interior (>2 km) using GIS. To measure the rain shadow effects, coastal samples are split into either east and west, excluding those sites on the island's southern coast.

All water samples were analyzed for stable isotopes of deuterium and oxygen, and used to assess the influences of all possible environmental factors. Waters were sealed in glass containers with no air space. Thermo TC/EA (High Temperature Conversion Elemental Analyzer) measured δ^2H concentrations, and a Delta S Mass Spectrometer and Ecotainer measured the concentration of $\delta^{18}O$. Three in-house standards corrected the data, which were then related to VSMOW. For a local meteoric water line (LMWL), values are used for the Northeastern Caribbean from Govender (2013). Stable water isotope values were averaged for each sample site and plotted in Esri™ ArcMap GIS software based on their GPS-measured sampling location. Isotope values are quantified using quantiles and colored accordingly.

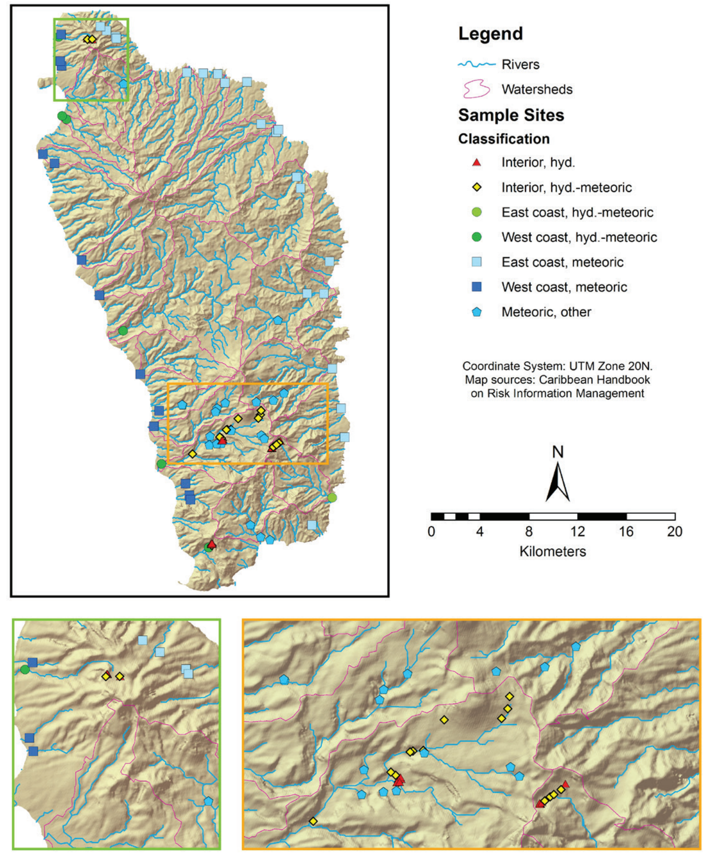

Figure 1. Map of the Dominica showing categorized sample locations.

To aid in assessment of wind direction, altitude, and storms, a contoured precipitation map from a 1967 soil and land-use report was digitized, using GIS to extrapolate values between contour lines. Stream catchments were imported to GIS, where the zonal statistics tool gave an average annual precipitation value associated with each stream catchment. To measure the impacts from tropical storms, a single event was examined. Tropical Storm Erika was the only major storm to pass significantly close to Dominica during the sampling period, passing by the island on August 27, 2015 and dropping over 500 mm of precipitation. The proceeding sampling occurred ten months later in June of 2016.

To further assess the influence of hydrothermal sources, major cations and anions were analyzed in addition to the previously discussed isotopes. At all sites from Figure 1, samples for major ion analysis were put into 60 mL Nalgene™ HDPE sterile sample bottles using a 0.2 mm filter, preserved with a drop of nitric acid and stored at 0-10°C. A Thermo Scientific

Dionex ion chromatography system analyzed the samples, using a 1/25 dilution for the hydrothermal samples. Samples for analysis of CO_3 and HCO_3^- were syringed into Falcon™ 50 mL Conical Centrifuge Tubes using a 0.2 mm filter. A MetrohmTM Titran-doTM 869 Compact Sample Changer Titrator ran the samples with NaOH as a standard to test for alkalinity, used to calculate CO_3 and HCO_3^-. Rockware AqQa software calculated the internal consistency of samples, cutting off anion-cation balances greater than 10%, and plotting the data on a Piper diagram.

In order to examine the downstream effects of hydrothermal mixing, the Roseau River is a good fit as it is well sampled along its north fork and features three different hydrothermal areas (Fig. 1). Along the Roseau River, sample sites MI5, MI4, TR3, TR5, TR2, WW3.5, WW9, and WW10 were chosen and their distance upriver measured using GIS.

RESULTS

Of the 104 sample sites, a total of 279 samples were collected and analyzed, an average of 70 per year from 2014 to 2017. Out of all sample sites, 55 are classified as Met (13 west coast, 21 east coast, 21 other), 8 as coastal Hyd-met (7 west coast, 1 east coast), 18 as interior Hyd-met, and 22 as Hyd. One sample site near the Valley of Desolation hydrothermal area, VOD10, has an unknown exact location and is excluded from analysis.

Climatic Factors

Dominica's east coast is slightly more depleted in $\delta^{18}O$ compared to the west coast, by ~0.20‰ (α=0.05) (Fig. 2). The difference in $\delta^{18}O$ between coasts is consistent throughout 2014 to 2017. However, if only meteoric streams are considered, then this difference is not statistically significant (P=0.07). There is no significant difference in δ^2H between east and west coasts (P=0.80). Turning to annual trends over the four-year period and the possible influence of Tropical Storm Erika, there is a small, but consistent positive trend in $\delta^{18}O$ of the purely meteoric samples, moving steadily from -2.38 ‰ in 2014 to -2.24 ‰ in 2017.

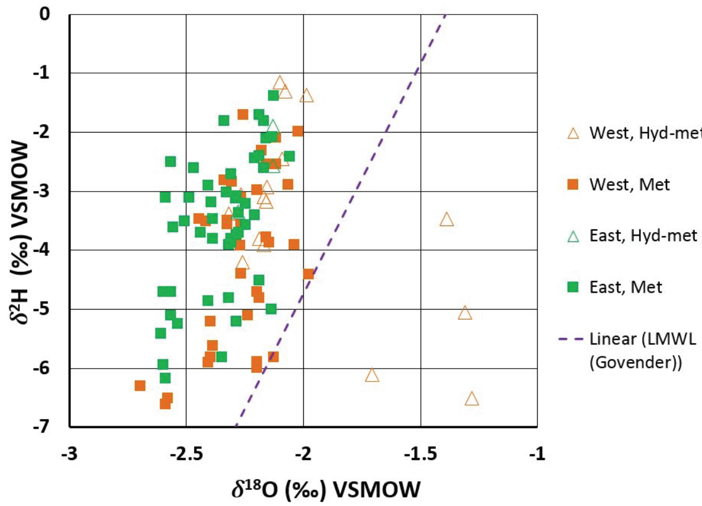

Figure 2. Graph of stable water isotopes showing difference between east and west coast sample sites. Note the lack of difference between Met samples.

Graphs were created to display $\delta^{18}O$ in relation to mean catchment precipitation and mean catchment altitude. However, a statistical relationship does not exist between $\delta^{18}O$ and mean catchment precipitation (R^2=0.0093), nor does one exist between $\delta^{18}O$ and mean catchment altitude (R^2=0.0642).

Hydrothermal Factors

Isotopically, there are distinct differences between the four categories of hydrothermal input to water (Fig. 3). Purely meteoric streams are the least enriched in both $\delta^{18}O$ and δ^2H, followed by interior Hyd-met, then coastal Hyd-met, then Hyd. The same trend is seen in respect to variability, with Met displaying the smallest standard deviation and Hyd the greatest. From a two-sample T-test assuming equal variances, interior streams with a known hydrothermal influence differ significantly from those without any known source in $\delta^{18}O$, but not in δ^2H (α=0.05). The mean differences are 0.19 ‰ for $\delta^{18}O$, and 0.46 ‰ for δ^2H.

Figure 4 displays a map of $\delta^{18}O$ values. Spatially, values are seen to be more positive in the vicinity of hydrothermal sites, with the exception of more negative values in the Morne Aux Diables (MAD) volcanic center. Deuterium show a less obvious trend, though values are generally more positive directly at hydrothermal sites.

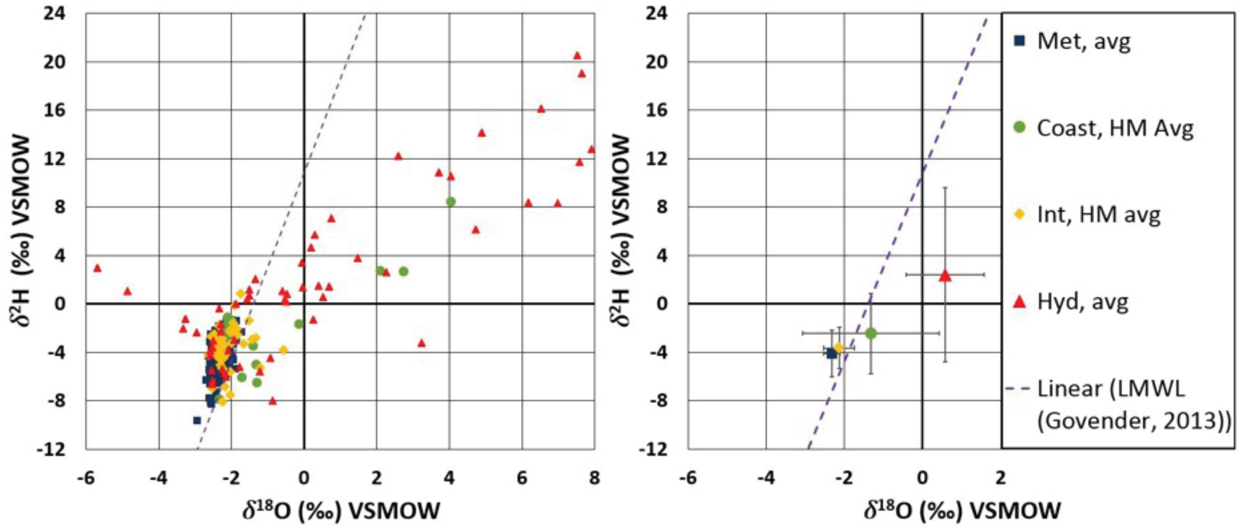

Figure 3. Stable water isotope graph split between hydrothermal categories. Left graph shows all data, right graph shows 4-year averages and standard deviations.

Piper diagrams show that stream waters sourced by hydrothermal springs are geochemically similar to their hydrothermal source, and generally contain more SO_4, Na, Mg, and Cl (Fig. 5). Hydrothermal springs display the highest concentrations of these ions.

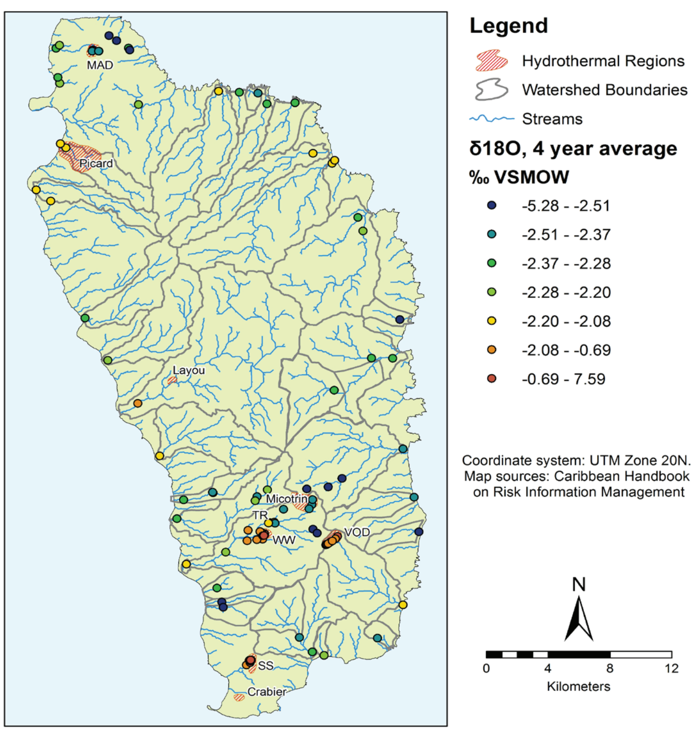

Figure 4. Map of δ¹⁸O values for all sample sites. Areas with any known degree hydrothermal contribution are generally mapped. MAD = Morne Aux Diables, WW = Wotten Waven, VOD = Valley of Desolation, and SS = Sulphur Springs. Note: Trafalgar (TR) has very minor thermal contribution but is generally not considered to be hydrothermal.

DISCUSSION

Climatic Factors

Stable water isotope values show no significant difference between east and west coast, suggesting any differences in precipitation or dominant weather direction are not significant enough to alter stream water chemistry. This is supported by the lack of correlations between $\delta^{18}O$ and either catchment parameter. It should be noted that the sampling period (June) has historically been the time of year when Dominica's east and west coast weather stations have been the most similar in precipitation (weather.gov.dm). If sampled during either May or November, when the east-west coast precipitation difference is most pronounced, then climatic effects may be more noticeable. A year-long study of Dominican stream waters revealed distinct chemical differences between the wet and dry seasons when corrected for precipitation difference with regards to dissolved ions (Goldsmith et al., 2009).

With regards to Tropical Storm Erika, no discernible effect is seen, with meteorically-fed streams staying on a consistent trend of positive shifts in $\delta^{18}O$ and no deviation from this trend in 2016. Since sampling occurred 10 months following the storm, it is likely the residence times of meteoric waters are shorter than this period, and that severe weather events do not have long lasting island-wide effects on stream chemistry. However, to confirm this more research is needed,

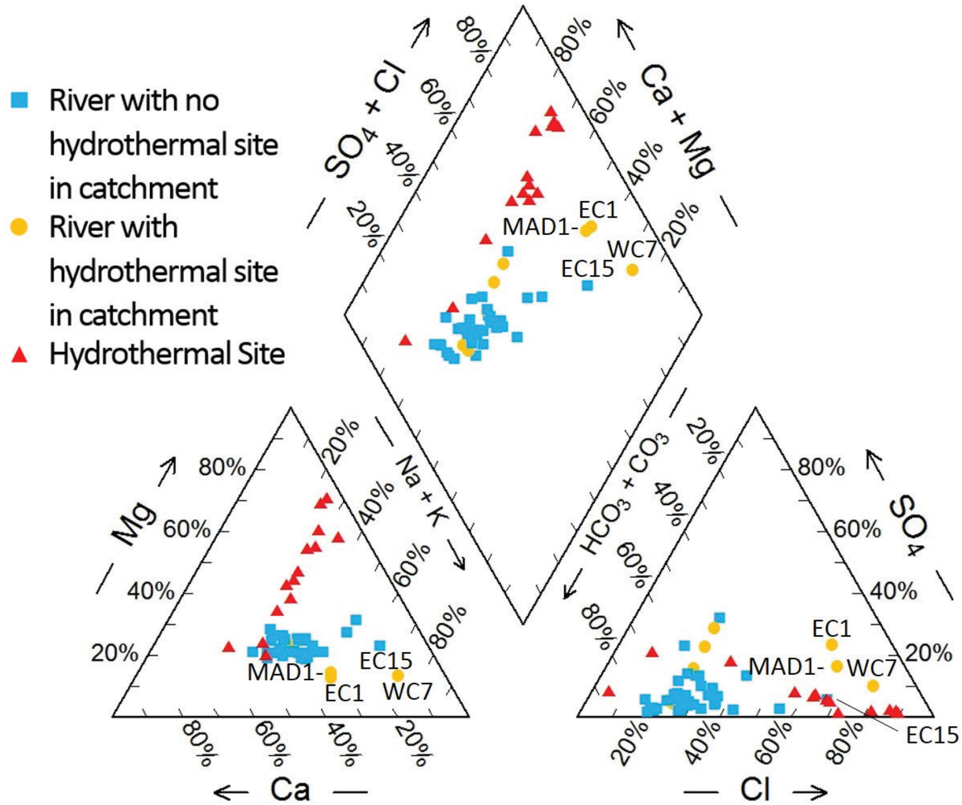

Figure 5. Major ion piper diagram, displaying Hyd, Hyd-met, and Met samples.

especially soon after storm events, on cases of stream water effects from storm events in the tropics. Recently, Hurricane Maria, a category 5 storm which was much more severe than Tropical Storm Erika, made landfall in Dominica in September 2017. A subset of stream waters were collected in January 2018, four months after the storm, and are currently being analyzed.

Hydrothermal Factors

Where stream water chemistry influences are most apparent is from the effects of mixing with hydrothermally altered waters. Figure 4 shows how streams downstream of hydrothermal sites also have ionic compositions between meteoric waters and their hydrothermal source, with the exception of higher Na + K concentrations for some of the Hyd-met samples. This could be due to mixing of some sea water in coastal sampling, as Na + K concentrations are high only in the case of a handful of coastal samples.

As expected, Figure 3 shows that waters generally become more enriched in both $\delta^{18}O$ and $\delta^{2}H$ with progressive input of hydrothermally altered water. As noted in previous Dominican stream chemistry reports, precipitation amount seems to be inversely correlated with $\delta^{18}O$ in Hyd and Hyd-met samples, due to dilution of hydrothermally altered stream water with more meteoric waters (Metzger, et al., 2015; DeFranco, et al., 2016; Metzger, et al., 2016). This effect is not seen in Hyd samples. However, in 2017 this trend is not followed, as both precipitation and $\delta^{18}O$ increases, suggesting that some other factor is influencing the overall isotopic signature of hydrothermal systems.

One peculiarity is that Hyd-met samples near the coast are more isotopically enriched than Hyd-met samples further inland, contrary to what would be expected due to progressive meteoric input downstream. However, interior Hyd-met are still contained within the variance of coastal Hyd-met. The few cases of coastal Hyd-met samples that significantly shift the average of the group in a more positive direction are the streams that drain the Sulphur Springs (SS) system near the southwestern coast. Here, several explanations are possible, and it is likely a result of a combination of these factors. The proximity of downstream sample sites to both the coast and to the hydrothermal sites means that hydrothermal waters are not getting as much meteoric input before being sampled, evident in the orange color and high temperatures at the downstream sampling site. Another factor that could contribute in the decrease the meteoric input is that the location of SS on the southwestern coast means that this area receives less rainfall compared with the rest of the island. This may also mean that the system itself is more vapor dominated as compared to the others that appear to be more liquid dominated. Hence, its difference in stable isotope composition.

In a few samples hydrothermal sites display a significant negative trend in $\delta^{18}O$, as in the case of the MAD volcanic center, situated in the north of the island. This trend is consistent for MAD and may be a result of $\delta^{18}O$ exchange between the thermal waters with dissolved CO_2, which takes place during equilibration in systems with high ratios of CO_2 to water (Joseph et al., 2011). In the case of rivers draining MAD, they show no deviation from nearby Met streams.

Looking at the spatial variation in isotopes, trends in $\delta^{18}O$ are expected, with samples downstream of hydrothermal sites showing $\delta^{18}O$ values similar to the hydrothermal source. There also appears to be a spatial component of enrichment. Near the Wotten Waven (WW) hot springs, there are enriched $\delta^{18}O$ values nearby the hot springs that are not downstream (samples TR1 and WW6-8). This suggests that the movement of hydrothermal waters may not be limited to the hot springs, but that there is unknown subsurface input of hydrothermal waters to the nearby streams. Goldsmith et al. (2010) suggest similar conduits from soil/bedrock interface to stream water. Locally in Wotten Waven, this release of hydrothermal waters could be due to faulting related to the underlying caldera and should be investigated further.

CONCLUSIONS

Based on these results, precipitation and weather factors do not play a significant role in stream chemistry. However, more sampling is needed throughout the year to examine the effects of seasonal variation. In our sampling period, hydrothermal sources are the dominant control on stable isotope and ionic composition. Streams draining hydrothermal sources are isotopically and ionically enriched. Input of hydrothermal waters to streams may not be limited to surface features such as springs, but may also be contributed from complex groundwater sources directly to streams from underlying hydrothermal reservoirs.

ACKNOWLEDGEMENTS

This material is based upon work supported by the Keck Geology Consortium and the National Science Foundation under Grant No. 1659322. I would also like to thank Sue Swanson for her guidance, Mazi-Mathias Onyeali, Jackie Buskop, Amanda Schmidt, Sarah Katz, and Matt Manon for help with lab and field work. Thank you to the Archbold Tropical Research and Education Center and Union College for hospitality and facilities.

REFERENCES

DeFranco, K., Frey, H.M. and Manon, M.R.F., 2016, Establishing island-wide water characterization in a volcano-hydrothermal system in Dominica, Lesser Antilles: Northeastern section Geological Society of America Abstracts with Programs. v. 48, no. 2.

Dominica Meteorological Service, 2018, Douglas-Charles Airport: 1981-2010 and Canefield Airport: 1982-2011: http://www.weather.gov.dm/climate-data.

Goldsmith, S.T., Carey, A.E., Johnson, B.M., Welch, S.A., Lyons, W.B., McDowell, W.H., and Pigott, J.S., 2010, Stream geochemistry, chemical weathering and CO_2 consumption potential of andesitic terrains, Dominica, Lesser Antilles: Geochimica et Cosmochimica Acta, v. 74, p. 85–103, doi: 10.1016/j.gca.2009.10.009.

Good, S.P., Mallia, D.V., Lin, J.C., and Bowen, G.J., 2014, Stable Isotope Analysis of Precipitation Samples Obtained via Crowdsourcing Reveals the Spatiotemporal Evolution of Superstorm Sandy: PLOS ONE, v. 9, p. e91117, doi: 10.1371/journal.pone.0091117.

Govender, Y., Cuevas, E., Sternberg, L.D.S., and Jury, M.R., 2013, Temporal Variation in Stable Isotopic Composition of Rainfall and Groundwater in a Tropical Dry Forest in the Northeastern Caribbean: Earth Interactions, v. 17, p. 1–20, doi: 10.1175/2013EI000534.1.

Johnson, L., Richards, C., Host, G. and Arthur, J., 1997, Landscape influences on water chemistry in Midwestern stream ecosystems: Freshwater Biology, v. 37, p. 193–208. doi:10.1046/j.1365-2427.1997.d01-539.x

Joseph, E.P., Fournier, N., Lindsay, J.M., and Fischer, T.P., 2011, Gas and water geochemistry of geothermal systems in Dominica, Lesser Antilles island arc: Journal of Volcanology and Geothermal Research, v. 206, p. 1–14, doi: 10.1016/j.jvolgeores.2011.06.007.

Lachniet, M.S., and Patterson, W.P., 2009, Oxygen isotope values of precipitation and surface waters in northern Central America (Belize and Guatemala) are dominated by temperature and amount effects: Earth and Planetary Science Letters, v. 284, p. 435–446, doi: 10.1016/j.epsl.2009.05.010.

Lang, D.M., 1967, Soil and land-use surveys No. 21. Dominica., in Report. Regional Research Centre, University of the West Indies, Dominica, p. 59.

McDowell, W.H., Lugo, A.E., and James, A., 1995, Export of Nutrients and Major Ions from Caribbean Catchments: Journal of the North American Benthological Society, v. 14, p. 12–20, doi: 10.2307/1467721.

Metzger, T., Frey, H.M., and Manon, M.R.F., 2015, Water geochemistry analysis of streams and hydrothermal waters in Dominica, Lesser Antilles: Northeastern section Geological Society of America Abstracts with Programs, v. 47.

Metzger, T., Frey, H.M., Manon, M.R.F., and DeFranco, K., 2016, Island-wide isotopic analysis of meteoric and hydrothermal waters in Dominica, Lesser Antilles: Geological Society of America Abstracts with Programs. v. 48, no. 7.

Ogden, F.L., 2016, Evidence of equilibrium peak runoff rates in steep tropical terrain on the island of Dominica during Tropical Storm Erika, August 27, 2015: Journal of Hydrology, v. 542, p. 35–46, doi: 10.1016/j.jhydrol.2016.08.041.

Smith, A.L., Roobol, M.J., Mattioli, G.S., Fryxell, J.E., Daly, G.E., and Fernandez, L.A., 2013, The Volcanic Geology of the Mid-Arc Island of Dominica: Geological Society of America, Geological Society of America Special Paper, https://books.google.com/books?id=FbmkAQAAQBAJ.

Learning Science Through Research
Published by Keck Geology Consortium

Short Contributions
Keck Geology Consortium
Volume 31
May 2018

DECOMPRESSION AND HEATING INDUCED AMPHIBOLE BREAKDOWN IN EFFUSIVE VOLCANISM ON DOMINICA, LESSER ANTILLES

ABADIE LUDLAM, Union College
Research Advisor: Holli Frey

INTRODUCTION

Amphibole stability is generally dictated by the water content of a melt, which can be changed by heating or decompression. As these processes occur and water content decreases, amphibole becomes unstable and begins to break down (Fig. 1). This breakdown occurs as an open system reaction with the surrounding melt, creating new minerals in the place of amphibole (Fig. 1; Buckley et al., 2006; Plechov et al., 2008). The result is a reaction rim usually composed of plagioclase, orthopyroxene (opx), clinopyroxene (cpx), and Fe-Ti oxides (Rutherford and Hill, 1993; Rutherford and Devine, 2003; Browne and Gardner, 2006; De Angelis et al., 2013; De Angelis et al., 2015). Many authors (Rutherford and Hill, 1993; Browne and Gardner, 2006; Plechov et al., 2008; De Angelis et al., 2013) have investigated both natural and experimentally created breakdown rim textures, but little consensus has been made about the types of textures that can be created and by what process.

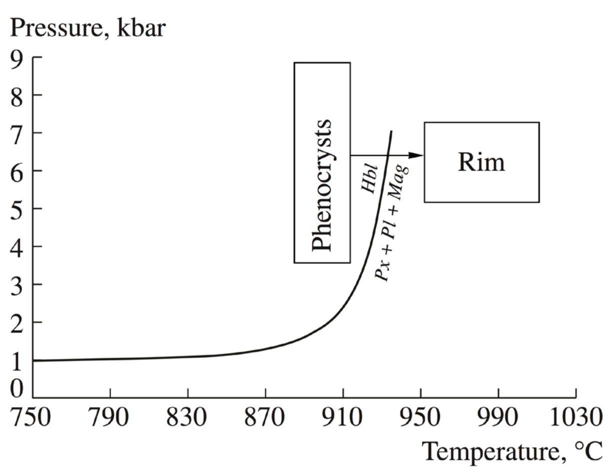

Figure 1. An experimentally derived amphibole stability field for dacite that was used in this as an approximate stability field for the samples in this study. From Plechov et al., 2008.

Decompression induced rims occur as magma rises slowly enough for amphibole to spend adequate time in pressures where it is unstable and can react with the melt. In decompression induced rims, the ascent rate of the magma determines the thickness of the rims (Rutherford and Hill, 1993; Rutherford and Devine, 2003; Plechov et al., 2008). A slower ascent pushes amphibole outside of its stability field for a longer time, allowing breakdown to occur, whereas a fast ascent moves the crystal to the surface quickly, minimizing time for reactions and creating a thin rim or no rim at all (Rutherford and Hill, 1993). Additionally, magma stalling at depth can create zoned rims, with multiple populations of grain sizes (Browne and Gardner, 2006). The relationship between ascent rate and rim thickness has been shown numerous times experimentally, and decompression experiments have allowed calibration curves for rates of ascent to be established for specific melt compositions (Rutherford and Hill, 1993; Plechov et. al, 2008). Ascent rates are generally on the order of days to weeks (Rutherford and Hill, 1993; Plechov et. al, 2008).

Heating induced reaction rims are often attributed to mafic injections and can occur in as little as 3 hours at 10-15 °C above the amphibole stability field (Rutherford and Devine, 2003; De Angelis et al., 2013; De Angelis et al., 2015). The extent of breakdown depends on the degree of heating. In extreme cases, complete breakdown can occur in just 36 hours, but prolonged heating at a lower temperature causes little change in rim thickness (De Angelis et al., 2015).

This study aims to characterize and understand the cause of amphibole breakdown in lava domes on Dominica, Lesser Antilles. Four andesitic-dacitic lava domes (60-64 % SiO_2) from different locations and varying ages were studied: Espagnol (ESP, 744 ± 44 ka), La Falaise (LF, 84 ± 5 ka), Canot (CAN, < 50 ka), and Patates (MPP, 510 ± 9 yrs) (Project Director's Fig. 1; Lindsay, 2003; Howe et al., 2015). ESP is on the northwestern coast, and the others are located in the Plat Pays complex in the southwestern region of the island. These domes exhibit drastically different extents of breakdown, and our goal was to understand what was causing breakdown and why it was different between domes.

METHODS

A Zeiss EVO-MA15 scanning electron microscope (SEM), along with a back scattered electron (BSE) detector were used to image thin sections of the samples. Running with the SEM, a Bruker EDX system was used to create elemental maps and determine compositions of minerals in the samples. Oxide quantitative analysis was performed using a 5 µm beam spot, standardizing Mg and Al on spinel, Ti on rutile, Fe on hematite, and Si, Ca, and Mn on spessartine, with ilmenite as a secondary standard. Plagioclase analysis was performed using a 10 µm by 10 µm rastered box, standardizing Mg and Si on augite, K on microcline, Na on albite, and Al, Ca, and Fe on grossular, with labradorite as a secondary standard. For all analyses, the beam current was 15 kV.

Rim thicknesses were measured on crystals in ESP and MPP using ImageJ. Thicknesses were taken at the thinnest and thickest points of each rim, and 2 to 3 other evenly spaced points on the rim.

After compositions were obtained, crystallization temperatures of all possible pairs of Fe-Ti oxides were found using the Ghiorso and Evans (2008) thermometer, aided by the Hora et al. (2013) Excel script. Due to the scarcity of oxides in our samples, all temperatures were considered, regardless of if the oxide pairs passed the Bacon-Hirschmann (1988) Mg/Mn test of equilibrium. Water contents and depths were found using these temperatures, plagioclase compositions, whole rock geochemistry as a proxy for magmatic liquid, and the plagioclase hygrometer of Waters and Lange (2015).

RESULTS

Amphibole Breakdown Textures

Six breakdown textures were observed among the four samples: two thin rimmed textures and four pseudomorph textures. Each sample contained either thin rimmed textures or pseudomorph textures, but not both. All textures were composed of plagioclase, pyroxene, and oxides.

Thin rimmed breakdown textures were observed in two samples: ESP and MPP (Fig. 2). Each sample had a distinct texture that made up 100% of their observed hornblende crystals. Type 1, found in ESP, is equigranular, fine grained, and ranged from 8 to 82 µm. Thicknesses does not correlate to crystal size, and rim thickness is highly variable on individual crystals. The texture often surrounds inclusions and extends into cleavage planes. Type 2, found in MPP, is also equigranular and fine grained, but with thinner rims than type 1, with nearly all rims between 6 and 22 µm. Thickness again does not correlate to crystal size. The texture is rarely found around inclusions or along cleavage planes, and rim thicknesses are more consistent on each crystal and throughout the sample than type 1. Oxides are notably scarce in type 2.

The four pseudomorph textures are shared between LF and CAN (Fig. 3). Types 3, 4, and 5 were found in both samples, and type 6 is unique to CAN. Type 3 consists of an equigranular center and a finer grained rim with noticeabley fewer oxides than the core. Type 4 is characterized by multiple zones of distinguishable differences in grain size and relative mineral abundances. Grains with this texture tend to sharply preserve amphibole shape. Type 5 is a grungy texture, with no distinguishable grain shape. Type 6 is the coarsest grained texture, and the amphibole shape appears to be disaggregating.

Oxide Temperatures

Temperatures were found for the matrix, reaction texture, and inclusions for LF and CAN, but only for the matrix and inclusions for ESP and MPP because their rims were too fine grained to obtain an accurate analysis (Fig. 4). Temperatures in ESP were 710-870 °C in the matrix (n = 42) and 820-920 °C in the

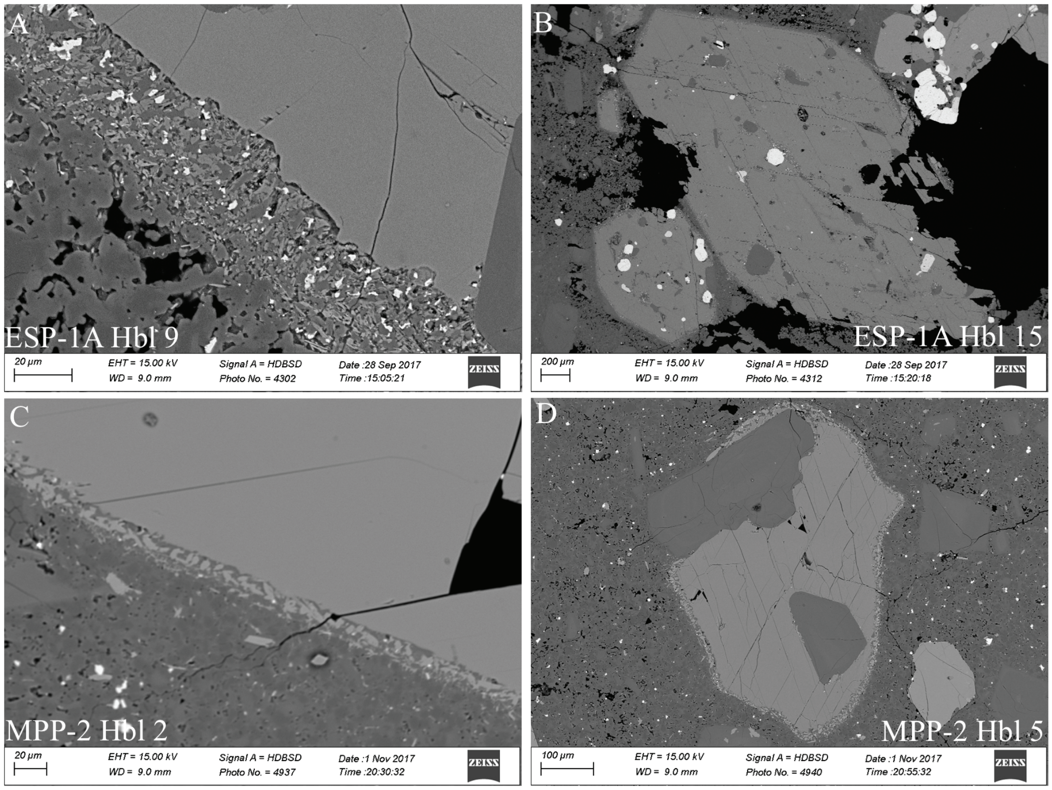

Figure 2. BSE images of thin rimmed reaction textures, both consisting of plagioclase, pyroxene, and oxides. A, B: Type 1, found in ESP only, is the thicker of the two textures. C, D: Type 2, found in MPP-2 only, contains noticeably fewer oxides than type 1.

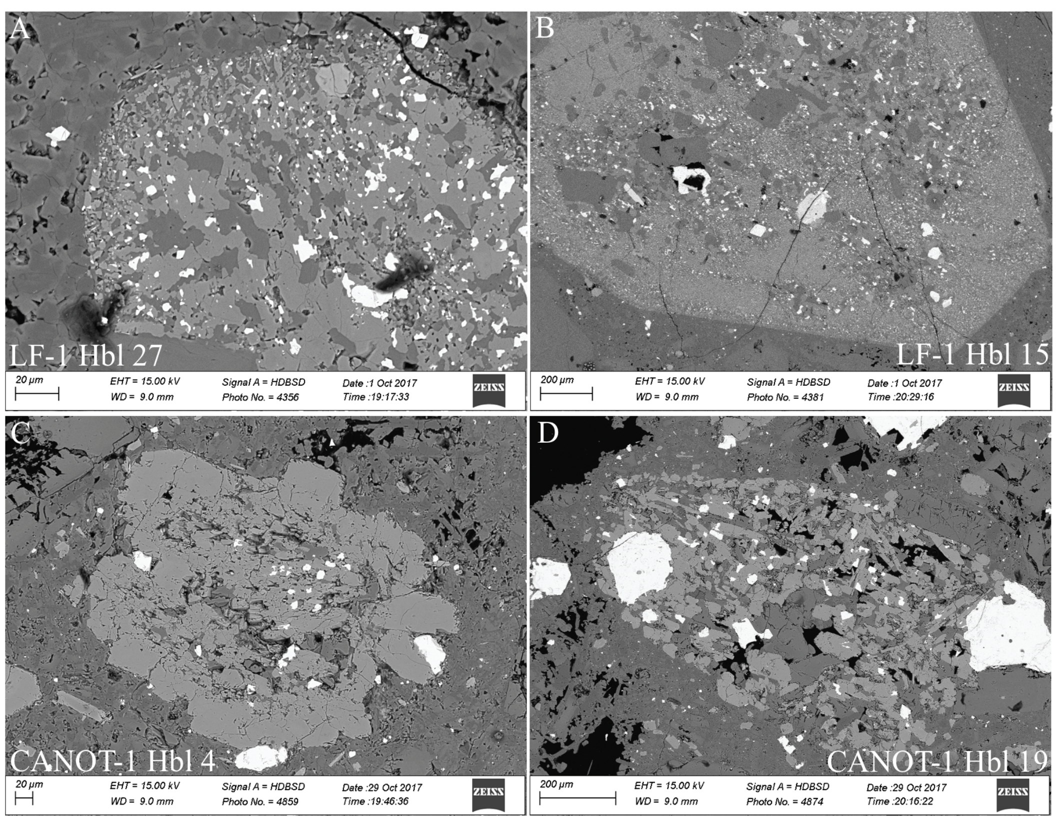

Figure 3. BSE images of hornblende pseudomorphs. A: Type 3, a coarse interior and fine grained, oxide poor exterior. B: Type 4, zoned by grain size. C: Type 5, grungy with indistinguishable shape. D: Type 6, coarse grained and shape disaggregating.

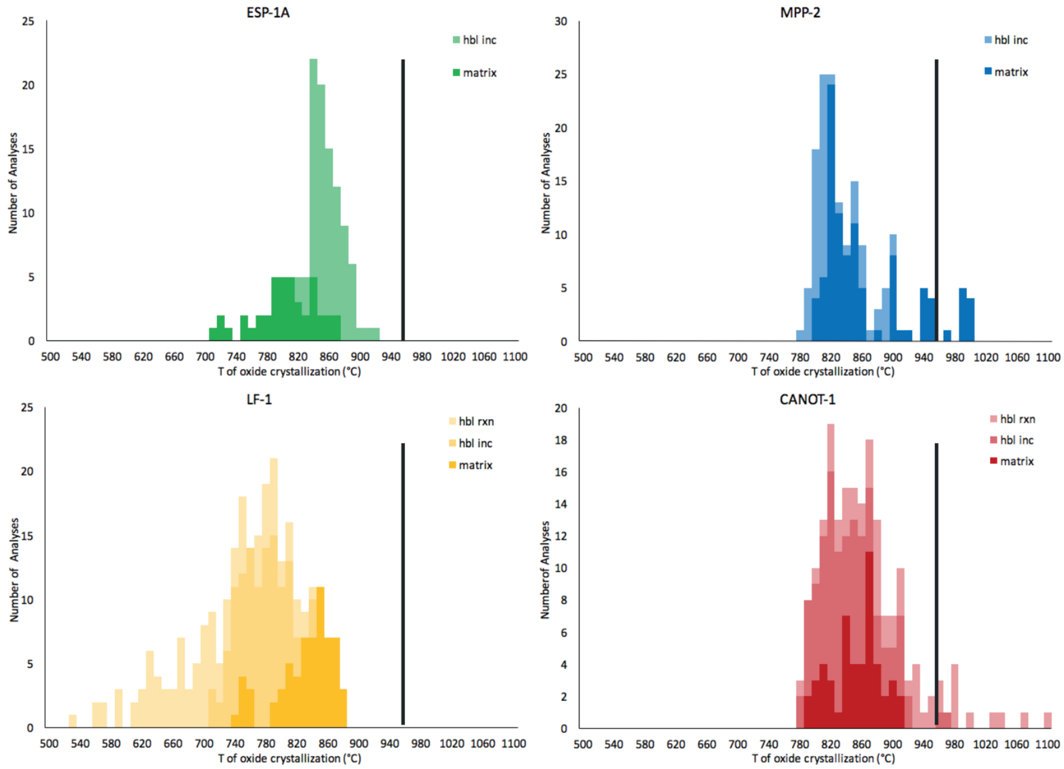

Figure 4. Temperatures of oxide crystallization, found using oxide compositions and Ghiorso and Evans 2008 geothermometer.

inclusions (n = 81). In MPP, temperatures ranged from 800-1000 °C in the matrix (n = 100) and 780-900 °C in inclusions (n = 60). In LF, temperatures ranged from 740-880 °C in the matrix (n = 64), 710-840 °C in inclusions (n = 100), and 530-830 °C in the reaction texture (n = 100). Temperatures in CAN were relatively constant. They ranged from 790-910 °C in the matrix (n = 50), 780-970 °C in inclusions (n = 88), and 780-1100 °C in the reaction texture (n = 50).

Plagioclase Compositions

Plagioclase rim compositions were found for all four samples, and core compositions were found for ESP and LF. In both ESP and LF, core compositions were more anorthitic and wider ranging than rim compositions. Rim compositions in ESP ranged from An_{34} to An_{62} (n = 36) and core compositions ranged from An_{48} to An_{82} (n = 54). LF rim compositions ranged from An_{42} to An_{66} (n = 27) and core compo-sitions from An_{44} to An_{90} (n = 67). In MPP, rim compositions ranged from An_{48} to An_{60} (n = 31). Rim compositions of CAN ranged from An_{46} to An_{92} (n = 30).

Plagioclase rim compositions, whole rock geochemistry, and oxide temperatures were used to determine the minimum and maximum water content of the latest crystallized melt, yielding 6.8-7.2 wt% in ESP, 6.7-6.8 wt% in MPP, 8.6-8.8 wt% in LF, and 6.5-6.8 wt% in CAN. These water contents, oxide temperatures, and whole rock geochemistry were then used to find the pressures when plagioclase rims were crystallizing. These pressures were 3100-3450 bars for ESP, 3050-3100 bars for MPP, 4800-5000 bars for LF, and 3000-3250 bars for CAN.

Elemental Mapping

Elemental maps displaying Mg, Ca, and Fe reveal the composition of pyroxenes in each samples' reaction textures (Fig. 5). MPP rims contain negligible Ca and significant Mg and Fe, indicating that cpx is absent in the rims, whereas opx is abundant. LF and CAN have many grains with a combination of Mg and Ca, as well as grains that contain only Mg, indicating an abundance of both cpx and opx. ESP rims shows two distinct zones, with an abrupt boundary between, of pyroxene composition. The inner looks similar to LF

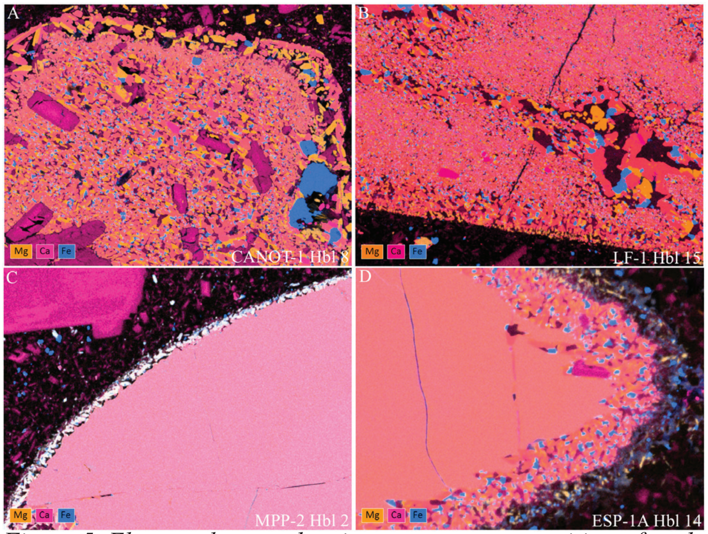

Figure 5. Elemental maps showing pyroxene composition of each sample's breakdown texture.

and CAN and is cpx rich, and the outer looks similar to MPP, lacking cpx.

DISCUSSION

The abundance, or lack thereof, of cpx in the reaction textures of the amphibole may be diagnostic of the cause of amphibole breakdown. De Angelis et al. (2015) found that in experiments at several temperatures, cpx was lost after 36 to 48 hours of heating, and for certain temperatures, prolonged heating did not cause a substantial growth in rim thickness.

The lack of cpx in MPP's rims and the finding that prolonged heating may not cause complete breakdown suggests heating is the cause of amphibole breakdown in MPP. This is consistent with several of its oxide temperatures exceeding 950 °C, the approximate upper limit of amphibole stability in an experimental dacite (Figs. 1 and 4; Plechov et al., 2008)

In LF and CANOT, the presence of cpx in breakdown textures points to decompression as the cause of amphibole breakdown. Zonation of breakdown textures into zones of varying grain size, like that observed in LF and CANOT, has been attributed to magmatic stalling at different depths (Fig. 3B; Browne and Gardner, 2006). The extent of breakdown in these samples, along with their zoning, indicates that they rose slowly, stalling several times on their ascent to the surface.

The mineralogically distinct reaction zones observed in ESP's elemental maps suggests two separate events causing breakdown. The inner zone, containing cpx, was likely caused by decompression, whereas the outer zone, lacking cpx, was likely caused by heating. Though none of the oxide temperatures found in ESP exceeded 950 °C, temperatures were not found for its rims. Amphibole breakdown is usually thought to occur from the outside in, so it is likely that the outer zone is the older one and heating occurred first (Rutherford and Hill, 1993). It is also possible that the outer zone is caused by a reaction between the melt and the inner zone, suggesting that decompression occurred first.

There are no trends connecting extent or cause of breakdown to the age, place, or geochemistry of each lava dome. ESP (heating and decompression) and LF (decompression) have slightly higher SiO2 content than CANOT (decompression) and MPP (heating), showing no correlation between whole rock chemistry and cause of breakdown. Though two of the southern domes, LF and CANOT, share pseudomorph textures and decompression induced breakdown, the third southern dome, MPP, contains thin rims created by heating. The northern dome, ESP, appears to have been created by a mix of these processes, so there is no relationship between geographic location and cause of breakdown. There is no consistent trend over time either. The oldest dome, ESP, and the youngest dome, MPP, are the two domes with evidence of heating. These results suggest that melt ascent paths are not consistent over time or space and may instead reflect small batches of melt with unique ascent paths.

CONCLUSIONS

Amphiboles from ESP and MPP are characterized by thin, fine-grained reaction rims, whereas those from LF and CAN exhibit complete breakdown. Six reaction textures were found in the four samples, all consisting of plagioclase, pyroxene, and oxides. ESP and MPP each possess a distinct thin rimmed texture, and LF and CAN share four pseudomorph textures. Elemental mapping was used to determine the abundance of cpx in each sample, as the presence of cpx would suggest heating induced breakdown. MPP's rims contain no cpx, indicating that breakdown was most likely caused by heating. This is consistent with temperatures found using oxide pair compositions, several of which are above amphibole's 950 °C temperature stability limit in dacite. Pseudomorphs in LF and CAN contain abundant cpx, making decompression the probable cause of breakdown. The complete breakdown of LF and CAN and zoning in their reaction textures imply that they ascended slowly, stalling multiple times. Elemental maps of ESP show two distinct zones, one with and one without cpx, suggesting two phases of breakdown caused by separate heating and decompression events. The lack of correlation between cause of breakdown and the age and location of samples suggests that lava dome ascent paths on the island are changing over time and space.

ACKNOWLEDGMENTS

This material is based upon work supported by the Keck Geology Consortium and the National Science Foundation under Grant No. 1659322. Thank you to Holli Frey and Matt Manon for their guidance throughout this project.

REFERENCES

Bacon, C.R., and Hirshmann, M.M., 1988, Mg/Mn partitioning as a test for equilibrium between coexisting Fe-Ti oxides: American Mineralogist, 73, p. 57-61.

Browne, B.L., and Gardner, J.E., 2006, The influence of magma ascent path on the texture, mineralogy, and formation of hornblende reaction rims: Earth and Planetary Science Letters, 246, p. 161-176.

Buckley, V.J.E., Sparks, R.S.J., Wood, B.J., 2006, Hornblende dehydration reactions during magma ascent at Soufriere Hills Volcano, Montserrat: Contributions to Mineralogy and Petrology, 151, p. 121-140.

De Angelis, S.H., Larsen, J., Coombs, M., 2013, Pre-eruptive magmatic conditions at Augustine Volcano, Alaska, 2006: Evidence from amphibole geochemistry and textures: Journal of Petrology, 54, p. 1939-1961.

De Angelis, S.H., Larsen, J., Coombs, M., Dunn, A., Hayden, L., 2015. Amphibole reaction rims as a record of pre-eruptive magmatic heating: An experimental approach: Earth and Planetary Science Letters, 426, p. 235-245.

Ghiorso, M.S. and Evans, B.W., 2008, Thermodynamics of rhombohedral oxide solid solutions and a revision of the Fe-Ti two-oxide geothermometer and oxygen barometer: American Journal of Science, 308, p. 957–1039.

Hora, J.M., Kronz, A., Moller-McNett, S., Worner, G., 2013, An Excel-based tool for evaluating and visualizing geothermobarometry data: Computers & Geosciences, 56, p. 178-185.

Howe, T.M., Schmitt, A.K., Lindsay, J.M., Stockli, D.F., 2015, Time scales of intra-oceanic arc magmatism from combined U-Th and (U-Th)/He zircon geochronology of Dominica, Lesser Antilles: Geochemistry, Geophysics, Geosystems, 16.

Lindsay, J.M., Stasiuk, M.V., Shepherd, J.B., 2003, Geological history and potential hazards of the late-Pleistocene to Recent Plat Plays volcanic complex, Dominica, Lesser Antilles: Bulletin of Volcanology, 65, p. 201-220.

Plechov, P.Y., Tsai, A.E., Shcherbakov, V.D., Dirksen, O.V., 2008, Opacitization conditions of hornblende in Bezymyanni Volcano andesites (March 30,1956 eruption): Petrology, 16, p. 19-35.

Rutherford, M.J. and Devine, J.D., 2003, Magmatic conditions and magma ascent as indicated by the hornblende phase equilibria and reactions in the 1995-2002 Soufriere Hills magma: Journal of Petrology, 44, p. 1433-1454.

Rutherford, M.J. and Hill, P.M., 1993, Magma ascent rates from amphibole breakdown: An experimental study applied to the 1980-1986 Mount St. Helens Eruptions: Journal of Geophysical Research, 98, p. 19667-19685.

Waters, L. E., Lange, R. A., 2015, An updated calibration of the plagioclase-liquid hygrometer-thermometer applicable to basalts through rhyolites, American Mineralogist, 100, p. 2172-2184.

KECK Geology Consortium
Learning Science Through Research
Published by Keck Geology Consortium
Short Contributions
Keck Geology Consortium
Volume 31
May 2018

INVESTIGATING VOLCANIC-HYDROTHERMAL SYSTEMS IN DOMINICA, LESSER ANTILLES: TEMPORAL CHANGES IN THE CHEMICAL COMPOSITION OF HYDROTHERMAL FLUIDS FOR VOLCANIC MONITORING USING GEOTHERMOMETERS

MAZI-MAZTHIS C. ONYEALI, University of Colorado, Boulder
Research Advisors: Holli Frey, Erouscilla Joseph, and Lon Abbott

INTRODUCTION

Since 2002, the UWI Seismic Research Centre has routinely monitored gas and water chemistry of the hydrothermal areas of Dominica. The primary goal being, that by monitoring changes in the water chemistry of active fumaroles and hot springs, the information can be used to monitor changes in volcanic activity on the island. The waters are predominantly acid-sulfate in character, and likely formed because of dilution of acidic gases in near surface oxygenated groundwater (Joseph et al., 2011). While the waters are of primarily meteoric origin, this study investigates yearly shifts in isotopic composition to explore how evaporation effects, water-rock interaction, and other factors play a role on the general geochemistry. With updated water chemistry data from five hydrothermal areas (Boiling Lake, Valley of Desolation, Sulphur Springs, Watten Waven, Cold Soufriere) for the period 2014 to 2017, we will re-evaluate the characteristics of these systems (last reported in 2011) and use geothermometers to evaluate reservoir temperatures.

METHODS

Field

Samples were collected in six areas: the Boiling Lake, Valley of Desolation, Sulphur Springs, Watten Waven, Colde Soufriere, Micotrin. In total, twenty-nine features were sampled, with six samples per sampling site. Each set consisted of one alkalinity sample (0.2 mm filter), one sample for analysis of anions, deuterium, and delta ^{18}O (0.2 mm filter); one sample for cations and trace elements (0.2 mm filter), preserved with nitric acid; and two samples for dissolved inorganic carbon (raw water).

ProDSS Multiparameter Water Quality Meter (YSI) measured water temperature (Celsius), pressure (mmHg), dissolved oxygen (DO%), specific conductivity (SPC), conductivity (C), total dissolved solids (TDS), salinity (Sal), pH, and pH voltage (mV). The YSI was calibrated daily for the most accurate readings.

Lab

Samples were brought to Union College Geoscience Lab and were analyzed using various equipment. The MetrOhm 888 autotitrator measures for total alkalinity determinations, which is key to finding bicarbonate concentrations (HCO_3^- and CO_3). The UIC Coulometrics™ Carbon Dioxide Coulometer measured organic and inorganic carbon in solid and aqueous phases by oxidizing samples to CO_2. Anions and cations were determined using the Dionex-Ion Chromatograph and the software Chromeleon.

The Delta S Mass Spectrometer and Ecotainer is used for analyzing delta ^{18}O. The water sample was injected into a high-temperature carbon reactor, which converts it into H_2 and CO. The H_2 and CO are separated by gas

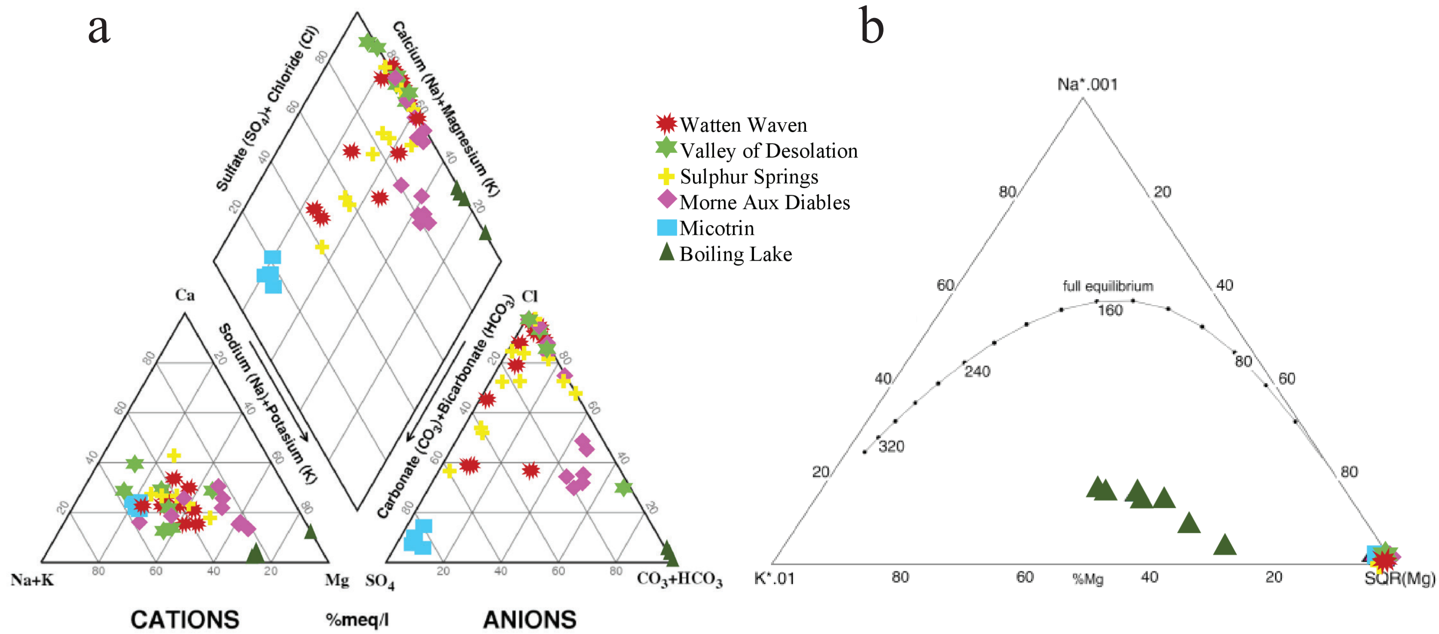

Figure 1. Chemical composition of hydrothermal waters from Dominica. (A) Na+K-SO_4-Mg, Cl-SO_4-HCO_3 and SO_4+Cl-Ca+Mg-Na+K-CO_3+ HCO_3 ternary (Piper) diagrams for hydrothermal water samples from 2000-2006 and 2014-2017 giving their relative concentrations. (B) Na-K-Mg ternary diagram that displays the maturity of the waters.

chromatography and carried by helium into the isotope ratio mass spectrometry, where the delta ^{18}O ratio is then measured (Lu FH, 2009).

The use of an Isotope-Ratio Mass Spectrometer was employed for the analysis of deuterium and carbon isotopes. To acidify and flush the sample vials, the manifold system (Schauer et al, 2004) was used in order to keep everything out of the vial besides the 500 micron sample and helium for the most accurate results. The Inductively Coupled Plasma Mass Spectrometer was used to determine trace elements such as aluminum and iron.

WATER GEOCHEMISTRY

General Compositions and classification

Water chemistry comparisons, comprise of data from 2000-2006 (Joseph et al, 2011), June 2014 (Metzger, 2015), June 2015 (Defranco, 2016), June 2016 (Aragosa, 2017) and June 2017. The chemical composition of the hydrothermal waters are plotted in ternary (Piper) diagrams (Fig. 1a). Overall, the hydrothermal waters in Dominica have seen little to no major shifts in cation compositions in every area besides the Boiling Lake. However, anion composition shifts have been observed.

Watten Waven

Manifestation of hydrothermal activity at Watten Waven is in the form of streams fed by boiling waters, and bubbling fumaroles. Orange colored sediment is observed surrounding its streams and fumaroles. The water has a pH = 3 to 7, and temperatures = 25°C to 89°C. The water is primarily acid-sulfate dominated; however, some waters are sulfate-bicarbonate type in composition. These sulfate-bicarbonate waters are mostly present in the streams with higher pH's and lower temperatures compared to the sulfate-based waters.

Valley of Desolation

Valley of Desolation (VoD) waters are overwhelming acid-sulfate and are characterized by pH = 2 to 7 and temperatures that range from 69°C to 99°C. The springs contain dark cloudy water with bubbling fumaroles that feed into larger streams. Unlike other areas, the VoD has remained sulfate dominated since monitoring began in 2000. A consistent minor shift in the dominant cation from sodium toward calcium is present from 2014-2017. Less readily leachable salts in shallow ground water may play a role in this gradual shift.

Boiling Lake

The lake is contained in a 50 m wide, 15 m deep and 1.22 x 103 m^3 crater (Fournier et al, 2009), at the heart of the Morne Trois Piton volcanic complex. The waters are characterized by pH = 3 to 4 and temperatures ranging from 85°C to 90°C. Unlike the other hydrothermal features, it has undergone significant changes in chemistry since 2000. The water of the Boiling Lake currently has a sodium/potassium chloride-type composition.

Sulphur Springs

Sulphur Springs waters have pH = 2 to 7 and temperatures from 35°C to 91°C dark black and dark-milky waters, vigorously bubbling fumaroles and strongly altered yellow-orange rocks/sediment. The waters have shifted towards a bicarbonate composition and now has a sulfate-bicarbonate type composition. The waters have lower sulfate concentrations on average from 2000 to 2017. The black color of the water is likely due to the precipitation of iron sulfide in the water because of the activity of high metabolic sulfate-reducing bacteria (Fauque et al, 1995).

Morne Aux Diables

Morne Aux Diables comprises an area of 1 m^2 to 5 m^2 with murky-white bubbling pools, heavily altered rocks/sediment coated with sulfur precipitates. The water is characterized by pH = 1.4 to 3 and low temperatures of 23°C to 24°C. Similar to Watten Waven, the waters of Morne Aux Diables is primarily sulfate-dominated. Unlike Watten Waven, it has seen a shift toward neutral chloride waters and a decline in sulfate content.

Micotrin

Sampling of Micotrin springs began in 2014 and is characterized as bicarbonate waters with a pH = 6 to 6.5 and temperatures = 20°C to 32°C. The clear waters flow over rocks with deep orange colored surface alteration. The waters are magnesium bicarbonate in character.

Table 1

Calculated Temperatures from Fournier 1977(F), Fournier and Truesdell 1976 (F/T), Giggenbach 1988 (G), Arnorsson et al. 1983 (A), Qz^a= no steam-loss, Qz^b= Maximum steam-loss

Sample	Site	Surface Temperature (C°)	Na-K (F)	Na-K (G)	Na-K (F/T)	Na-K-Ca (F/T)	Chalcedony (A)	Qz^a (F)	Qz^b (F)
Boiling Lake	Valley of Desolation	99	319	314	307	452	137	165	156
Bubbling Pool 1	Valley of Desolation	79	308	305	293	347	103	131	128
Bubbling Pool 2	Valley of Desolation	99	295	294	276	338	123	151	144
Black Water Spring	Valley of Desolation	40	268	270	241	313	70	98	100
Nico's Spring	Sulphur Springs	91	150	163	100	223	159	185	172
Jan's Pool	Watten Waven	59	341	332	337	351	61	90	92
Yellow Pool	Watten Waven	78	339	331	335	351	74	102	103
River Blanc	Watten Waven	28	282	282	259	329	57	89	86
Eric's Pool	Morne aux Diables	24	268	270	240	313	49	78	81
Micotrin Warm Spring	Micotrin	32	265	267	237	295	75	104	104

Cation/Anion 2014-2017 Comparisons

The hydrothermal waters of Dominica have been consistently sampled since 2014. Sampling sites like Eric's Pool (Morne Aux Diables), Jan's Pool (Watten Waven) and Nico's Pool (Sulphur Springs) concentrations have stayed fairly consistent throughout the four years of sampling, only varying by 1-5% year to year for Na, K, Mg, Ca, F, Cl, and HCO_3. Sulfate, on the other hand, has seen the greatest shifts in concentration from year to year. The highest concentrations of sulfate has been observed in 2015. This correlates with 2015 having the lowest precipitation (59.8 mm) in the four-year sampling period, based on rainfall data collection at the Canefield Airport. June 2014 saw precipitation of 104.4 mm, while June 2016 and June 2017 saw precipitation 227.5 mm and 142.6 mm respectively. Lower precipitation leads to less dilution and higher concentrations, most significantly in sulfate.

The Boiling Lake follows the trends in other hydrothermal areas, with the exception of its sulfate concentrations. The other hydrothermal areas have concentrations of sulfate in the hundreds and thousands of parts per million (ppm) with sulfate being the dominant anion. The Boiling Lake on the other hand, has sulfate concentrations of tens of ppm with chloride in the thousands of ppm. A high of 2189 ppm was recorded in 2000 (Joseph et al, 2011). Since the draining events in 2004, which caused the lake to drain and refill over a period of four months (2004), there has been a yearly decline of SO_4 that has never recovered since the 2004 event (Fournier et al, 2009). In November 2016, another drainage event occurred that lasted for six weeks. No change in the pattern of SO_4 concentration was observed after this event.

Maturity

The Na-K-Mg ternary diagram is a powerful tool (Fahrurrozie et al, 2015) to help assess the deep equilibrium reservoir temperatures and evaluate the state of equilibrium and mixing effects of hydrothermal waters. The diagram is divided into three sections that inform on how much water-rock interaction/mixing has occurred. The top section shows the full equilibrium between the waters with the surrounding rock; the middle shows partial equilibrium between the waters and the surrounding rock and the bottom section shows if the waters are immature (Fig. 1b). Immature waters signify little to no water-rock interaction/mixing. For the purpose of geothermometry, this can help indicate which geothermometers are best suited to estimate reservoir temperatures.

The hydrothermal waters of Dominica are primarily immature. This is indicative that the waters are mixing with meteoric groundwater and are not at equilibrium with the host lithology. Due to the waters immaturity, silica based geothermometers are more useful than Na-K geothermometers to get better estimates of reservoir temperatures. Boiling Lake shows more mixing and equilibrium than other areas.

Isotope Geochemistry

Stable isotopes can indicate the source of the water present in hydrothermal springs and groundwater reservoirs. The stable isotopes are expressed relative to the Vienna Standard Mean Ocean Water (VSMOW) in parts per thousand (0/00, per mil). The equation used for hydrogen is:

$$\delta^2 H - \left(\frac{{}^{2}H/{}^{1}H(sample)}{{}^{2}H/{}^{1}H(VSMOW)} - 1 \right) x10^3$$

and the oxygen equation used is:

$$\delta^{18} O - \left(\frac{{}^{18}O/{}^{16}O(sample)}{{}^{18}O/{}^{16}O(VSMOW)} - 1 \right) x10^3$$

Past investigations in Dominica, conducted by Joseph et al. (2011), have found that the isotopes of many of these springs lie on a trend between magmatic sources and the meteoric water line (MWL) with some influence from water-rock interaction and surface evaporation. This interpretation is based on the natural processes of the waters stable hydrogen and oxygen isotopes that are controlled by kinetic and equilibrium fractionation. The natural processes that can affect $\delta^{18}O$ and δ^2H values are shown in Figure 2b.

Isotope data for the hydrothermal waters of Dominica began to be regularly collected in 2015 and there is isotope data for 2002 (Joseph et al., 2011). The stable isotopes of water in the hydrothermal areas of Dominica are primarily seeing the effects evaporation from the surface year to year. 2017 on average saw a decrease in $\delta^{18}O$ and δ^2H in comparison to 2015 and 2016. Valley of Desolation's $\delta^{18}O$ vs δ^2H graph (Fig. 2), displays a similar trend to the Boiling Lake and Watten Waven. Sulphur Springs shows a negative shift in $\delta^{18}O$ in 2017. Though minor, this may be indicative of the increased presence of CO_2, which can promote low temperature primary mineral dissolution and secondary mineral precipitation reactions. This process can preferentially consume $\delta^{18}O$ (Karolyte et al., 2017; D'more and Panichi, 1987). It also means that equilibrium oxygen isotope exchange between CO_2 and the water may have taken place.

GEOTHERMOMETRY

Geothermometers have the theoretical basis of a multicomponent thermodynamic calculation based on

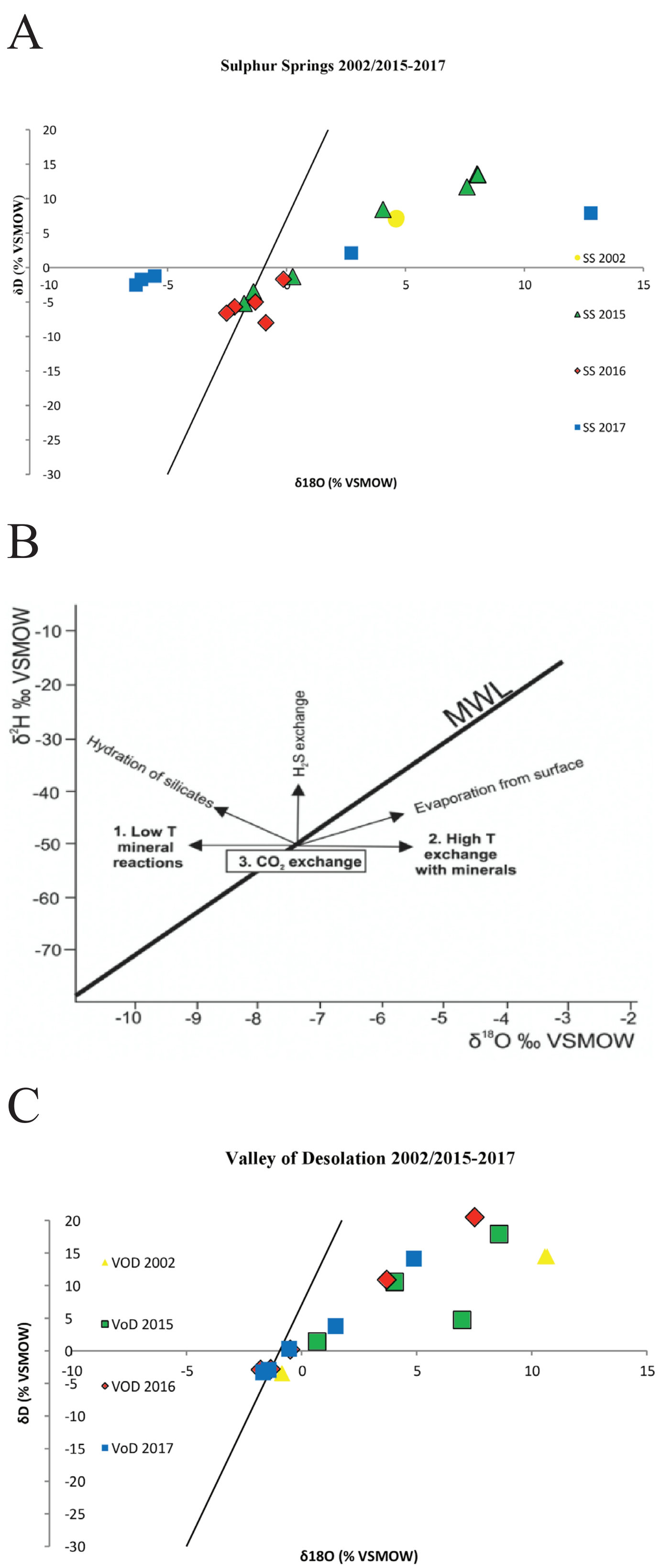

Figure 2. Stable isotope composition of hydrothermal waters from Dominica. (A) Average natural trends in $\delta^{18}O$ vs $\delta^{2}H$ at Sulphur Springs. (B) Natural processes affecting water $\delta^{18}O$ vs $\delta^{2}H$ values (Karolyte et al., 2017). (C) Average natural trends in $\delta^{18}O$ vs $\delta^{2}H$ at Valley of Desolation.

the equilibria of water, mineral, and gas phases (Reed) et al., 1984; Wishart, 2015). It evaluates whether degassing or dilution has occurred, determines the equilibrium status of the system, and obtains temperatures if equilibrium exists for a mineral assemblage. While theoretically it is sound, in practice calculated reservoir temperatures can be less accurate due to factors like degassing and precipitation of calcium carbonate. The most accurate temperatures would come from in situ boreholes. Geothermometers still can be useful because they show increases and decreases in temperatures even if the reservoir temperature itself may not be completely accurate.

The Dominican hydrothermal waters are overwhelmingly immature (Fig. 1b). Subsequently, silica based geothermometers offer a more reliable option as compared to Na/K geothermometers, since the host lithology has not equilibrated with the waters. Silica solubility-based geothermometers are determined by variations in the solubility of different silica species (quartz and chalcedony) in water as a function of temperature, pressure, and fluid acidity at the time of mineralization (Wishart, 2015). Silica geothermometers are best for surface temperatures above 150°C (below this chalcedony controls the dissolved silica content) and when the effects of steam separation are due to subsurface boiling (Yock, 2009; Karingithi, 2009). For the quartz geothermometers two equations are required, the adiabatic (maximum steam loss):

$$\boldsymbol{T^{0}C = \frac{1522}{5.75 - \log(SiO_2)} - 273.15\,(Fournier, 1977)}$$

and the conductive (no steam loss):

$$\boldsymbol{T^{0}C = \frac{1112}{4.91 - \log(SiO_2)} - 273.15\,(Fournier, 1977)}$$

Na-K geothermometers work best with fluids that are from a thermal environment that are above 180°C, contain low calcium, and have equilibrated with albite and K-spar (Yock F. 2009). Na-K-Ca geothermometers assume equilibrium between Na and K-feldspar but can be affected by boiling and dilution. Thus, these both are best used for more mature and less volatile waters. However, these geothermometers still can be useful to get general temperature differences.

Silica geothermometers were used to calculate equilibrium temperatures for the Boiling Lake, Nico's Pool and Jan's Pool for water samples in 2006 (Joseph et al., 2011). When compared with these temperatures, samples from 2017 indicate that the reservoir that feeds the Boiling Lake, has dropped by ~30°C, Sulphur Springs has seen an increase in reservoir temperature of ~31°C, while Watten Waven has no significant change in temperature.

CONCLUSION

Analysis of the hydrothermal waters of Dominica have indicated that while the origin of the hydrothermal systems are still dominantly meteoric, surface evaporation effects and variable amounts of mixing with shallow ground water plays an important role in most of the hydrothermal areas. New $\delta^{18}O$ isotopic shifts in Sulphur Springs, suggest that low temperature mineral reactions are driving oxygen to exchange with CO_2. This is evident by the significant $\delta^{18}O$ shift from 2014 to 2016 and then again in 2017, as seen for Nico's Pool in Sulphur Springs. Variable levels of degassing year to year and the action of high metabolic sulfate-reducing bacteria may possibly be the key contributing factors. Sulphur Springs has shown a significant increase in reservoir(s) temperature. Future monitoring of this site is needed to see if this trend continues. The change in chemistry of the Boiling Lake to a more chloride dominant system may be indicative of the system being fed more directly from a deeper hydrothermal brine reservoir (Fournier et al., 2009) and the calculated reservoir temperature drop may play an active role in the decline in SO_4.

ACKNOWLEDGEMENTS

This material is based upon work supported by the Keck Geology Consortium and the National Science Foundation under Grant No. 1659322. The first extension of gratitude is to my research advisors Holli Frey and Erouscilla Pat Joseph. Their help, guidance and kindship were invaluable to my growing knowledge as a scientist and a person. National Science Foundation - MRI #1229258 (Isotope ratio mass spectrometer), National Science Foundation - CCLI#9952410 (Perkin Elmer ICP-MS), Union College - Summer Research Fellowship were all key to funding my research. Matthew Manon's assistance in the IC and ICP-MS Lab and Anouk Verheyden-Gillikin for assistance in IRMS lab. ODM in Dominica for guiding and helping us throughout our travels and Springfield Estate for the food and beds.

REFERENCES

Arnórsson, S., 2000, Isotopic and chemical techniques in geothermal exploration, development anduse. Sampling methods, data handling, interpretation. International Atomic Energy Agency,Vienna, 351pp.

D'Amore, F., Panichi, C., 1987, Geochemistry in geothermal exploration. Appl. Geotherm. 9, 69e89.

Fahrurrozie, A., Saputra, M. P., & Nugraha, T., 2013, The Application of Na-K-Mg, Na-K/Mg-Ca and K-Mg/Quartz Diagrams to Evaluate Water Geochemistry in West Java Geothermal Prospects, Indonesia, p. 4-7.

Fauque, G., Le Gall, J., and Barton, L. L., 1991, Sulfate-reducing and sulfur-reducing bacteria, in: Variations in Autotrophic Life (J. M. Shively and L. L. Barton, eds.) Academic Press, London, pp. 271–338.

Fournier, R.O., 1977, Chemical Geothermometers and Mixing Models for Geothermal Systems, Geothermics, p. 5, 41-50.

Fournier, N., F. Witham, M. Moreau-Fournier, and L. Bardou., 2009, Boiling Lake of Domiica, West Indies: High-temperature volcanic crater lake dynamics, J. Geophys. Res., 114.

Giggenbach, W.F., 1988, Geothermal solute equilibria. Derivation of Na-K-Mg-Ca geoindicators. Geochim Cosmochim Acta, v. 52, p. 2749-2765.

Giggenbach, W. F., and Soto, R. C., 1992, Isotopic and chemical composition of water and steam discharges from volcanic-magmatic-hydrothermal systems of the 75.

Goldsmith, S. T., Carey, A. E., Johnson, B. M, Welch, S. A., Lyons, W. B., Mcdowell,W. H., and Pigott, J. S., 2010. Stream Geochemistry, Chemical Weathering and CO_2 Consumption Potential of Andesitic Terrains, Dominica, Lesser Antilles: Geochimical Cosmochimica Acta, v. 74, no. 1, p.85-103.

Joseph, E. P., Fournier, N. Lindsay, J. M., Robertson, R., and Beckles, D. M., 2013, Chemical and isotopic characteristics of geothermal fluids from Sulphur Springs, Saint Lucia: Volcanology and Geothermal Research, v. 254, p. 23-36.

Joseph, E. P., Fournier, N., Lindsay, J. M., Fischer, T. B., 2011, Gas and water geochemistry of geothermal systems in Dominica, Lesser Antilles island Arc:Volcanology and Geothermal Research, v. 206, p.1-14.

Karingithi, C.W., 2009, Chemical geothermometers for geothermal exploration, Short Course IV on Exploration for Geothermal Resources, v. SC-10, p. 3-7

Karolyet, R, Serno, S, Johnson, G & Gilfillan, S., 2017, 'The influence of oxygen isotope exchange between CO_2 and H_2O in natural CO_2-rich spring waters: implications for geothermometry' Applied Geochemistry.

Lindsay, J. M., Stasiuk, M. V., Shepherd, J. B., 2005, Geological history and potential hazards of the late Pleistocene to Recent Plat Pays volcanic complex, Dominica, Lesser Antilles: Bull Volcanol, v. 65, p. 201– 220.

Lu, F. H., 2009, Online high-precision δ^2H and δ^{18}O analysis in water by pyrolysis. Rapid Commun. Mass Spectrom., v. 23, p. 3144–3150.

Reed, M. H., Spycher, N., 1984, Calculation of pH and Mineral Equilibria in Hydrothermal Waters with Application to Geothermometry and Studies of Boiling and Dilution, Geochimica et Cosmochimica Acta, v. 48, p.1479-1492.

Schauer, A. J., Lott, M. J., Cook, C. S. and Ehleringer, J. R., 2005, An automated system for stable isotope and concentration analyses of CO_2 from small atmospheric samples. Rapid Commun. Mass Spectrom., v. 19, p. 359–362.

Torres Marta E. , Mix Alan C. , Rugh William D., 2005, Precise δ^{13}C analysis of dissolved inorganic carbon in natural waters using automated headspace sampling and continuous-flow mass spectrometry., Limnol. Oceanogr. Methods, v. 3.

Wishart, DeBonne., 2015, Comparison of Silica and Cation Geothermometers of Bath Hot Springs, Jamaica WI.

Yock, A., 2009, Geotermomertry in Costa Rica, Short Course on Surface Exploration for Geothermal Resources, v. SC-09, p. 2-5

Learning Science Through Research
Published by Keck Geology Consortium

Short Contributions
Keck Geology Consortium
Volume 31
May 2018

INVESTIGATION OF MINERAL ALTERATION IN ANDESITE AND DACITE FROM THREE DIFFERENT VOLCANO HYDROTHERMAL SYSTEMS ON DOMINICA, LESSER ANTILLES

CLARISSA ITZEL VILLEGAS SMITH, Carleton College
Research Advisors: Cameron Davidson, Holli Frey, and Erouscilla Joseph

INTRODUCTION

Dominica is geologically similar to the nearby islands of Guadeloupe, Montserrat, and St. Lucia in the Lesser Antilles. Unlike the latter three, a comprehensive study has yet to be conducted on the alteration minerals resulting from the hydrothermal and fumarolic environments on this island. Dominica has nine volcanoes and is primarily composed of andesite and dacite. Four of these volcanic centers are associated with geothermal activity where hot sulfur-bearing gases from magmatic sources mix with meteoric water to produce steam-heated acidic-sulfate waters. One of the geothermal areas, the Cold Soufriere has colder surface temperatures compared to others on the island. The hydrothermal waters of Dominica are classified as acid-sulfate and are immature with respect to bedrock interaction (Joseph et al., 2011; Onlyeali et al., 2017). Immaturity depends on the degree of interaction and mixing that has occurred between the water and the host lithology in the reservoir. Immature waters do not achieve equilibrium with the host rock composition and therefore the use of solute (Na, K, and Mg) geothermometry is not appropriate. Silica thermometry may be a more reasonable option for estimating reservoir temperatures in this case. Silica thermometry of the hydrothermal waters shows that the reservoir temperature of the Cold Soufriere is <80 °C, whereas Sulfur Springs and the Valley of Desolation have reservoir temperatures of 100-200 °C (Onlyeali et al., 2017). Rocks in these hydrothermal areas typically are observed with a rind of sublimates and incrustations composed of secondary alteration minerals.

Samples of the altered rock were collected from three different hydrothermal site locations in Dominica, which vary in temperature, as well as moisture level. The aim of this research project is to address the following questions: What minerals are present in the rocks and associated alteration rinds at these sites? What were the processes causing this alteration? Finally, what differences exist between these three sites?

FIELD SITES AND SAMPLE DESCRIPTIONS

Samples were collected from three hydrothermal areas on the island of Dominica: 1) Valley of Desolation, 2) Sulfur Springs, and 3) Cold Soufriere.

The Valley of Desolation hydrothermal area covers an area of about 0.5 km^2 and is characterized by high inputs of surface water and fumarolic gases containing H_2S and CO_2. Water and gas temperatures range from 69-98 °C and pH ranges from 1– 4 (Onlyeali et al., 2017). Alteration rinds are found on andesite and dacite blocks, cobbles and pebbles and vary in thickness from 1-20 mm. Some rinds are well lithified whereas other rinds are poorly lithified and argillitic. The rinds display distinctive colors including white, dark grey, orange, yellow, green, pink, and purple.

The predominantly gaseous hydrothermal site at Sulfur Springs is very dry, with little to no surface water inputs. Temperatures of the gas fumaroles range from 41-97 °C and the pH range from 1-3. Sulfur Springs covers the largest area out of the three sites. The dominant lithology of this site is rounded andesite cobbles.

The unaltered cores of the cobbles are grayish white in color with a very well lithified thin white rind that is 3-13 mm thick. In some cases there are two layers of rinds around the unaltered core that are easily separable from each other.

The smallest site, the Cold Soufriere, covers an area of 25 m^2. There are significant surface water inputs in the form of several small pools. Temperatures in these water pools range from 18-32 °C and the pH from 1-4. The rocks in this area appear to be the most altered of the three sites. Most of the rock samples are argillic and crumble easily, whereas others have harder rinds 2-10 mm in thickness and pinkish gray cores.

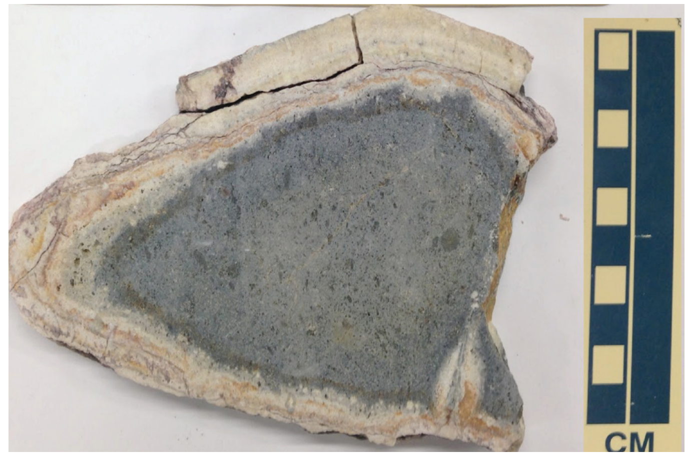

Fig. 1: A cross section of an andesite cobble from the Valley of Desolation showing the well lithified alteration rind characteristic of the area.

METHODS

Due to the fine-grained nature of the alteration rinds, we used the Phillips PW-1840 powder X-ray diffractometer at Union College to identify the minerals present in sixteen samples of rock rinds. This was also done for one unaltered rock core from Sulfur Springs. To make powders for XRD analysis, the weathered rind of the rock (Fig. 1) was scraped from the rock surface with a dental pick, then ground into a fine powder using a mortar and pestle. In some cases, multiple powder samples were taken from a single hand sample, separated by differences in alteration colors or by inner vs. outer rind layers.

PANalytical HighScorePlus was used with the Crystallography Open Database (Grazulis et al., 2009) for mineral identification and Rietveld analysis yielded the abundance of each mineral type in a given sample. In addition, we measured the whole-rock major and trace element geochemistry of one unaltered core of a rock sample from Valley of Desolation using ICP-OES at Acme Labs and ICP-MS at Union College, respectively.

Thin-sections were prepared to examine the boundary between the alteration rind and unaltered core. X-ray maps and quantitative elemental analyses of the minerals present were done with the Union College Zeiss EVO-MA15 equipped with a Bruker EDX system.

RESULTS

Rietveld analysis of the XRD spectra yielded a total of fifteen different minerals across all the samples (Fig. 2). The types of minerals present include: silica polymorphs, hematite, alunite minerals, sulfates, sulfides, and feldspars. Silica polymorphs are dominant with about 70% of the samples containing cristobalite, and only one sample, from the Cold Soufriere, contains jarosite, a mineral commonly found in inactive fumaroles on the island of Guadeloupe (Salaün et al., 2011). Alunite, a mineral characteristic of higher temperatures (Aguilera et al., 2016), is present in the Valley of Desolation and Sulfur Springs samples, but it is not present in any Cold Soufriere samples. Six of the altered rinds contain feldspar and no sulfates (Fig. 3).

DISCUSSION

The minerals across all three sites are typical of rock alteration by low temperature (<300 °C) acid-sulfate fluids, suggesting that the alteration observed is a result of interaction with shallow groundwater and sulfur gases (Joseph et al., 2011). At the Cold Soufriere, the site with the lowest temperatures, there was an absence of the mineral alunite. A hydrous sulfate mineral, alunite was found in the two other field locations. This may be a clue as to how differences in the minerals present for each site may be attributed to distinct hydrothermal systems with different temperatures (Aguilera et al., 2016).

	Minerals Present (Determined by XRD) in Alteration Rind																			
	Cristobalite	Quartz	Tridymite	Hematite	Alunite	Natroalunite	Minamiite	Sulfur	Gypsum	Jarosite	Caminite	Greigite	Pyrite	Carrolite	Plagioclase	Albite	Anorthite	Anorthoclase	Sodalite	Pyroxene
SS4Unaltered																X	X			X
SS1Rind		X	X		X				?							?				
CS1BlackRind	X		X													X				
CS2OrangeRind	X		X	X																
CS3Sulfur	X							X												
CS4Purple	X		X	X										?						
CS5AcidRock	X		X							X										
VOD1Rind	X	X			X	X								X						
VOD1InnerRind		X			?		X								?	X				
VOD1OuterRind		X				X									X					
VOD4PinkWhite	X	X	X					X												
VOD5OuterRind		X			X	?					X	?								
VOD6Rind	X							X		?									?	
VOD7Gray	X	X			X			X					X							
VOD7White	X				X									?	X					
VOD8Orange	X		X														X	X		
VOD9Purple	X	X		X														X		

Fig. 2: Minerals detected in the XRD spectra are indicated as an "X" in this table while minerals that were present in small amounts are indicated with a "?".

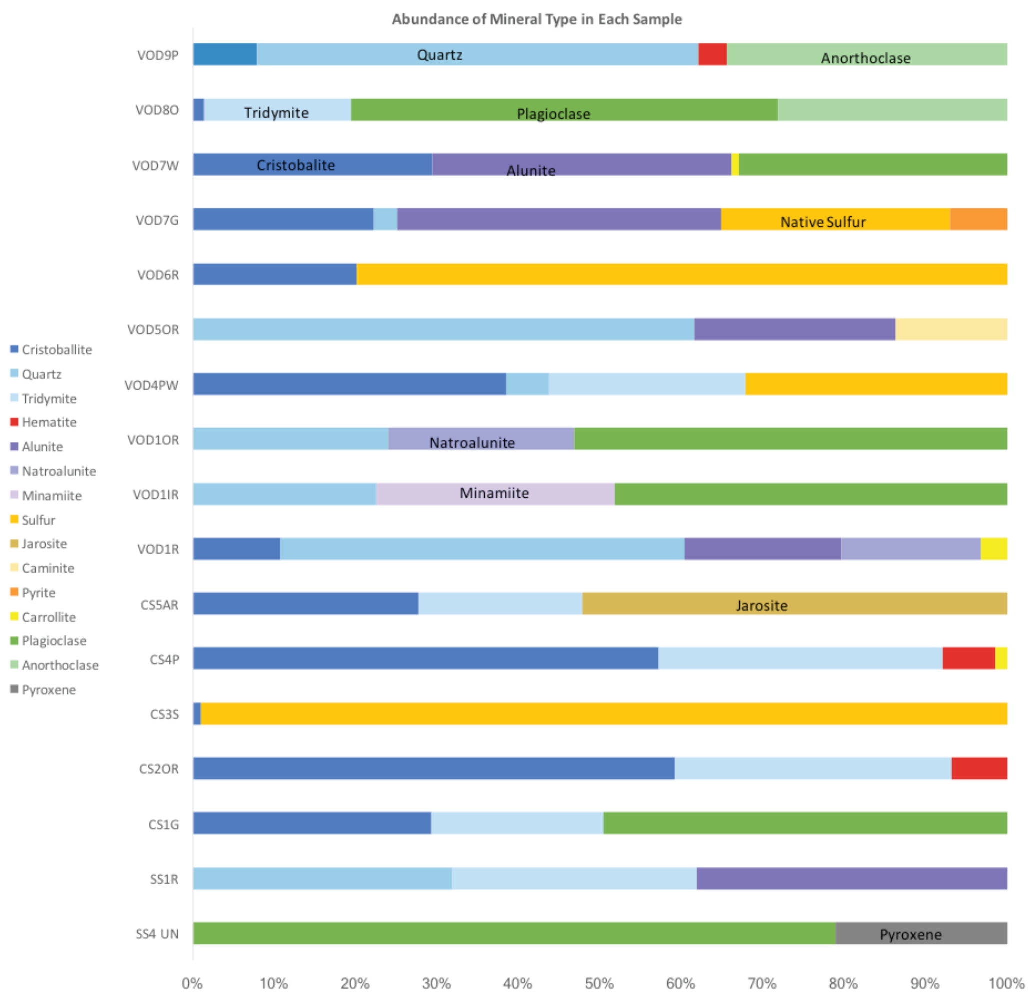

Fig. 3: Rietveld analysis yielded mineral abundances for each XRD sample.

Cristobalite, sulfide, and sulfate minerals likely originate from hydrothermal vents, whereas fine grained iron oxides come from the alteration of Fe-Mg minerals such as pyroxene. Native sulfur crystals observed in the field are attributed to precipitation of the sulfur present in fumarole gases (Mayer et al., 2017).

Africano et al. (2000) studied the Hsu volcano in Hokkaido, Japan. They found that cations from the original minerals had been completely leached, leaving only silica. The cations were found precipitated as secondary minerals in microcracks where fluid had entered and filled in the spaces. Similarly, in the Dominica samples, elemental maps (Fig. 4) show how silica polymorphs have replaced minerals such as plagioclase. Veins containing very fine grains of hematite and various sulfate minerals crosscut plagioclase and pyroxene crystals. Clay minerals, typical of argillic alteration, are often formed in hydrothermally active areas and are common in the andesites of the nearby island of Guadaloupe (Mas et al., 2006). Mayer et al. (2017) found the clay minerals montmorillonite and kaolinite in argillic samples from Valley of Desolation. However, no clay minerals have been detected in this study.

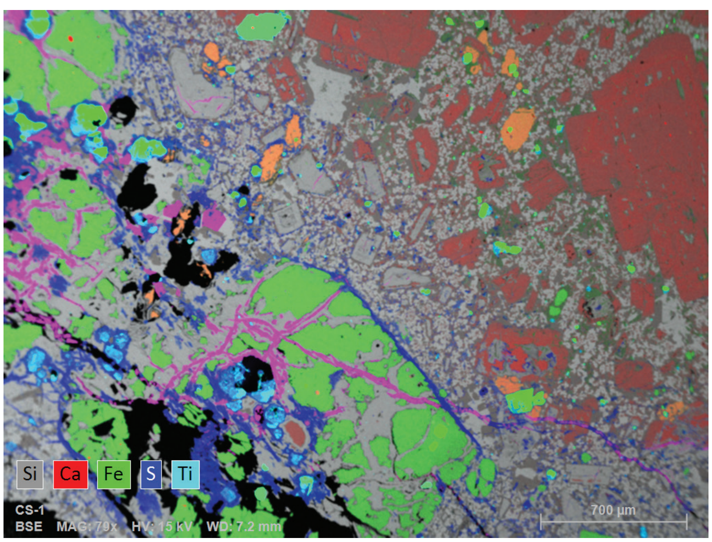

Fig. 4: An elemental map of a sample from the Cold Soufriere. False colors represent the elements present in the thin section. The alteration rind is located in the bottom left corner. Opx (green) is cross-cut by veins (blue, pink) of hematite and various sulfate minerals. Outlines of plagioclase phenocrysts are visible and have been replaced by silica polymorphs (gray) although a small amount of plagioclase remains in the center of the crystals.

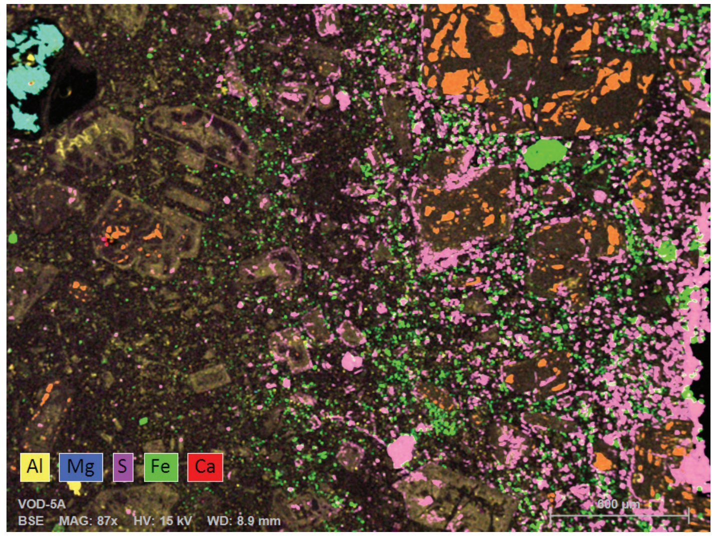

Fig. 5: An elemental map of a sample from the Valley of Desolation. The thick outer rim on the right shows the gradation in alteration from across the boundary from rock to rim. Very fine sulfide, sulfate and iron-titanium oxides minerals and alunite are found in this location. Plagioclase crystals have been replaced with silica.

Some minerals like gypsum, were found in the thin section using the SEM, but not detected by the XRD. A plausible explanation is that the XRD powders only contain minerals from the thinner sublimate on the outermost layer of the rock surface, excluding the core of the cobble, which may alter differently. Further work is necessary to characterize the varying degrees of alterations throughout the rock sample. Several rinds still contain plagioclase feldspar, suggesting that some of the original minerals have withstood the weathering conditions. Interestingly, of all samples that still contained feldspar, none contained sulfates (Fig 2). This indicates that these plagioclase-bearing rinds are less weathered. This is observed at all three sites. It is possible that the absence of sulfates is dependent on proximity to fumaroles and running water, as samples that are closer to the fluid discharge will have more exposure to alteration.

One sample from the Cold Soufriere includes a fine grained mix of oxide minerals consisting of iron, sulfur, and titanium. Minerals containing all three elements are rare, though this mineralogy has been discovered on Mars, which is known to have evidence of hydrothermal systems: the Spirit Rover discovered opaline silica, a hydrothermally derived silica polymorph, in the Gusev crater (Ruff et al., 2011).

In the oxides on Dominica, there is a trend of iron concentration decreasing and sulfur concentration increasing moving from the core to outer edge of the rind. The amount of titanium, a relatively immobile element, remains constant. A possible explanation for this pattern is that the outer surface of the rind is more exposed to the sulfur bearing gases and fluids which cannot penetrate deeply into the core. Some of these oxides may have replaced ilmenite that was present in the host rock.

CONCLUSIONS

Both acidity and fluid availability in the environment caused differences in the degree of alteration of minerals, with those from the drier Sulfur Springs showing the least amount of alteration. Sulfur Springs is a hot and dry environment, Valley of Desolation is a hot and wet environment, and the Cold Soufriere is a wet and cold environment. The presence of water allowed for the movement of different elements and ions to enter and leave the rock, forming alteration minerals. Furthermore, acidity contributed to the degree of lithification of the rock regardless of temperature and may explain the alteration of the original mineralogy.

ACKNOWLEDGEMENTS

This material is based upon work supported by the Keck Geology Consortium and the National Science Foundation under Grant No. 1659322. A big thank you to the Commonwealth of Dominica for allowing this research to be conducted and to the mentors who advised me on this project: Holli Frey, Matt Manon, Erouscilla Joseph, Cam Davidson and Laura Waters.

REFERENCES

Africano, F., and Bernard, A., 2000, Acid alteration in the fumarolic environment of Usu volcano, Hokkaido, Japan: Journal of Volcanology and Geothermal Research, v. 97, p. 475–495, doi: 10.1016/s0377-0273(99)00162-6.

Aguilera, F., Layana, S., Rodríguez-Díaz, A., González, C., Cortés, J., and Inostroza, M., 2016, Hydrothermal alteration, fumarolic deposits and fluids from Lastarria Volcanic Complex: A multidisciplinary study: Andean Geology, v. 42, doi: 10.5027/andgeoV43n2-a02.

Onyeali, M. C., Joseph, E. P., and Frey, H. M., 2017, Investigating Volcanic-Hydrothermal Systems in Dominica, Lesser Antilles: Temporal Changes in the Chemical Composition of Hydrothermal Fluids for Volcanic Monitoring Using Geothermometers: Abstract 215815 presented at 2017 Fall Meeting, AGU, New Orleans, Louisiana, 11-15 December

Grazulis, S., Chateigner, D., Downs, R. T., Yokochi, A. T., Quiros, M., Lutterotti, L., Manakova, E., Butkus, J., Moeck, P. & Le Bail, A., 2009, Crystallography Open Database - an open-access collection of crystal structures,. J. Appl. Cryst. 42, 726-729.

Joseph, E.P., Fournier, N., Lindsay, J.M., and Fischer, T.P., 2011, Gas and water geochemistry of geothermal systems in Dominica, Lesser Antilles island arc: Journal of Volcanology and Geothermal Research, v. 2016, p. 1–14.

Mas, A., Guisseau, D., Mas, P.P., Beaufort, D., Genter, A., Sanjuan, B., and Girard, J., 2006, Clay minerals related to the hydrothermal activity of the Bouillante geothermal field (Guadeloupe): Journal of Volcanology and Geothermal Research, v. 158, p. 380–400, doi: 10.1016/j.jvolgeores.2006.07.010.

Mayer, K., Scheu, B., Yilmaz, T.I., Montanaro, C., Gilg, H.A., Rott, S., Joseph, E.P., and Dingwell, D.B., 2017, Phreatic activity and hydrothermal alteration in the Valley of Desolation, Dominica, Lesser Antilles: Bulletin of Volcanology, v. 79, doi: 10.1007/s00445-017-1166-0.

Onyeali, M. C., Joseph, E. P., and Frey, H. M., 2017, Investigating Volcanic-Hydrothermal Systems in Dominica, Lesser Antilles: Temporal Changes in the Chemical Composition of Hydrothermal Fluids for Volcanic Monitoring Using Geothermometers: Abstract 215815 presented at 2017 Fall Meeting, AGU, New Orleans, Louisiana, 11-15 December

Ruff, S.W., Farmer, J.D., Calvin, W.M., Herkenhoff, K.E., Johnson, J.R., Morris, R.V., Rice, M.S., Arvidson, R.E., Bell, J.F., Christensen, P.R., and Squyres, S.W., 2011, Characteristics, distribution, origin, and significance of opaline silica observed by the Spirit rover in Gusev crater, Mars: Journal of Geophysical Research, v. 116, doi: 10.1029/2010je003767.

Salaün, A., Villemant, B., Gérard, M., Komorowski, J.-C., and Michel, A., 2011, Hydrothermal alteration in andesitic volcanoes: Trace element redistribution in active and ancient hydrothermal systems of Guadeloupe (Lesser Antilles): Journal of Geochemical Exploration, v. 111, p. 59–83, doi: 10.1016/j.gexplo.2011.06.004

KECK Geology Consortium
Learning Science Through Research
Published by Keck Geology Consortium

Short Contributions
Keck Geology Consortium
Volume 31
May 2018

COMPOSITION AND SHORT-TIMESCALE EROSION PATTERNS OF RIVER SEDIMENTS ON DOMINICA

HALEY TALBOT-WENDLANDT, Ohio Wesleyan University
Research Advisor: Bart Martin

INTRODUCTION

Dominica is located in the Caribbean, which is generally an under-studied area of the world for geomorphology (Portenga et al., 2009). There has not been very much prior research conducted in tropical climates because these areas are often less easily accessible than more temperate climates (Alcántara-Ayala, 2002). However, it may be more important to study tropical areas than it is to study temperate ones; natural disasters such as volcanic activity and flooding are common in the tropics, and countries located in these areas are often still developing and do not have excess resources readily available to take preventative safety measures or rebuild after a disaster (Alcántara-Ayala, 2002). Because areas with tropical climates receive more rainfall per year than places with temperate climates, various erosive processes can play larger roles in tropical areas than in temperate ones (Vijith et al., 2011). Increased rainfall can lead to more frequent and more intense storm-related hazards such as landslides (Van Westen, 2016), so it is impossible to simply generalize erosion rates associated with temperate areas and apply those rates to tropical areas (Portenga et al., 2009). Therefore, it is important to determine the background erosion rates in various tropical climates.

Dominica is a young volcanic island, with no known rocks formed more than 7 million years ago (Lindsay et al., 2005). Many of these rocks are ignimbrites, which are easily eroded, especially in a tropical, wet environment such as the Caribbean (Frey, 2016). The exact type of erosion is unknown though, so it would be helpful to use beryllium-7 analyses to determine whether erosion is occurring on horizontal surfaces. Fallout radionuclide research has already been performed in many other areas of the world, so it will be interesting to analyze this data in the context of a tropical area, and this project will contribute to the continued characterization of tropical processes (Campbell et al., 2015; Hancock et al., 2016). It is especially important to characterize the watersheds and carry out these studies now, while there is relatively little development in most upstream areas.

In order to determine the effects of landslides, storm events, and other erosive processes on different watersheds of Dominica, we collected sediment samples on which we performed compositional, beryllium-7, and lead-210 analyses; and we identified landslides using satellite imagery of the island. I hypothesized that we would be able to differentiate between different watersheds of the island based on the different erosion rates and sediment compositions, with some differences in iron and magnesium ratios between different watersheds and relatively little variation between the fine and coarse sediments from the same watersheds. I expect that fine sediments will be characteristic of more weathered material, since the clay minerals present in Dominica's ignimbrites undergo a weathering sequence (Frey, 2016). I also hypothesized that landslides would tend to occur in the same general areas, and that those areas would be the ones identified as having a high risk of landslides in the World Bank report (Van Westen, 2016).
Van Westen (2016) included factors such as slope steepness, elevation, soil type, distance from roads, land use, and underlying geology when evaluating landslide susceptibility in this report.

METHODS

Field work

On Dominica, we sampled twenty watersheds with an area greater than 10 km^2 found using ArcMap (Fig. 1). We then sampled each watershed as close as possible to the mouth of the river, while still avoiding tidal influence. At each sample site, we collected active channel sediments from multiple points in the streambed in order to get a more representative sample of the sediments carried by the fluvial system (Gonzalez et al. 2017). For example, we attempted to collect sediment from the channel, point bars, and along the river banks from a longitudinal section of the river whenever possible. We then sieved the mixed sediment to collect only grain sizes of <63 μm and 250-850 μm. We also took pictures and made written observations of each sample location, including notes on channel width and depth; average channel sediment size, sorting, and rounding; land use; channel type; relative flow velocity; and bank sediment size. We also noted the location of current bridges in addition to old, washed-out bridges still in place along the river.

XRD analysis

After collecting the samples, we dried them in an oven. We then re-powdered the finer-grained samples with a mortar and pestle as necessary and performed x-ray diffraction analysis on these samples. We ran each sample from 2θ=5°-85° at 4°/min, with the diffractometer set to Bragg-Brentano geometry and λ=1.54056. We found peaks using a computer program, PDXL.

XRF analysis

We used a handheld XRF device to analyze the chemistry of the fine-grained and powdered coarse-grained samples. We used the USGS Majors 3 method and ran each coarse-grained sample for 180 seconds and each fine-grained sample for 240 seconds. Although this data was uncalibrated, we were able to compare the ratios of various elements in the different samples.

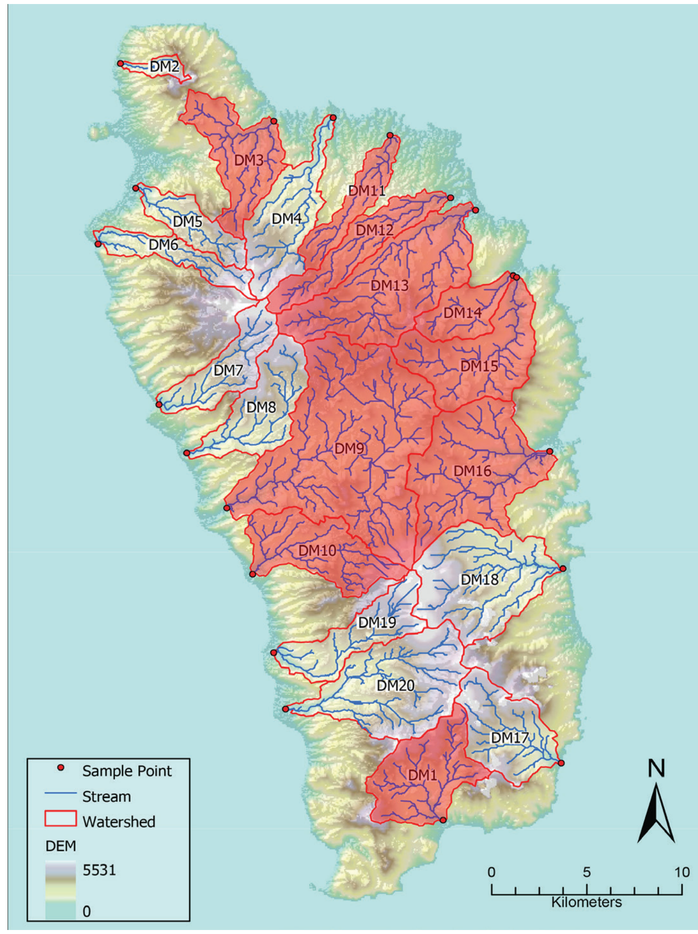

Figure 1. A map of Dominica displaying boundaries (outlined in red) and sampling locations (red points) of 20 watersheds with areas greater than 10 km^2. Watersheds with higher than average iron ratios are highlighted in red. The watershed map was created by Kira Tomenchok.

Radioactive isotope analysis

We followed a procedure similar to Singleton et al. (2017): we prepared samples by leaching them in hydrochloric acid, then used a gamma counter to analyze the amounts of ^{7}Be, ^{137}Cs, and ^{210}Pb. We were only able to analyze 12 samples so far.

Satellite image analysis

I used Adobe Photoshop to compile composite pictures of Dominica before Tropical Storm Erika hit the island in August 2015. I stitched satellite images together in order to reduce cloud interference, then made a visual inspection to identify possible landslides. These landslides were marked in a new layer in Photoshop (Fig. 2). We were able to use imagery from the World Bank taken between Tropical Storm Erika and

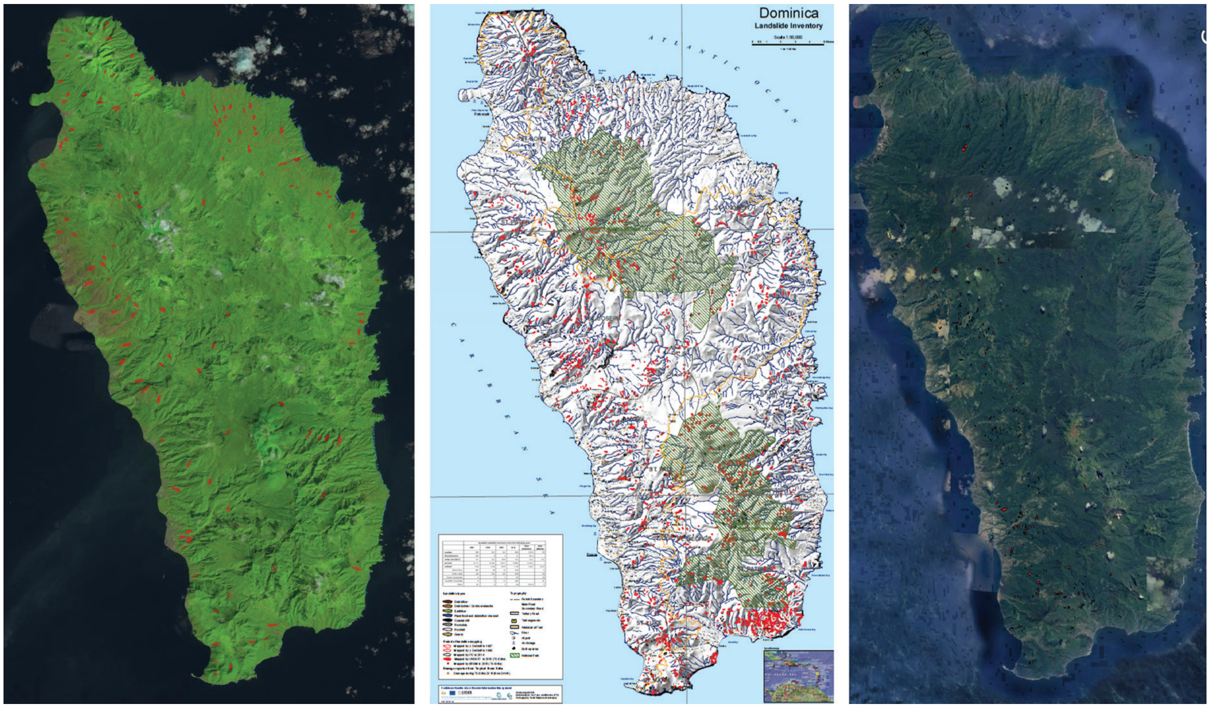

Figure 2. On the left, a stitched satellite image of Dominica using raw images from a range of dates between 2010 and 2015 (before Tropical Storm Erika) in order to reduce cloud cover in the stitched image, with disturbed land areas overlain in red. In the center, a map of landslides present after Tropical Storm Erika, from Van Westen (2016). On the right, satellite imagery from Google Earth overlain with landslides which Marcus Hill identified in post-Hurricane Maria (September 2017) imagery.

Hurricane Maria. The post-Hurricane Maria landslides were mapped by Marcus Hill using ArcGIS.

RESULTS

XRD analysis

All of the samples returned very similar results, with peaks at 2θ≈44.7°, 65.1°, 78.2°, 38.4°, and 22.0°, in decreasing order of intensity (Fig. 3). We attempted to utilize an online mineral database to match the peaks with known minerals, but were unable to find matches within the known mineral families present on the island. The closest mineral matches based on the peaks were minerals such as periclase, heterosite, and triphylite, which are unlikely to exist in this geologic setting.

XRF analysis

We found that the coarse samples and fine samples from the same location often differed in their relative proportions of various elements, including iron to silicon and iron to aluminum (Table 1). For example, the coarse sample from location DM-01 has a relatively high proportion of iron in the fine sample and a relatively low proportion of iron in the coarse sample.

We also found some patterns within the fine and coarse sediment groups. There is a group of fine-grained samples, numbers DM-01, 03, and 09 - 16, with higher than average iron:silicon and iron:aluminum ratios (with the exception of the iron:aluminum ratio in DM-10). These watersheds are for the most part located in the central and northeast part of the island (Fig. 1).

Radioactive isotope analysis

None of the samples analyzed contained detectable amounts of ^{137}Cs, and only DM-15AL contained a detectable amount of ^{7}Be. However, all of the samples contained at least some ^{210}Pb (Fig. 4).

Satellite image analysis

In the post-Maria landslide map, we were able to detect more and smaller landslides than in the pre-Erika map, but this was because we used satellite imagery from different sources for the two maps and the post-Maria satellite imagery was much higher resolution

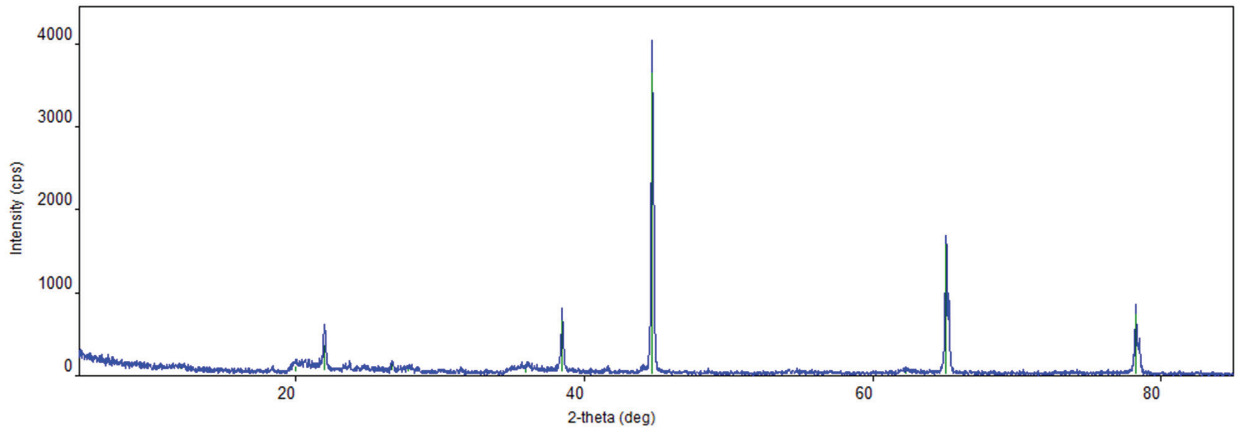

Figure 3. A plot of intensity (cps) vs 2θ (deg) for sample DM-11. This sample's plot is representative of those obtained for other samples.

than the pre-Erika imagery. In all maps, we found more landslides on the western half of the island than on the eastern half, with the exception of a cluster of landslides in the southeast in the post-Erika map. It appears that landslides are generally reactivated or occur in similar locations following storm events, but the varying resolutions of the three maps make it difficult to make accurate comparisons.

Table 1. Cation ratios in sediment samples from Dominica

	Fine			Coarse		
Sample number	Fe:Si	Fe:Al	Al:Mg	Fe:Si	Fe:Al	Al:Mg
1	15.62	102.15	20.29	8.39	56.97	22.89
2	8.16	52.77	23.39	12.06	82.47	17.34
3	13.03	72.41	31.81	16.93	103.62	25.32
4	9.04	55.04	28.82	13.24	93.19	15.50
5	11.15	66.25	23.42	9.35	61.84	20.02
6	9.29	58.19	25.43	11.53	81.59	19.75
7	11.08	69.92	25.05	13.65	88.28	17.92
8	10.66	64.15	27.17	16.99	132.33	11.84
9	13.25	79.49	24.29	11.77	67.82	18.89
10	12.31	62.47	22.82	10.25	60.37	23.12
11	15.05	69.53	19.13	24.20	117.27	21.83
12	15.30	81.61	28.11	9.89	61.25	19.85
13	14.18	69.55	33.28	10.19	73.77	17.59
14	18.56	78.72	20.08	15.04	74.84	25.98
15	17.77	78.17	19.62	15.91	68.05	24.64
16	15.96	72.07	25.38	11.41	54.87	20.47
17	8.77	49.88	23.73	9.22	62.45	20.02
18	9.95	55.21	26.47	12.54	83.82	17.38
19	7.88	47.89	23.38	10.32	68.66	16.19
20	8.03	51.00	24.87	6.07	39.59	24.19

Note: Cells highlighted in orange are cation ratios greater than the average value for samples the same grain size.

DISCUSSION

Although our XRD analysis does not allow us to differentiate which minerals are present in our samples, we are able to conclude that all of our samples have a similar mineralogy (Fig. 3). Considering that Dominica is an island where many parent rocks have similar mineral assemblages which then go through a clay mineral weathering sequence (Frey 2016), we are able to conclude that the watersheds which we studied undergo processes which produce similarly weathered sediments.

There are some samples where, based on our XRF data, the fine and coarse sediment vary in composition. Not all displayed the same pattern of differences though; some sample locations had higher iron-to-silicon and iron-to-aluminum ratios in the fine portion, while others had a larger ratio in the coarse portion (Table 1). This lack of systematic difference indicates that there are not specific elements that are preferentially weathered across the island. In addition, there are more spatial patterns in the fine-grained sediments. Specifically, fine samples from adjacent watersheds often had similar iron:silicon, iron:aluminum, and magnesium:aluminum ratios, while these ratios varied more widely in coarse samples from adjacent watersheds (Fig. 1). The fine-grained sediments could therefore serve as a more sensitive indicator for weathering than the coarse-grained sediments.

The lack of ^{137}Cs in these samples indicates that there has been deep erosion since the time of ^{137}Cs deposition, as modern sediment sources are deeper than

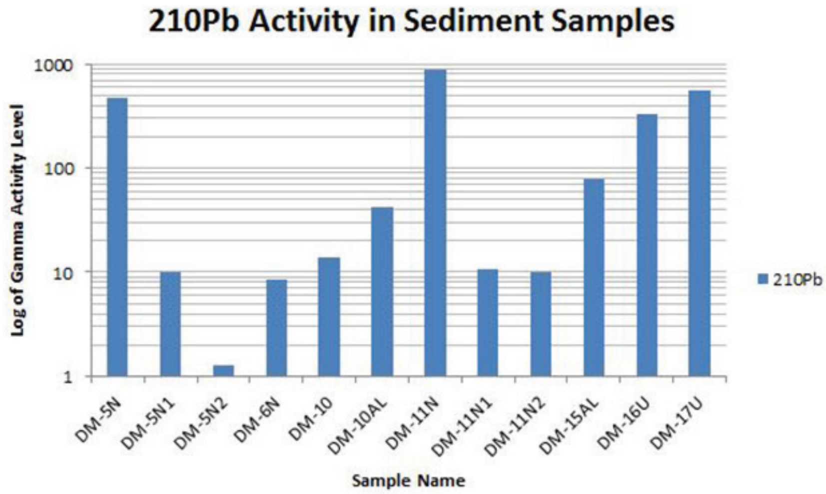

Figure 4. A logarithmic plot depicting the amount of ^{210}Pb detected in various sediment samples.

where ^{137}Cs would have been deposited (Singleton et al., 2017). This conclusion is also supported by the lack of ^{7}Be. The presence of ^{210}Pb in all samples indicates that more recent erosion has been somewhat slower and sources some surface material, as the sediments must have been exposed on the surface for at least some time in order to allow ^{210}Pb to accumulate (Singleton et al., 2017).

Our satellite landslide maps are consistent with what the Van Westen (2016) report predicts. This report highlighted the northwest and south central mountains as areas where there was a relatively higher risk of "soil slides," and we found the majority of landslides were in these areas (Fig. 2). The pre-Erika map includes a cluster of large landslides in the northeast coastal plain, where there is a low risk of soil slides in the Van Westen (2016) report and only a few small ones were found in the post-Maria images; this cluster is most likely the result of mislabeling land that was disturbed by something other than a landslide (such as human activities). There does not appear to be any correlation between the landslides and our XRF data.

CONCLUSIONS

Based on XRD analysis, we found that there are similar erosive processes are occurring throughout the different watersheds we analyzed. We were unable to differentiate different watersheds based on the XRD results. We also conclude that fine-grained sediments serve as better markers for weathering of different elements based on their higher spatial correlation in XRF tests. This could be applied to continued research by prioritizing fine-grained sediment collection if resources and time are severely limited.

We found that landslides are relatively common across the island, and that post-storm landslides generally occurred in areas where they had occurred before. The importance of landslides as an erosive factor is partly confirmed by the fallout radionuclide data; there has to have been enough erosion in the recent past to remove ^{137}Cs deposits, and this erosion could have been achieved through landslides. Landslide frequency is also emphasized in our satellite image mapping. They are present across the island in images from three different points in time, sometimes in large clusters. Post-storm landslide locations can be predicted based on past landslides, but they can also be predicted based on factors such as slope steepness and soil type (Van Westen, 2016). In their report, Van Westen discusses how there were many individual landslides following Hurricane Erika which occurred in areas that had been predicted as low or moderate risk and notes this as an area for future improvement in landslide prediction. Van Westen (2016) discusses how some of the data sets they used were low resolution, and this discussion coupled with the varying resolutions of the satellite imagery we acquired emphasize the need for continued, and detailed, research in the Caribbean. Some islands might be relatively well-studied, but each one is different and requires its own data collection in order to allow scientists to accurately create and compare hazard maps. Failing to thoroughly study and evaluate all the risks inherent to any one island could lead to continued loss of life and property from natural disasters such as landslides and volcanic eruptions, which is why it is so important to continue researching and collecting data on Dominica and throughout the Caribbean.

ACKNOWLEDGEMENTS

This material is based upon work supported by the Keck Geology Consortium and the National Science Foundation under Grant No. 1659322 and made possible by a research permit from Dominica's Ministry of Forestry. I would also like to thank Amanda Schmidt for all her guidance and encouragement throughout this entire process, and the rest of Team Geomorph for being excellent collaborators and partners.

REFERENCES

Alcántara-Ayala, I., 2002, Geomorphology, natural hazards, vulnerability and prevention of natural disasters in developing countries: Geomorphology, v. 47, p. 107-124.

Campbell, M. K., Bower, J. A., Schmidt, A. H., Neilson, T. B., Sosa-Gonzalez, V., and Bierman, P. R., 2015, Fallout radionuclides in soil profiles and history of land use in Yunnan Province, China: Geological Society of America Abstracts with Programs, v. 47, no. 7, p. 515.

Frey, H., 2016, Dominica: The sleeping giant in the Caribbean: Franklin & Marshall Scientist 2016, p. 3-37.

Gonzalez, V. S., Schmidt, A. H., Bierman, P. R., and Rood, D. H., 2017, Spatial and temporal replicability of meteoric and in situ ^{10}Be concentrations in fluvial sediment: Earth Surface Processes and Landforms, v. 42, p. 2570-2584.

Hancock, G. R., Coulthard, T. J., and Lowry, J. B. C., 2016, Predicting uncertainty in sediment transport and landscape evolution–the influence of initial surface conditions: Computers & Geosciences, v. 90, P.B., p. 117-130.

Lindsay, J. M., Smith, A. L., Roobol, M. J., and Stasiuk, M. V., 2005, Dominica: Volcanic Hazard Atlas of the Lesser Antilles, p. 1-48.

Portenga, E. W., Bierman, P. R., Rizzo, D. M., 2009, A global summary and analysis of exposed bedrock erosion rates estimated using in situ ^{10}Be: Geological Society of America Abstracts with Programs, v. 41, no. 7, p. 619.

Singleton, A. S., Schmidt, A. H., Bierman, P. R., Hood, D. H., Neilson, T. B., Greene, E. S., Bower, J. A., and Perdrial, N., 2017, Effects of grain size, mineralogy, and acid-extractable grain coatings on the distribution of the fallout radionuclides ^{7}Be, ^{10}Be, ^{137}Cs, and ^{210}Pb in river sediment: Geochimica et Cosmochimica Acta, v. 197, p. 71-86.

Van Westen, C. J., 2016, National scale landslide susceptibility assessment for Dominica, in CHARIM Caribbean Handbook on Risk Information Management: World Bank GFDRR.

Vijith, H., Suma, M., Rekha, V. B., Shiju, C., and Rejith, P. G., 2011, An assessment of soil erosion probability and erosion rates in a tropical mountainous watershed using remote sensing and GIS: Arabian Journal of Geosciences, v. 5, p. 797-805.

KECK Geology Consortium

Learning Science Through Research

Published by Keck Geology Consortium

Short Contributions
Keck Geology Consortium
Volume 31
May 2018

APPROXIMATING METEORIC ^{10}BE USING THE CONCENTRATION OF ACID-EXTRACTABLE GRAIN COATINGS: A CASE STUDY TRACING EROSION DEPTH ON DOMINICA, LESSER ANTILLES

KIRA TOMENCHOK, Washington and Lee University
Research Advisors: David Harbor and Amanda Schmidt

INTRODUCTION

Dominica, an island in the Caribbean, experiences the harmful social and economic effects of landslides (De Graff et al., 1989). Steep topography, geology and heavy precipitation create an environment conducive to damaging erosional processes. Intense rainfall events are the principle mechanism for inducing landslides (De Graff et al., 1989). Tropical Storm Erika in 2015 and most recently Hurricane Maria in September 2017 devastated the island and resulted in major landslides and flooding (van Westen et al., 2018). Due to the immediate and prominent impact, several studies have characterized and quantified landslides on Dominica. However, additional erosional processes in the Caribbean are relatively understudied (Portenga and Bierman, 2011).

We use sediment tracers to gain a larger scope of the geomorphic processes on Dominica. Sediment tracing is important to understanding the correlation between surface processes and factors such as climate, tectonics and human activity (Singleton et al., 2017). We assume the geochemical signature of detrital sediment is representative of an entire upstream basin. The tracer of our focus is meteoric beryllium-10 ($^{10}Be_m$), which is important in determining the depth of erosion in a watershed. Due to the expensive nature of $^{10}Be_m$ our study focuses on developing the concentration of grain coatings as a proxy for $^{10}Be_m$.

The purpose of this paper is twofold. We intend to characterize the erosional processes of an entire upstream basin using the elemental concentration of grain coatings on detrital sediment (Greene, 2016). We will develop a baseline understanding of the erosional processes within each watershed on Dominica, inferring landslide, riverbanks/scarps and surface erosion. Furthermore, we intend to determine the validity of using the concentration of grain coatings as a proxy for meteoric ^{10}Be in detrital sediment. With catchment sediment-source identification, our goal is to better assess sediment dynamics on Dominica and ultimately improve hazard mitigation.

Sediment Tracers

Meteoric ^{10}Be is a cosmogonic radionuclide (half-life of 1.39 million years) formed in the atmosphere by the spallation of oxygen or nitrogen (Graly et al., 2010). From the atmosphere, $^{10}Be_m$ is delivered to Earth's surface by precipitation or dry deposition (Graly et al., 2010). At the surface, $^{10}Be_m$ adheres to the upper few meters of soil and surface sediment (Willenbring, 2010). The concentration of meteoric $^{10}Be_m$ in detrital river sediments is an important metric in surface processes; specifically, $^{10}Be_m$on (Reusser and Bierman, 2010) and the residence time of sediment (Willenbring, 2010). Soils in slowly eroding landscapes tend to have higher concentrations of $^{10}Be_m$ due a greater residence time and shallow erosion. Low $^{10}Be_m$ concentrations are present in sediment from rapidly eroding landscapes and sediment sourced from below the $^{10}Be_m$ accumuluation zone (i.e. deeply penetrating gullies or deep-seated landslides) (Fig. 1) (Reusser and Bierman, 2010).

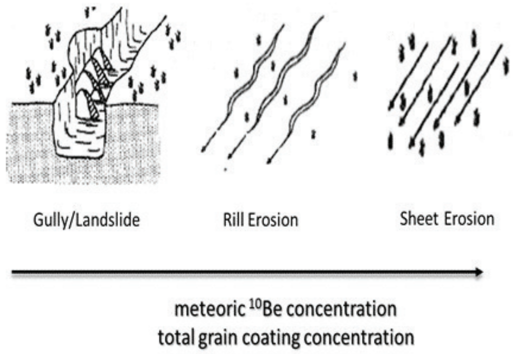

Figure 1. Relative concentration of meteoric ^{10}Be and total grain coatings in types of erosion. Adapted from Wallbrink and Murray (1993).

A strong, positive correlation exists between total $^{10}Be_m$ and acid-extractable grain coating concentrations, suggesting $^{10}Be_m$ is associated with weathering materials (Greene, 2016). Grain coatings form during podsolization, the process in which Fe^+, Al^+, and weathering products translocate through soil and form a thin film around grains in the B horizon (Birkeland, 1984). Atoms adhere to reactive surfaces of weathering materials such as oxides, hydroxides and 2:1 clay minerals. Thus, organic Be complexes sorb to sediment by associating with existing grain coatings (Greene, 2016). We measure depth of erosion using elemental concentration of grain coatings on detrital sediment as a proxy for $^{10}Be_m$ concentrations.

With the extensive landslide analysis that other studies have conducted, we evaluate erosional processes using previously mapped landslides. By quantifying the concentration of grain coatings, we determine the impact of landslides on the geochemical signature of river sediment. We hypothesize that watersheds with stabilizing landslide scars will have medium grain coating concentrations (Fig. 1). Watersheds with river bank/scarp erosion or active landslides will have low grain coating concentrations and watersheds with widespread surface erosion will have high elemental concentrations (Fig. 1). Furthermore, we will compare our grain coating concentrations with $^{10}Be_m$ data to evaluate the validity of our method in the Caribbean climate.

METHODS

Field Work

During two weeks in July 2018, a team collected detrital sediment from 20 active river channels of watersheds greater than 20 km^2 in Dominica. At each site, we wet sieved two sediment sizes, <63 and 250-850 µm. During sediment collection we spanned a 50 m radius to ensure a thorough collection of well mixed sediment (Sosa Gonzalez et al., 2017) and we sampled upstream of any tidal influence. In general, our sample sites were located near urban features. Vegetated banks were common at each location but bank steepness varied. Water depth ranged from 10 cm to 1m and channel width ranged from 20-50 m. Rock size varied greatly between each location. Some sites had a maximum rock size of gravel and other locations had large boulders up to 3-5 m.

Lab Analysis

The geochemical analysis, adopted from Greene (2016), leaches acid-extractable grain coatings as a proxy for meteoric ^{10}Be. I dried all sediment in the oven, powdered the coarse-grained sediment in a shatter box, and performed the following leaching procedure identically for both the <63 and 250-850 µm samples. I added 2 mL of 6M HCl to 0.5 g of sample, heated the sample in a sonic bath for 24 hours, and centrifuged and separated the leachate from the sediment. For using a ratio of the ICP-OES analysis, I diluted the leachate by 1:370 (sample:acid), where the acid is a 1% HCl and 1% HNO_3 solution. I sent the samples to the Nano Research Facility (EECE) at Washington University in Saint Louis where they analyzed the concentrations of Al, Fe, Mn, Na, Ca, K, Mg, Si and Ti in an ICP-OES. I also performed a microscopy analysis on two coarse-grained samples, Belfast and Mamelabou, under the microscope and SEM to understand grain composition and grain coating composition.

We measured $^{10}Be_m$ concentrations of both grain sizes from eight watersheds, including: Picard, Macoucherie, Belfast, Mamelabou, Pagua North, Pagua South, Castle Bruce, and White. Using methods from (Stone, 1998), the sediment was powdered, ^{9}Be carrier added and beryllium extracted at the University of Vermont. $^{10}Be_m$ concentrations were measured with accelerator mass spectrometry (AMS) at Lawrence Livermore National Laboratory.

ArcGIS analysis

I used GIS to quantify the following basin average parameters: geology, land use, slope, local relief, rainfall, and landslide frequency. The geology data layer classifies the rock types into Andesitic Dacite Lava, Block and Ash Flows, Block and Ash Flow Ignimbrites, Ignimbrites, Sedimentary and Volcanics. The land use map is from the Caribbean Handbook on Risk Information Management (CHARIM) database, generated by image classification of satellite images acquired between 1996 and 1999 as part of the Caribbean Land cover project. We simplified the categories into five main classifications: Forest, Urban, Agriculture, Grasslands, and Other. I downloaded global DEM layers of Dominica to create slope and local relief. To calculate precipitation we digitized the mean annual precipitation map from Lang (1967). Furthermore, I used the landslide layer from van Westen (2016)—which mapped landslides pre- and post-Tropical Strom Erika in 2015 using satellite imagery—and performed zonal statistics to quantify landslide area per watershed of pre- and post-TS Erika landslides.

RESULTS

Grain Coating Concentrations

The ICP-OES analysis revealed the elemental concentrations of HCl-extractable coatings for Al, Fe, Mn, Na, Mg, Si, and Ti. A strong positive correlation exists between relative concentrations of Al, Fe, and Mn. The correlation between Al, Fe, and Mn shows that an increase in one of these elements leads to a linear increase in the other two elements. Conversely, no relationship exists between Na, Mg, and Ti demonstrating no correlation in relative concentration. Furthermore, meteoric ^{10}Be correlates positively with elemental concentrations of Al, Fe and Mn, but inversely with Na and does not correlate at all with Mg and Ti (Fig. 2). The positive correlations between $^{10}Be_m$ and Al, Fe, and Mn confirms that the total concentration of grain coatings will be processed as the summation of Al, Fe and Mn concentrations

Landslides

Landslide density decreases within the northern and northeastern watersheds, ranging from 0.5 to 1.3% (Fig. 3). The lowest density watershed is Mamelabou, with a density of 0.05%. Landslide density increases in southern watersheds, ranging from 1.3 to 3.2%. The northwestern watersheds have an intermediate

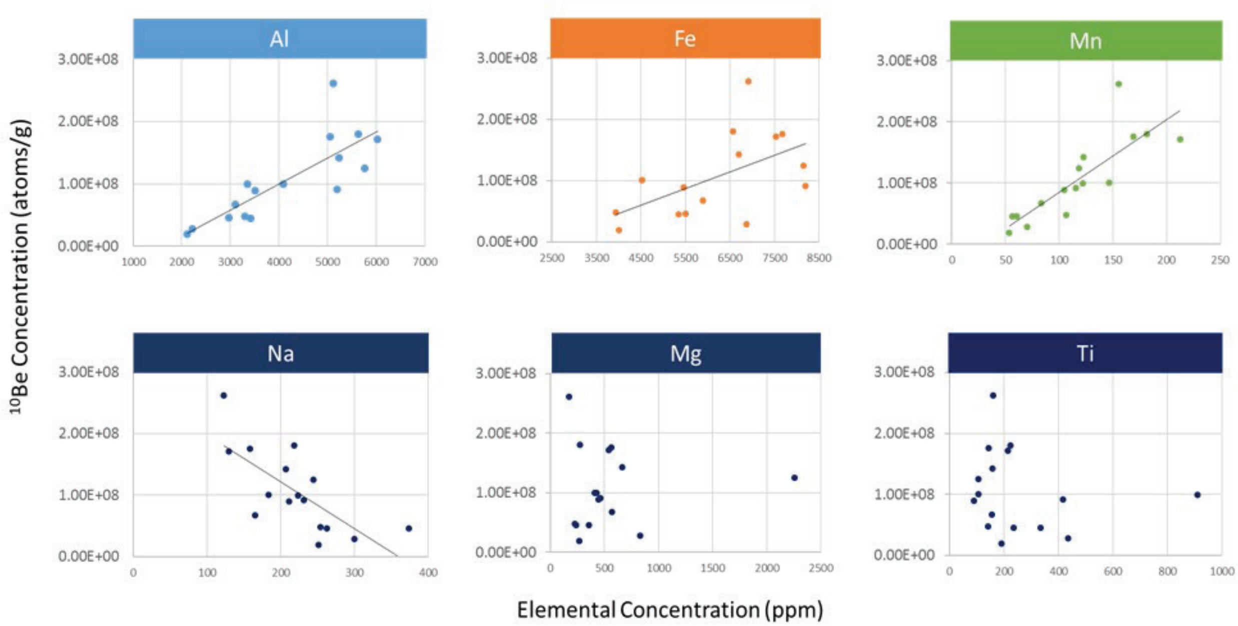

Figure 2. $^{10}Be_m$ vs. elemental concentrations of HCl-extractable grain coatings.

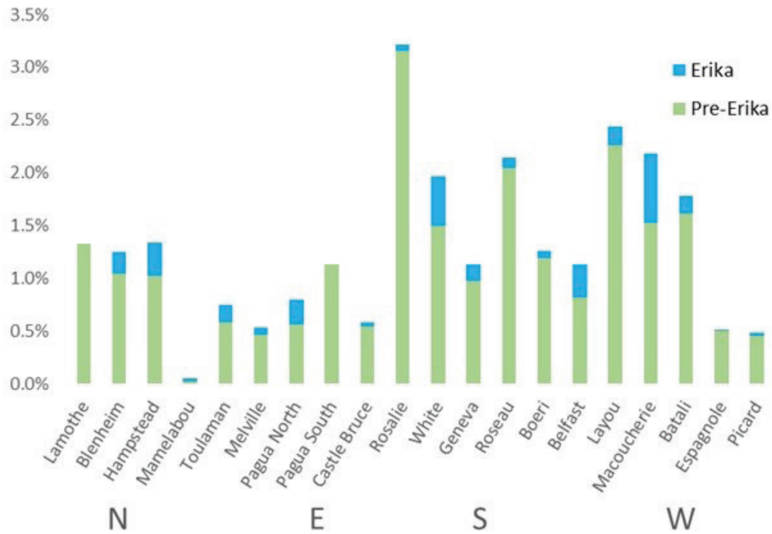

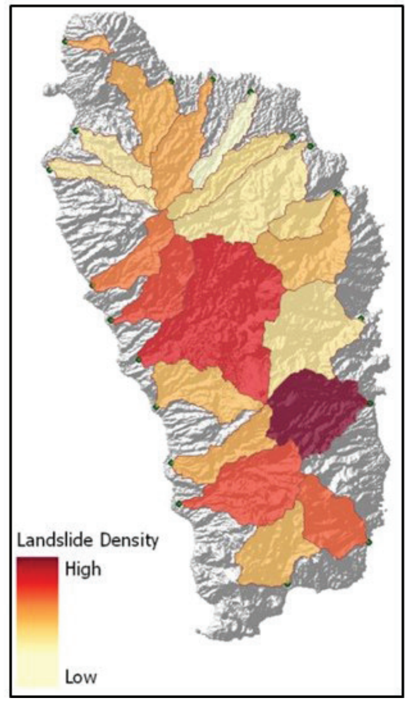

Figure 3. Landslide Density. (Left) Graphical representation (Right) Map representation.

landslide density of 1.1-2.4%. Landslide density is inversely and strongly related (R^2 value of 0.305) to total grain coating concentrations from fine-grained samples (Fig. 4a). Grain coatings from coarse-grained samples show an inverse but weak relationship (R^2 value of 0.032) with landslide density (Fig. 4b). In addition, $^{10}Be_m$ concentrations from all samples and landslide density (Fig. 4c), show a strong inverse relationship similar to the grain coating concentration from fine-grained sediment and landslide density.

Watershed Characteristics

Watershed characterization provides a broader view of controls on weathering and erosion within each watershed (Fig. 5). The relationship between mean annual rainfall and landslide density shows no significant relationship. Mean annual rainfall varies little between watersheds; the general trend shows consistent total rainfall with a range of 3.4-6.1 m/yr between each watershed. Slope generally correlates with landslide density. The northeastern watersheds have shallow slopes (15-18°), the southern watersheds are the steepest (20-27°), and the northwestern watersheds are intermediate (18-20°). Local relief shows similar trends to slope. The main variation of volcanic flows between watersheds is the abundance of ignimbrites and block and ash flows. Generally, watersheds with a landslide density less than 1.3% have a total ignimbrite abundance less than 10% and a block and ash flow abundance greater than 70%. Agriculture and forest abundance vs landslide density show a weak correlation. The main variation of land use is between forest and agriculture, while urban and grassland areas contribute only marginally to the total land use.

DISCUSSION

Acid-extraction of detrital sediment grain coatings from Dominica provides a valid proxy for $^{10}Be_m$. HCl-extraction predominantly leached Fe and Al, suggesting reactive grain coatings are composed of these minerals. The large concentrations of Fe found in the ICP-OES and SEM-EDS analysis suggest that the bulk of the grain coatings are composed of amorphous Fe oxy-hydroxides (Wittmann et al., 2012). Additionally, acid-extractable Al is part of the weathering material; the large concentrations of Al suggest some of the grain coatings are composed of Al oxy-hydroxides (Greene, 2016). The HCl method primarily leaches crystalline and amorphous oxides/hydroxides (Greene, 2016), therefore the grain coating concentrations are primarily composed of Fe and Al oxide sourced from weathering products.

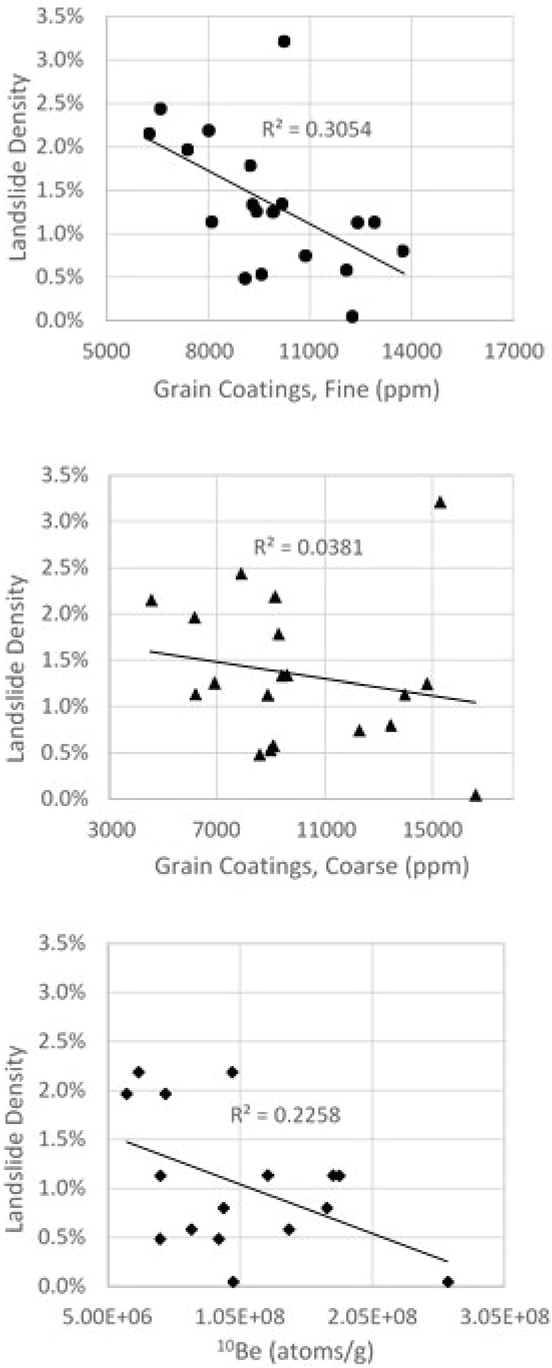

Figure 4. a) Fine Grain Coatings vs Landslide Density. b) Total Grain Coatings vs Landslide Density. c) ^{10}Be *atoms/g vs landslide density.*

Singleton et al., (2017) found $^{10}Be_m$ is strongly correlated with site-specific acid-extractable elements, which in turn is positively related to the accumulation of reactive phases during pedogenesis. It is likely, given a positive relationship between Fe, Al and Mn, that these elements accumulate directly within grain coatings during pedogenesis. Mn—which has a concentration an order of magnitude lower than Fe and Al—also showed a direct relationship with Fe and Al; suggesting Mn in the reactive phase accumulates directly within grain coatings. Furthermore, the HCl-extractable elements of Fe, Al, and Mn show a positive correlation with meteoric ^{10}Be; consistent with Greene (2016), who found acid-extractable Fe, Mn and Al strongly and positively correlate with $^{10}Be_m$ concentrations. Therefore, we use concentrations of Fe, Al and Mn, as the total concentration of grain coatings and exclude Na, Mg and Ti concentrations. Na may have an inverse relationship with grain coatings and $^{10}Be_m$ due to the leaching of Na through soil, rather than accumulating into grain coatings during pedogenesis (Birkeland, 1999). Mg and Ti may have a weak/lack of correlation due to the resistant weathering nature of Mg and Ti oxides (Birkeland, 1999). These elements do not behave in the same manner as Fe, Al and Mn during pedogenesis and this likely explains why they do not correlate with $^{10}Be_m$.

Based on the strong positive relationship between elemental concentration of grain coatings and $^{10}Be_m$, grain coatings will behave similarly to $^{10}Be_m$ as a sediment tracer. When compared to landslide density, both coatings from fine-grained sediment and $^{10}Be_m$ show a strong inverse relationship (Fig. 4a, 4c), suggesting both tracers reveal similar erosional processes. However, coatings from coarse-grained sediment compared with landslide density show an inverse but weak relationship (Fig. 4b); this trend may be a result of one of the major assumptions in sediment tracing. We assumed that grain coating concentrations are associated only with upland erosion processes and not transport processes. The abrasion of coarse-grained material may decrease the total concentration of grain coatings, depending on transport distance. Therefore in this study, grain coatings from fine-grained sediment are a more viable sediment tracer than coarse-grained coatings when assessing basin-scale erosional processes.

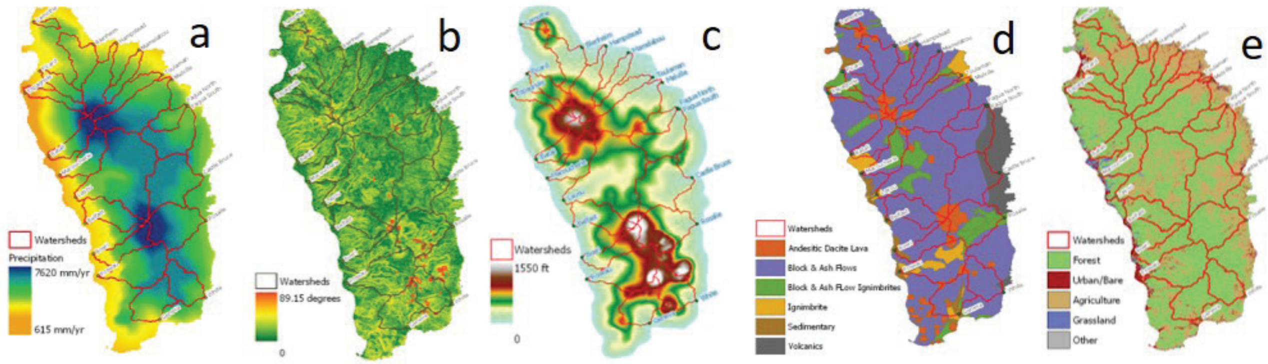

Figure 5. Watershed Characteristics. a) Rainfall b) slope c) local relief d) land use e) geology.

Using the fine-grained coatings as a sediment tracer proxy for $^{10}Be_m$ reveals the erosional processes on Dominica. The northeastern watersheds, with high grain coating concentrations, have mostly shallow erosional processes (Reusser and Bierman, 2010). Shallow erosion allows time for the accumulation of $^{10}Be_m$, as well as grain coating concentrations (Reusser and Bierman, 2010). Low landslide densities in the northeastern watersheds and high grain coating concentrations show that deeply sourced sediment is not a main contributor to outlet sediment. The southern watersheds contain lower concentration of grain coatings, suggesting that the erosional processes are sourcing rapidly eroded material or deep material. Rapidly eroding and deep-sourced sediment fail to accumulate $^{10}Be_m$ and correspondingly, grain coating concentrations (Reusser and Bierman, 2010). The correlation of low grain coating concentration with high landslide density in these watersheds supports the idea that landslides are significant contributors to the outlet sediment. Therefore, the outlet sediment is characteristic of the erosional processes in the corresponding watersheds.

Evaluating Watershed Characteristics

Even though precipitation is the main mechanism for inducing landslides (De Graff et al., 1989), the little variability of mean annual rainfall fails to explain changes in landslide density between watersheds. However, landslides instead can be initiated by single heavy precipitation events. Nugent and Rios-Berrios (2017) mapped radar-derived precipitation values for Tropical storm Erika over a 24 hour period on August 27, 2015. Mapped isohyets from this event correlate weakly but positively with TS Erika induced landslides (van Westen, 2016). Thus, landsliding events may be induced by single storm events, rather than mean annual rainfall. Additionally, slope and local relief correlate strongly with landslide density. Steep slopes are favorable for initiating landslides (Andereck, 2007), thus suggesting that steep slopes are a main driver for erosional processes on Dominica. The weak correlation between forest and agriculture abundance vs landslide density suggests that land use is not a major driver for landslides on Dominica. The weak correlation with landslide density and geology also suggests that variability in rock type plays only a minor role in erosional processes. Therefore, scatter in our landslide dataset falls to environmental factors such as rainfall distribution during a single storm event and variability in slope.

CONCLUSION

This work continues the nascent efforts to characterize erosional processes on Dominica. This study shows that fine-grained coating concentrations from detrital sediments works as a proxy for $^{10}Be_m$ in order to interpret upstream erosional processes. In Dominica, grain coatings primarily consist of Al, Fe and Mn. Total concentration of these elements negatively correlated with mapped landslides. The correlation between coatings from fined-grained samples and landslides suggests that landslides are a significant driving sediment source within Dominican watersheds. Additionally, individual rainfall events and slope variability are the main drivers for erosional processes on Dominica.

ACKNOWLEDGEMENTS

This material is based upon work supported by the Keck Geology Consortium and the National Science Foundation under Grant No. 1659322. Thank you to the Keck Geology Consortium and the Kozak, Spencer, McGuire, Schwab Award for making this research project possible. Thank you to Melinda Quock for extracting $^{10}Be_m$, UVM lab space for extraction, LLNL for running samples, and Sanmathi Chavalmane Subbenaik at WashU for running samples. Special thank you to my Washington and Lee advisors, David Harbor and Margaret Anne Hinkle, and my Keck Project advisor, Amanda Schmidt. Additional thanks to Emily Falls and Sarah Wilson at Washington and Lee University, and Holli Frey, the Head Keck Project advisor. Finally, thank you to the Team Geomorph members, Haley Talbot-Wendlandt, Cole Jimerson and Marcus Hill.

REFERENCES

Andereck, Z.D., 2007, Mapping Vulnerability of Infrastructure to Destruction by Slope Failures on the Island of Dominica, WI: A Case Study of Grand Fond, Petite Soufriere, and Mourne Jaune: Miami University, 72 p.

Birkeland, P.W., 1984, Soils and Geomorphology: Oxford University Press, 372 p.

Birkeland, P.W., 1999, Soils and Geomorphology: Oxford University Press, 452 p.

De Graff, J., Brice, R., W. Jibson, R., Mora Castro, S., and Rogers, C., 1989, Landslides: their extent and economic significance in the Caribbean, in p. 51–80.

Graly, J.A., Bierman, P.R., Reusser, L.J., and Pavich, M.J., 2010, Meteoric ^{10}Be in soil profiles – A global meta-analysis: Geochimica et Cosmochimica Acta, v. 74, p. 6814–6829, doi: 10.1016/j.gca.2010.08.036.

Greene, E.S., 2016, Comparing ^{10}Be, *in situ* ^{10}Be, and native ^{9}Be across a diverse set of watersheds [Master of Science Thesis]: University of Vermont, 110 p.

Lang, D.M., 1967, Soil and land-use surveys No. 21. Dominica.: Soil and land-use surveys No. 21. Dominica., https://www.cabdirect.org/cabdirect/abstract/19721905097 (accessed April 2018).

Nugent, A.D., and Rios-Berrios, R., 2017, Factors Leading to Extreme Precipitation on Dominica from Tropical Storm Erika (2015): Monthly Weather Review, v. 146, p. 525–541, doi: 10.1175/MWR-D-17-0242.1.

Portenga, E.W., and Bierman, P.R., 2011, Understanding Earth's eroding surface with ^{10}Be: GSA Today, v. 21, p. 4–10, doi: 10.1130/G111A.1.

Reusser, L.J., and Bierman, P.R., 2010, Using meteoric ^{10}Be to track fluvial sand through the Waipaoa River basin, New Zealand: Geology, v. 38, p. 47–50, doi: 10.1130/G30395.1.

Singleton, A.A., Schmidt, A.H., Bierman, P.R., Rood, D.H., Neilson, T.B., Greene, E.S., Bower, J.A., and Perdrial, N., 2017, Effects of grain size, mineralogy, and acid-extractable grain coatings on the distribution of the fallout radionuclides ^{7}Be, ^{10}Be, ^{137}Cs, and ^{210}Pb in river sediment: Geochimica et Cosmochimica Acta, v. 197, p. 71–86, doi: 10.1016/j.gca.2016.10.007.

Sosa Gonzalez, V., Schmidt, A.H., Bierman, P.R., and Rood, D.H., 2017, Spatial and temporal replicability of meteoric and *in situ* ^{10}Be concentrations in fluvial sediment: Earth Surface Processes and Landforms, v. 42, p. 2570–2584, doi: 10.1002/esp.4205.

Stone, J., 1998, A rapid fusion method for separation of beryllium-10 from soils and silicates: Geochimica et Cosmochimica Acta, v. 62, p. 555–561, doi: 10.1016/S0016-7037(97)00340-2.

Wallbrink, P.J., and Murray, A.S., 1993, Use of fallout radionuclides as indicators of erosion processes: Hydrological Processes, v. 7, p. 297–304, doi: 10.1002/hyp.3360070307.

van Westen, C.J., 2016, National Scale Landslide Susceptibility Assessment for Dominica:, doi: 10.13140/RG.2.1.4313.2400.

van Westen, C., Zhang, J., and Sijmons, K., 2018, Tropical Cyclone Maria. Inventory of landslides and flooded areas: UNITAR, https://unitar.org/unosat/node/44/2762 (accessed March 2018).

Willenbring, 2010, Meteoric cosmogenic Beryllium-10 adsorbed to river sediment and soil: Applications for Earth-surface dynamics: Earth-Science Reviews, v. 98, p. 105–122, doi: 10.1016/j.earscirev.2009.10.008.

Wittmann, H., Von, B., Bouchez, J., Dannhaus, N., Naumann, R., Christl, M., and Gaillardet, J., 2012, The dependence of meteoric ^{10}Be concentrations on particle size in Amazon River bed sediment and the extraction of reactive ^{10}Be/^{9}Be ratios: Chemical Geology, v. 318–319, p. 126–138, doi: 10.1016/j.chemgeo.2012.04.031.

KECK Geology Consortium
Learning Science Through Research
Published by Keck Geology Consortium

Short Contributions
Keck Geology Consortium
Volume 31
May 2018

EVIDENCE FOR COLD, HYDROUS PARENTAL MAGMAS ON DOMINICA: PETROLOGY OF THE FOUNDLAND BASALTS

KATHRYN VONSYDOW, California State University San Bernardino
Research Advisors: Laura Waters (Sedona College), Holli Frey (Union College), and Joan E. Fryxell (California State University San Bernardino)

INTRODUCTION TO RESEARCH QUESTION

Dominica is the center island of the Lesser Antilles island arc. The island hosts a variety of volcanic features that all contribute to the story of its formation. The Foundland (FND) region is in the southeastern portion of Dominica. FND is one of the few locations on the island where basalt has been erupted. The petrology of the basalts and their field relations in FND will contribute to an understanding of the primitive magmas that formed under Dominica. These findings can then be compared to the data collected from another basalt location, proto-Morne aux Diables (pMAD), in the northern section of the island which is thought to have erupted around the same time to determine if they originated from the same magmatic source.

GEOLOGIC BACKGROUND

FND is in the southeast corner of Dominica and is thought to represent one of the most primitive magmas erupted on the island. One notable feature of this region is the absence of felsic deposits and the eruption of basalts. The basalts of the FND stratovolcano are thought to have erupted 3.72 to 1.12 mya during the Pliocene Epoch (Smith et al., 2013). The oldest rocks of FND can be found along the base of sea cliffs and are volcanic breccia deposits (Wills, 1974). The inland regions of FND are dominated by up to 30 m thick basalt flows interbedded with scoriaceous pyroclastic deposits and some andesites (Lindsay et al., 2005).

METHODS

One major obstacle of fieldwork was finding locations to collect viable rock samples. Wills (1974) gave the GPS coordinates of locations of his sample sites around FND. Due to road damage from Tropical Storm Erika that hit the island in 2015, it was very difficult to reach the interior portion of FND. We were only able to collect samples from Foundland's easternmost and westernmost edges. Samples were collected from outcrops exposed along roadcuts and river floodplains using 6-pound and 10-pound sledgehammers.

At Union College, the best pieces were selected from each sample and were cut to the proper dimensions for 11 thin sections using a diamond tipped rock saw. The resulting billets were epoxied, cut, and polished in the Geology Department at Union College. Three of the thin sections were given a carbon coat and examined under a scanning electron microscope (SEM) along with a sample previously collected by Frey (Foundland-2B). Images and compositions of spinel (mostly magnetite), olivine, and plagioclase were collected using energy dispersive spectrometry (EDS) with the Zeiss EVO-MA15 Scanning Electron Microscope (SEM) at Union College. The EDS analyses were conducted following a calibration method, where the initial beam intensity is obtained by collecting the energy emitted by a copper plate, then EDS spectra are collected for natural mineral standards in the Union College collection.

Using a Rocklabs hydraulic press provided by Union College, samples were crushed into rock fragments and then dried in an oven before being broken down into smaller fragments with a small sledgehammer.

Table 1. Bulk chemistry of Foundland samples

Sample Number	FB-1A	FB-2A	FB-2M	FB-3	FB-4	FB-5	FB-6	FB-7A	FB-7B	FB-8	FB-9
Major Elements, in weight percent											
SiO2	52.74	52.54	48.74	52.10	51.67	59.32	51.51	48.79	48.81	49.37	52.95
TiO2	0.83	0.81	1.06	0.86	0.90	0.69	0.82	0.97	1.05	1.02	0.83
Al2O3	19.36	19.72	19.82	20.80	20.27	17.94	21.41	21.18	21.01	20.40	19.93
Fe2O3	9.74	9.20	11.39	8.84	9.52	7.75	8.94	9.89	10.30	10.67	9.17
MnO	0.20	0.19	0.20	0.19	0.19	0.14	0.19	0.17	0.18	0.19	0.20
MgO	4.50	4.59	5.52	3.81	4.14	2.74	3.70	5.38	4.83	5.10	4.08
CaO	9.07	9.53	10.70	9.93	10.11	7.07	10.32	10.77	10.94	10.44	9.55
Na2O	2.75	2.64	2.09	2.58	2.49	2.78	2.32	2.14	2.08	2.19	2.51
K2O	0.54	0.51	0.26	0.61	0.47	1.34	0.53	0.49	0.53	0.39	0.54
P2O5	0.15	0.14	0.08	0.14	0.12	0.10	0.12	0.11	0.11	0.09	0.13
Total	99.87	99.87	99.84	99.87	99.86	99.87	99.88	99.88	99.84	99.87	99.88
Trace Elements, in parts per million											
Rb											
Sr	11	11	4	14	9	44	11	14	15	5	16
Ba	295	294	278	284	348	226	271	240	294	234	235
Zr	117	108	106	129	105	231	105	123	153	93	118
Y	53	51	37	64	45	79	57	21	51	48	57
Nb	21	18	15	19	17	24	18	0	17	20	22
Cs	0	3	4	4	0	5	4	0	7	0	7
Sc	0	0	0	0	7	0	0	0	0	0	7
V	28	30	45	28	32	24	23	49	34	37	25
Cr	221	226	389	237	255	191	220	354	365	344	221
Ni	15	19	11	7	13	7	10	0	3	19	14
Cu	10	11	10	8	11	3	8	0	13	10	8
Zn	52	78	129	83	76	55	79	46	121	66	37
Ga	79	77	77	77	70	61	75	47	76	69	76
La	20	19	19	21	19	19	20	14	19	19	20
Ce	10	9	11	0	10	19	8	0	18	12	8
Nd	21	16	27	26	23	32	20	20	29	12	20
Hf	12	11	22	21	13	18	17	0	22	5	12
Pb	6	2	2	0	2	0	6	5	0	6	4
Th	4	4	3	5	6	5	4	0	9	6	3
U	0	0	3	0	0	4	0	8	2	0	0

The fragments were then placed inside a Rocklabs shatter box with aluminum oxide vessel and porcelain plate and ground into a fine powder. A powder was made from each sample (11 in total).

We determined major and trace element abundances using a 3.0 kW Panalytical Axios wavelength-dispersive X-ray fluorescence (XRF) spectrometer at Pomona College. Each of the 11 powders were prepared for analysis by mixing them with a flux in a 2:1 ratio (3.5 g basalt powder to 7.0 g dilithium tetraborate ($Li_2B_4O_7$)). A vortex blender was then used to ensure the mixture was homogeneous. Each mixture was placed in a graphite crucible and fused into a glass bead at 1000 °C for 15 minutes, left to cool to room temperature, and reheated for an additional 15 minutes at 1000 °C to burn off any extra water still present, as well as eliminate any air pockets within the bead. The cooled beads where then polished on diamond polishing wheels and by hand with 400-grit sandpaper. Using XRF equipment provided by the Pomona College Geology Laboratory, we were able to analyze major, minor, and 22 trace elements from each bead (Table 1). Reference calibration curves were defined by using 55 certified reference materials (Lackey et al., 2012).

Modal counts were collected for 1000 points each on four slides at Union College using a Petrog point count stage, the PetrogLite computer program, and a petrographic microscope. The modal counts of the remaining slides (excluding sample FB-5 which was determined to be an andesite) were collected for 1000 points each by hand using a petrographic microscope at CSUSB.

RESULTS

Major and Minor Elements

Table 1 shows major and trace element data for the FND samples. For the major elements, the silica content averaged 51.69 wt. % for each sample (except FB-5) and is classified as a basalt. The average Al_2O_3 content was 20.17 wt. % which can be an indicator that the parental melt experienced fractional crystal-

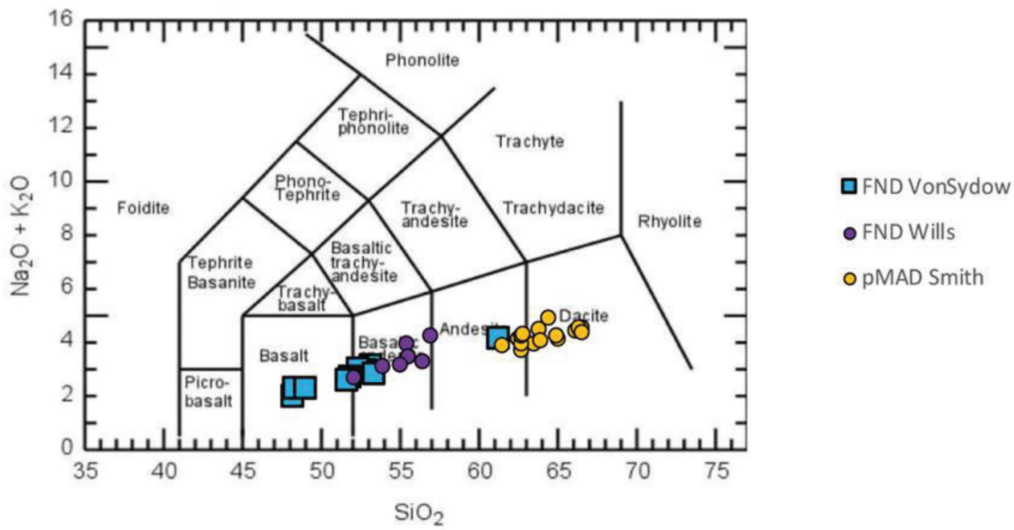

Figure 1. TAS Diagram (modified from LeBas et al., 1986) showing the relationship between SiO_2 content vs Alkali content of samples collected from FND and pMAD.

lization. For the minor elements, the average amount of TiO_2 was 0.89 wt. % and the average MnO was 0.18 wt.% which suggests the influence of oxidizing conditions. Sample FB-2M, a boulder that was collected in the Savanna River floodplain and contained mafic nodules, had the highest concentrations of TiO_2, Fe_2O_3, MnO, and MgO, which further supports oxidizing conditions. Alkali concentrations ($Na_2O + K_2O$) vs silica concentrations are plotted on Figure 1 and shows that the samples range from a basalt to basalt-andesite composition; however, Sample FB-5 was found to be an andesite.

Modal Abundances

Modal abundances, excluding sample FB-5, were determined from samples collected in FND. For each sample, plagioclase was the most frequently observed phenocryst, composing between 21.1 and 47.6%. Clinopyroxene (cpx) was the second most common phenocryst found in each sample constituting between 4% and 13.6%. Most olivine (olv) crystals were highly weathered and difficult to recognize; those that were observed composed between 1.1% and 8.7%.
The abundance of orthopyroxene (opx) phenocrysts ranged between 1.1% and 3.2%. In most samples, groundmass (gm) was a major component of the rock and ranged between 25.1% and 62.3%.

Plagioclase Compositions

From the same four samples, the rim and core from five different phenocrysts each were analyzed using a SEM at Union College. We were unable to collect data from the rim of the second phenocryst in sample FB-2B. The composition of plagioclase rims ranged between An_{54} and An_{97} and the composition of cores ranged between An_{78} and An_{95}.

Olivine Compositions

Olivine compositions were established from rims and cores of phenocrysts from four samples. It was difficult finding unweathered olivine phenocrysts to analyze from each sample. Of those that were found, sample FB-2 has an average composition of Fo_{69}, FB-7A has an average composition of Fo_{70}, and FB-9 is the most forsteritic with an average composition of Fo_{78}.

Fe-Ti Oxide Compositions

Iron-titanium oxide composition were also determined from four samples. Fe-Ti oxide compositions fall on the titanomagnetite-ulvospinel continuum with trace amounts of the spinel end member. Higher oxygen environments cause ulvospinel components of magnetite to chemically weather by oxidation to form ilmenite.

Relatively high concentrations of Ti can only occur in low-oxidation environments; therefore, the low TiO_2 concentrations coupled with presence of ilmenite support the hypothesis that these samples formed under oxidizing conditions. Furthermore, the existence of both magnetite and ilmenite in samples (i.e. FB-2M and FB-9) require that the parental melt be subjected to a limited range of temperatures. Using an Fe-Ti oxide geothermobarometer created by Ghiorso and Evans (2008), we used all possible pairs to determine a temperature range as low as 714 °C and as high as 925 °C with an average of temperature around 816 °C.

Amphibole Phenocrysts

Amphibole phenocrysts were analyzed in sample FB-9 and fall on the cummingtonite-grunerite solid series; they also all contain trace amounts of calcium. Amphiboles appear late in the crystallization sequence associated with mafic rocks, specifically if the melt is enriched in silica and H_2O. The oxidized rims had formed around the phenocrysts indicating they grew from the melt and were not plucked a cumulate or country rock.

DISCUSSION

FND and pMAD are volcanic centers located at opposite ends of Dominica. Both centers erupted around the same time (Pliocene Epoch) and one outstanding question in the literature is whether they erupted from the same magma source (Smith et al., 2013). We note the presence of the same mineral phases (plagioclase + clinopyroxene + titanomagnetite ± ilmenite ± olivine ± orthopyroxene) in lavas erupting from both volcanic centers, however it is still outstanding if their major element patterns are both similar and consistent with the observed mineral phases.

FND samples are plotted along with those collected by Smith et al. (2013) and Wills (1974) for both FND and pMAD in Figure 2. Despite being relatively mafic samples, each suite of volcanics has a low concentration of MgO with markedly elevated alkali concentrations. The most striking pattern of all the FND and pMAD lavas is that all samples are saturated in abundant plagioclase crystals; this modality is largely consistent with elevated Al_2O_3 contents for each sample, which should stabilize plagioclase. The trends of Al_2O_3 and CaO for all the lavas are consistent with the crystallization of plagioclase through a liquid line of descent. Additionally, the pattern of continuous depletion in Fe_2O_3 and TiO_2 throughout both volcanic series is consistent with the presence of magnetite-ulvospinel in all samples. The similar patterns in geochemistry for each of these areas suggests that they are derived from a similar source.

The most notable difference between both volcanic centers is the presence of amphiboles collected in FND (FB-9) and their absence in pMAD (Smith et al., 2013). This may be explained by both the water content and the pre-eruptive temperature of the melt during the two eruptive episodes. The phase stability curves for plagioclase and amphibole determined from experiments on high-Al basalt from Grove et al. (2003), demonstrate that the co-existence of plagioclase and amphibole only occurs at relatively cold pre-eruptive temperatures for a basalt (1000 °C – 1050 °C). Moreover, saturation in plagioclase and amphibole additionally requires between 7 – 8 wt. % H_2O to be in equilibrium with the melt (under pure H_2O vapor saturated conditions) (Fig. 3). One possible explanation for the presence of amphibole in the FND lavas is that they separated from their parental cumulates at lower temperatures. Additionally, Ca-rich plagioclase was observed in both FND and pMAD. In pMAD, phenocryst compositions covered a narrow range and were more anorthite-rich than FND, suggesting that pMAD's melt was in the earlier stages of crystallization (i.e. hotter) at the time of eruption.

With respect to mantle source, sample geochemistry and petrology reported in this study and from Smith et al. (2013) indicated that both the FND and the pMAD magmas were likely derived from a parental magma that originated from a metasomatized mantle. The calcic nature of the plagioclase crystals and the presence of amphibole in one sample from FND in all samples strongly supports high water contents. The discrepancy (i.e. differentiation) beneath FND occurs at lower temperatures, which suggests an interval of cooling occurred between the eruption of pMAD and FND.

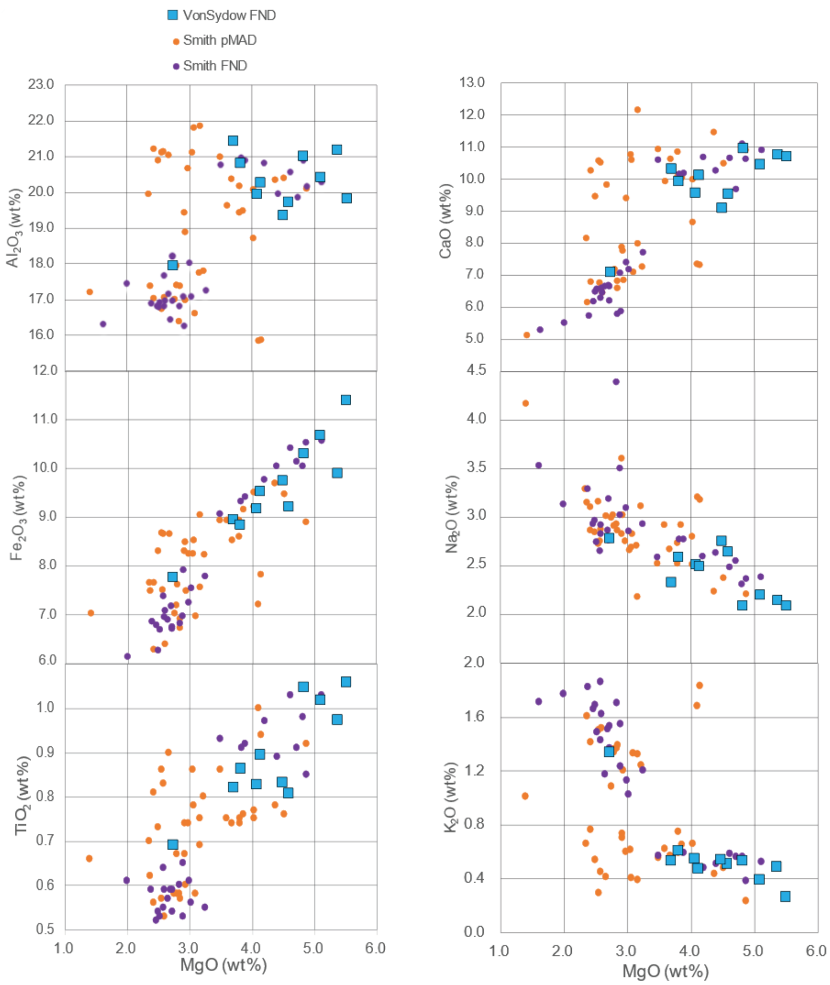

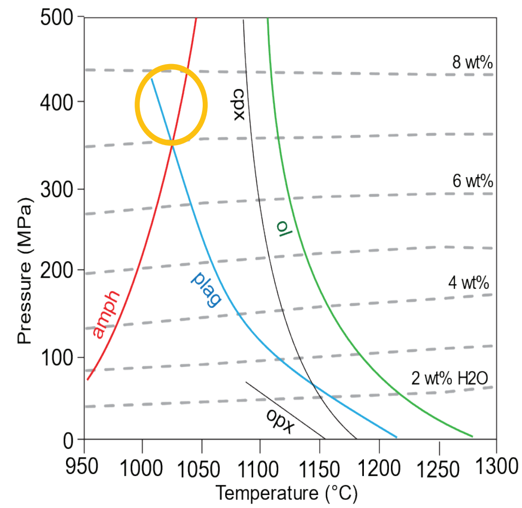

Figure 3. Results of a H_2O saturated phase equilibrium experiments modified from Grove et al. (2003). Amphibole (amph), plagioclase (plag), clinopyroxene (cpx), orthopyroxene (opx), and olivine (olv) lines are plotted to show the conditions necessary for their growth from a melt. The area circled in yellow suggests the conditions necessary for plagioclase and amphibole to coexist.

Figure 2. Harker diagrams showing the relationship between MgO concentration and major/minor element concentrations from FND and pMAD (Wills, 1974 and Smith et al., 2013).

CONCLUSION

The overall bulk chemistry of samples collected from FND and pMAD show very similar trends. Both locations are characterized by the same mineral phases, highly calcic plagioclase, little to no olivine, and Fe-Ti oxides. The overall mineral composition of the samples from FND indicate they are aluminous, subduction zone basalts. When these basalts are compared to those collected in pMAD (Smith et al., 2013), we see that the compositions are very similar which suggests both locations shared the same magma source. The main difference between the two centers is the presence of amphibole phenocrysts in FND. The presence of amphibole crystals and the coexistence of magnetite and ilmenite, suggest that between the eruption of pMAD and the eruption of FND, the melt cooled and crystallized, explains the inferred increase in water and lower inferred temperature.

FURTHER STUDY

• Olivine phenocrysts collected from pMAD need to be analyzed to be compared to those collected in FND.

• More SEM work to be done on samples collected in FND to add to the data set.

ACKNOWLEDGEMENTS

This material is based upon work supported by the Keck Geology Consortium and the National Science Foundation under Grant No. 1659322. This research was funded by a National Science Foundation grant to the Keck Geology Consortium (EAR 1659322 to K. Wirth, Macalester College).

I would like to thank Keck and the National Science Foundation (NSF) for funding this project and offering me the opportunity to travel abroad and experience a research project as an undergraduate. I would also like to give a very special thanks to my Keck advisors Laura Waters and Holli Frey, my home advisor Joan E. Fryxell, and all my fellow Keck students for their friendship and making this experience one I will always cherish. I would also like to thank Union College and Pomona College for providing equipment needed to analyze samples collected from Foundland. I would like to thank to Bill Neubeck of Union College for making our thin sections, to Matt Manon of Union College for his support in learning to use a SEM, and to Jonathan Harris of Pomona College for his guidance in preparing samples for XRF analysis. A final and very special thanks goes to the people of Dominica who welcomed us with open arms to their country and allowed us the opportunity (through our experience) to grow as scientists and as people.

REFERENCES CITED

Frey, H.M., Dominica: The Sleeping Giant in the Caribbean: Franklin and Marshall Magazine Issue 84, 52 p.

Ghiorso, M.S. and Evans, B.W., 2008, Thermodynamics of Rhombohedral Oxide Solid Solutions and a Revision of the Fe-Ti Two-oxide Geothermometer and Oxygen-barometer: American Journal of Science, v. 208, p. 957 – 1039.

Grove, T.L., Elkins-Tanton, L.T., Parman, S.W., Chatterjee, N., Müntener, O., and Gaetani, G.A., 2003, Fractional crystallization and mantle-melting controls on calc-alkaline differentiation trends: Contributions to Mineralogy and Petrology, v. 145, doi: 10.1007/s00410-003-0448-z.

Lackey, J.S., Cecil, M.R., Windham, C.J., Frazer, R.E., Bindeman, I.N., and Gehrels, G.E., 2012, Fine Gold Intrusive Suite: The roles of basement terranes and magma source development in the Early Cretaceous Sierra Nevada batholith: Geosphere, v. 8, no. 2, doi: 10.1130/GES00745.1.

LeBas, M.J., LeMaitre, R.W., Streckeisen, A., and Zanettin, B., 1985, A Chemical Classification of Volcanic Rocks Based on the Total Alkali-Silica Diagram: Journal of Petrology, v. 27, no. 3, p. 745 – 750.

Lindsay, J.M., Smith, A.L., Roobol, M.J., and Stasiuk, M.V., 2005, Volcanic Hazard Atlas of the Lesser Antilles: Dominica: West Indies, Seismic Research Centre, 279 p.

MacDonald, R., Hawkesworth, C.J., and Heath, E., 1999, The Lesser Antilles Volcanic Chain: A Study in Arc Magmatism: Earth-Science Reviews, v. 49, p. 1-76.

Smith, A.L., Roobol, M.J., Mattioli, G.S. Fryxell, J.E., Daly, G.E., and Fernandez, L.A., 2013, The Volcanic Geology of the Mid-Arc Island of Dominica, Lesser Antilles: The Surface Expression of an Island-Arc Batholith: Boulder, Colorado, Geological Society of America Special Paper 496, 249 p.

Wills, K.J.A., 1974, The geologic history of Southern Dominica and plutonic nodules from the lesser Antilles [Doctoral thesis]: Durham University, 211 p.

KECK Geology Consortium
Learning Science Through Research
Published by Keck Geology Consortium

Short Contributions
Keck Geology Consortium
Volume 31
May 2018

MULTIPLE PROXIES FOR INVESTIGATING GLACIAL HISTORY OF ANTARCTICA FROM ODP SITES 696 & 697

SUZANNE O'CONNELL (Wesleyan University) and **JOSEPH ORTIZ** (Kent State University)

INTRODUCTION

The Antarctic ice sheets and the Southern Ocean have played a central role in controlling global sea level and deep and intermediate water formation, upwelling intensity, and ultimately the storage and exchange of carbon dioxide with the atmosphere. Major goals in this Antarctic Pliocene and upper Miocene research include determining the presence and behavior of Antarctic ice sheets using the sediment record from ODP sediment cores and well-logs. This knowledge of the patterns and rates of past ice behavior can provide important analogues for predicting ice sheet retreat over the next few decades and centuries as atmospheric carbon dioxide levels exceed the present 410 ppm CO_2 and temperatures increase by more than 1 degree Celsius.

The Weddell Sea is one of the main formation sites for Antarctic Bottom Water and an outlet for about one fifth of Antarctica's continental ice volume, draining ice from both West and East Antarctica (Fig. 1). We chose the Weddell Sea embayment as the location for this study because there are many unresolved questions about ice-sheet history in this sector that can be readily addressed using diatom floral abundance, grain-size analysis and geochemical provenance techniques.

Sediment from two Ocean Drilling Program (ODP) Sites (113-696 and 113-697) and well logs from the circumAntarctic were examined (Figure 1). Both sites are dominated by terrigeneous sediment, contain no carbonate and small amounts of biosilica, primarily diatoms. Ice-rafted detritus and dropstones (>1mm), indicators of ice-berg melting, and hence glacial history, are present at both sites. Core recovery is variable, ranging from 100% to no recovery at all.

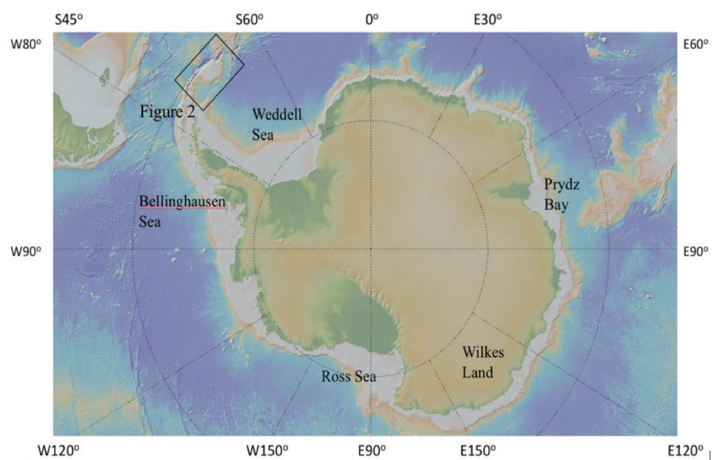

Figure 1. Polar projection of Antarctica produced with the GeoMapApp software depicting the location of the areas studied in this research. The two Leg 113 sites are shown in more detail in the insert (Figure 2). The well-logs of the circum-Antarctic sites are identified by basin. The IODP Wilkes Land sites are offshore of the land, in the ocean.

This research utilized a wide variety of sedimentological and geophysical techniques to describe the deposition of these circum-Antarctic sediments. Four different projects were completed as part of this study:

1) Eduardo Centeno (Wesleyan University) examined Pliocene diatom assemblages from Core 697B-14X (Figure 2), which we think represents sediment from Marine Isotope Stage (MIS) M2 (3.312-3.264 Ma) a Southern Ocean warming interval during which there was rapid turnover in diatom species.

2) Mark LePan (Colgate University) examined what–according to the shipboard initial results report–was thought to be Pleistocene diatoms from Core 113-696A-2H (Figure 2). His findings suggest that the core may well be Pliocene.

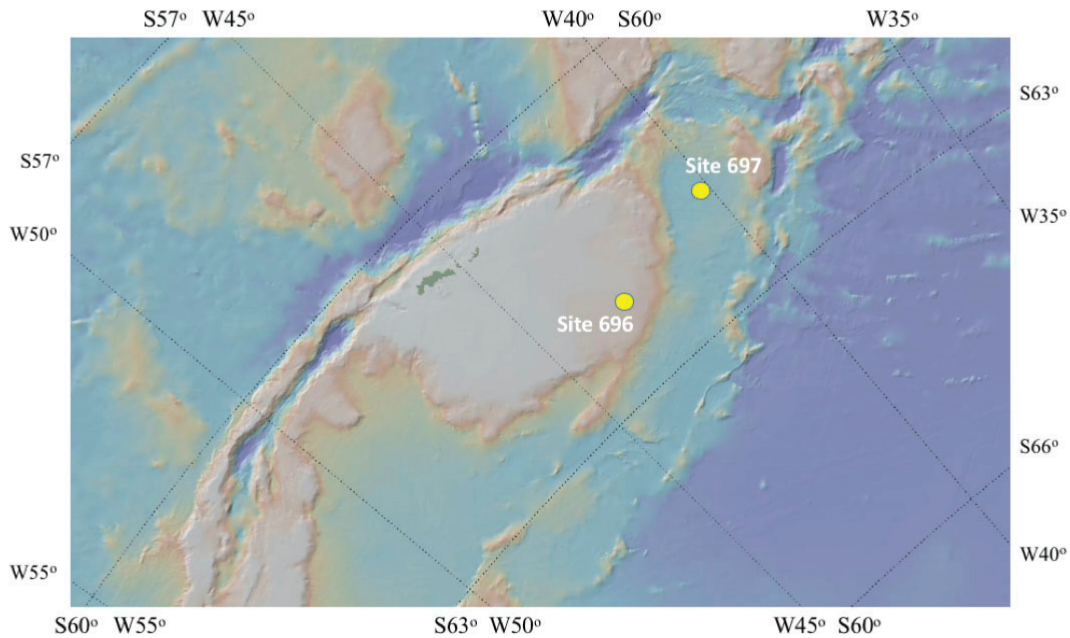

Figure 2. Polar projection of the insert shown in Figure 1 produced with the GeoMapApp software. The location of the two ODP Sites 696 and 697 are shown, clearly identifying that they were part of a depth transect, at 650 and 3480 m water depth respectively.

3) Forrest Lloyd (Beloit College) examined sediment chemistry and grain-size of the oldest section of Site 697, Cores 697B-31X and 32X (302.6-322.9 mbsf), with an estimated age around 5 Ma.

4) Andrew Hollyday (Middlebury College) conducted the widest ranging studies, examining split core measurements and geophysical well logs from several circum-Antarctic sites to identify the pace of lithologic variations.

In addition to these specific reports, data and samples collected by this Keck team will be available for further research projects in years to come.

SPECIFIC RESEARCH PROJECTS

Two diatom projects were undertaken as part of this research. The work of these investigators attests to how difficult diatom slide preparation and identification can be. Species identification requires using a high magnification microscope to identify the intricate patterns on both the edges and center of the rigid silica frustules. Diatoms reproduce both sexually and asexually.

Eduardo Centeno completed the diatom identifications for three samples in an interval that spans the crucial Marine Isotope Stage M2, a brief cooling event in the warmer Pliocene. His first two samples, at 697B-14X-5, 55-57 cm (~3.29 Ma) and 697B-14X-4, 68-70 cm (~3.27 Ma) are from the coldest part of interval M2, when benthic $\delta^{18}O$ values were ~3.7‰ (LRO4, Lisiecki and Raymo, 2005). By the time the youngest sample, 679B-14X-2, 66-68 cm, (3.2 Ma) was deposited, the M2 isotope excursion had ended. The benthic $\delta^{18}O$ values had lightened (warmed or freshened) to ~3.1‰, indicating both rapid ice melting and probably concurrent warming of the deep ocean. The youngest sample, also had the highest weight percent biosilica, supporting the interpretation of a warmer, more productive, ocean. The decrease in Chaetocerous resting spores in the youngest (warmest) sample supports more open ocean conditions at 3.2 Ma, while sea-ice tolerant, Eucampia Antarctica, confirms the continued presence of sea-ice at this location. Centeno will continue this work as part of his senior honors thesis.

Mark LaPan also conducted a diatom research project. His project was to identify diatoms from Core 113-686A-2H, which according to the shipboard biostratigraphers was Quaternary in age (Barker, Kennett et al., 1988). He chose this interval because his research mentor specializes in Antarctic Pleistocene diatoms. Site 696, in 650 m water depth is the shallowest of a 3-site depth transect in the Jane Basin. As with the other Antarctic sites, it is dominated by terrigeneous sediment. To identify areas that were more likely to contain diatoms, magnetic susceptibility measurements were taken on the core. Areas with the lowest magnetic susceptibility are likely to have a higher percentage of biosilica and are likely to be the warmer intervals (Leventer et al., 1996). These intervals were preferentially sampled. Post-expedition examination of the samples by Gersonde and Burckle (1990), suggest that the Core spanned the Quaternary to late Pliocene. Since that paper was published, the diatom zonation has continued to evolve and two of the species identified by LaPan, Thalassiosira torokina and Thalassiosira inura are both now considered to be older than 2 and 3.5 million years respectively (Cody et al., 2008). With several Antarctic IODP expeditions in the austral summer of 2018 and 2019, it is likely that the diatom zonation will be further refined in the next several years, as additional diatom data and better paleomagnetics are combined to produce a revised diatom chronostratigraphy.

Forrest Lloyd examined the two oldest recovered cores from Site 697. Extensive work has been done during a previous Keck program on the younger Pliocene sections. The interval between 205.9 mbsf (Core 113-697B-20X) and 293.0 mbsf (Core 113-697B-30X) had very poor recovery (30%). The resulting lack of continuity in this interval makes it a low priority to examine, hence the decision to go to the cores at the base of the hole.

The goal of this study was to examine sediments from the early Pliocene, a warmer interval, to see if ice-rafted sediment, based on $^{40}Ar/^{39}Ar$ age determinations of biotite and hornblende were sourced from closer locations (Williams et al., 2010) and if bottom currents were weaker based on mean sortable silt size determinations (McCave et al., 1995). Both of these measurements would support a warmer early Pliocene.

Cores 113-697B-31X and 32X (302.6-322.9 mbsf) were dated as lower Pliocene by the shipboard biostratigraphers (Barker, Kennett et al., 1988), relying primarily on radiolarian zonations (Lower *Tau* zone). These two cores were hampered by the lack of paleomagnetic reversals to provide an age determination and therefore a more accurate determination of sedimentation rates. The two closest reversals, occur at the top of C3N-3 and top of C3N-4 (Table 1). Pudsey (1990) also shows a reversal at 261 mbsf, but there is no core at that depth. But if that depth is used, it suggests an even higher sedimentation rate for Cores 31X and 32X. Given this constraint, there was the option of extrapolating the average sedimentation rate for the upper part of the core (6.8 cm/ky) or using the much higher sedimentation rate based on the two closest ages (27 cm/ky), or the imaginary core age from 261 mbsf (Table 2). All three approaches show that by the base of the Core 32X, the sediments are likely to be in the upper Miocene. The lower age of the radiolarian lower Tau zone was extended post- Leg 113 (Lazarus, 1990) and, does extend into the uppermost Miocene (5.5-4.2 my), so a Miocene age is possible and is in agreement with a higher sedimentation rate at the base of the hole.

Whether upper Miocene or lower Pliocene, the objective of this investigation was to contrast this time interval with the middle Pliocene. This research shows more variable IRD and more common contourite deposits in these cores than those of the middle-Pliocene. This clearly shows that glaciation as documented by IRD was occurring during this time interval and that bottom currents were strong enough to develop contourites. Additional work will continue with both the dating of the hornblendes and biotites.

Andrew Hollyday employed cyclostratigraphic analysis of continuous split core measurements and well logs to identify orbital forcing at selected circum-Antarctic ocean drilling sites (Figure 1) and from that determined sedimentation rates. Although sedimentation rates are usually calculated from biostratigraphic and paleomagnetic data, at sites where such data is lacking, this is an alternative, first-order method to identify sedimentation rates.

The sedimentation rate calculations for Site 697 are based on the down core XRF measurements for seven Pliocene-age cores with good recovery. Collected in 1987, the cores have shrunk and cracked due to dehydration. To generate a sedimentation rate, the domi-

Table 1. Paleomagnetic Boundaries for Site 697 Identified in Pudsey (1990) With Sample Information and Sedimentation Rates

Magnetic boundaries	Sample identification	Depth (meters below seafloor)	Gee & Kent (2007) age (Ma)	Pudsey (1990) age (Ma)	Sedimenta tion rate cm/kyr
Matuyama chron, base / C2AN-1, top	697B-10H-1, 99-111 cm	105.7	2.608	2.47	
C2AN-2, top	697B-13X-3, 119-121 cm?	132.8	3.11	2.99	5.40
C2AN-2, base	697B-14X-1, 49-51 cm	138.7	3.22	3.08	5.36
C2AN-3, top	697B-14X-7, 39-41 cm	147.6	3.33	3.13	8.09
Gauss chron, base / C2AN-3, base	697B-16X-4, 49-51 cm	162.25	3.58	3.4	5.86
C3N-1, top	697B-20X-4, 29-31 cm	201	4.18	3.88	6.46
C3N-1, base	697B-21X-2, 9-11 cm	207.5	4.29	3.97	5.91
C3N-3, top	697B-25X-2, 119-121 cm	247.2	4.8	4.4	7.78
C3N-3, base	? No core at this interval ?	261	4.89	4.47	
C3N-4, top	697B-30X-2, 119-121 cm	295.7	4.98	4.57	26.94

nant elemental components of the XRF data are found through a series of statistical steps, which allow the identification of the dominant elemental components - varimax-rotated, principal components (VPCAs) - that explain the variance in the data. The VPCAs are then analyzed the same way as the well-log data from the other sites.

The down hole geophysical well logs (gamma-ray spectrometry and dual-induction resistivity) and the XRF VPCAs were analyzed using wavelet analysis, which detrends the data and uses frequency-domain transformations to decompose the time series into time-frequency phase space. The Pliocene cycles are identified by their power spectra and assigned Milankovitch periodicities (Hollyday, Figure 2). The strongest peak was assigned to either obliquity (41,000 years) or eccentricity (100,000 years) and in several cores precession (23,000 years) was also identified. The obliquity assignments are in agreement with prior Antarctic Pliocene investigations (Nash et al., 2009). Agreement between the periodicities identified by the different types of measurements confirms the validity of this technique (Hollyday, Table 1). Even where there is disagreement, e.g. an order of magnitude difference between the gamma-ray and resistivity

Table 2. Age Calculations for the Top of Cores 31X and 32X Using Different Sedimentation Rates

Location	Depth (mbsf)		Age (Ma)	Age (Ma)	Age (Ma)	Sedimentation rate (cm/kyr)
C3N-4	295.7		4.98	Top 31X	Top 32X	
Top of core 31X	302.6			5.99	7.41	6.8
Top of core 32X	312.2			5.24	5.59	26.9
				5.16	5.41	38.6

sedimentation rates determined for Site 1059 in the Bellingshausen Sea, the assigned rates are still within the range of those determined by biostratigraphic and paleomagnetic techniques (Hollyday, Figure 3).

For the Weddell Sea, the focus of the rest the investigations, Hollyday's, average sedimentation rates where consistent within each core. Only in Cores 697B- 3H and 4H (37.1-56.5 mbsf), was there no obliquity signal identified. Sedimentation rates determined based on paleomagnetic age picks (Table 1, Figure 3) are surprisingly consistent, averaging between 5 and 8 cm/kyr, and in good agreement to his rate determinations of 4-8 cm/kyr (Hollyday, Table 1)

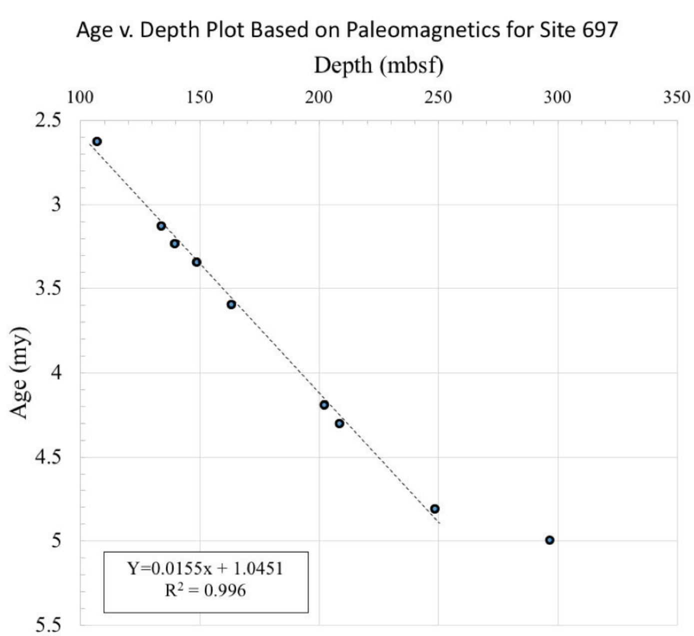

Figure 3. Sedimentation rate curve for Site 697 based on paleomagnetic age picks. The line through all but the oldest age pick shows a surprisingly constant sedimentation rate of 5.4-8.1 cm/kyr.

SUMMARY

These four studies provide a rich beginning to understanding Antarctic glacial history and the importance of using older ocean drilling program cores and well logs to understand this critical environment. Continued work on these cores and with this data will provide additional insight to describing and interpreting the glacial history of the Weddell Sea sector of Antarctica.

ACKNOWLEDGEMENTS

This material is based upon work supported by the Keck Geology Consortium and the National Science Foundation under Grant No. 1659322. We would like to extend thanks to the staff at the Gulf Coast Repository of the International Ocean Discovery Program, especially Phil Rumford, who facilitated our viewing and sampling of cores and Brian LeVay who taught us about the many complexities of core scanning XRF and coached us through the intracacies of collecting and processing, split core XRF measurements.

REFERENCES

Barker, P.F., Kennett, J. P., et al., (1988). Proc. ODP, Init. Repts., 113: College Station, TX (Ocean Drilling Program).

Cody, R.D. , Levy, R.H., Harwood, D.M., Sadler, P.M., (2008). Thinking outside the zone: High-resolution quantitative diatom biochronology for the Antarctic Neogene, Palaeogeography, Palaeoclimatology, Palaeoecology, 260 92–121.

Gee, J.S., and Kent, D.V., (2007). Source of Oceanic Magnetic Anomalies and the Geomagnetic Polarity Timescale: Treatise on Geophysics, v. 5, p. 419–4607.

GeoMapApp, http://www.geomapapp.org/, accessed May 15, 2018

Gersonde, R. and Burckle, L.H. (1990) Neogene Diatom Biostratigraphy of ODP Leg 113, Weddell Sea (Antarctic Ocean). in Barker, P. R, Kennett, J. P., et al., Proc. ODP, Sci. Results, 113: College Station, TX (Ocean Drilling Program), v. 7, 61-789.

Lazarus, D., Middle Miocene to Recent radiolarians from the Weddell Sea, Antarctica, (1990) in Barker, P. R, Kennett, J. P., et al., Proc. ODP, Sci. Results, 113: College Station, TX (Ocean Drilling Program). v. 41, p.709-727.

Lisiecki, L., and Raymo, M. (2005). A Pliocene-Pleistocene stack of 57 globally distributed benthic $\delta^{18}O$ records, Paleoceanography, 20, pa1003. doi.org/10.1029/2004PA001071.

Leventer, A., E. W. Domack, S. Ishman, S. Brachfeld, C. McClennen, and P. Manley, (1996). 200–300-year productivity cycles in the Antarctic Peninsula region: Understanding linkages among the Sun, atmosphere, oceans, sea ice and biota, Geol. Soc. Am. Bull., 108, 1626–1644.

McCave, I.N., Manighetti, B., and Robinson, S.G., (1995). Sortable silt and fine sediment size/composition slicing: Parameters for palaeocurrent speed and palaeoceanography: Paleoceanography, v. 10, p. 593–610.

Naish, T., Powell, R., Levy, R., Wilson, G., Scherer, R., Talarico, F., Krissek, L., Niessen, F., Pompilio, M., Wilson, T., Carter, L., DeConto, R., Huybers, P., McKay, R., Pollary, D., Ross, J., Winter, D., Barrett, P., Browne, G., Cody, R., Cowan, E., Carmpton, J., Dunbar, R., Dunbar, N., Florido, F., Gebhardt, C., Graham, I., Hannah, M., Hansaraji, D., Harwood, D., Hellings, D., Henrys, S., Hinnov, L., Kuhns, G., Kyle, P., Laufer, A., Maffioli, P., Magens, D., Mandernack,, K., McIntosh, W., Millan, C., Morin, R., Ohneiser, C., Paulsen, T., Persico, D., Raine, I., Reed, J., Riesselman, C. , Sagnotti, L., Schmitt, D., Sjunneskog, C., Strong, P., Taviani, M., Vogel, S., Wilch, T., Williams, T. (2009). Obliquity-paced Pliocene West Antarctic ice sheet oscillations. Nature, 458 (7236), 322–328. https://doi.org/10.1038/nature07867

Pudsey, C. J. (1990) Grain size and diatom content of hemipelagic sediments at Site 697, ODP Leg 113: A record of Pliocene-Pleistocene climate. in Barker, P. R, Kennett, J. P., et al., Proc. ODP, Sci. Results, 113: College Station, TX (Ocean Drilling Program), v.8, p. 111-120.

Williams, T., van de Flierdt, T., Hemming, S., Chung, E., Roy, M., Goldstein, S. (2010). Evidence for Iceberg Armadas from East Antarctica in the Southern Ocean during the Late Miocene and Early Pliocene.” Earth and Planetary Science Letters, p. 351–361.

KECK Geology Consortium
Learning Science Through Research
Published by Keck Geology Consortium

Short Contributions
Keck Geology Consortium
Volume 31
May 2018

DIATOMS OF THE ANTARCTIC – ENVIRONMENTAL INTERPRETATION OF THE MIDDLE PLIOCENE AT SITE 697

EDUARDO CENTENO, Wesleyan University
Research Advisor: Suzanne O'Connell

ABSTRACT

Understanding the effects of warming events on sea ice during the geologic past is critical for predicting future sea ice behavior. In the last 15 million years (Ma), five major episodes of Southern Ocean diatom species turnover (origination rate plus extinction rate) have been identified and linked to times of cooling and ice expansion. However, the highest turnover rate occurred between 3.55–3.40 Ma and aligns with an increase in biosiliceous activity, rising CO_2 concentrations, warming temperature and ice retraction The goal of this application is to determine the mechanisms that catalyzed this anomalous turnover pulse by creating a record of the diatom community in the Weddell Sea off the coast of the Antarctic Peninsula. Preliminary results show that during the 100,000 year period (3.2-3.29 Ma), toward the end of MIS M2, Site 697 was marked by open ocean conditions and indicate sea ice conditions were unstable. A more comprehensive dataset will allow us to explore conditions during both MIS M2 and the earlier Turnover Pulse D. We will be able to identify relationships between the two events and discover the mechanisms by which they were catalyzed.

INTRODUCTION

Diatoms are of critical interest today because they contribute an estimated 45% of total oceanic primary production (Yool, 2003), they are the dominant living marine phytoplankton group, and their macroevolutionary history is linked to changes in climate (Lazarus, 2014). This important group of microalgae are a common tool for paleoclimate scientists because diatoms are diverse, with estimates of the number of species on the order of 105 (Mann and Droop, 1996). They are also sensitive to environmental conditions and are able to inhabit virtually any environment with moisture and sunlight, making them an especially versatile and accessible paleoclimate indicator (Crosta and Koc, 2007).

One third of the diatoms of the genus Chaetoceros are known to form resting spores within the vegetative cell associated with unfavorable conditions such as nitrogen deficiency and low light conditions (Hargraves and French, 1975, Leventer, 1991). Previous work has not detected a relationship between the abundance of Chaetocerous resting spores and sea surface temperature (Zielinski and Gersonde, 1997). However, high productivity has been shown to be very important to the distribution of Chaetocerous resting spores (Donegan and Schrader, 1982, Leventer, 1991, Karpuz and Jansen, 1992, Zielinski and Gersonde, 1997). Chaetocerous resting spore dominance has been suggested to be catalyzed by surface water stratification produced by sea ice melt water (Leventer et al., 1993, Leventer et al., 1996).

Site 697

The Ocean Drilling Program (ODP) was an international cooperative effort that conducted 110 expeditions and drilled 2000 drill holes (IODP website). Site 697 is a drill hole located in the Weddell Sea within the Jane Basin and is 3480 meters below sea level. Site 697 is the deepest of a three-site depth transect of the South Orkney microcontinent (SOM) drilled during ODP Leg 113 (Barker, Kennett et al., 1988)[See O'Connell, Fig. 1, this volume].

Southern Ocean Phytoplankton Turnover

Five major episodes of Southern Ocean diatom species turnover (origination rate plus extinction rate) [Fig. 1] have been identified and linked to times of cooling and ice expansion in the last 15 million years (Ma). Figure 1 (Crampton et al., 2016) was created using a model reconstruction of diatom speciation and extinction rates to examine phytoplankton response to climate change in the southern high latitudes over the past 15 My. The ages of the five major pulses are approximately 14.65–14.45 Ma (A), 13.75–13.55 Ma (B), 4.90–4.40 Ma (C), 3.55–3.40 Ma (D), and 3.00–1.95 Ma (E) (Crampton et al., 2016). However, it is unclear why the turnover pulse that occurred between 3.55–3.40 Ma (turnover pulse D) - the highest of all five turnover rates - correlates with an increase in biosiliceous activity (Fig. 1, Graph D), rising CO_2 concentrations (Fig. 1, Graph E), warming temperature and ice retraction (Fig. 1, Graph C) [Crampton et al., 2016].

Marine Isotope Stage M2

The Marine Isotope Stage (MIS) M2 (3.312-3.264 Ma) [Tab. 1] was a global glaciation event that corresponded to a 20 to 60 m sea-level drop (Tan et al., 2017). This glaciation event interrupted the period of global warmth and high CO_2 concentration of the mid-Piacenzian (Tan et al., 2017). Unlike the late Quaternary glaciations, M2 only lasted 50 thousand years and occurred under uncertain CO_2 concentration (Tan et al., 2017).

Objective

The goal of this research study is to determine the mechanisms that catalyzed the turnover pulse that occurred between 3.55–3.40 Ma by creating a record of the diatom community at Site 697. This is a data sparse region that plays a key role in our climate (Salzmann et al., 2011). Diatom species are highly endemic in the Southern Ocean and form two distinct biomes: a specialized flora occupying the sea ice zone (Armand et al., 2005) and a high-nutrient, low-chlorophyll flora occupying the open ocean (Crosta et al. 2005). Past plankton turnover has been inferred to occur when a warmer-than-present climate state is terminated by a major period of glaciation that results in loss of open-ocean habitat due to increase sea ice cover, driving non-ice adapted diatoms to regional or global extinction [Figure 2] (Crampton et al., 2016).

The central hypothesis underpinning this research is that turnover pulse D was caused by a warming event that decreased ice cover, in turn driving ice adapted diatoms to extinction and non-ice adapted diatoms to rapid speciation. By calculating the relative abundance of sea ice and non-sea ice diatoms through time, we

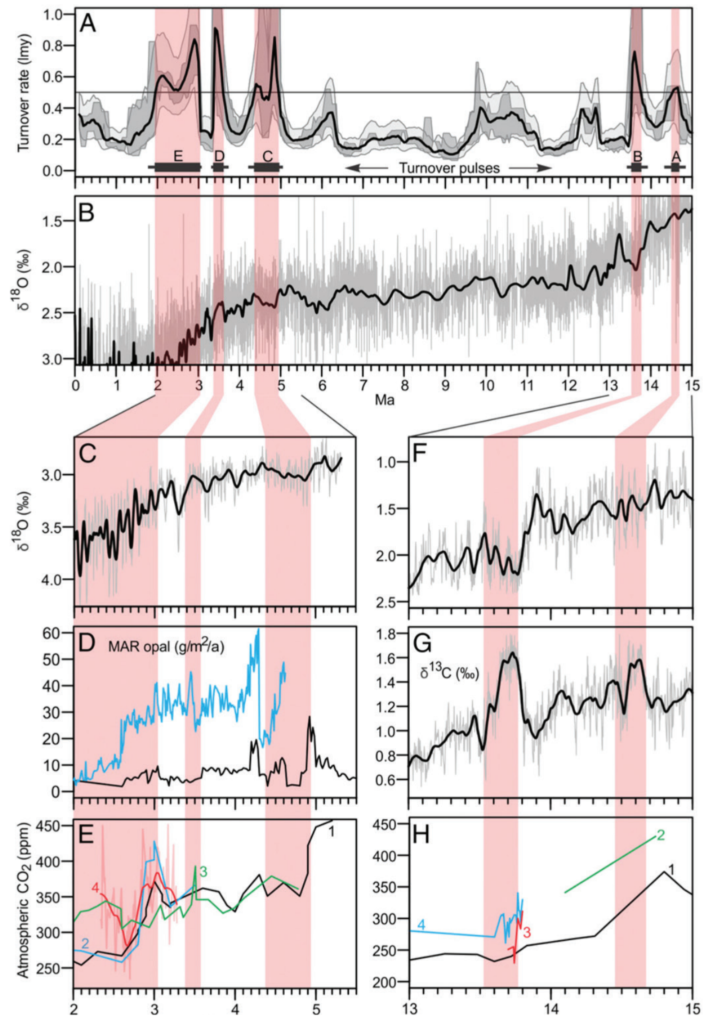

Figure 1. Turnover pulses of diatoms in the Southern Ocean and Antarctic margin over the past 15 Ma compared with key paleoenvironmental proxies. (A) A plot of species lineage-million-year (lmy) turnover rate, with major pluses identified by pink bars. (B) Benthic δ^{18}O curve for the time interval 15-0 Ma. (C) Benthic δ^{18}O curve for the time interval 5-2 Ma. (D) Opal accumulation rates, which acts as a proxy for sea ice extent on the Antarctic margin for the time interval 5-2 Ma. Declining opal accumulation indicates an expansion in sea ice. (E) Estimate of atmospheric pCO_2 for the time interval 5-2 Ma, based on alkenone (1 and 2) and boron (3 and 4) proxies. (F) Benthic δ^{18}O curve for the time interval 15-13 Ma. (G) Benthic δ^{13}C curve for the time interval 15-13 Ma. (H) Estimates of atmospheric pCO_2 based on alkenone (2 and 4), boron (1), and B/Ca (3) proxies (Crampton et al., 2016).

Table 1. Table of absolute ages which are calculated for magnetic time scale reversals and corresponded to samples in the 697 core.

Magnetic boundaries	Sample	Depth (meters below seafloor)	G&K (2007) model age (millions of years)	Pudsey (1990) model age (millions of years)
Matuyama chron, base / C2AN-1, top	697B-10H-1-100	105.7	2.608 (LR05)	2.470
C2AN-2, top	697B-13X-4-8	132.8	3.11	2.99
C2AN-2, base	697B-14X-1-50	138.7	3.22	3.08
C2AN-3, top	697B-14X-7-40	147.6	3.33	3.13
Gauss chron, base / C2AN-3, base	697B-16X-4-50	162.25	3.58	3.40
C3N-1, top	697B-20X-4-30	201	4.18	3.88

Note: Original ages were determine by Pudsey (1990), but were never published. Absolute ages were redeveloped by Gee and Kent (2007) and are the ones used in this study.

can construct a diatom-inferred record of sea ice fluctuation. The relative abundance of sea ice adapted and non-sea ice adapted diatoms is also supplemented by additional data on biosilica weight percent (wt. %) and course fraction analysis by our research team. Comparing the microfossil abundances to our biosilica wt. % and course fraction data gives us a holistic perspective with which to consider the causes for turnover pulse D. This information regarding the timing of climatic events and the paleoenvironmental conditions that characterized them (i.e., SST, extent of sea ice, and ice sheet size) are relevant to help constrain paleoclimate and ice sheet models for the early-middle Pliocene.

METHODS

Sample Collection and Supplementary Data

Samples for the working half of Site 697 were collected at the Integrated Ocean Discovery Program Core Repository. Excluding areas of the core with poor recovery, 20 cubic centimeters of samples were brought back to the Wesleyan University campus for further study.

For course fraction analysis, samples were washed according to standard wet-sieving procedures. Course fraction is a proxy for melting from land-derived icebergs.

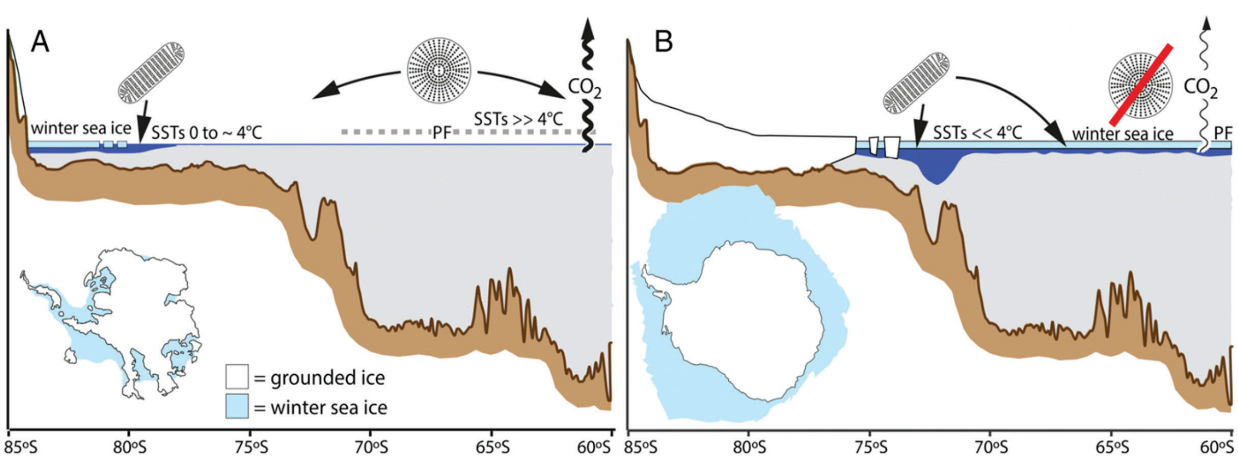

Figure 2. Modified figure from Crampton et al. (2016), showing schematic environmental reconstruction for the Antarctic continental shelf and Southern Ocean during intervals of (A) warmth and ice minimum and (B) peak cold and maximum ice extent. Crampton et al. (2016) hypothesizes that rapid transitions between these two environmental states is the main cause of major species turnover, as it drives extinction/ speciation of warm/cold-adapted phytoplankton. Ventilation of CO_2-enriched deep water is indicated by wavy arrow (thin line indicates reduced ventilation due to stratified surface water and sea ice cover). PF, polar front.

Biosilica wt. % for our samples is determined mostly by diatom abundance, with minor contributions from radiolarians and other siliceous organisms. Therefore, the wt. % biosilica is a proxy for diatoms, which in turn, are an indicator of productivity in the waters around Site 697.

Preparing Diatom Slides

For each sample, approximately 0.5g of sediment was placed in a desiccator for at least 24 hours to ensure they were completely dry. Next, 0.3g of sample is placed in a 50mL centrifuge tube and softened in deionized water. The sample is then treated with 20mL of 35% hydrogen peroxide in order to oxidize organic material. After effervescence stops, samples are rinsed multiple times with deionized water and centrifuged at 1500 rpm for 10 minutes. To further disaggregate sediments, samples are treated with a dilute Calgon (sodium hexametaphosphate) solution and later rinsed as described above.

The next step of this procedure uses a random settling method to evenly distribute the diatoms in solution over three quantitative slides per sample. For each sample, 5 mL of randomized suspended sediment was extracted and added to a small beaker containing 45 mL of deionized water to allow for good dissemination. The diluted solution was then poured into a petri dish containing 20 mL of deionized water. After waiting 30 minutes for the sediment to settle in the petri dish, short strips of paper towel were inserted into the water and connected to a sponge under the petri dish. Through capillary action this step drains the water and expedites drying. After allowing for all of the water in the petri dish to dry, coverslips were removed from the petridish, dried on a hot plate, and mounted to glass slides using Norland Optical Adhesive #61.

Identifying and Counting Diatoms

One slide per sample was examined under a light microscope at 1,000x magnification. Random traverses are made across the coverslip until at least 500 diatom valves are counted for each sample to ensure an accurate representation of the fossil assemblage (Chang, 1967).

Diatoms were only counted when at least half of a valve was visible. Each diatom was identified to the species level unless diagnostic features were missing, in which case they were categorized at the generic level. Diatoms from the lineolate genera, such as Thalassiothrix and Thalassionema, are usually fractured along its length, in which case two ends counted as one valve. Chatoceros resting spores were included in the results because they are often associated with high levels of productivity in a stratified setting. Environmental preferences were assigned to species according to the findings of Armand et al. (2005) and Crosta et al. (2005)

Age Model

The ages for this study are based on the reversal stratigraphy given in Pudsey (1990) and then tied to the Gee and Kent (2007) timescale. Between reversals, ages are extrapolated.

Statistical Analysis

P values and statistical data were collected with the program language R. A chi square test was performed on the data to determine statistical significance.

RESULTS

Preliminary Data

Diatom assemblages were characterized for three samples. This study will be continued and we plan to analyze around 100 samples in Site 697 before the end of the calendar year. All three samples were located in section 14x of the core, between 3.2-3.29 Ma (~140.4-144.6 mbsf). The oldest sample, 14X-5, 55-57 cm (sample 1), occurs at the coldest time period of MIS M2 at around 3.29 Ma (Fig. 3). This section in the core is characterized by relatively low biosilica levels (5 wt. %), very low course fraction (~0-2 wt. %). Sample 2, 14X-4, 68-70 cm was deposited around 3.27 Ma, and marks the end of the large peak during the earliest parts of MIS M2. Sample 2 exhibits similar values of biosilica and course fraction wt. % as Sample 1. Sample 3, 14X-2, 66-68 cm, is the youngest sample analyzed in this study and occurs around 3.2 Ma. Sample 3 contains 11 wt. % biosilica and a slight increase in course fraction to 3 wt. %.

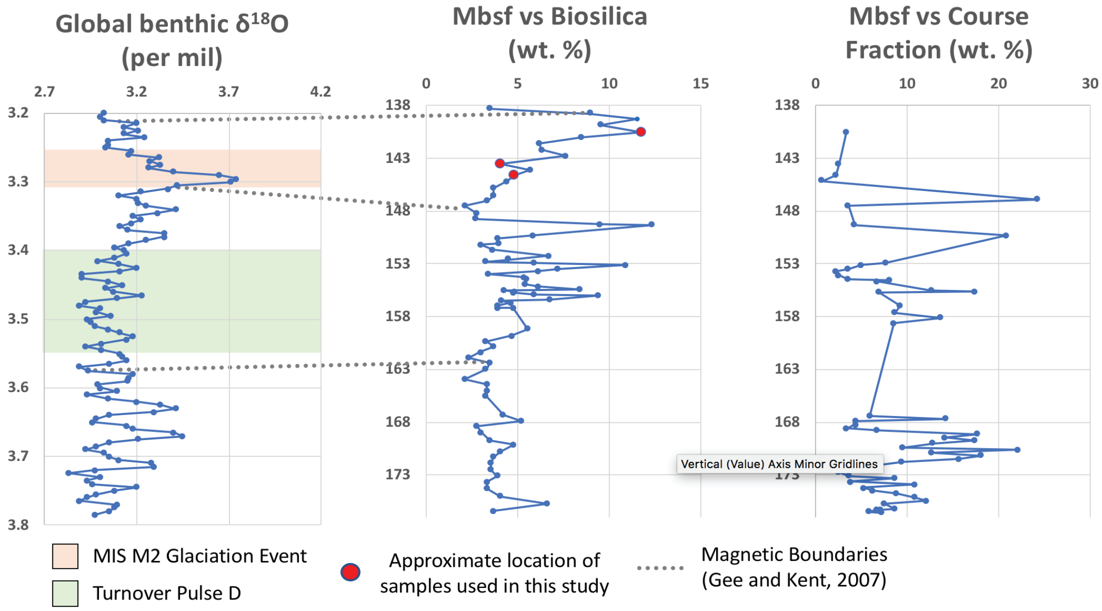

Figure 3. On the left, benthic foraminiferal $\delta^{18}O$ stack is plotted from ~3.2 to 3.8 Ma (sections 14x-17x in the core), which is an average of 57 globally distributed $\delta^{18}O$ records (Lisiecki and Raymo, 2005). MIS M2 (3.312-3.264 Ma) is highlighted by an orange box. The event produced a ~0.5‰ shift of benthic foraminiferal $\delta^{18}O$ (Tan et al., 2017). Turnover Pulse D is highlighted by a green box. The graph in the center is a plot of biosilica wt. % for sections 14x-17x, and serves as a proxy for productivity. The three samples used in this study are denoted by a red dot and tie lines for magnetic boundaries are connected to their corresponding samples by the grey dotted lines. The graph on the right is a plot of course fraction weight % for sections 14x-17x, and serves as a proxy for sea ice retreat.

Diatom Data

A diverse assemblage of diatoms was found in the three samples, which incorporated 54 distinct species or species groups. The abundance of representative species is presented as percent of the total assemblage. The complete data set is available on request.

Figure 4 shows similar trends in all the samples with respect to our open ocean and sea ice affinity diatoms. The sea ice diatom assemblage is very small, except for the species Eucampia Antarctica which consistently dominated all three assemblages and had the highest count for any species in the youngest sample.

In sample 1, characteristic species include Thalassiothrix spp. (9.6%), Chaetoceros resting spores (9.6%), Eucampia Antarctica (13%), Fragilariopsis barronii (5.9%), and Rouxia Antarctica (4%). Present in low abundances are Rouxia naviculoides (1.7%), Thalassiosira torokina (1.7%), and Fragilariopsis sublinearis (0.4%) (Fig. 4).

In sample 2, dominant species include Rouxia Antarctica (8.1%), Rouxia naviculoides (8.5%), and Chaetoceros resting spores (11%) (Fig. 4). Decreasing in abundance are Fragilariopsis barronii (3.3%), Thalassiothrix spp. (6.6%), and Eucampia Antarctica (7.9%). Thalassiosira torokina (1.5%) and Fragilariopsis sublinearis (0.4%) remain in low abundance

In sample 3, the abundance Fragilariopsis barronii (3.1%), Rouxia Antarctica (9.7%), Rouxia naviculoides (3.9%), Thalassiothrix spp. (5.2%), Chaetoceros resting spores (5.4%) decreases, while Eucampia Antarctica increases to 15%. Fragilariopsis sublinearis (1.2%) increases slightly in this sample but remains in low abundance. Thalassiosira torokina (1.2%) remains in low abundance (Fig. 4).

DISCUSSION

The low wt.% biosilica and wt.% course fraction data from Samples 1 and 2 seem to suggest a cold period marked by low productivity and stable ice covered conditions. These data are consistent with the global benthic $\delta^{18}O$ data that show very fast cooling during

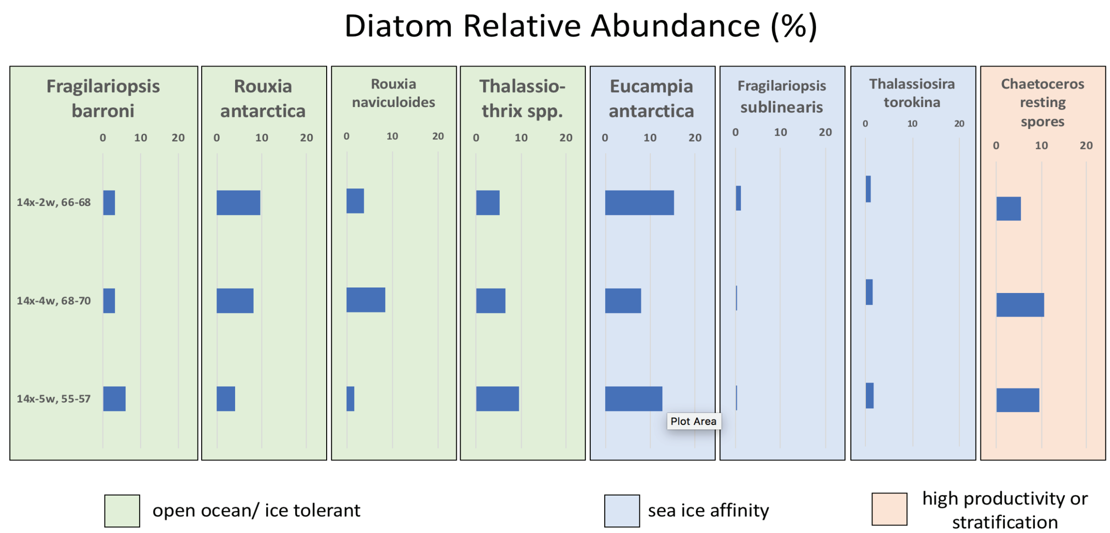

Figure 4. Relative abundance of select Site 697 diatom species. Environmental preferences were assigned using information from Crosta et al. (2005) and Armand et al. (2005). Open ocean/ ice tolerant species are highlighted in green. Diatom species with a sea ice affinity are highlighted in blue. Diatom species associated with high productivity or stratification are highlighted in orange.

this time (Lisiecki and Raymo, 2005). However, these samples are also characterized by high values of Chaetocerous resting spores (9.6 and 11%, respectively) often associated with high productivity in a stratified setting. Heavily silicified diatom resting spores have a faster sinking rate than vegetative cells and are therefore less vulnerable to dissolution (Mcquoid and Hobson, 1996). A preservation bias might be responsible for the high counts of resting spores that we see in our data. The count data for Chaetocerous resting spores was determined to be statistically significant (p value of 0.009).

Chaetocerous counts for Sample 3 are lower than expected, which suggests that an environment change that made it less conducive to the growth of this species even though there is a 6% increase in biosilica wt. % and a slight increase in course fraction. This time interval also occurs during the late warming period of MIS M2. These data suggest this warming period saw a decrease in ice cover which lead to an increase in productivity. The Chaetocerous resting spore data suggests that there was a decrease in stratification, which might suggest a decrease in ice melt. Ice was melting prior to the deposition of Sample 3 (ca. 3.2 Ma), at which time the rate of ice melt had decreased.

The Pliocene Epoch spans a time when the Earth experienced a transition from relatively warm conditions to a cooling climate. It was a generally warmer and wetter interval with atmospheric CO_2-concentrations at or slightly above modern levels (Pagani et al., 2009, Salzmann et al., 2011). This explains why all three samples are dominated by mostly open ocean and ice tolerant species and gives us a sense of ice sheet dynamics. The size of polar ice sheets might have been significantly reduced during the Pliocene causing ca. 25 m higher sea levels than today and serves as an analog to future climate conditions (Dowsett et al., 2010). However, the consistently high abundance of Eucampia Antarctica, a species with a higher affinity for sea ice, ensures that sea ice was, in fact, consistently present through this time interval.

CONCLUSION

To explore the relationship between sea surface conditions and ice cover variability in a sensitive location off of East Antarctica, we have initiated a diatom-based paleo environmental reconstruction of Site 697 in the mid-Pliocene. Our data indicate the area was influenced by sea ice but was marked by open ocean conditions through 3.2-3.29 Ma. Fluctuating percentages of open ocean diatoms indicate ice conditions were unstable during this 100,000 year period.

A more comprehensive dataset will allow us to gather paleoenvironmental data through Cores 14-17X. This will allow us to explore conditions, not only during MIS M2, but also Turnover Pulse D. We will be able to observe relationship between the two events and discover the mechanisms by which they were catalyzed.

ACKNOWLEDGEMENTS

This material is based upon work supported by the Keck Geology Consortium and the National Science Foundation under Grant No. 1659322. I would like to thank Professor Suzanne O'Connell for her leadership and mentorship during my KECK experience and throughout my experience as a researcher. I would also like to thank David Harwood for teaching me how to identify diatoms and for his continued support. Lastly, I would like to thank all the members of our research team at Wesleyan University, Melissa Luna, Noah Spriggs, Eliza Carter, and Sophia Ptacek, and my fellow KECK participants, Mark Lapan, Forrest Lloyd, and Andrew Hollyday.

REFERENCES

Armand LK, Crosta X, Romero O, Pichon JJ, 2005, The biogeography of major diatom taxa in Southern Ocean sediments: 1. Sea ice related species. Palaeogeogr Palaeoclimatol Palaeoecol 223:93–126.

Barker, P.F., Kennet, J.P., Scientific Party, 1988, Weddell sea paleoceanography: Preliminary results of ODP Leg 113: Palaeogeography, Palaeoclimatology, Palaeoecology 67 (1): 75-102.

Crampton, J.S., Cody, R.D., Richard Levy, R., Harwood, D., McKay, R., Naish, T.R., 2016. Southern Ocean phytoplankton turnover in response to stepwise Antarctic cooling over the past 15 million years: Proc. Natl. Acad. Sci. USA 113 (25), 6868–6873.

Chang, Y., 1967. Accuracy of Fossil Percentage Estimation. Journal of Paleontology, Vol. 41, No. 2, p. 500-502.

Crosta X, Romero O, Armand LK, Pichon JJ ,2005, The biogeography of major diatom taxa in Southern Ocean sediments: 2. Open ocean related species: Palaeogeogr Palaeoclimatol Palaeoecol 223:66–92.

Crosta, Xavier and Koç, Nalan, 2007. Diatoms: From Micropaleontology to Isotope Geochemistry, In Hillaire-Marcel, C., and De Vernal, A. (Eds.) Developments in Marine Geology, Proxies in Late Cenozoic Paleoceanography, Vol 1, p. 327-358.

Donegan, D., and Schrader, H., 1982, Biogenic and abiogenic components of laminated hemipelagic sediments in the central Gulf of California: Marine Geology, v. 48, p. 215–237, doi: 10.1016/0025-3227(82)90098-6.

Dowsett, H.J., Robinson, M., Haywood, A., Salzmann, U., Hill, D., Sohl, L., Chandler, M., Williams, M., Foley, K., Stoll, D., 2010. The PRISM3D paleoenvironmental reconstruction. Stratigraphy 7, 123–139.

Escutia, C., Brinkhuis, H., and Klaus, A., 2011, IODP Expedition 318: From Greenhouse to Icehouse at the Wilkes Land Antarctic Margin: Scientific Drilling, v. 12, p. 15–23, doi: 10.5194/sd-12-15-2011.

Gee, J., and Kent, D., 2007, Source of Oceanic Magnetic Anomalies and the Geomagnetic Polarity Timescale: Treatise on Geophysics, p. 419–460, doi: 10.1016/b978-0-444-53802-4.00106-8.

Given, H. Home: IODP - International Ocean Discovery Program, https://www.iodp.org/about-iodp/history

Hargraves, P.E., French, F.W., 1975, Observations on the survival of diatom resting spores: Beih. Nova Hedw. v. 53, p. 229-238.

Karpuz, N.K., and Jansen, E., 1992, A high-resolution diatom record of the last deglaciation from the SE Norwegian Sea: Documentation of rapid climatic changes: Paleoceanography, v. 7, p. 499–520, doi: 10.1029/92pa01651.

Lazarus D, Barron J, Renaudie J, Diver P, Türke A, 2014, Cenozoic planktonic marine diatom diversity and correlation to climate change: PLoS One 9(1):e84857.

Leventer, A., 1991, Sediment trap diatom assemblages from the northern Antarctic Peninsula region: Deep Sea Research Part A. Oceanographic Research Papers, v. 38, p. 1127–1143, doi: 10.1016/0198-0149(91)90099-2.

Leventer, A., Dunbar, R.B., and Demaster, D.J., 1993, Diatom Evidence for Late Holocene Climatic Events in Granite Harbor, Antarctica: Paleoceanography, v. 8, p. 373–386, doi: 10.1029/93pa00561.

Leventer, A., Domack, E.W., Ishman, S.E., Brachfeld, S., Mcclennen, C.E., and Manley, P., 1996, Productivity cycles of 200–300 years in the Antarctic Peninsula region: Understanding linkages among the sun, atmosphere, oceans, sea ice, and biota: Geological Society of America Bulletin, v. 108, p. 1626–1644, doi: 10.1130/0016-7606(1996)108<1626:pcoyit>2.3.co;2.

Lisiecki, L. E., and M. E. Raymo, 2005, A Pliocene-Pleistocene stack of 57 globally distributed benthic $\delta^{18}O$ records: Paleoceanography, 20, PA1003, doi:10.1029/2004PA001071

Mann, D., & Droop, G. (1996). 3. Biodiversity, biogeography and conservation of diatoms. Hydrobiologia, 336(1), 19-32.

Mcquoid, M.R., and Hobson, L.A., 1996, Diatom Resting Stages: Journal of Phycology, v. 32, p. 889–902, doi: 10.1111/j.0022-3646.1996.00889.x.

Pagani, M., Caldeira, K., Berner, R., and Beerling, D.J., 2009, The role of terrestrial plants in limiting atmospheric CO_2 decline over the past 24 million years: Nature, v. 460, p. 85–88, doi: 10.1038/nature08133

Salzmann, U., Williams, M., Haywood, A.M., Johnson, A.L.A., Kender, S., Zalasiewicz, J., 2011, Climate and environment of a Pliocene warm world. Palaeogeogr. Palaeoclimatol. Palaeoecol., v. 309, p. 1–8. http://dx.doi.org/10.1016/j.palaeo.2011.05.044.

Tan, N., Ramstein, G., Dumas, C., Contoux, C., Ladant, J. B., Sepulchre, P., Zhang, Z.S., De Schepper, S., 2017, Exploring the MIS M2 glaciation occurring during a warm and high atmospheric CO_2 Pliocene background climate: Earth and Planetary Science Letters, v. 472, p. 266-276.

Yool, A., and Tyrell, T., 2003, Role of diatoms in regulating the ocean's silicon cycle: Global Biogeochemical Cycles, v. 17.

Zielinski, U., and Gersonde, R., 1997, Diatom distribution in Southern Ocean surface sediments (Atlantic sector): Implications for paleoenvironmental reconstructions: Palaeogeography, Palaeoclimatology, Palaeoecology, v. 129, p. 213–250, doi: 10.1016/s0031-0182(96)00130-7.

KECK Geology Consortium
Learning Science Through Research
Published by Keck Geology Consortium

Short Contributions
Keck Geology Consortium
Volume 31
May 2018

PRELIMINARY WAVELET ANALYSIS OF CIRCUM-ANTARCTIC ODP WELL LOGS AND SPLIT-CORE XRF SCANS FROM ODP SITE 697 CORES INFERS OBLIQUITY SIGNAL

ANDREW HOLLYDAY, Middlebury College
Research Advisors: Suzanne O'Connell, Will Amidon, and Joe Ortiz

ABSTRACT

Circum-Antarctic marine sediment archives in this study preserve late Pliocene and early Pleistocene depositional geochronology linked to continental erosional systems, and surface and bottom currents. Geophysical IODP/ODP down hole well logs from the Plio-Pleistocene offer the only available offshore (>100 km and ~3000 m water depth) marine sediment record for circum-Antarctic scientific ocean drilling sites. Even though recovered cores are commonly discontinuous, they can provide a higher resolution window into sedimentary process. Principal component analysis of XRF elemental counts from Weddell Sea ODP Leg 113 Site 697 split-cores reveals a dominant terrigenous elemental component, which may be linked to proximal ice erosional regimes. Wavelet analysis on both the well log and XRF datasets allows us to cross-calibrate proxies and identify 23, 41, and 100-kyr Milankovitch periodicities, with 41-kyr dominating. Wavelet analysis is also used to derive discretized linear sedimentation rates that agree with available IODP/ODP paleomagnetic and biostratigraphic age models and imply spatiotemporal changes in Antarctic depositional history. Finally, the dominating obliquity signal in these offshore marine deposits provides evidence for coupling between nearshore glacial sequence stratigraphy.

INTRODUCTION

Global geological evidence from marine and terrestrial systems has demonstrated that prior to the onset of vast northern hemisphere glaciation in the Pleistocene, early Pliocene atmospheric CO_2 levels were near 400 p.p.m.v., and global mean temperatures were approximately 3°C warmer than present (Raymo et al., 1996; Pagani et al., 2010). These conditions offer a powerful analogue in the paleoclimate record that can be used to inform modern anthropogenic warming and sea level rise. Well-dated marine lithostratigraphic constraints from the Ross Sea by the ANDRILL program have linked 40-kyr fluctuations in the ice sheet extent and sediment record to orbitally-driven cycles in solar insolation (changes in Earth's obliquity; Naish et al., 2009).

This project utilizes Ocean Drilling Program (ODP) cores from Expedition 113 in the Weddell Sea and Integrated Ocean Drilling Program (IODP) and ODP geophysical down-hole well logs from Expeditions 119 and 188 from Prydz Bay, Expedition 178 from the Bellingshausen Sea, and Expedition 318 offshore Wilkes Land to study the connection between nearshore diatomite-diamicton sequences (ANDRILL) and distal circum-Antarctic continental shelf sediments. While the ANDRILL program was able to study glacial cycles by directly identifying lithological facies diagnostic of either glacial advance or retreat, this project uses sediment cores (XRF) and borehole measurements (gamma ray and resistivity) in its analysis.

LOCALITIES

This study considers four circum-Antarctic marine ODP/ IODP locations: the Weddell Sea, Prydz Bay, the Bellingshausen Sea, and offshore Wilkes Land (see O'Connell, this volume for location map).

Expedition 113 Site 697 is located northeast of the Antarctic Peninsula in the northwestern Weddell Sea, close to where the Weddell Gyre joins the Antarctic Circumpolar Current, both of which flow clockwise. This site is approximately 800 km from the modern terminus of the Filchner-Ronne Ice Shelf, which is a primary source of sediment at this site (Bentley & Anderson, 1998).

The Pyrdz Bay ODP Sites (739, 742, and 1166) from Expeditions 119 and 188 are located approximately 110 km from the modern terminus of the Amery Ice Shelf, which is also the primary regional sediment source. All three Pyrdz Bay sites are located on the modern continental shelf.

The Bellingshausen Sea ODP Sites (1095, 1096, and 1103) from Expedition 178 are located 400 km to the west of the Antarctic Peninsula. These sites are dominated by erosional input from the proximal Transantarctic Mountains via paleo-ice streams (Barker, Camerlenghi, &Acton, 1999).

The Wilkes Land IODP sites (U1359 and U1360) are located to the west of the Ross Sea along the Wilkes and Adelie coasts. Sediment delivered to these sites, which are located approximately 200 km offshore, is sourced from the East Antarctic Ice Sheet (Verma et al., 2014).

DATA COLLECTION

High resolution *in situ* x-ray fluorescence (XRF) intensities were collected for 22 major and trace elements on Expedition 113 Site 697 split cores at the International Ocean Discovery Program (IODP) facility in College Station, TX using an Avaatech XRF Core Scanner with Brightspec silicon drift detectors (SDD). Spot measurements (spot size ~1 cm^2) were analyzed every 2 cm along the cores for 10, 30, and 50 kVp energy profiles. A peak area integration and background model was developed and the data were processed using bAxil.

ANALYSIS OF WELL LOGS AND XRF SCANS

Principal component analysis (PCA) with varimax rotation and Kaiser normalization, which is a statistical technique that uses orthogonal transformation to isolate linearly uncorrelated components, was performed on the continuous segments of the XRF elemental counts dataset (3H-4H, 8H, 14X-15X, and 19X-20X) from Hole 697B from the Weddell Sea using SPSS. This analysis produces a dominant component that explains approximately 35% of variance across the distribution (Fig. 1). PCA shows that Mg, Al, Si, K, Ti, Fe, Ga, Rb, Zr, Ni, and Ag systematically explain the majority of variance within this component which

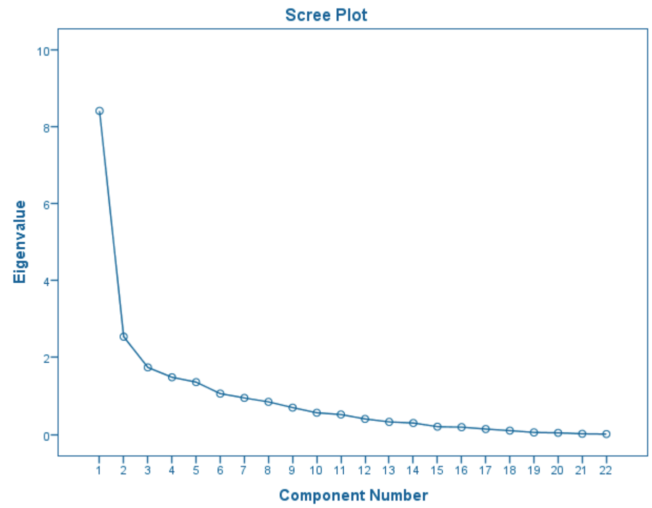

Figure 1: Principal Component Analysis (PCA) scree plot of component numbers versus eigenvalues indicating clear orthogonally-independent Component 1, which explains ~35% of the variability of the entire dataset and is dominantly explained by Mg, Al, Si, K, Ti, Fe, Ga, Rb, Zr, Ni, and Ag input variables. These elements correspond to terrigenous sediment input, which is analyzed with wavelet analysis.

The dominant PCA terrigenous component scores were then analyzed using wavelet code developed at the University of Colorado, Boulder using Interactive Data Language (IDL). The code first detrends the data with a third-degree polynomial, then uses the Mortlet wavelet and Fourier transformations to decompose time series into time-frequency phase space, and ultimately deconvolves cycles recorded in the stratigraphy (Fig. 2; Torrence & Compo, 1998). Only continuous segments of Site 697, Weddell Sea cores were selected in order to avoid coring unconformities which violate fundamental assumptions within wavelet analysis methodology. In this analysis, the recovered sections are conformable. In order to capture the 100-kyr periodicity, a minimum of 1000 centimeters—an overestimate given speculated sedimentation rates during the Pliocene—was run through wavelet analysis. Down hole geophysical well log datasets including gamma ray spectrometry and dual-induction resistivity from Prydz Bay, the Bellingshausen Sea, and off shore Wilkes Land were analyzed with the same wavelet code.

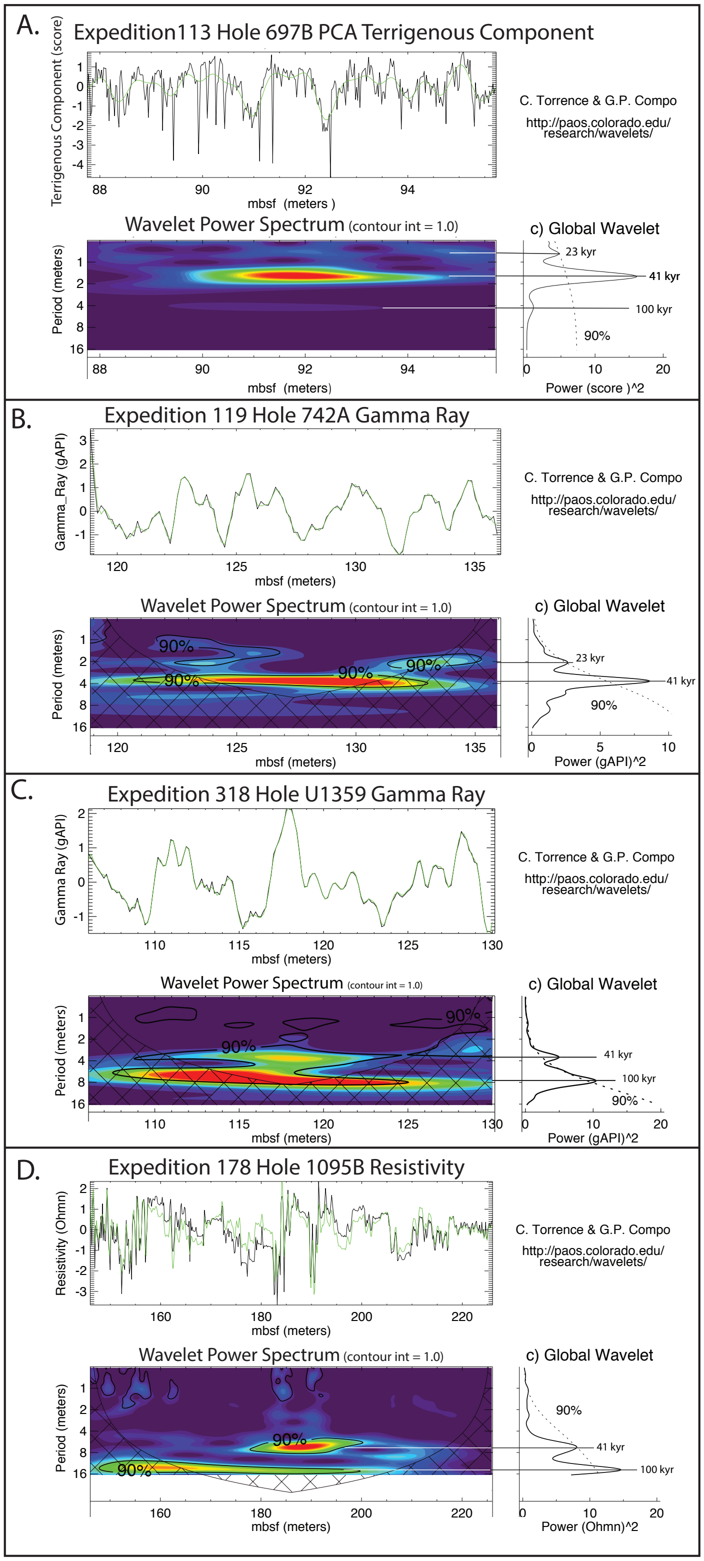

Figure 2: Wavelet analyses of circum-Antarctic sediment archives from ODP/IODP Expeditions 113, 119, 318, and 178. Raw and detrended (green) datasets (PCA component, gamma ray, and resistivity) versus meters below sea floor (mbsf). A: PCA terrigenous component from XRF core measurements from Expedition 113 in the Weddell Sea, Hole 697B Core 8H. This late Pliocene segment extends 7.9 meters, and according to internal (wavelet) age control represents >190-kyrs of deposition. Milankovitch assigned periodicities show dominant 41-kyr signal in Global Wavelet. B: Gamma Ray well-log from Expedition 119 in Prydz Bay from well-logging. This Pliocene segment extends 17.07 meters, and according to internal (wavelet) age control, represents >187-kyrs of deposition. A 41-kyr assigned periodicity dominates the Global Wavelet. C: Gamma Ray well-log from Expedition 318, Hole U1359, offshore of Wilkes Land from post coring logging. This early Pliocene segment extends 23.91 meters, and according to internal (wavelet) and external (biostratigraphic and paleomagnetic) age control, represents between 359-kyrs (internal) and 543-kyrs (external) of deposition. This record is dominated by the 41-kyr obliquity periodicity, with an insignificant 100-kyr signal that is primarily contained within the cone of influence. D: Resistivity well-log from Expedition 178 Hole 1095B in the Bellinghausen Sea from post coring logging. This early Pliocene segment extends 79.85 meters, and according to internal (wavelet) and external (biostratigraphic and paleomagnetic) age control, represents 505-kyrs (internal) to 1.3-Ma (external). This resistivity archive shows dominant 41-kyr and 100-kyr periodicities, but the 100-kyr is mostly contained in the cone of influence, which indicates it should be rejected. Overall, the geophysical well-log wavelet signal is more ambiguous from the Bellinghausen Sea, which may be a function of more complex sedimentary mechanisms (Scheuer et al., 2006).

RESULTS

Milankovitch orbital periods (23, 41, and 100 kyrs) were assigned to zones of significantly elevated power scores on the Global Wavelet, which translates frequencies in space to frequencies in time with the ultimate goal of deriving linear sedimentation rates (Table 1; True-Alcala, 2015). For most datasets, all three Milankovitch periodicities are visible and statistically significant. Sedimentation rates agree across periodicities (maximum standard deviation of 3.3 cm/kyr), which suggests assignments are correct. In Weddell Sea Hole 697B, the 41-kyr assigned obliquity signal primarily dominates during the Pliocene (Fig. 2A) with some exceptions where the dominant Global Wavelet signal is 100-kyr (eccentricity); these analyses are within the cone of influence, which may suggest the signal is an artifact of a padding feature in the code designed to remove edge effects. Prydz Bay well logs show the most dominant 41-kyr signal, while the Bellingshausen Sea and offshore Wilkes Land well-logs (Fig. 2C-D) show greater ambiguity between obliquity and eccentricity.

Derived circum-Antarctic sedimentation rates agree within an order of magnitude with a standard deviation of 3.6 cm/kyr. Weddell Sea sedimentation rates agree within core segments and range from approximately 4.0 to 7.6 cm/kyr; variability is likely a function of temporal (stratigraphic) sedimentation variation. In Prydz Bay, derived sedimentation rates range from 8.5 to 15.0 cm/kyr; Wilkes Land sedimentation rates are also within range with 6.7 to 9.4 cm/kyr. Lastly, Bellingshausen Sea derived rates range from 5.1 to 15.7 cm/kyr (Table 1).

DISCUSSION

This preliminary wavelet analysis of terrigenous component XRF data and geophysical well log measurements from circum-Antarctic sites demonstrates that offshore (>100 km and ~3000 m deep) marine sediments from the Pliocene record obliquity-paced deposition from continental erosion. While the ANDRILL program shows clear nearshore glacial sequence stratigraphy driven by obliquity during the Pliocene, IODP/ODP offshore cores and wells logs provide evidence for depositional obliquity signals as far as 800 km from the sediment source (Naish et al., 2009). The geographic diversity of IODP/ ODP sites can also inform spatiotemporal changes in ice volume. Obliquity dominates in each study region presented here, except in the Bellingshausen Sea, where local sedimentary mechanisms and architecture may obfuscate the signal (Scheuer et al., 2006). Scheuer et al. (2006) suggests that despite clear ice sheet sediment contribution during the Pliocene, bottom currents also had a significant influence on Bellingshausen Sea depocenters, which may explain ambiguity between obliquity and eccentricity-dominated wavelet analysis.

Otherwise, the Weddell Sea, Prydz Bay, and Wilkes Land sites show consistent obliquity-driven sedimentation (Fig. 2B). The Prydz Bay sites—the most nearshore locality presented—show the most decisive wavelet signal compared to more offshore circum-Antarctic study localities. This agrees with Hambrey et al. (1991) who indicates ice advance and retreat cycles strongly influence sediment mobilization and transport from the Amery Ice Shelf. While sediment from the Weddell Sea Site (697) is also sourced, in part, from a vigorous ice stream that terminates in the Filchner-Ronne Ice Shelf, it may also be receiving sediment from as far away as Dronning Maud Land (Kaufman, 2016). The Site 697 record is characterized by lower sedimentation rates, which hinder how well the depocenter records the three Milankovitch

Locality	Dataset	Orbital Cycle (kyr)	Length (cm)	Sedimentation Rate (cm/kyr)
Weddell Sea	XRF Site 697 3-4H	23	180	7.82
Weddell Sea	XRF Site 697 3-4H	100	700	7
Weddell Sea	XRF Site 697 8H	23	80	3.47
Weddell Sea	XRF Site 697 8H	41	180	4.39
Weddell Sea	XRF Site 697 8H	100	430	4.3
Weddell Sea	XRF Site 697 14X	23	100	4.34
Weddell Sea	XRF Site 697 14X	41	220	5.36
Weddell Sea	XRF Site 697 14X	100	480	4.8
Weddell Sea	XRF Site 697 19X	23	180	7.82
Weddell Sea	XRF Site 697 19X	41	320	7.8
Weddell Sea	XRF Site 697 19X	100	710	7.1
Prydz Bay	Gamma Ray 1166A	23	290	12.6
Prydz Bay	Gamma Ray 1166A	41	710	17.31
Prydz Bay	Gamma Ray 739C	23	180	7.82
Prydz Bay	Gamma Ray 739C	41	380	9.26
Prydz Bay	Gamma Ray 742A	23	200	8.69
Prydz Bay	Gamma Ray 742A	41	390	9.51
Bellingshausen Sea	Resistivity 1103A	41	310	7.56
Bellingshausen Sea	Resistivity 1103A	100	900	9
Bellingshausen Sea	Gamma Ray 1095B	41	200	4.87
Bellingshausen Sea	Gamma Ray 1095B	100	540	5.4
Bellingshausen Sea	Resistivity 1095B	41	700	17.07
Bellingshausen Sea	Resistivity 1095B	100	1450	14.5
Wilkes Land	Gamma Ray U1359D	41	300	7.317073171
Wilkes Land	Gamma Ray U1359D	100	600	6
Wilkes Land	Gamma Ray U1361A	41	400	9.756097561
Wilkes Land	Gamma Ray U1361A	100	900	9

Table 1: Discretized linear sedimentation rates derived according to assigned Milankovitch periodicities from wavelet analysis. Approximate agreement across orbital cycle assignments within each dataset suggests robust assignment. Variability across datasets implies spatiotemporal differences in sedimentation rate for circum-Antarctic Pliocene localities.

periodicities (i.e. longer periodicities are favored). Unlike the Weddell Sea and Prydz Bay sites, the Wilkes Land archives are not sourced by major ice streams that terminate in ice shelves—a configuration known to accelerate ice flow. That said, wavelet analysis demonstrates obliquity governing and sedimentation rates that are within the range of Prydz Bay and the Weddell Sea localities, which could provide corroborating evidence for a dynamic East Antarctic Ice Sheet (EAIS) during the Pliocene (Cook et al., 2013; Barker, Kennett, & et al., 1988). Minor disagreement between dominating obliquity and eccentricity in the Wilkes Land well logs can likely be attributed to their distance offshore, slightly lower sedimentation rates (Table 1), and turbidite and bottom current influences (Escutia et al., 2005).

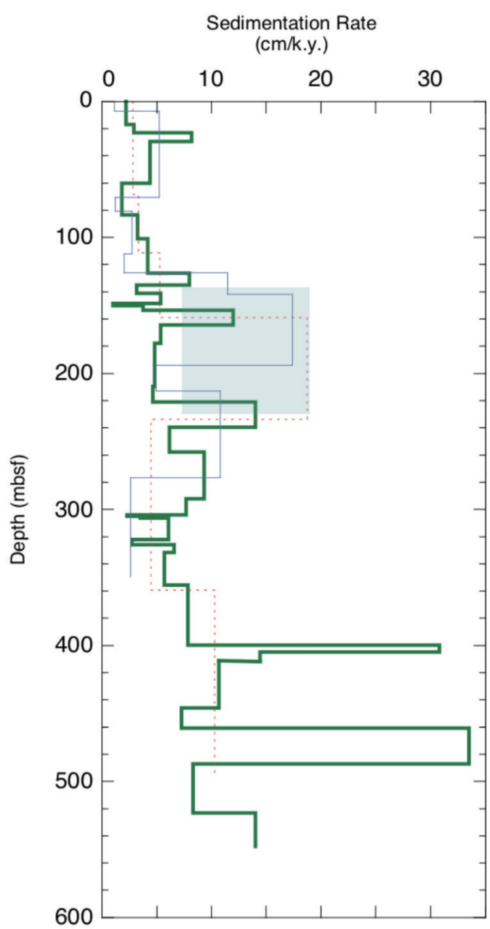

Figure 3: Independent age model (sedimentation rate versus meters below sea floor) from Bellinghausen Sea Expedition 178 Site 1095 based on paleomagnetic (dark green), radiolarian (dashed), and diatom (thin) data. Light green box indicates range of wavelet-derived sedimentation rates (cm/ kyr) for this section from gamma ray and resistivity well-log datasets, demonstrating agreement with independent geochronology. Adapted from Barker & Camerlenghi (1999).

Wavelet-derived sedimentation rates confirm accurate Milankovitch cycle assignments but also can be used in the absence of paleomagnetic and biostratigraphic age control. The mean wavelet-derived sedimentation rate for Bellingshausen Sea Site 1095 is approximately 15.8 cm/kyr, which is within the 5 to 18 cm/kyr geomagnetic, radiolarian, and diatom constraint (Fig. 3; Barker & Kennett et al., 1999). Similarly, wavelet analysis of XRF Weddell Sea cores produce a mean sedimentation rate of approximately 5.9 cm/kyr, which corresponds to an independent paleomagnetic age model suggesting 4.0 cm/kyr during the Pliocene (Barker et al., 1988). Wilkes Land well-log wavelet analysis calculates sedimentation rates that are within an order of magnitude of the well-constrained paleomagnetic, radiolarian, and diatom age model (2.5 and 4.4 cm/kyr) but still is systematically slightly overestimating. Overall, these cross-calibrated sedimentation rates exemplify the utility of wavelet analysis of continuous well-logs, such as gamma ray and resistivity, and geochemcial datasets to produce robust age control. Further cross referencing can improve the reliability of wavelet analysis in providing age models.

CONCLUSION

Both wavelet analysis and PCA provide new insights regarding how subtle geochemical and geophysical marine sediment dataset can be used to inform changes in Antarctic ice volume. We present three circum-Antarctic gamma ray and resistivity well log datasets and one split core geochemical dataset from the Weddell Sea to demonstrate ubiquitous obliquity-paced sedimentation during the Pliocene. These offshore records demonstrate that distal marine archives record orbital forcings. Linear sedimentation rates are also derived through wavelet analysis and compared with independent age models.

ACKNOWLEDGEMENTS

This material is based on work supported by the Keck Geology Consortium and the National Science Foundation under Grant No. 1659322. I would also like to acknowledge Suzanne O'Connnell, Joe Ortiz, and Will Amidon for their support. The staff at the IODP repository in Texas, especially Brian LaVey, was especially helpful with the initial data collection.

REFERENCES

Barker, P. F., Camerlenghi, A., & Acton, G. D. (1999). *Proceedings of the Ocean Drilling Program, Initial Reports* (Vol. 178).

Barker, P. ., Kennett, J. P., & et al. (Eds.). (1988). *Proceedings of the Ocean Drilling Program, 113 Initial Reports* (Vol. 113). Ocean Drilling Program. Retrieved from http://www-odp.tamu.edu/publications/113_IR/113TOC.HTM

Bentley, M. J., & Anderson, J. B. (1998). Glacial and marine geological evidence for the ice sheet configuration in the Weddell Sea–Antarctic Peninsula region during the Last Glacial Maximum. *Antarctic Science*, *10*(3), 309–325. https://doi.org/10.1017/S0954102098000388

Cook, C. P., van de Flierdt, T., Williams, T., Hemming, S. R., Iwai, M., Kobayashi, M., … Yamane, M. (2013). Dynamic behaviour of the East Antarctic ice sheet during Pliocene warmth. *Nature Geoscience*, *6*(9), 765–769. https://doi.org/10.1038/ngeo1889

Escutia, C., Santis, L., Donda, F., Dunbar, R. B., Cooper, A., Brancolini, G., & Eittreim, S. L. (2005). Cenozoic ice sheet history from East Antarctic Wilkes Land continental margin sediments. *Global and Planetary Change*, *45*, 51–81. https://doi.org/10.1016/j.gloplacha.2004.09.010

Hambrey, M. J., Ehrmann, W., & Larsen, B. (1991). Cenozoic glacial record of the Prydz Bay continental shelf, East Antarctica. In: Barron, J; Larsen, B, et al. (eds.), Proc. ODP, Sci. Results, College Station, TX. (Ocean Drilling Program), 119, 77-132, 119(10.2973/odp.proc.sr.119.200.1991), 77–132. https://doi.org/Hambrey, M. J. , Ehrmann, W. and Larsen, B. (1991)   Cenozoic glacial record of the Prydz Bay continental shelf, East Antarctica ,   In: Barron, J; Larsen, B, et al. (eds.), *Proc. ODP, Sci. Results, College Station, TX. (Ocean Drilling Program)*, *119*, 77-132, *119*, pp. 77-132.doi:10.2973/odp.proc.sr.119.200.1991 <http://doi.org/10.2973/odp.proc.sr.119.200.1991>, hdl:10013/epic.41574

Hemming, S. R. (2007). Paleoceanography, physical and chemical proxies | Terrigenous sediments. In *Encyclopedia of Quaternary Science* (pp. 1776–1785).

Kaufman, Z. (2016). Sediment interpretations of ice-rafted debris in the Weddell Sea, Antarctica: a 3-3.8 mya record from ODP Site 697. *Honors Theses - All*. Retrieved from https://wesscholar.wesleyan.edu/etd_hon_theses/1605/

Latimer, J., & Filippelli, G. (2001). Terrigenous input and paleoproductivity in the Southern Ocean. *Paleoceanography*, *16*. https://doi.org/10.1029/2000PA000586

Naish, T., Powell, R., Levy, R., Wilson, G., Scherer, R., Talarico, F., … Williams, T. (2009). Obliquity-paced Pliocene West Antarctic ice sheet oscillations. *Nature*, *458*(7236), 322–328. https://doi.org/10.1038/nature07867

Pagani, M., Lui, Z., LaRiviere, J., & Ravelo, A. C. (2010). High Earth-system climate sensitivity determined from Pliocene carbon dioxide concentrations. *Nature Geoscience. 3*(1), 27-30 https://doi.org/10.1038/ngeo724

Raymo, M., Grant, B., Horowitz, M., & H. Rau, G. (1996). Mid-Pliocene warmth: Stronger greenhouse and stronger conveyor. *Marine Micropaleontology - MAR MICROPALEONTOL*, *27*, 313–326. https://doi.org/10.1016/0377-8398(95)00048-8

Scheuer, C., Gohl, K., D. Larter, R., Rebesco, M., & Udintsev, G. (2006). Variability in Cenozoic sedimentation along the continental rise of the Bellingshausen Sea, West Antarctica. *Marine Geology*, *227*, 279–298. https://doi.org/10.1016/j.margeo.2005.12.007

Scheuer, C., Gohl, K., & Udintsev, G. (2006). Bottom-current control on sedimentation in the western Bellingshausen Sea, West Antarctica. Geo-marine letters, (10.1007/s00367-006-0019-1). https://doi.org/Scheuer, C. , Gohl, K. and Udintsev, G. (2006)   Bottom-current control on sedimentation in the western Bellingshausen Sea, West Antarctica, Geo-marine letters. doi:10.1007/s00367-006-0019-1 <http://doi.org/10.1007/s00367-006-0019-1> , hdl:10013/epic.23546

Torrence, C., & Compo, G. P. (1998). A Practical Guide to Wavelet Analysis. *Bulletin of the American Meteorological Society*, *79*(1), 61–78. https://doi.org/10.1175/1520-0477(1998)079<0061:APGTWA>2.0.CO;2

True-Alcala, T. (2015). Diffuse Spectral Reflectance-derived Pliocene and Pleistocene Periodicity from Weddell Sea, Antarctica Sediment Cores. *Honors Theses - All*. Retrieved from https://wesscholar.wesleyan.edu/etd_hon_theses/1479

Verma, K., Bhattacharya, S., Biswas, P., Shrivastava, P. K., Pandey, M., Pant, N. C., & Party, I. E. 318 S. (2014). Clay mineralogy of the ocean sediments from the Wilkes Land margin, east Antarctica: implications on the paleoclimate, provenance and sediment dispersal pattern. *International Journal of Earth Sciences*, *103*(8), 2315–2326. https://doi.org/10.1007/s00531-014-1043-4

Learning Science Through Research
Published by Keck Geology Consortium
Short Contributions
Keck Geology Consortium
Volume 31
May 2018

ANTARCTIC WEDDELL SEA ODP SITE 696 PLEISTOCENE-PLIOCENE DIATOMS

MARK LAPAN, Colgate University
Research Advisor: Amy Leventer

INTRODUCTION

Pleistocene-Pliocene Antarctic Glacial History

As the impacts of climate change become clearer, scientists look to the earth's climatic history to place modern warming into a longer term perspective. In particular, scientists look to past warm periods to measure and model such important environmental parameters as sea level, atmospheric circulation, ice accumulation and atmospheric chemistry. The mid-Pliocene, from 4.5-3.3 million years ago is considered a potential analog for future climate given its many similarities to the modern world - with a similar geography of continents and oceans, intensity of solar radiation reaching the earth, and critically, carbon dioxide levels that are similarly high (Naish et al., 2009; Pollard and DeConto, 2009; Federov et al., 2013; Golledge et al., 2017). The Pleistocene interglacial periods, especially some of which appear to have been warmer than the present interglacial, for example Marine Isotope Stage 31 (Scherer et al., 2008) and Marine Isotope Stage 11 (Raymo and Mitrovica, 2012) are also ideal candidates to explore the consequences of a warmer world.

This project examines the Pleistocene using diatoms, plankton with silica tests, in a 10-m sediment core (2H) recovered from the Weddell Sea, from ODP Leg 113, Site 696 (see Figure 1). Diatoms are excellent as climatic indicators, given their sensitivity to a suite of environmental factors, including temperature, salinity, light levels, nutrient content, and the presence or absence of sea ice (Armand et al. 2005). For this study, the extent of seasonal sea ice cover was considered to be a critical factor controlling the concentration of diatom valves in sea floor sediments. As Burckle and Cirilli (1987) noted, for example, heavy sea ice cover restricts light penetration, and decreases primary productivity. Consequently, downward flux of diatoms is minimal during times of cooler climate and associated sea ice expansion. In contrast, warmer intervals with decreased sea ice cover, contain more biosiliceous sediments. The goal of this study was to evaluate diatom assemblage and abundance patterns in silica-rich sediments from the Jane Basin, at the northern tip of the Antarctic Peninsula, in order to understand past warm periods in this region.

International Ocean Discovery Program

The Ocean Drilling Program (ODP) and its successor, the International Ocean Discovery Program (IODP), is a scientific ocean drilling program that collects ocean floor geological data that are used to advance our understanding of a wide range of questions regarding Earth's history and dynamics. ODP Leg 113 took place in 1987 and was focused on the climatic and oceanographic evolution of the Weddell Sea. For this specific project, sediments from Hole 696A were selected for analysis, given shipboard biostratigraphic data that suggested the recovery of Pleistocene interglacial material (Gersonde and Burckle, 1990). Hole 696A is located at 61O50.945'S, 42O55.984'W. The total depth of the hole was 106 meters and 58.3 m were recovered (Barker et al., 1988).

METHODS

Core 696A-2H was run through a multi-track sensor at the IODP repository at Texas A&M University in College Station. Two downcore measurements, magnetic susceptibility and bulk density, were made on the archive half of Core 686A-2H to guide sampling. Dropstones, > 2mm were removed before the measurements were made. The core had shrunk and had numerous cracks, which disrupted the continuous measurements.

Magnetic Susceptibility

Magnetic Susceptibility (MS) is a measure of the relative proportion of magnetic material within a given sample. In sediments from the Southern Ocean, MS often indicated the relative contribution of terrigenous material versus biogenic material to the sediment (Leventer et al., 1996). This is because most biogenic input is in the form of biogenic silica and organic carbon, which do not contribute to MS. Measurements were taken at 0.1 cm intervals. These data (Fig 1) were used to determine sampling intervals for diatom identification, since this project focused on addressing the past periods of ocean warmth, which were most likely to have been recorded as intervals of low MS, due to greater biogenic production in open waters.

Bulk Density

Bulk density measurements were also collected via the non-destructive tool of the multi-track sensor. These data, also collected at 0.1 cm intervals are illustrated in Figure 1.

Diatom Sampling, Processing and Identification

Samples for qualitative and quantitative diatom analyses were selected based on the MS record, with low MS intervals presumed to be richer in diatomaceous material. Samples were dried at <50 degrees C, followed by weighing out a mass between 20-50 milligrams. Samples then were placed in glass vials on a warming tray set to 50 degrees C. Samples were cleaned using 10% hydrogen peroxide to remove organic material; after several days on the warming tray, samples were then placed into settling chambers and quantitative slides were made according to the method from Warnock and Scherer (2014). Microscopy was completed using an Olympus BX40 microscope. Observations were made at a magnification of 1000x. Microphotographs were taken using a Lumenara camera system. A total of 17 samples were taken (Fig 1). Of those 17 samples, 11 species were found that could be used to help date the core. Although the initial intent of the study was to find absolute and relative abundance of the diatom species observed, this result was not reached due to various obstacles. Thus, the end goal of the project was more preliminary taxonomy and slide creation for further quantitative work in the future.

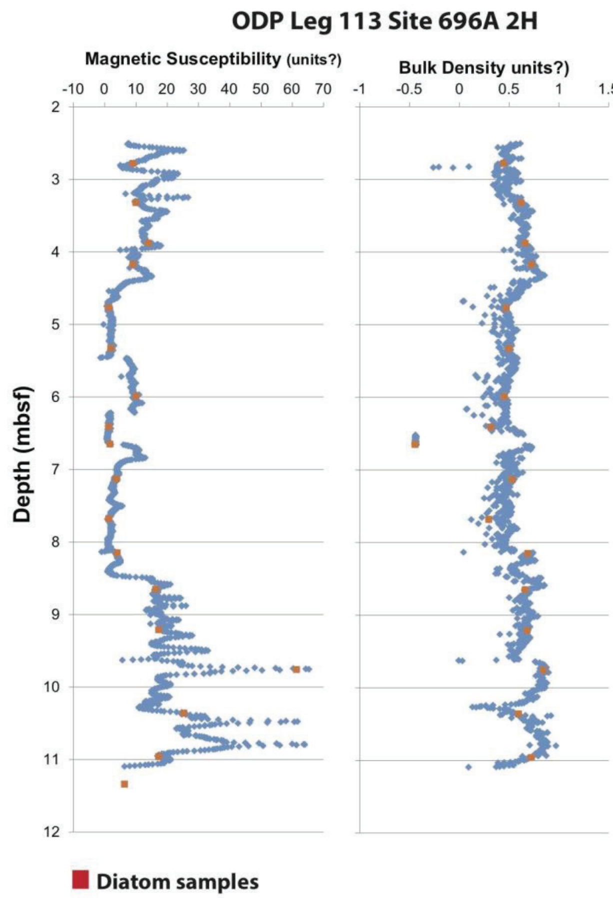

Figure 1. Magnetic Susceptibility and Bulk Density with location of samples examined for diatoms.

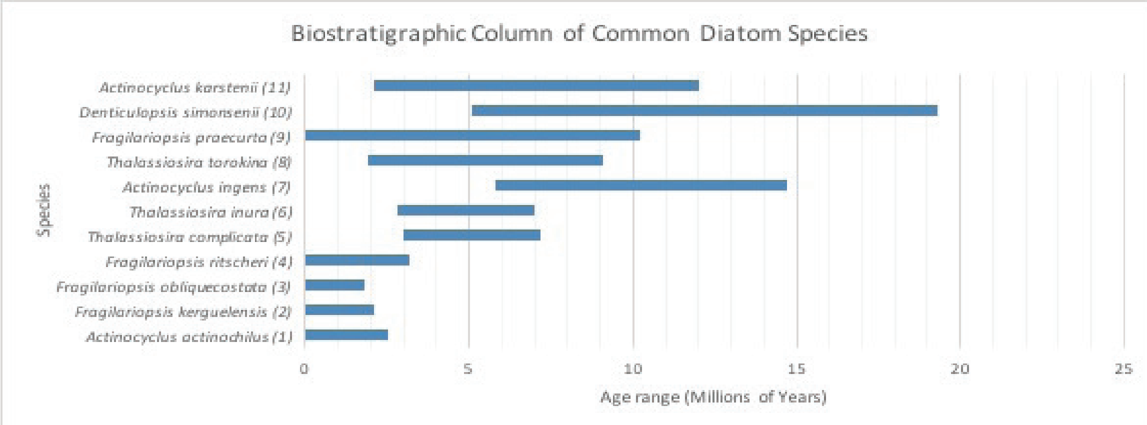

Figure 2. Biostratigraphic column of commonly observed diatom species.

RESULTS

Diatom Images

Diatom images were compiled using Photoshop to alter the coloration so that the images would match in color tone to account for differences in lighting when the photos were taken. The images taken and edited in Photoshop were then put in pdf format to create a taxonomic guide, this could be used as a template for counting the number of a specific species of diatom in the future (Fig. 3).

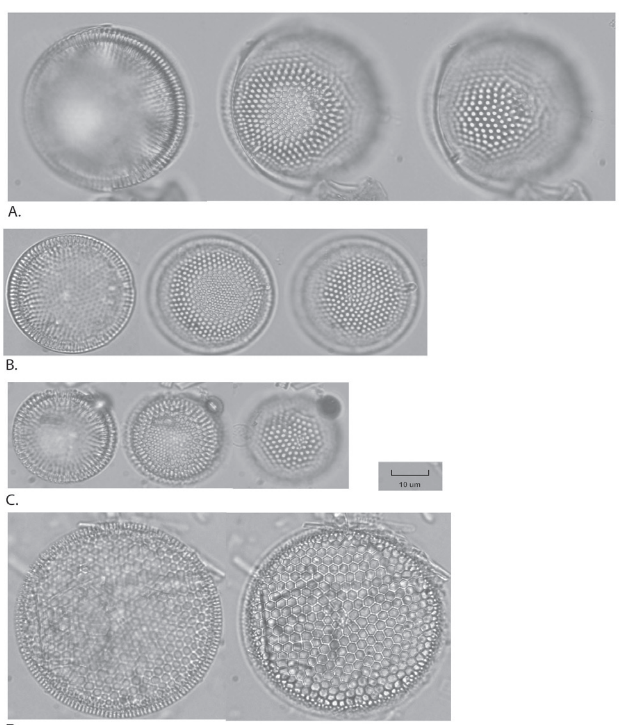

Figure 3. Images of Diatom species A-D: Thalassiosira torokina.

Biostratigraphic Position

From Cody et al. (2008), we can create a time sequence for when a majority of diatom species lived during the Pliocene and Pleistocene. Figure 2 illustrates a focused version of this graph with respect to the diatoms observed in this core. Using this information we can estimate the time during which the sediments in this core were deposited.

DISCUSSION

One goal of this project was to study the paleoceanographic record of warm intervals of Earth's history, based on diatoms from ODP Leg 113 Site 696. The first step toward accomplishing this goal was to understand the stratigraphic framework for the samples selected for study, by comparing their diatom assemblage with stratigraphic zonations for the Southern Ocean (Cody et al., 2008). Among the first to contribute to this field of study were Weaver and Gombos (1981), who proposed the Neogene (last 24 m.y.a.) diatom zonation by summarizing species into easily recognizable and broad geographic distributions. Gersonde and Burckle (1990), more specifically examined Neogene sediments from Leg 113, and given the excellent core recovery, were able to revise earlier zonation schemes. They addressed several critical and unresolved points, including the use of Last appearance datums (LADs), and the previous use of several poorly described species as biostratigraphic markers which led to incorrect age assignments. For example, Miocene zones were not directly tied to the magnetic time scale, and long (4 m.y.) zone ranges needed to be refined. These issues were addressed by initial studies at Site 696. Gersonde and Burckle (1990) presented 16 diatom zones that were described along with several stratigraphically useful diatom datums of late early Miocene to Pleistocene age. This work stands as the foundation for the research conducted during this project.

Based on the diatom biostratigraphy (Gersonde and Burckle 1990, Gersonde et al. 1990), this core which was located at depth of 0-550 meters below sea floor, dates back to the early to late Pliocene. This new work aimed to re-address the timing of biosiliceous sections of 696A-2H, following upon the earlier findings. A brief taxonomic guide to species observed in this core section (Fig 3) documents the microscopy, and provides some preliminary guidance. However, the findings of this new work remain inconclusive, due to the presence of many unidentified species, and a large range in morphology within individual species. In addition, some stratigraphically significant species here were not identified in Gersonde and Burckle (1990).

For example, in the samples studied, *Thalassiosira torokina* was found to be abundant, yet Gersonde and Burckle (1990) do not record this species from the same section of Core 2H-696A. This may be due to a wide range in the morphology of this species. Larger *Thalassiosira torokina* are more three dimensional for example, while smaller specimens of *Thalassiosira torokina* are flatter, making it easier to have the entire valve in focus in a single view. As presented in Gersonde and Burckle (1990) we also observed *Thalassiosira inura*. Figure 2 is a graphical represen-tation of the ages that species observed.

Conclusions and Challenges with this study

The identification and counting of diatoms from these samples was challenging for several reasons. First, this researcher was new to the field of micropaleontology, so learning the fundamentals of diatom taxonomy was more time intensive than initially anticipated. In addition, the nomenclature of diatom species has evolved over time, primarily through detailed study of DSDP, ODP and IODP materials. Consequently, the names of many species have changed over time; for this reason, species identification required a thorough acquaintance with the large body of taxonomic literature. Overall, development of a biostratigraphic and paleoceanographic story based on samples from Leg 113 will require continued effort.

Moving forward from this study, the next step is to complete both absolute and relative diatom abundance counts. This would enable us to develop a biostratigraphic framework for the core, and to reconstruct changes in the oceanic environment over time. In addition, comparison of diatom abundance data and physical parameters, such as magnetic susceptibility, could provide information on changes in paleoproductivity that could be extrapolated beyond the scope of individual micropaleontologic analysis.

ACKNOWLEDGEMENTS

This material is based upon work supported by the Keck Geology Consortium and the National Science Foundation under Grant No. 1659322.

REFERENCES

Armand, L.K., Xavier, C., Romero, O., and Pichon, J.J., (2005). *The biogeography of major diatom taxa in Southern Ocean sediments: 1. Sea ice related species*, Palaeogeography, Palaeoclimatology, Palaeoecology 223 93-126.

Barker, P.F., Kennett, J. P., et al., (1980). *Proc. ODP, Init. Repts*., 113: College Station, TX (Ocean Drilling Program).

Burckle, L.H. and Cirilli, J., (1987). *Origin of diatom ooze belt in the Southern Ocean: implications for paleoceanography and paleoclimatology*, Micropaleontology 33, 82-86.

Cody, R.D. , Levy, R.H., Harwood, D.M., Sadler, P.M., (2008). *Thinking outside the zone: High-resolution quantitative diatom biochronology for the Antarctic Neogene.*Palaeogeography, Palaeoclimatology, Palaeoecology 260 92–121.

Fedorov, A.V., Brierley, C. M., Lawrence, K. T., Liu, Z., Dekens, P.S., Ravelo, A.C. (2013) *Patterns and Mechanisms of early Pliocene warmth.* Nature, 496 43–49. doi:10.1038/ nature12003.

Gersonde, R.(1990) *Taxonomy and morphostructure of Neogene diatoms from the Southern Ocean, ODP Leg 113.* Proceedings of the Ocean Drilling Program, Scientific Results, 113 791-802.

Gersonde, R. and Burckle, L.H. (1990) *Neogene Diatom Biostratigraphy of ODP Leg 113, Weddell Sea (Antarctic Ocean)*. Proceeding of the Ocean Drilling Program, Scientific Results, 113 7 61-789.

Golledge, N.R., Thomas, Z.A., Levy, R.H., Gasson, E.G., Naish, T.R., McKay, R.M., Kowalewski, D.E. and Fogwill, C.J., (2017). *Antarctic climate and ice-sheet configuration during the early Pliocene interglacial at 4.23 Ma.* Climate of the Past 13(7): 959-975.

Naish, T., Powell, R., Levy, R., Wilson, G., Scherer, R.,Talarico, F., Krissek, L., Niessen, F., Pompilio, M., Wilson, T., Carter, L., Deconto, R.,Huybers, P., McKay, R., Pollard, D., Ross, J., Winter, D., Barrett, P., Browne, G., Cody, R., Cowan, E., Crampton, J., Dunbar, G., Dunbar, N., Florindo, F., Gebhardt, C., Graham, I., Hannah, M., Hansaraj, D., Harwood, D., Helling, D., Henrys, S., Hinnov, L., Kuhn, G., Kyle, P., Läufer, A., Maffioli, P., Magens, D., Mandernack, K., McIntosh W., Millan, C., Morin, R., Ohneiser, C., Paulsen, T., Persico, D., Raine, I., Reed, J., Riesselman, C., Sagnotti, L., Schmitt, D., Sjunneskog, C., Strong, P., Taviani, S., Vogel, S., Wilch, T., Williams, T. (2009) *Obliquity-paced Pliocene West Antarctic ice sheet oscillations*, Nature, 458(7236):322-8. doi: 10.1038/nature07867.

Pollard, D. and DeConto, R. M. (2009) *Modelling West Antarctic ice sheet growth and collapse through the past five million years*, Nature, 458, 329–332.

Raymo, M. E., and Mitrovica, J.X., 2012, *Collapse of polar ice sheets during the stage 11 interglacial*, Nature, doi:10.1038/nature10891.

Scherer, R. P., Bohaty, S., Dunbar, R., Esper, O., Flores, J., Gersonde, R., Harwood, D., Roberts, A. and Taviani, M. *Antarctic records of precession-paced insolation-driven warming during early Pleistocene Marine Isotope Stage 31*. Geophysical Research Letters, 35, doi:10.1029/2007GL032254.

Warnock, J. P., Scherer, R. P. (2014) *A Revised Method for Determining the Absolute Abundance of Diatoms*. Journal of Paleolimnology, Doi: 10.1007/s10933-014-9808-0

Weaver, F.M., and Gombos, A.M.(1981) *Southern high latitude diatom biostratigraphy*, DSDP: Decade of Progress: Society of Economic Palaeontologists and Mineralogists Special Publication, 32, 445-470.

KECK Geology Consortium

Learning Science Through Research

Published by Keck Geology Consortium

Short Contributions
Keck Geology Consortium
Volume 31
May 2018

ZANCLEAN (EARLY PLIOCENE) SEDIMENT RECORDS OF ICE-SHEET INSTABILITY AT ODP SITE 697 (JANE BASIN), NW WEDDELL SEA, SOUTH ORKNEY MICROCONTINENT

FORREST W. LLOYD, Beloit College
Research Advisors: Suzanne O'Connell (Wesleyan University) and Jim Rougvie (Beloit College)

INTRODUCTION

Accounting for an approximate tenth of the Earth's land surface, Antarctica stores about 70% of the world's freshwater (29.46 million km^3) in the form of ice which covers 90% of its continental surface (Fretwell et al. 2013; Kennicut et al., 2014). During climatic transitions, mechanisms related to melting or fracturing destabilize the voluminous Western/ Eastern Antarctic Ice-sheets (WAIS/EAIS) and their freshwater stores are released, further increasing sea-level and destabilizing ice-sheets (Bamber et al., 2013; Favier et al., 2014).

Although complete ice-sheet destabilization is not possible on decadal timescales, sea-level rise affects all peoples, especially those living in coastal poverty, as a 0.8 m sea-level rise would result in massive rebuilding and relocation efforts for inundated areas (Hallegatte et al., 2013; Hauer et al., 2016). The study and mitigation of WAIS/ EAIS destabilization is further necessitated by increased anthropogenic activity which has accelerated rates of sea-level rise approximately 0.08 mm annually since 1993; melt from glaciers and ice-sheets account for 61 ± 19% of this change alone (Gardner et al., 2013; Albrecht and Levermann, 2014; Nerem et al., 2018).

As ice ablation occurs at one of Antarctica's five distinctive crustal regions, glaciers entrain geologic material, transport it seaward, and calve to form iceberg armadas (Bischof, 2001; Boger et al., 2011). Prevailing ocean currents, such as the counter-clockwise flowing East Wind Drift (Antarctic Coastal Current), often transport these armadas for several years at an approximate rate of 5 cm/s and are the only regional mechanism capable of depositing entrained material as ice-rafted detritus (IRD) thousands of km from provenance to pelagic depths (Le and Shi, 1997; Diekmann and Kuhn, 1999). The transfer of IRD from a terrestrial source to the oceanic depths can be used to infer sediment provenance, paleo-ocean circulation, paleo-environmental conditions, and possible Heinrich-like Events which reflect glacial/interglacial cycles at high latitudes via iceberg abundance (Heinrich, 1988; Alley and MacAyeal, 1994; Naish et al., 2009; Williams et al., 2010; Passchier; 2017). Although the definition of IRD is subjective, the term is here defined as material >63 µm due to the infrequent ice rafting of silt sized (<63 µm) particles (Drewry and Cooper, 1981; Heinrich, 1988; Darby et al., 2002).

By measuring the changes in mean size of sortable silt (10-63 µm), a better understanding of the velocity of bottom water can be reached as responses to Pliocene environmental change often result in a change in flow velocity (McCave et al., 1995). In polar regions, where sortable silt from melting ice can be mixed with that transported by bottom currents, changes in sortable silt for bottom currents need to be carefully evaluated (McCave et al, 2013).

The Pliocene epoch (2.58 to 5.33 mya) is characterized by an early and middle warming period and is marked by similarities to those of present and predicted conditions: atmospheric CO_2 concentrations (~400 ppm), average surface temperatures (2-3°C warmer), and southern landmass configurations (Pagani et al., 2009); therefore, the study of ice-sheet instability during the Pliocene epoch serves as a suitable proxy for current and predicted future environmental conditions concerning sea-level rise and ice-loss.

Environmental proxies such as biogenic silica (bSi), ice-rafted detritus (IRD), sortable silt, and XRF elemental counts from Pliocene aged marine sediment cores can be used to better understand responses to environmental change, identify regions of future ice-sheet instability, and learn more about paleo-ocean circulation conditions at ODP Site 697 (Jane Basin).

METHODS

Two well-preserved Weddell Sea sediment cores (31X and 32X), from the B-hole of ODP Site 697 (Leg 113), with inter-dispersed IRD intervals were selected from the IODP Gulf Coast Repository (GCR) for XRF, bSi, grain size, and IRD provenance analyses.

Split cores were scraped with a standard glass microscope slide to homogenize surface relief and remove accumulated dust and mold; lithic bodies such as pebbles were removed, measured, and identified. Once prepared, cores were covered with a 4 µm SPEX CertiPrep Ultralene film and analyzed using an Avaatech XRF Core Scanner at 10, 30, and 50 kV every 2 cm to provide quantitative elemental data.

Ten cc sediment aliquots were taken downcore every 10 cm. If a disturbance, such as a crack, was present at the sampling interval a five-cc aliquot was taken; if the region was greatly disturbed it was skipped altogether.

At Wesleyan, approximately 2 g of sample from 22 separate (n31X= 3, n32X= 19) intervals were prepared for a time-step wet alkaline digestion method modified by the University of Minnesota Limnological Research Center (LCR). Following initial preparation samples were digested in 0.5 molar NaOH solution and the rate of bSi dissolution was recorded after 60, 90, 120, 150, and 200-minute intervals; one aliquot was extracted following each digestion. Sample absorption was measured via spectrophotometry and a bSi weight percentages were calculated.

Samples were separated into size fractions for different analyses. 35 mL of a sodium hexametaphosphate Calgon dispersing agent and a Vortex Genie were used to disaggregate bulk samples, these were later segregated into four grain fractions (<63 µm, 63-150 µm, 150-500 µm, >500 µm) via standard wet-sieving practices. Fractions were dried via heat lamp, weighed with a Mettler AE 240 balance, transferred to a 1 mL vial; sample percent weights were calculated.

In order to estimate accumulation rates (>63 µm) for each core, paleomagnetic reversal stratigraphy from Pudsey et al. (1988) and a geomagnetic polarity timescale by Gee and Kent (2007) were used to estimate absolute ages and linear sedimentation rates (LSR). Due to the lack of age control for Cores 31X and 32X the nearest paleomagnetic reversal (Chron 3N-4), located 295.7 mbsf in Core 30X-2, was used to extrapolate ages; since accumulation values are expected to meet or exceed those nearest to sea-level, the linear sedimentation rate (LSR) closest to the top of Core 31X (150 m/my) was applied to the following equation:

$$\textbf{Sample Age} = \textbf{Chronological Age}_i + [(\textbf{Mbsf}_{sample} - \textbf{Mbsf}_i) * (1/\textbf{LSR}_{sample})]$$

where LSR_{sample} is the linear sedimentation rate (LSR) at the specified sample depth, Mbsf refers to "meters below sea floor," and Chron Age_i, $Mbsf_i$ (i =initial) refer to values at the upper paleomagnetic boundary used in calculating LSR_{sample} (Pudsey, 1990; Gee and Kent, 2007).

A lithium heteropolytungstate (LST) heavy liquid was used to density separate the 150 - 500 µm sized particles and liquid nitrogen was used to freeze the densest mineral fraction; individual hornblende grains were picked from the resulting heavy fraction for Ar geochronology dating at Columbia University's Lamont-Doherty Earth Observatory. Results from Ar geochronology and Malvern analyses are not available at this time.

RESULTS

Core Descriptions

Core 31X is composed of a highly disturbed silty-mud that is dark green to grey in color; evidence of oxidation, sand sized quartz rich material, dropstones, and light banding are found throughout. Geologic material found in 32X is slightly warmer in color than that of 31X as it ranges from dark greenish-grey to brown, is clay rich, and has sedimentary structures that have been mixed and disturbed by drilling. A highly laminated area is found in 32X-4; pyrite nodules and an abundance of pebble sized igneous drop-stones are found throughout the core (Fig.1).

Figure 1. Photo showing variability in core section 32X-4-90-98. Core images, such as this one taken from approximately 317.66 to 317.72 mbsf, display a range of colors and particle sizes as found throughout the hole. The light, silt-rich laminae are indicative of contourite deposits which form as a result of contour currents which are turbid and caused by bottom water interaction.

Analysis of XRF spectra

Downcore trends, based on normalized ratios are highly variable. High ratios of Fe/Ti, Fe/Al, and S/Cl signal the presence of anoxic conditions in the core with peaks at 306.6 and 314.72 mbsf (Fig. 2). XRF proxies related to bSi production such as Si/Al and Si/Ti, are found to match trends in bSi accumulation (Fig. 3).

Accumulation of biogenic silica (bSi)

The percent composition of bSi tends to increase in sync with increased IRD accumulation (Fig. 4). Biogenic silica averages 1.97 weight percent (n=22) and biosilica ranges from 1.34% to 7.36% with a standard deviation of 1.41. The mean for the three measurements from 31X is 2.45% and the standard deviation is 0.525. Values calculated from Core 32X (n=19) range from 1.34 % to 7.36 %, have a mean of 2.36% with a standard deviation of 1.52.

Grain size analysis

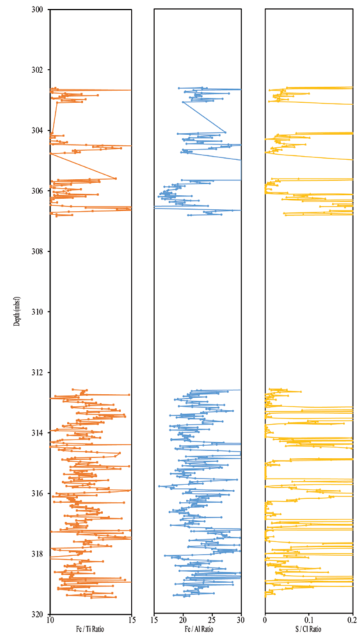

Figure 2. Anoxic pyrite forming conditions in XRF spectra. All XRF proxies for anoxic conditions (Fe/Ti, Fe/Al, and S/Cl ratios) which are necessary for pyrite formation are found peaking at the same depths downhole for Core 31X and Core 32X; pyrite is found at these depths.

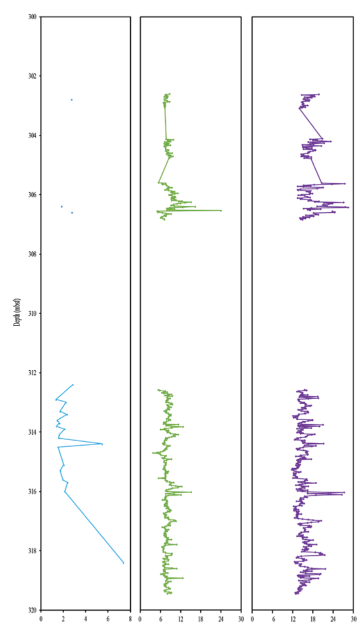

Figure 3. Record of biogenic productivity in XRF spectra. The bSi curve (solid light blue) is plotted downcore with proxies for bSi production; notice that although samples were not taken down the entire hole peaks match and can be used to infer other periods of productivity as they relate to glacial/interglacial periods.

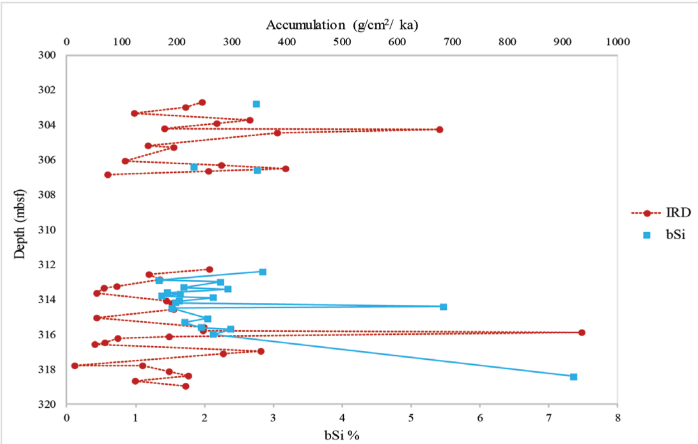

Figure 4. Downhole ice-rafted detritus (IRD) and biogenic silica (bSi) accumulation. Peaks from IRD (dashed red) and bSi accumulation (solid light blue) tend to be synchronous and exhibit similar trends in warming.

Fine particles (<63 µm) compose a majority ($\bar{x}$ = 92.4%) of the cores while the >500 µm fraction composes the smallest percent of the cores with values ranging from 0.07 to 0.47%. Per sample weight percent values from the 63-150 fraction ($\bar{x}$ = 3.42%) range from 0.44% to 14.54% and the slightly smaller ($\bar{x}$ = 2.94%) 150-500 µm interval ranges from 0.06% to 14.91%.

Accumulation of ice-rafted detritus (IRD)

According to estimates from the paleomagnetic reversal at 4.908 Ma (Chron 3N-4) Cores 31X and 32X together preserve an approximate 108 kyr sediment record spanning the Zanclean age of the Pliocene this assumes LSR has remained unchanged. These cores exhibit downcore variability with abrupt peaks associated with IRD accumulation appearing at 304.3 mbsf (31X) and 315.9 mbsf (32X). Abundant IRD accumulation ($\bar{x}$ = 216.1 g/cm^2 / ka) in these cores range from 14.06 to 934.3 g/cm^2 / kyr. and account for 0.49% to 32.8% of the total per sample sediment weight; the median accumulation rate and standard deviation is 185.9 and 170.7 respectively. Core 31X records approximately 27 kyr of geologic history and has weight percent values ranging from 2.58% to 23.71%; the mean accumulation rate for 31X is 258.5 g/cm^2 / ka. Core 32X comprises a majority (n= 25) of the total samples (n= 41) and has a high mean sedimentation rate (190.6 g/cm^2/ka) with values ranging from 14.1 to 934.3 g/cm^2/ka, a median of 180.8, and a standard deviation of 176.5; per sample weight percent values for the core ranged from 0.49% to 32.8% with a standard deviation of 6.19 and a median of 6.34; the mean per sample weight percent was 6.69%.

DISCUSSION

Lack of age control for Cores 31X and 32X has made correlating depth to age difficult for ODP cores 697B-31X and 32X as the only paleomagnetic reversal occurs in Core 30X where the top of Chron 3N-4 (4.980 Ma) is identified at 295.7 mbsf (Pudsey, 1990; Gee and Kent, 2007). Assuming a linear sedimentation rate of 150 m/my sediment, as accumulation is posited to increase with Jane Basin depth, these cores record an approximate 108 kyrs (5.03 Ma to 5.13 Ma) with the base of Core 32X aging approximately 16 kyrs older than that of the base of Core 31X.

In conjunction with an abundance of Si and relative lack of Ca in Core 31X and Core 32X, contourite deposits suggest that the site is located at depth, cool, and turbid as laminae is reworked by contour currents to form contourites; larger inter-dispersed dark bands are representative of interglacial cycles as terrigenous material was deposited by icebergs during episodic warming periods (Fig. 1). IRD and bSi peaks suggest that the period recorded by Core 31X and Core 32X during the Zanclean age of the Pliocene was relatively warm and underwent a total of 17 interglacial periods, with seven being minor, as evident in Figure 4. Kaufman (2016) focuses on Cores 13X-17X and finds that the mean IRD accumulation rate during the mid-Pliocene warming period was 57.45 g/cm^2/kyr with a range between 2.7 g/cm^2/kyr to 254 g/cm^2/kyr. These rates are much lower than those from Cores 31X and 32X, as values range from 14.06 g/cm^2/kyr to 934.3 g/cm^2/kyr and average 216.1 g/cm^2/kyr; such change in accumulation rate may suggest increased ice rafting over the site, a change in provenance, increased entrainment potential of water due to increased discharge, or may reflect an increase in Jane Basin depth. Such data also suggest that the Pliocene is characterized by a series of warming and cooling cycles which began in the Zanclean and culminated in the mid-Pliocene. It should be noted however that when calculating IRD accumulation rates, values are sensitive to reasonable but poorly constrained LSR values (150 m/my).

Despite the presence of data from the early and mid-Pliocene, more data from Cores 18X-30X would be beneficial in discerning when glacially dominated periods were most prevalent as such information could be applied to aid in mitigation efforts, environmental models, and contribute better understanding of environmental conditions at ODP Site 697 during the Pliocene epoch. Unfortunately, poor recovery and disturbed sediment for most of these cores do not make such research likely.

Comparison of Si/Al and Si/Ti XRF spectral count ratios in Figure 3 show that local Si is biogenically sourced, likely from diatom frustules, as bSi accumulation and these XRF spectra align; variance, especially at 316.04 mbsf, can likely be attributed to the deposition of silicates by icebergs (Agnihotri et al., 2008; Dickson et al., 2010). This change in composition may reflect a change in provenance. In conjunction with pyrite occurring at depth, XRF spectral proxies (Fe/Ti, Fe/Al, and S/Cl ratios) follow similar trends suggesting the presence of anoxic conditions or formation of bottom water at this time; such conditions occurred as a result of increased eutrophication following ice-rafted mineral deposition as both conditions reduce abundant oxygen flow (Fig. 2).

FUTURE WORK

Hornblende age dates ($^{40}Ar/^{39}Ar$) and results from the analysis of fine grains (<63 μm) will be used to determine IRD provenance and understand conditions related to bottom water formation during the Pliocene; results will be compared to those of Kaufman (2016) to determine if source regions have changed during this earlier interval.

ACKNOWLEDGEMENTS

This material is based upon work supported by the Keck Geology Consortium and the National Science Foundation under Grant No. 1659322; further financial support was made possible through the ExxonMobil Corporation. The author would like to thank the International Ocean Discovery Program-Gulf Coast Repository (IODP- GCR), Wesleyan University and Beloit College for allowing access to their instrumentation. Special thanks are extended to Brian LeVay at IODP, Elmo Rawling at the Wisconsin Geologic & Natural History Survey, Team Antarctica (Andrew Hollyday, Eduardo Centeno, Eliza Carter, Mark LaPan, Melissa Luna, Noah Spriggs, and Sophia Ptacek), the project directors (Suzanne O'Connell and Joseph Ortiz), and to Jim Rougvie as their collective support and collaboration was pivotal to the project's overall success.

REFERERENCES

Agnihotri, R., Altabet, M.A., Herbert, T.D., and Tierney, J.E., 2008, Subdecadally resolved paleoceanography of the Peru margin during the last two millennia: Geochemistry, Geophysics, Geosystems, v. 9, p. 1–15.

Albrecht, T., and Levermann, A., 2014, Spontaneous ice-front retreat caused by disintegration of adjacent ice shelf in Antarctica: Earth and Planetary Science Letters, v. 393, p. 26-30.

Alley, R.B., and MacAyeal, D.R., 1994, Ice-rafted debris associated with binge/purge oscillations of the Laurentide Ice Sheet: Paleoceanography, v. 9, p. 503–511.

Bamber, J. L., and Aspinall, W. P., 2013, An expert judgement assessment of future sea level rise from the ice sheets: Nature Climate Change, v. 3, no. 4, p. 424-427.

Bischof, J., 2001, Ice Drift, Ocean Circulation and Climate Change, Heidelberg, Springer.

Boger, S. D., 2011, Antarctica - Before and after Gondwana: Gondwana Research, v. 19, no. 2, p. 335-371.

Darby, D.A., Bischof, J.F., Spielhagen, R.F., Marshall, S.A., and Herman, S.W., 2002, Arctic ice export events and their potential impact on global climate during the late Pleistocene: Paleoceanography, v. 17, p. 15–17.

Dickson, A.J., Leng, M.J., Maslin, M.A., and Röhl, U., 2010, Oceanic, atmospheric and ice-sheet forcing of South East Atlantic Ocean productivity and South African monsoon intensity during MIS-12 to 10: Quaternary Science Reviews, v. 29, p. 3936–3947.

Diekmann, B., and Kuhn, G., 1999, Provenance and dispersal of glacial-marine surface sediments in the Weddell Sea and adjoining areas, Antarctica: ice-rafting versus current transport: Marine Geology, v. 158, no. 1-4, p. 209-231.

Drewry, D. J., and Cooper, A. P. R., 1981, Processes and Models of Antarctic glaciomarine sedimentation: Annals of Glaciology, v. 2, p. 117-122.

Favier, L., Durand, G., Cornford, S.L., Gudmundsson, G.H., Gagliardini, O., Gillet-Chaulet, F., Zwinger, T., Payne, A.J., and Brocq, A.M.L., 2014, Retreat of Pine Island Glacier controlled by marine ice-sheet instability: Nature Climate Change, v. 4, p. 117–121.

Fretwell, P., Pritchard, H. D., Vaughan, D. G., Bamber, J. L., Barrand, N. E., Bell, R., Bianchi, C., Bingham, R. G., Blankenship, D. D., Casassa, G., Catania, G., Callens, D., Conway, H., Cook,. J., Corr, H. F. J., Damaske, D., Damm, V., Ferraccioli, F.,Forsberg, R., Fujita, S., Gim, Y., Gogineni, P., Griggs, J. A., Hindmarsh, R. C. A., Holmlund, P., Holt, J. W., Jacobel, R. W., Jenkins, A., Jokat, W., Jordan, T., King, E. C., Kohler, J., Krabill, W., Riger-Kusk, M., Langley, K. A., Leitchenkov, G., Leuschen, C., Luyendyk, B. P., Matsuoka, K., Mouginot, J., Nitsche, F. O., Nogi, Y., Nost, O. A., Popov, S. V., Rignot, E., Rippin, D. M., Rivera, A., Roberts, J., Ross, N., Siegert, M. J., Smith, A. M., Steinhage, D., Studinger, M., Sun, B., Tinto, B. K.,Welch, B. C., Wilson, D., Young, D. A., Xiangbin, C., and Zirizzotti, A., 2013, Bedmap2: improved ice bed, surface and thickness datasets for Antarctica: Cryosphere, v. 7, no. 1, p. 375-393.

Gardner, A. S., Moholdt, G., Cogley, J. G., Wouters, B., Arendt, A. A., Wahr, J., Berthier, E., Hock, R., Pfeffer, W. T., Kaser, G., Ligtenberg, S. R. M., Bolch, T., Sharp, M. J., Hagen, J. O., van den Broeke, M. R., and Paul, F., 2013, A Reconciled Estimate of Glacier Contributions to Sea Level Rise: 2003 to 2009: Science, v. 340, no. 6134, p. 852-857.

Gee, J.S., and Kent, D.V., 2007, Source of Oceanic Magnetic Anomalies and the Geomagnetic Polarity Timescale: Treatise on Geophysics, v. 5, p. 419–460.

Hallegatte, S., Green, C., Nicholls, R.J., and Corfee-Morlot, J., 2013, Future flood losses in major coastal cities: Nature Climate Change, v. 3, p. 802–806.

Hauer, M.E., Evans, J.M., and Mishra, D.R., 2016, Millions projected to be at risk from sea-level rise in the continental United States: Nature Climate Change, v. 6, p. 691–695.

Heinrich, H., 1988, Origin and Consequences of Cyclic Ice Rafting in the Northeast Atlantic Ocean During the Past 130,000 Years: Quaternary Research, v. 29, p. 142–152.

Kaufman, Z.S., 2016, Sediment Interpretations of Ice Rafted Debris in the Weddell Sea, Antarctica: a 3-3.8 mya Record from ODP Site 697 [thesis]: Wesleyan University.

Kennicutt, M.C., Chown, S.L., Cassano, J.J., Liggett, D., Massom, R., Peck, L.S., Rintoul, S.R., Storey, J.W.V., Vaughan, D.G., Wilson, T.J., and Sutherland, W.J., 2014, Polar research: Six priorities for Antarctic science, v. 512, p. 23–25.

Le, K., and Shi, J., 1997, A study of circulation and mixing in the region of Prydz Bay, Antarctica: Studia Marina Sinica, v. 38, p. 39-52.

McCave, I.N., Crowhurst, S.J., Kuhn, G., Hillenbrand, C.-D., and Meredith, M.P., 2013, Minimal change in Antarctic Circumpolar Current flow speed between the last glacial and Holocene: Nature Geoscience, v. 7, p. 113–116.

McCave, I.N., Manighetti, B., and Robinson, S.G., 1995, Sortable silt and fine sediment size/composition slicing: Parameters for palaeocurrent speed and palaeoceanography: Paleoceanography, v. 10, p. 593–610.

Naish, T., Powell, R., Levy, R., Wilson, G., Scherer, R., Talarico, F., Krissek, L.,Niessen, F., Pompilio, M., Wilson, T., Carter, L., DeConto, R., Huybers, P., McKay, R., Pollard, D., Ross, J., Winter, D., Barrett, P., Browne, G., Cody, R., Cowan, E., Crampton, J., Dunbar, G., Dunbar, N., Florindo, F., Gebhardt, C., Graham, I., Hannah, M., Hansaraj, D., Harwood, D., Helling, D., Henrys, S., Hinnov, L., Kuhn, G., Kyle, P., Laufer, A., Maffioli, P., Magens, D., Mandernack, K., McIntosh, W., Millan, C., Morin, R., Ohneiser, C., Paulsen, T., Persico, D., Raine, I., Reed, J., Riesselman, C., Sagnotti, L., Schmitt, D., Sjunneskog, C., Strong, P., Taviani, M., Vogel, S., Wilch, T., and Williams, T., 2009, Obliquity-paced Pliocene West Antarctic ice sheet oscillations: Nature, v. 458, no. 7236, p. 322-U384.

Nerem, R.S., Beckley, B.D., Fasullo, J.T., Hamlington, B.D., Masters, D., and Mitchum, G.T., 2018, Climate-change–driven accelerated sea-level rise detected in the altimeter era: Proceedings of the National Academy of Sciences, v. 115, p. 2022–2025.

Pagani, M., Liu, Z., Lariviere, J., and Ravelo, A.C., 2009, High Earth-system climate sensitivity determined from Pliocene carbon dioxide concentrations: Nature Geoscience, v. 3, p. 27–30.

Passchier, S., Ciarletta, D., Miriagos, T., Bijl, P., Bohaty, S., 2017. An Antarctic stratigraphic record of step-wise ice growth through the Eocene-Oligocene Transition. Geological Society of America Bulletin, Vol. 129.

Pudsey, C. J. “Grain size and diatom content of hemipelagic sediments at Site 697, ODP Leg 113: A record of Pliocene-Pleistocene climate. “Proceedings of the Ocean Drilling Program, Scientific Results. Vol.113. 1990.

Pudsey, C.J., Barker, P.F., and Hamilton, N., 1988, Weddell Sea abyssal sediments a record of Antarctic Bottom Water Flow: Marine Geology, v. 81, p. 289–314.

Williams, T., et al. “Evidence for iceberg armadas from East Antarctica in the Southern Ocean during the late Miocene and early Pliocene.” Earth and Planetary Science Letters 290.3 (2010): 351-361.